SVENSKA GEOFYSISKA FÖRENINGEN

VOLUME 10, NUMBER 3 **Tellus** AUGUST 1958

*A QUARTERLY JOURNAL OF GEOPHYSICS*

# Comparative Studies of 500 mb Barotropic Forecasts Based on Different Analyses

By ROY BERGGREN, Swedish Meteorological and Hydrological Institute, Stockholm

(Manuscript received October 2, 1957)

*Abstract*

Some barotropic 500 mb forecasts are compared in the following manners:

1) comparison of the differences between forecasts made from analyses with identical boundary regions but different inner parts

2) comparison of forecasts made from two independent analyses based on identical material, and

3) comparison between forecasts based on two analyses with identical inner region but different boundary regions.

The result of a computation of the standard deviation of the vorticity and the Jacobian $J(\eta, \phi)$ is given and discussed, the deviation being due entirely to the personal factor in upper air analysis.

## Introduction

When discussing numerical forecasts such as barotropic 500 mb forecasts one has a definite need of some kind of verification figures. The ones mostly used in the past have been the correlation coefficient between observed and forecast height changes, the root-mean-square difference of these values and so on. In an earlier paper (1957, in the following called paper I) the author reported the result of an experiment in which the initial 500 mb chart as well as the barotropic 24h and 48h forecasts were kept constant, while different verification analyses were used. Thus, the forecast height changes were the same all through the experiment, while the observed changes varied with the different verification analyses. The latter analyses were based on identical observation material and the reported deviations were entirely due to the personal factor in upper air analysis.

In this paper another experiment will be discussed, in which the verification charts are the same all the time while the initial charts vary, the variation being entirely due to the method of analysis. The observation material was identical for all the four different analyses used for the experiment. Thus, the observed changes varied this time with the initial analysis as did the forecast changes.

The 500 mb forecasts were performed as discussed in papers by Staff Members, Dept. of Met., Univ. of Stockholm (1954) and BOLIN (1955). The grid size was about 300 km and the area used is indicated in fig. 1. The total forecast area was about 12,000 km × 9,000 km and the verification was performed over an area of 8,000 km × 4,000 km (see fig. 1).

Among the 29 analyses discussed in paper I three were picked out. The first one was the author's analysis (from here on called analysis

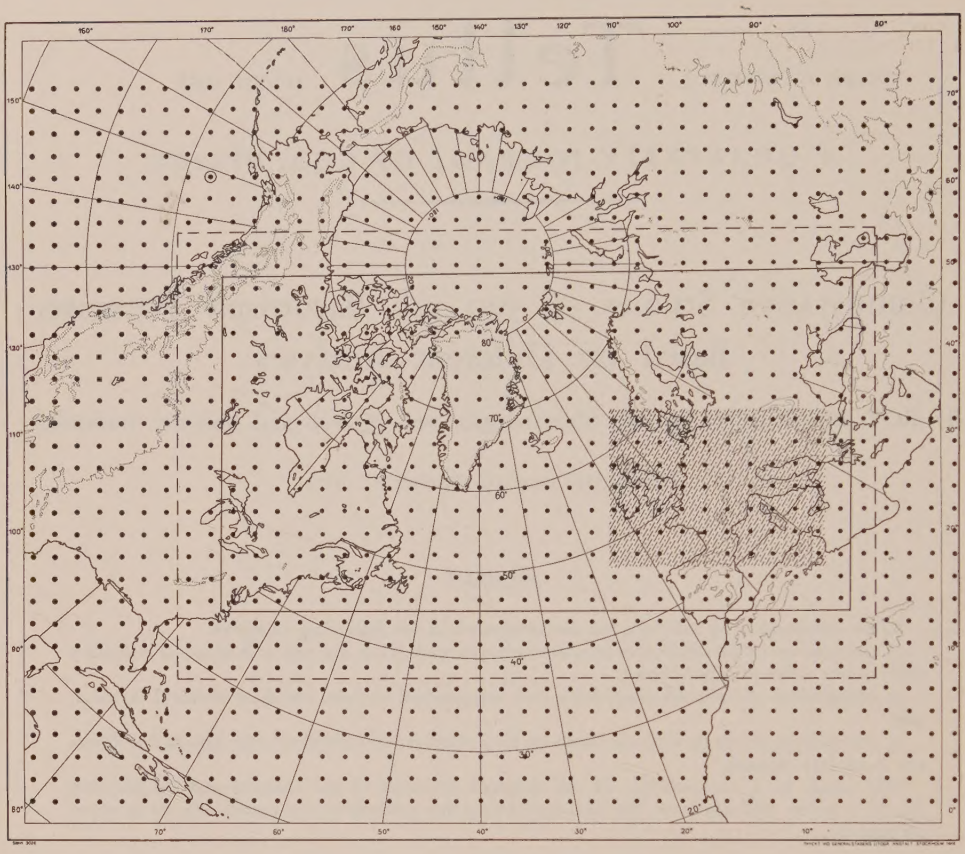

Fig. 1. Location of the grid used in the numerical foreasts. The solid line indicates the region within which verification was made. The dashed line gives the boundary outside which the analyses discussed in paragraph 1 were identical. The calculations discussed in paragraph 5 were performed over the small region with the dash-dotted lines.

A) which gave a low value for the correlation coefficient for the 24h forecast. The second one (analysis B) was the analysis that gave the highest 24h correlation coefficient and as the third analysis a numerical analysis was chosen (analysis C). The numerical analysis was used already in paper I and was constructed according to the scheme laid down by Bergthorson and Döös (1955) and by Döös and Eaton (1957).

In the earlier experiment the analysis was restricted to a region slightly larger than the verification area indicated in fig. 1. Thus, it was necessary to increase the analysis area of analyses B and C. This was done in such a way that the boundary region from analysis A was fitted to the inner part of analyses B and C. In fig. 1 is indicated the boundary outside which the three analyses were identical.

Furthermore, the analyst who once performed analysis B completed his analysis to the outer boundary of fig. 1 (analysis $B^1$). Thus, the author had at his disposal four analyses that were to be brought together and compared in three different ways:

1) Comparison of the differences between forecasts made from analyses with identical boundary regions but different inner parts, (analyses A, B and C),

2) comparison of forecasts made from two independent analyses based on identical material (analyses A and $B^1$), and

3) comparison between forecasts based on two analyses with identical inner region but different boundary regions (analyses B and $B^1$).

Before going into numerical details two things must be stressed:

a) this discussion deals only with one

**Table I. The standard deviation of the difference between analyses A, B, B¹ and C and the corresponding forecasts. The computations were made over the inner area given in fig. 1, consisting of 420 grid points.**

| Analysis pairs | A—B | B—C | A—C | A—B¹ | B¹—C | B—B¹ |
|---|---|---|---|---|---|---|
| Analysis | 26 gdm | 24 | 31 | 26 | 24 | 0 |
| 24h forecasts | 29 | 33 | 31 | 30 | 33 | 9 |
| 48h | 54 | 41 | 30 | 56 | 50 | 39 |

single case and it is not claimed that general conclusions can be drawn from it. The goal of this paper is only to show what may happen under certain conditions,

b) the case studied in this paper and in paper I represents a simple case from the analyst's point of view. The observed differences in analysis are therefore relatively small.

Let us first examine numerical estimates of the differences between the analyses used during the experiment. As a measure of the deviations between the analyses the author has used the standard deviation ($d$) of the difference between the height values at the 420 grid points of the verification area indicated in fig. 1.

In the literature on numerical analysis the root-mean-square difference (RMS) is sometimes given.

The difference between $d$ and RMS is small when $(\overline{A}-\overline{B})$ is a small quantity ($\overline{A}$ and $\overline{B}$ being the mean value of the height of the 500 mb surface over the area considered) as is always the case when we compare different analyses over a relatively large area. The reason for using $d$ in this paper is the fact that the same quantity is calculated for the different forecasts and in these the differences $(\overline{A}-\overline{B})$ may reach very large values (in one case 148 geodynamic meters (gdm)).

In table I the values of $d$ are given and they ought to be compared with those given by earlier authors. CRESSMAN and GILCHRIST (1954) have given the values in table II. They used three different analyses together with a numerical one. The two first analyses (1 and 2) "were prepared very carefully by experienced analysts who took all the time they needed for their completion. Analysis 3 was made hurriedly under operational conditions."

Cressman and Gilchrist made the computation over a grid of 19 × 19 points or approximately 5,400 × 5,400 km. From this grid 222 points were selected "as being those where sufficient data were available to permit a fair comparison". Thus, the number of points involved was only slightly more than half that used in this paper. Furthermore, the investigated area was to a large extent situated over the North-American continent in the former case while the one used in this paper covers wide parts of the northern part of the Atlantic Ocean. It is therefore reasonable to get larger $d$-values in the latter case.

If we now compare the values given by BERGTHORSON and DÖÖS (1954) (table III) with those in table I we find that the mean value for seven cases is about the same as the ones given in table I. A smaller area (3 000 km × 2 400 km) gave values 5 – 6 m

**Table II. The standard deviation of the difference between three conventional analyses (1, 2 and 3) and a numerical one (0) as given by Cressman and Gilchrist (1953).**

| Analysis pairs | 1—2 | 1—3 | 2—3 | 0—1 | 0—2 | 0—3 |
|---|---|---|---|---|---|---|
| d | 15 gdm | 20 | 18 | 21 | 22 | 21 |

**Table III. The root-mean-square difference between two conventional routine analyses ($C_1$ and $C_2$) and one numerical analysis (N). The values within brackets represent values for a small area with a dense net work of observing stations. Bergthorson and Döös (1955).**

| Analysis pairs | N—$C_1$ | N—$C_2$ | $C_1$—$C_2$ |
|---|---|---|---|
| 7 cases (12h forecast) | 26 (21) m | 24 (18) | 26 (20) |
| 2 cases (24h forecast) | 43 (29) | 49 (33) | 36 (28) |

lower. In the seven cases a 12h forecast was used as a first approximation. The numerical analysis discussed in this paper, however, was based on a 24h forecast. For that reason we ought to compare the values for the two cases that included a 24h forecast. From these values we can see that the values given in table I are lower than the ones in table III. This is in agreement with the above-mentioned fact that the case studied in this paper represents a simple case from the analyst's point of view.

The mean value of the root-mean-square difference given by Döös and Eaton (1957) was 34 m and was based on a five month trial period (about 125 cases) during which the numerical analysis technique was used on a routine basis. The investigated area was the northern part of the Atlantic Ocean between 25° N and 65° N, i.e. an area with a scanty net work.

1. *Comparison between forecasts based on analyses with identical boundary regions*

In fig. 2 are given all analyses and forecasts discussed in the three first paragraphs of this paper. The upper row contains four different versions of the 500 mb pattern for 7 November 1949, 0300 GMT. The boundary regions of the three analyses A, B and C are identical and in addition to these analyses, analysis $B^1$ is indicated in fig. 2 b with dashed lines. The verification charts for 8 and 9 November 1949, 0300 GMT are given in figs. 2 g and k, respectively. Figs. 2 d – f and 2 h – j give the 24h and 48h forecasts, respectively, placed below the corresponding initial chart. The forecasts based on analysis $B^1$ are given by dashed lines on the forecasts based on analysis B.

As can be seen at a first rapid visual inspection of the forecast charts they all contain the same main error, viz. the trough over Central Europe and the Mediterranean is forecast to move too far to the northeast. Furthermore, the cyclogenesis over the Atlantic east of Newfoundland was missed by all forecasts. Over she westernmost part of the verification area the forecasts show better agreement with the verification charts. On the whole the difference between the forecasts are rather small.

On the forecast charts in fig. 2 d, f, h, and j are also indicated the errors in the forecast, given as the difference between the forecast chart and the verification chart. Thus, a minus-sign on fig. 2 indicates a region in which the forecast gives too low height values. No error fields are given on figs. 2 e and i in order not to overload these figures. The positions of the centres for extreme values of the errors are, however, approximately the same as the ones indicated on the other forecast charts. Especially, this is the case if we compare forecasts B and C.

On fig. 2 g and k are given the observed 24h and 48h changes, respectively. From the error field the following conclusions may be drawn.

The most serious errors are those connected with (1) the trough from Iceland to the central part of the Mediterranean; (2) the low over the Atlantic and (3) the strong anticyclogenesis in the upper left corner of the chart. The errors (1) is brought about by the fact that this trough maintained its position under filling, while the forecast moved it to the northeast keeping its central value unchanged. The errors (2) are obviously connected with a baroclinic development of a low east of Newfoundland. Finally the errors (3) are caused by an intense fictitious anticyclogenesis over the Alaska region and the area south thereof. This must be due to the boundary error effect as pointed out by Bolin (1955). Keeping the boundary values constant in such an area with strong cyclonic activity means a serious drawback to the value of the forecast. The numerical value of the error in this area exceeds 400 gdm even for the 24h forecasts.

A striking feature of the error fields in fig. 2 d and h is the large increase of the numerical value of some of the extreme areas. Over Canada a change from −50 gdm to −250 gdm was observed. The maximum value of −200 gdm over Central Europe in fig. 2 d increased, numerically speaking, to −340 gdm over Scandinavia in fig. 2 h.

In spite of the fact that the numerical values of the error sometimes increase or decrease radically, a certain conservatism in the error field can be seen, if we compare the field for a 24h and 48h forecast. Comparing consecutive 24h forecasts and their corresponding error field this is more obvious. When using numerical forecasts on an operational basis this fact must be of some value. Petterssen (1956)

**Table IV. Some verification parameters computed for different 500 mb 24h forecasts valid for 0300 GMT 8 November 1949. Heights are given in geodynamic meters and wind speeds in m/s.**

| Analysis | A | B | C | $B^1$ | $B^{11}$ |
|---|---|---|---|---|---|
| $\bar{y}$ | −22 | −6 | −5 | −7 | −6 |
| $\sigma_y$ | 77 (69) | 66 (70) | 62 (73) | 66 (69) | 69 (73) |
| $\overline{\lvert y \rvert}$ | 63 | 54 | 51 | 52 | 56 |
| $\varepsilon_0$ | 64 | 52 | 58 | 49 | 50 |
| $r_{xy}$ | 0.67 (0.68) | 0.74 (0.73) | 0.68 (0.67) | 0.77 (0.75) | 0.77 (0.78) |
| $\delta_e$ | 11.4 | 9.4 | 10.5 | 9.1 | 9.2 |
| $\delta_p$ | 12.3 (10.7) | 10.2 (11.2) | 9.1 (11.5) | 9.9 (10.9) | 10.1 (11.1) |
| $\bar{d}_p$ | 10.4 (9.3) | 9.0 (9.9) | 7.9 (9.6) | 8.8 (9.6) | 9.0 (9.8) |
| $\bar{d}_e$ | 9.0 | 7.8 | 8.6 | 7.7 | 7.8 |
| $(d_e)$max | 38.2 | 28.5 | 36.1 | 27.5 | 27.5 |
| $r_{d_0 d_p}$ | 0.40 (0.44) | 0.56 (0.49) | 0.55 (0.37) | 0.54 (0.48) | 0.53 (0.48) |

**Table V. Some verification parameters computed for different 500 mb 48h forecasts valid for 0300 GMT 9 November 1949. Heights are given in geodynamic meters and wind speeds in m/s.**

| Analysis | A | B | C | $B^1$ |
|---|---|---|---|---|
| $\bar{y}$ | −48 | −2 | 6 | 38 |
| $\sigma_y$ | 146 (137) | 124 (129) | 124 (132) | 112 (106) |
| $\overline{\lvert y \rvert}$ | 125 | 99 | 101 | 95 |
| $\varepsilon_0$ | 133 | 92 | 87 | 88 |
| $r_{xy}$ | 0.66 (0.61) | 0.72 (0.70) | 0.74 (0.77) | 0.72 (0.69) |
| $\delta_e$ | 15.8 | 13.7 | 12.6 | 12.7 |
| $\delta_p$ | 16.8 (15.1) | 15.5 (16.9) | 14.1 (15.8) | 15.5 (16.7) |
| $\bar{d}_p$ | 15.0 (13.4) | 14.1 (13.2) | 12.7 (13.9) | 14.0 (13.1) |
| $\bar{d}_e$ | 14.2 | 12.2 | 11.4 | 11.4 |
| $(d_e)$max | 31.4 | 29.5 | 27.0 | 28.0 |
| $r_{d_0 d_p}$ | 0.23 (0.11) | 0.31 (0.38) | 0.39 (0.49) | 0.39 (0.32) |

has reported on an experiment carried out at the research centre in Chicago. The numerical forecasts were scrutinized by experienced forecasters using their general knowledge of the behaviour of the atmosphere from a barotropic point of view as well as statistics of the misbehaviour of the barotropic model published among others by GATES ET AL. (1956). On top of this a systematic use of the quasi-conservatism of the error fields might be of some value. It would lead too far, however, to enter on a detailed discussion on this subject in this paper.

In tables IV and V some verification figures are given. These values ought to be compared to the corresponding values in table VI. Subscripts $x$ and $y$ stand for observed and forecast changes, respectively.

The same symbols are used as in paper I (p. 332).

The variations of the numerical values in table IV are mostly between 10 and 30 per cent of the mean values. In two cases the differences are quite large: the value of $\bar{y}$ varies between −5 and −22 gdm and the value of $r_{d_0, d_p}$ between 0.40 and 0.56. Comparing the values of $\bar{x}$ in table III we find that the variation in $\bar{y}$ is much larger than in $\bar{x}$.

**Table VI. Some observed quantities for the 24h (48h) period ending at 0300 GMT 8 (9) November 1949. Heights are given in geodynamic meters and wind speeds in m/s.**

| | 24h | | | 48h | | |
|---|---|---|---|---|---|---|
| Analysis | A | B | C | A | B | C |
| $\bar{x}$ | 2 | −3 | −3 | 23 | 19 | 18 |
| $\sigma_x$ | 69 | 74 | 78 | 117 | 117 | 112 |
| $\overline{\lvert x \rvert}$ | 53 | 56 | 59 | 90 | 90 | 86 |
| $\delta_0$ | 10.8 | 11.8 | 12.4 | 16.9 | 16.4 | 15.4 |
| $d_0$ | 9.1 | 9.9 | 10.2 | 14.4 | 14.1 | 13.3 |
| $(d_0)$max | 32.5 | 38.7 | 39.9 | 39.6 | 38.4 | 33.8 |

The percentage variations in table V are for most quantities larger than the corresponding values in table IV.

If we now compare tables IV and V with table II in paper I (p. 333) we notice that the variations given in this paper are larger and in some cases much larger than the earlier ones. This is natural as we now deal with

differences in forecasts based on different analyses and in the earlier case with differences caused by different verification analyses. The effect is, however, counteracted by the fact that in paper I 26 (29) analyses were discussed while in this paragraph we are only discussing three different forecasts.

As was already stated in the introduction the situation chosen for this and the earlier study is a rather simple one from the analyst's point of view. It would be rather difficult to find a case that were definitely simpler to analyse if we regard the rather large area covered. For that reason it is the author's opinion that the values given in this paper and in paper I represent near minimum values.

When combining the $x$- and $y$-values in order to get the numerical quantities in table IV and V the $x$-values were taken as the differences between analyses A, B and C, respectively, and the verification analyses for the 8th and 9th of November 1949. It is possible to combine, say, an $x$-value taken as the difference between the verification analysis and analysis A and combine it with a $y$-value corresponding to analysis B. This was done for all possible combinations between $x$- and $y$-values corresponding to analyses A, B and C. The values that showed the largest numerical deviation from the ones calculated with the aid of the natural combinations are given within parantheses in table IV and V. Thus, for each forecast we get three different sets of verification quantities. If we compare the values corresponding to the same forecast we have almost the same combination of charts as was discussed in paper I: fixed values of the forecast changes correlated with values of observed changes varying with differences in the analysis of either the initial or the verification chart. In the earlier case the verification chart varied and this time the initial chart is the variable one. The values within parantheses deviate in some cases rather much from the already discussed values. In table V we get a value of $r_{xy}$ for analysis A, that is 0.61 instead of 0.66. The values of $\bar{d}_p$ in the same table and the same column are 13.4 and 15.0 m/s, respectively, and those of $r_{d_0,\,dp}$ 0.11 and 0.23, respectively.

It is natural to expect that the deviations due to different forecasts should represent larger values than those due to differences in verification analyses or in the initial analyses as the values are calculated in this special case. As can be seen in tables IV and V this is the rule except in a few places.

Let us now return to table I and compare the standard deviation of the difference between analyses A, B and C, respectively, with the same quantities for the corresponding forecasts. The largest increase is observed for the analysis pair A – B, for which the $d$-value increased from 26 to 54 gdm. For the pair B – C the increase is somewhat less, from 27 to 41 gdm. We notice that the $d$-values are approximately the same for all combinations of 24h forecasts. It is remarkable that the pair A – C shows a constant $d$-value during 48 hours.

2. *Comparison between two forecasts based on two different analyses*

As can be seen from fig. 2 there are some differences between analyses A and B$^1$. The largest deviations are observed over northeast Greenland and the area around the North Pole, over the Alps and northern Italy and the region south of the Azores. Minor differences are found in the upper part of the area given in fig. 2. Very much alike are the position of the low over northeast Canada and of the trough from Iceland to the Mediterranean.

From table IV we get the resulting verification figures. The correlation coefficient ($r_{xy}$) increased to the highest value in the table (0.77) and all the wind verification figures were lower for the B$^1$-case. The largest percentage drop was observed for the $\bar{y}$-value ( – 22 and – 7 gdm, respectively), and the second to the largest for the $\varepsilon_0$-value. The $r_{d_0,\,dp}$-value increased from 0.40 to 0.54. On the whole one must conclude, however, that the variation of the verification figures does not increase noteworthy when we include analysis B$^1$ and the corresponding 24h forecast in table IV. This is of course due to the fact that the difference between the forecasts based on analyses B and B$^1$, respectively, are rather small. This fact will be subject to a somewhat more detailed discussion in the next paragraph.

For the 48h forecasts the differences are larger than for the 24h ones, but the deviations are by no means great. A large difference is observed, however, in the $\delta_e$-value, this "wind

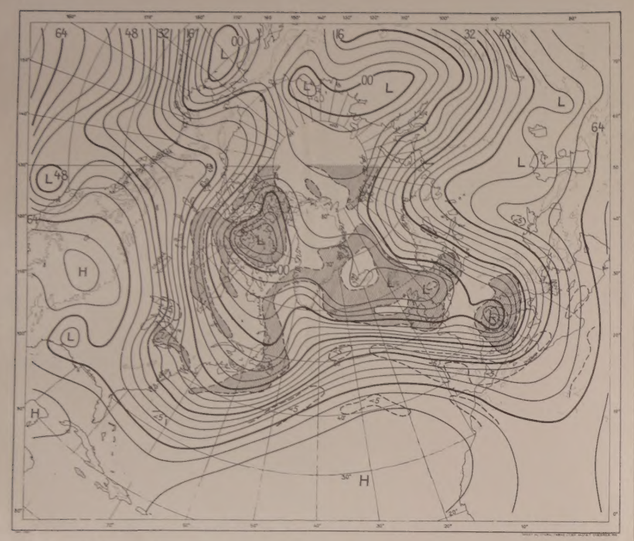

Fig. 2a. 500 mb, 0300 GMT 7 November 1949, with isohypses for every 4 geodynamic decameters and isolines for the absolute geostrophic vorticity in $10^{-5}$ $sec^{-1}$ (dashed lines, isoline interval $10^{-4}$ $sec^{-1}$). Hatched areas indicate vorticity values larger than $15 \cdot 10^{-5}$. Analysis A.

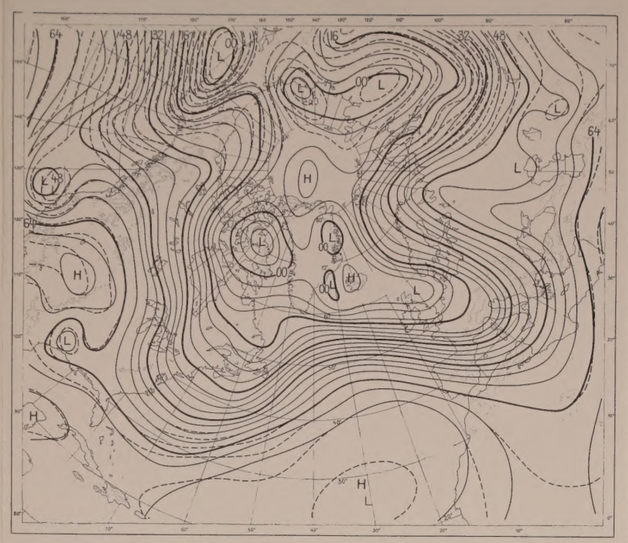

Fig. 2b. 500 mb, 0300 GMT 7 November 1949. Analysis B (solid lines) and $B^1$ (dashed lines).

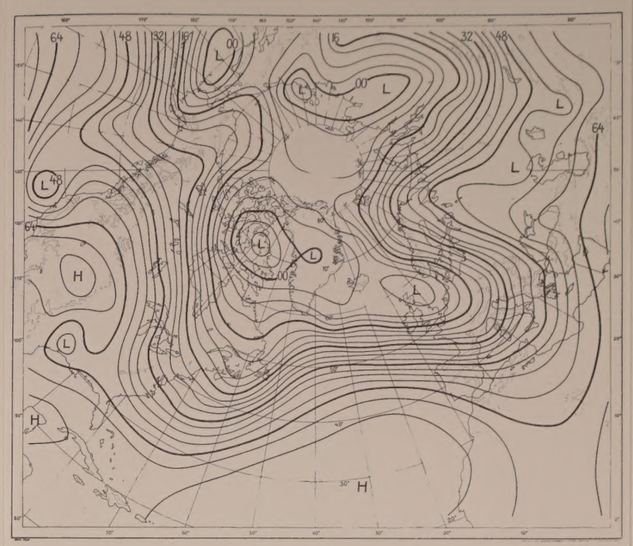

Fig. 2c. 500 mb, 0300 GMT 7 November 1949. Analysis C.

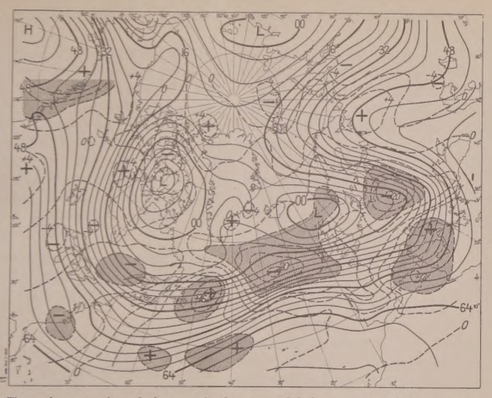

Fig. 2d. 500 mb 24h barotropic forecast valid for 0300 GMT 8 November 1949 (solid lines). Dashed lines (interval 4 geodynamic decameters) give the error of the forecast; a plus sign means that the forecast value is too high. Hatched areas indicate errors *numerically* larger than 8 geodynamic decameters. Based on analysis A.

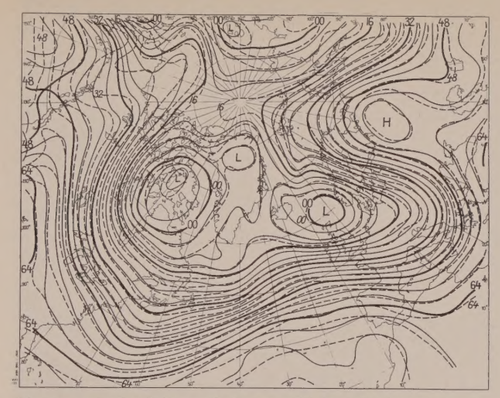

Fig. 2e. 500 mb 24h barotropic forecast valid for 0300 GMT 8 November 1949. Based on analysis B (solid lines) and $B^1$ (dashed lines), respectively.

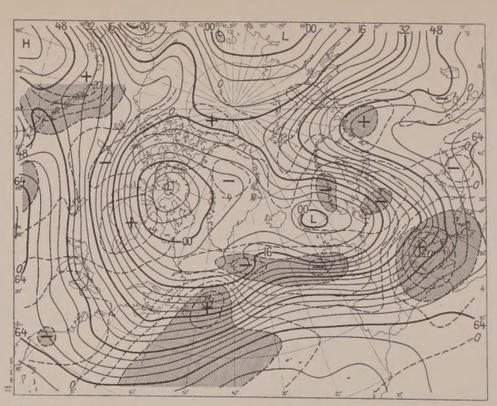

Fig. 2f. 500 mb 24h barotropic forecast valid for 0300 GMT 8 November 1949. Based on analysis C.

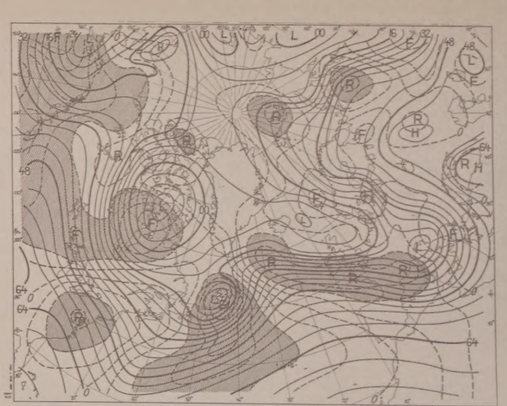

Fig. 2g. Verification 500 mb, 0300 GMT 8 November 1949 (solid lines). Observed changes are given by dashed lines (isoline interval 4 geodynamic decameters); hatched areas indicate changes *numerically* larger than 8 geodynamic decameters.

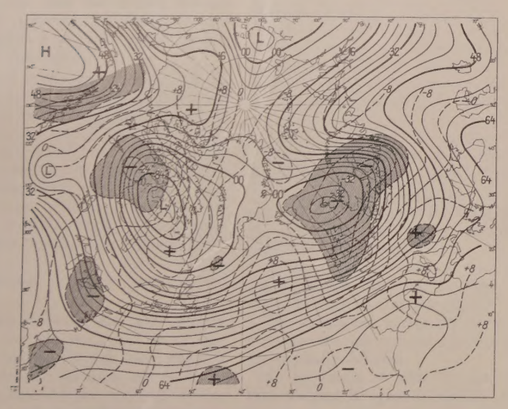

Fig. 2h. 500 mb 48h barotropic forecast valid for 0300 GMT 9 November 1949. Hatched areas indicate errors *numerically* larger than 16 geodynamic decameters. Isoline interval for dashed lines 8 geodynamic decameters. Based on analysis A.

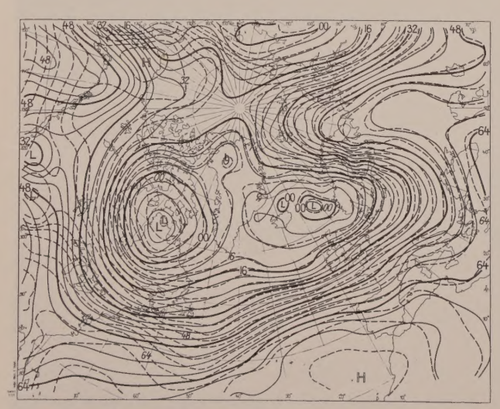

Fig. 2i. 500 mb 48h barotropic forecast valid for 0300 GMT 9 November 1949. Based on analysis B (solid lines) and $B^1$ (dashed lines), respectively.

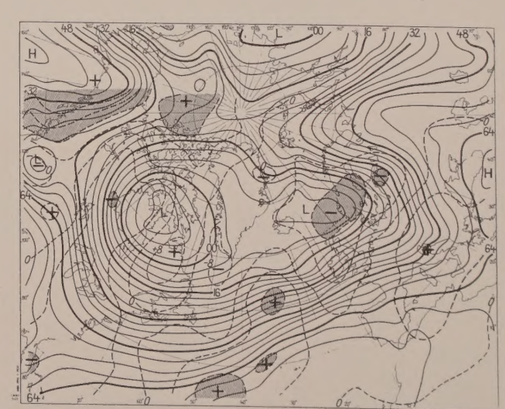

Fig. 2j. 500 mb 48h barotropic forecast valid for 0300 GMT 9 November 1949. Based on analysis C.

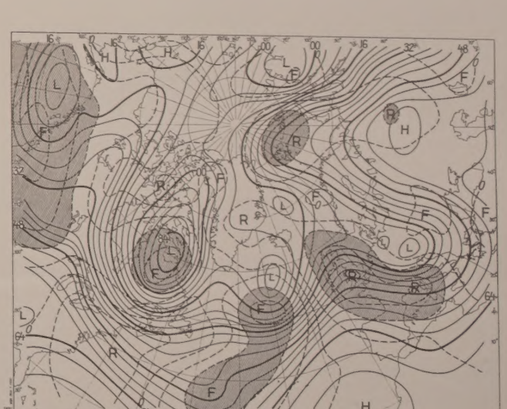

Fig. 2k. Verification 500 mb, 0300 GMT 9 November 1949. Hatched areas indicate regions with observed changes *numerically* larger than 16 geodynamic decameters. Isoline interval for dashed lines 8 geodynamic decameters.

Digitized by the Internet Archive
in 2024

https://archive.org/details/tellus-series-a-dynamic-meteorology-and-oceanography_1958-08_10_3

error" being 15.8 and 12.7 m/s, respectively. The largest difference is that of the $\bar{y}$-value, −48 and +38 gdm, respectively. If we disregard this difference the following conclusion can be given from an inspection of the parts of tables IV and V discussed so far: *in this case the inclusion of a new analysis with a different boundary region did not give rise to larger differences than were already observed using analyses with identical boundary analysis and different inner region analyses.*

The above conclusions are the same if we look at table I. The *d*-values show only small differences if we compare the analysis pair A − B¹ instead of A − B.

A visual inspection of the 24h forecast charts of fig. 2 gives the result that both sets of forecasts fail to predict the right position of the Mediterranean trough. Due to the extreme vorticity values combined with large wind velocities given by analysis A over Italy, the forecast based on this chart moved the trough more to the northeast than did the corresponding forecast based on analysis B¹ and at the same time the trough became sharper. It is, however, interesting to note that a new trough is situated over the Central part of the Mediterranean.

The low over northeastern Canada has the same position on the two forecast charts and the same is true for the ridge from the North Sea to Spitzbergen. Apart from the trough over Central Europe the two forecast charts ought not to result in two substantially different general forecasts for the verification area, i.e. the translation of forecast upper stream patterns into weather ought to be rather similar. In other words: if we disregard the trough over Central Europe there is no significant operational difference between the two forecasts.

A comparison between the 48h forecast charts shows that the deviations are larger than was the case for the 24h forecasts. It is beyond all doubt that for some areas a translation into weather of the 500 mb stream pattern would result in significantly different forecasts. This is true over the Baltic and adjacent areas, over the Central part of the Atlantic Ocean and the Mediterranean and finally over portions of the North-American continent. Subjectively speaking one could say that there exists an operational difference between the 48h forecast charts.

Best (1956) has given some examples on deviations between forecasts based on different analyses of (practically) the same observation material.

His conclusion was that "the prognostic differences do not appear to be of major importance on the 24h forecasts. However, for forecast periods of 48h and 72h, the prognostic differences seem large enough to be operationally significant."

A very large deviation was reported by Newton (1954) who by reanalyzing a 500 mb chart over the area southwest of Ireland got an increase of $r_{xy}$ from 0.06 to 0.41. In his case mean values of computed instantaneous tendencies twelve hours apart were compared with twelve hour observed changes.

3. *Comparison between forecasts based on two analyses with identical inner region but with different boundary regions.*

As already stated in the foregoing paragraph the difference between forecasts based on analyses B and B¹ did not differ too much from each other. Fig. 2 indicates that as far as the 24h forecasts are concerned the only noteworthy difference within the verification area is to be found over westernmost Atlantic. On the 48h forecast charts some differences are noteworthy over the North-American continent. The low over eastern Canada has deepened somewhat on the B-forecast while the B¹-forecast shows a slight filling. The low off the American westcoast on the initial charts is situated west of the Rocky Mountains on one chart and over or just east of the divide on the other.

In the boundary area in the upper left corner of the chart the boundary error are very different on the two charts.

The conclusion is that for some areas the two 48h forecasts may be regarded as slightly operationally different.

An inspection of table IV gives the result that analysis B¹ gave a slightly better 24h forecast than did analysis B. Practically all verification parameters show a decrease in their numerical value but the decrease is small, indeed. The correlation coefficient rose from 0.74 to 0.77. The differences given in table IV can hardly be said to be significant.

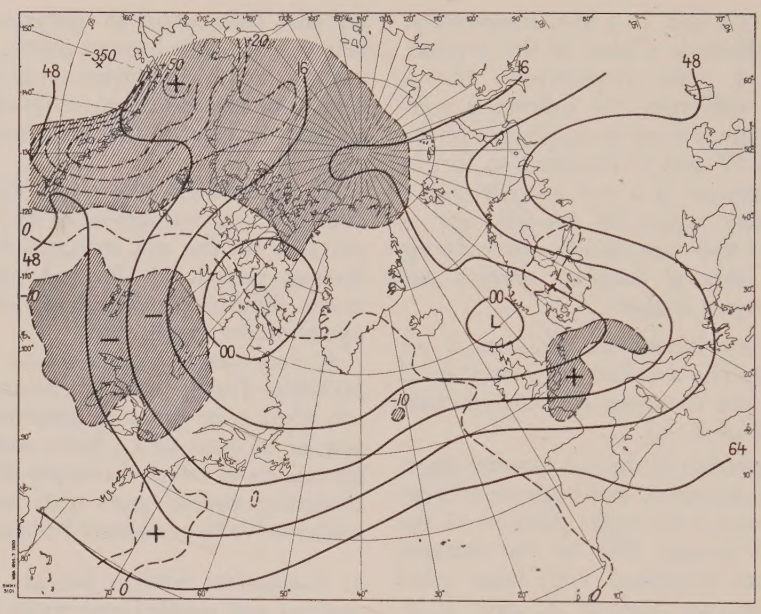


Fig. 3. 500 mb 24h barotropic forecast valid for 0300 GMT 8 November 1949 (cf. fig. 2e, solid lines). Dashed lines give the difference between the forecast and an "erroneous" one (see paragraph 4) with values *numerically* larger than 10 gdm indicated by hatching.

The differences for the 48h forecasts are larger for some quantities. This is especially true for the $\bar{y}$-value and also to some degree for the $\delta_e$-value and $\bar{d}_e$-value.

## 4. *Discussion of the influence of an isolated erroneous grid value on the forecast*

During the punching of the initial data for analysis $B^1$ in order to get it into a form suitable for the BESK computer, an error in the punching equipment gave a wrong grid point value for the point encircled in fig. 1. The grid point is situated over the Gulf of Alaska. Instead of the correct value (5)280 gdm the machine punched (5)080 gdm. This error was not traced because in the first print-out the value 280 was given.

This large point error seemed to have a peculiar influence on the computations. The 24h forecast was received without trouble, but when plotted and analyzed it was discovered that in the region of the wrong initial grid value a very peculiar pattern was obtained. During the continued calculation the number of iterations ran to rather high values and after 11 timesteps the calculations were stopped, i.e. after $24\text{h} + 11 \times 1.2 \simeq 37\text{h}$. The 37h forecast contained some very odd values south of Alaska and it was not possible to analyze that area without getting enormous gradients and a couple of small distinct lows and highs.

The fact that the wrong initial grid point was situated quite a long distance from the verification area gave the result that the verification figures for the 24h forecast based on the "wrong" analysis (called $B^{11}$ in the following) did not differ much from those of the $B^1$-forecast. In table IV are given the verification figures and we can see that the differences are very slight.

It is interesting to study the distribution o the difference between the $B^1$- and $B^{11}$-forecasts. These differences are given in fig. 3. Within the verification area the differences for large regions are less than 5 gdm, numerically speaking. The mean value of the absolute value of the difference calculated for the verification area was 5.7 gdm. As can be seen from the figure the influence of the error over the inner region is very slight. The computation did, however, break down, the number of iterations increasing from 2 – 4

during the first 24 hours to 26 just before the calculations were stopped.

5. *Differences between the value of some parameters calculated from a set of analyses.*

In the forecast scheme used in connection with the forecasts discussed in this paper the following equations are used

$$\xi = \nabla^2 \phi \tag{1}$$

$$\eta = \frac{m^2}{f}\,\xi + f \tag{2}$$

$$\frac{\partial \xi}{\partial t} = \frac{\partial \eta}{\partial x}\cdot\frac{\partial \phi}{\partial y} - \frac{\partial \eta}{\partial y}\cdot\frac{\partial \phi}{\partial x} = J(\eta, \phi) \tag{3}$$

where $\phi$ is the geopotential of the 500 mb surface, $\xi = fm^{-2}\,\zeta$ ($\xi$ is the relative vorticity), $\eta$ the absolute vorticity, $m$ the mapping factor $\left(m = \frac{1+\sin 50^\circ}{1+\sin\phi}\text{ in this case}\right)$ and $f$ the Coriolis parameter.

During the computation the quantity

$$\nabla^2\phi_{i,j} = \phi_{i,j+1} + \phi_{i,j-1} + \phi_{i+1,j} + \\ + \phi_{i-1,j} - 4\phi_{i,j} \tag{4}$$

is computed. Furthermore the quantity

$$J_{i,j}(\eta, \phi) = (\eta_{i+1,j} - \eta_{i-1,j})\,(\phi_{i,j+1} - \\ - \phi_{i,j-1}) - (\eta_{i,j+1} - \eta_{i,j-1})\,(\phi_{i+1,j} - \phi_{i-1,j}) \tag{5}$$

is calculated (scale factors is also applied in the two cases but they are disregarded here).

The differences observed between the forecasts as discussed in the paragraphs 1 – 3 must be due to differences in the initial distribution of the geopotential of the 500 mb surface. As they occur in the initial charts discussed in this paper, they are entirely due to differences between the analyses caused by the personal factor in upper air analysis. It might be of interest to calculate some parameters from the 26 different analyses referred to earlier. For a small area centered over Central Europe (see fig. 1) a calculation was made of the standard deviation ($s$) of $\zeta$ and $\nabla^2\phi_{i,j}$ and of $J(\eta, \phi)$ and $J_{i,j}(\eta, \phi)$. The first two quantities were computed for all 70 grid points within the indicated area and the other two for 23 grid points evenly spaced over the area.

A visual inspection of charts containing the distribution of the $s$-values for the four quantities (not shown in this paper) defined above gives the following result. The $s$-value for $\zeta$ and $\nabla^2\phi_{i,j}$ show rather confused patterns and it is not possible to notice any connection between these and the isohypse pattern or the pattern of the isotachs of the geostrophic wind. The highest values were found at one grid point over Poland and the second to the largest over Italy. Minimum values occurred over Scotland and in a narrow band from northern Ireland to Central Germany.

As for the $s$-values for $J_{i,j}(\eta, \phi)$ and $J(\eta, \phi)$ they were much more regularly distributed. The highest values was observed in the northwesterly current from the Bay of Biscay to Sardinia while the minimum values occurred in the trough from the North Sea to the Alps.

**Table VII. The standard deviation (s) of some parameters in equations 1—5.**

| | $\bar{s}$ | $s_{max}$ | $s_{min}$ | units |
|---|---|---|---|---|
| $\nabla^2\phi_{i,j}$ | 28.4 | 49.1 | 13.6 | gdm |
| $J_{i,j}(\eta,\phi)$ | $561 \cdot 10^{-4}$ | $1110 \cdot 10^{-4}$ | $132 \cdot 10^{-4}$ | MTS |
| $\zeta$, $\eta$ | $3.2 \cdot 10^{-5}$ | $5.1 \cdot 10^{-5}$ | $1.1 \cdot 10^{-5}$ | MTS |
| $J(\eta,\phi)$ | $16.3 \cdot 10^{-14}$ | $32.6 \cdot 10^{-14}$ | $3.4 \cdot 10^{-14}$ | MTS |

In table VII are given mean values of $s$ over the 70 (23) grid points together with the extreme grid point values observed within the area.

Taking the $\bar{s}$-value of 28.4 gdm for $\nabla^2\phi_{i,j}$ from table VII, it might be of interest to compare it to the value of the standard deviation of the height of the 500 mb ($\sigma_h$) as given in paper I. The value of $\sigma_h$ represents the variations due to the personal factor in analysis. Its mean value over the area considered in this paragraph was 13.1 gdm. Assuming that the value at one grid point is independent of the value at nearby grid points, we get the value $\sqrt{20}\cdot 13.1 = 58.7$ gdm for the value of $s$ for $\nabla^2\phi_{i,j}$. The actual value in table VII is 28.4 gdm, the difference being due to the correlation between the value of $\sigma_h$ at adjacent grid points.

The mean value of $s$ for the vorticity is $3.2 \cdot 10^{-5}$ sec$^{-1}$ and this value ought to be compared to the mean values of the relative and absolute vorticity for the investigated area. These mean values are $3.2 \cdot 10^{-5}$ and $14.0 \cdot 10^{-5}$ sec$^{-1}$, respectively.

The mean value of $s$ for $J_{i,j}(\eta, \phi)$ ought to be compared to the mean deviation of the mean value of the same quantity calculated for the 23 grid points and from the 26 analyses, this value being $96 \cdot 10^{-4}$ MTS. The mean value for the whole area is $4 \cdot 10^{-4}$ MTS, while the mean value of the range at each grid point is $2{,}270 \cdot 10^{-4}$ MTS.

Considering equation (3) and the mean value of $s$ for $J(\eta, \phi)$ given in table VII, we notice that the corresponding value of $\triangle\xi$ is equal to $5.9 \cdot 10^{-10}$ MTS, when the time step is one hour.[1]

Thus, the value of $\bar{s}$ for $J(\eta, \phi)$ corresponds to a value of $\triangle\xi$ (for a time step of one hour) that is 1/6 of the value of $\xi$ itself as the mean value and the mean deviation of $\xi$ for the area under consideration is $35.7 \cdot 10^{-10}$ and $40.3 \cdot 10^{-10}$ MTS, respectively.

The first conclusion one draws when faced with the values in table VII may be that forecasts based on these different analyses ought to be quite different. As has been pointed out in paragraph 1 through 3, this is not the case. The explanation for this apparent discrepancy is given by THOMPSON in an article published in 1954. In his paper Thompson shows that the solution of the vorticity equation for quasi-geostrophic flow can be given in terms of the first derivatives of the height of the pressure surface used. The errors in computing second and third order derivates are cancelled out in the process of solving the vorticity equation. Thompson emphasizes that errors in reported observations are non-systematic and therefore the percentage errors in the solution of the vorticity equation are generally much less than the percentage errors in the computed vorticity advection at individual points. In the case studied here, however, the differences in the analyses are to some extent systematic as they depend largely on the character of the network of upper air observing stations. Furthermore, the reported deviations are mean values for an area of approximately 2,700 × 1,800 km and do not represent errors at individual points.

[1] The calculations are actually performed in such a way that $\triangle\xi = \xi^t - \xi^{t-2\triangle t}$ and the corresponding Jacobian is computed for $(t - \triangle t)$. For the first two time steps it is not possible to use centered differences and then $\triangle\xi = \xi^{\triangle t/2} - \xi^0$ with the corresponding Jacobian for $t = 0$ and $\triangle\xi = \xi^{\triangle t} - \xi^0$ together with $J(\eta^{\triangle t/2}, \phi^{\triangle t/2})$, respectively.

## REFERENCES


BERGGREN, R., 1957: On the accuracy of 500 mb analysis with special reference to numerical forecasting. Tellus, 9, No. 3, pp. 323—340.

BERGTHORSON, P., and DÖÖS, B., 1955: Numerical weather map analysis. Tellus, 7, No 3, pp. 329—340.

BEST, W. H., 1956: Differences in numerical prognoses resulting from differences in analyses. Tellus, 8, No. 3, pp. 351—356.

BOLIN, B., 1955: Numerical forecasting with the barotropic model. Tellus, 7, No. 1, pp. 27—49.

CRESSMAN, G. P., and GILCHRIST, 1954: An experiment in objective analysis. Tellus, 6. No. 4, pp. 310—318.

DÖÖS, B., and EATON, Mc., 1957: Upper-air analysis over ocean areas. Tellus, 9, No. 2, pp. 184—194.

GATES, W. L., POCINSKI, L. S., and JENKINS, C. F., 1956: Results of numerical forecasting with the barotropic and thermotropic atmospheric models. Geophys. Res. Pap., No. 46.

NEWTON, C. W., 1954: Analysis and data problems in relation to numerical prediction. Bull. Am. Met. Soc., 35, No. 7, pp. 287—294.

PETTERSSEN, S. ET AL., 1957: An experiment in prognostication (Studies in weather analysis and forecasting, Part G) Final Rep. Contract AF 19 (604)—1293. Dept. Met., Univ. of Chicago, 32 pp.

Staff Members, Inst. of Met., Univ. of Stockholm, 1954: Results of forecasting with the barotropic model on an electronic computer (BESK), Tellus, 6, No. 2, pp. 139—149.

THOMPSON, P. D., 1954: A note on the integration of the vorticity equation for quasi-geostrophic flow. Tellus, 6, No. 6, p. 319—325.

# On the General Circulation over Eastern Asia (III)

Staff Members of the Section of Synoptic and Dynamic Meteorology, Institute of Geophysics and Meteorology, Academia Sinica, Peking

(Manuscript received October 24, 1957)

*Abstract*

The averaged vertical motion and the heat sources and sinks have been computed for the normal maps for January and July. The perturbations in the westerlies due to large-scale heat sources and sinks and to the earth's topography are discussed, first using the theory of small perturbations and secondly allowing the perturbations to be of a finite amplitude.

Section 2 contains a discussion of the dynamic influence of the topography on the daily weather systems.

## III. Dynamical studies on the general circulation over Eastern Asia

In the first two parts★ (Staff Members, 1957, 1958), we have presented the principal results of the synoptic and aerological studies on the general circulation over Eastern Asia. Here in the third part we are going to summarize the dynamical studies. In the dynamical investigations we are primarily concerned with the formation of the mean winter upper air flow pattern and the dynamical influences of the large-scale topography on the daily weather systems over Eastern Asia.

### *1. The formation of mean winter flow pattern over Eastern Asia*

In general there are two extreme views about the cause of formation of the mean upper air circulation. One school emphasizes the thermal origin while the other stresses the dynamical or topographical origin. Here we shall discuss the dynamics of formation of the mean upper air flow over the Far East from a combined view-point.

The large-scale topography over the northern hemisphere is already well-known. However, the distribution of heat sources and sinks is not yet clear. Different authors computed it in different ways. Therefore their results are not at all comparable. Here we have adopted the following three ways for computation:

a. Taking mean of the thermodynamic equation in the steady state, we have

$$Q_m = \frac{gc_p}{R}\frac{1}{\ln p_0/\overline{p}}\left[\mathbf{v}_m \cdot \nabla h - \frac{R\Gamma_p}{g}\ln\left(\frac{p_0}{\overline{p}}\right)\omega_m\right]. \qquad (1)$$

Here $h$ is the 1,000—500 mb thickness; $\omega \equiv dp/dt$; $\Gamma \equiv \frac{\gamma_d}{g_e} - \frac{\partial T}{\partial p}$, used as constant; $\gamma_d$ is the dry adiabatic lapse rate and $Q$, defined as the heat source (if positive) or sink (if negative), is the rate of heat gained or lost per unit mass and unit time through radiation, turbulence, condensation and evaporation. The remaining symbols are used as usual. Further the subscript "$m$" represents the mean for 1,000—500 mb; "bar", the value on 500 mb; and subscript "0", values on 1,000 mb or the surface.

★ Hereafter these references will be referred as (I).

The first term on the right of (1) may be calculated from the mean charts of 1,000—500 mb thickness and 700 mb by the geostrophic approximation, $\mathbf{v}_m$ being taken as the wind on 700 mb.

Assuming $\omega$ to be a linear function of $p$, $\omega_m$ may then be computed from $\omega_0$ (due to the earth's topography) and $\overline{\omega}$ which in turn may be evaluated from the divergence at 1,000 mb and 500 mb and $\omega_0$. The divergence at 1,000 mb is obtained from the mean surface vector wind, while that on 500 mb is computed as follows: By introducing the vertically-integrated wind components.

$$\overline{u} = \frac{1}{p_0}\int_0^\infty g\varrho u dz, \quad \overline{v} = \frac{1}{p_0}\int_0^\infty g\varrho v dz$$

in the tendency equation in the steady state, we get

$$\frac{\partial \overline{u}}{\partial x} + \frac{\partial \overline{v}}{\partial y} = -\frac{1}{p_0}\left(\overline{u}\frac{\partial p_0}{\partial x} + \overline{v}\frac{\partial p_0}{\partial y}\right) + \frac{g}{RT_0} w_0 \quad (2)$$

Here $w_0 = \mathbf{v}_0 \cdot \nabla \eta(x, y)$, $\eta(x, y)$ being the topography of the earth's surface. The expression on the left of (2) may be considered as divergence on 500 mb. $\overline{u}$ and $\overline{v}$ on the right of (2) are taken as the geostrophic wind on 500 mb. Thus the last term of (1) may be calculated.

b. The vertical motion is computed from the divergence of actual wind observations. Advection is also calculated from wind data under the geostrophic assumption. The result of heating obtained from these two terms is checked against radiation (short and long wave) and turbulence.

c. Adopting Sawyer and Bushby's (1953) two-parameter model for numerical integration we have

$$\overline{\mathbf{v}} \cdot \nabla (\overline{\zeta} + f) + \frac{1}{3}\mathbf{v}_T \cdot \nabla \zeta_T = \frac{8}{3}\frac{\overline{\omega}\,\zeta_T}{p_0 - p_1}.$$

Here $\overline{\mathbf{v}}$ and $\overline{\zeta}$ are respectively the geostrophic wind and relative vorticity at the mean level; $\mathbf{v}_T$ and $\zeta_T$, respectively the thermal wind and thermal relative vorticity and $f$, the Coriolis parameter. In obtaining the above equation the boundary conditions $\omega = 0$ at $p = p_0$ and $p = p_1$ are used. In the same model equation (1) may be written as

$$Q_m = c_p \overline{\mathbf{v}} \cdot \nabla T_0 - \frac{2}{3}\Gamma\overline{\omega}.$$

Eliminating $\omega$ from the above two equations we get

$$Q_m = c_p \mathbf{v} \cdot \nabla T_0 - \frac{\Gamma}{4}\frac{p_0 - p_1}{\zeta_T}\left[\overline{\mathbf{v}} \cdot \nabla (\overline{\zeta} + f) + \frac{1}{3}\mathbf{v}_T \cdot \nabla \zeta_T\right], \quad (3)$$

where $\Gamma = \frac{\gamma_a - \gamma_d}{\gamma_d \cdot \varrho}$ assumed to be independent of height.

We have calculated the heat sources by the first method over the northern hemisphere for January and July, by the second method over the Tibetan Plateau and its surroundings for winter and summer and by the third method for northern Asia for winter. The first and second methods give practically the same results while the third method gives similar distribution but too high intensity. We shall give the results by the first method.

The average vertical motion in the lower half atmosphere over the northern hemisphere is shown in fig. 1a (January) and 1b (July). Fixing our attention to Asia and its adjacent regions we see that in winter (fig. 1a) downward motion prevails almost over the whole Asia and Western Pacific which is due to the outbreak of cold air. In summer (fig. 1b) upward motion is present over almost the whole Eurasia with a center over the Tibetan Plateau.

Multiplying $\omega_m$ by $c_p\Gamma_p$ we obtain the part of the heat source or sink balanced by vertical motion. This part which is of the same order of magnitude as that part balanced by temperature advection is usually neglected in the computation of heat sources. The distribution of total heat source is shown in fig. 2a (January) and fig. 2b (July). Again fixing our attention to Asia and its adjacent regions we find that in winter (fig. 2a) a cold source is present over the greatest part of Asia and the heat source is centered over the Western Pacific. In summer (fig. 2b) the distribution is almost reversed.

In the following we shall discuss the perturbations on the westerlies due to the large-scale heat sources and sinks and the earth's topography. Using again Sawyer and Bushby's

a b

Fig. 1. Mean vertical motion in the lower half atmosphere over the northern hemisphere. (a) January and (b) July (unit: cm $sec^{-1}$).

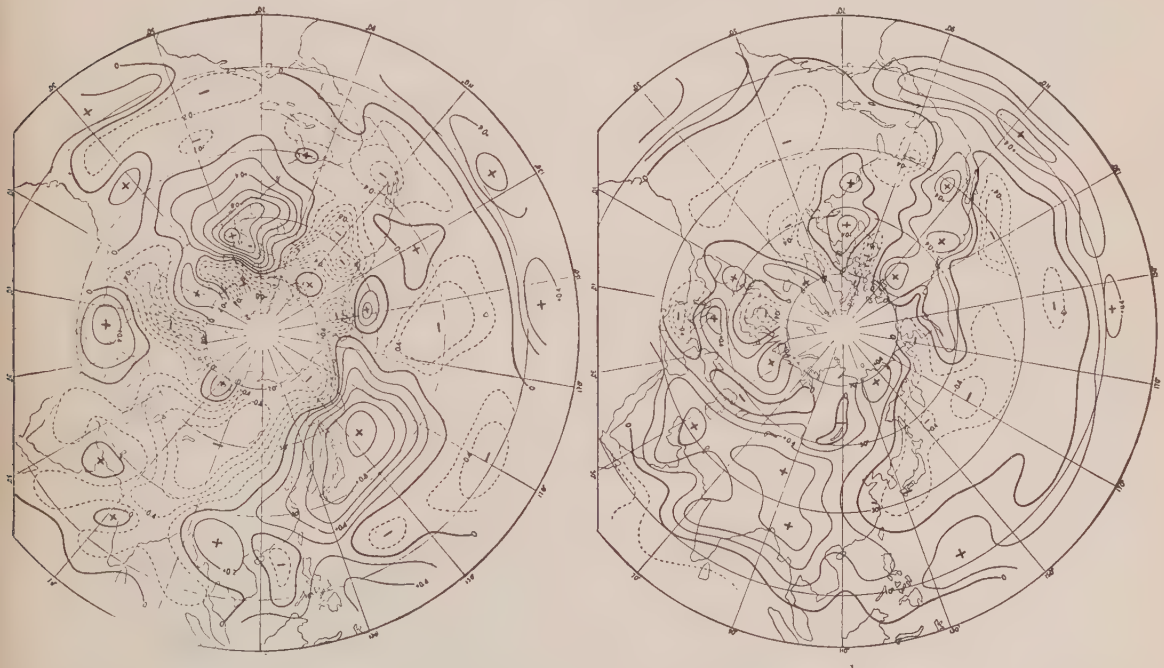

a b

Fig. 2. Distribution of heat sources and sinks in the lower half atmosphere over the northern hemisphere (a) January and (b) July (unit: $10^{-5}$ cal $gm^{-1}$ $sec^{-1}$).

model we obtain the vertically integrated vorticity equation for the steady state:

$$\overline{\mathbf{v}} \cdot \nabla(f+\overline{\zeta}) + \frac{1}{3}\mathbf{v}_T \cdot \nabla\, \zeta_T = -\frac{f}{H}\mathbf{v}_0 \cdot \nabla\eta, \quad (4)$$

where $H = RT_0/g$ is the height of the homogeneous atmosphere. In deriving equation (4) the lower boundary condition

$$-\frac{1}{\varrho_0 g}\omega_0 = w_0 = \mathbf{v}_0 \cdot \nabla\eta \qquad \text{at } p = p_0$$

is used. Introducing the assumptions that

$$\mathbf{v}(x, y, p) = \overline{\mathbf{v}}(x, y) + A(p)\,\mathbf{v}_T(x, y),$$
$$\omega(x, y, p) = B(p)\,\overline{\omega}(x, y) + C(p)\,\omega_0(x, y),$$

where $A(p) = (p_0 + p_1 - 2p)/(p_0 - p_1)$, $B(p) = 1 - A^2$ and $C(p) = \dfrac{p - p_1}{p_0 - p_1}$ ($p_0 = 1{,}000$ mb, $p_1 = 200$ mb), into the steady state vorticity equation, multiplying with $A(p)$, and then integrating it with respect to $p$ from $p_0$ to $p_1$, we find

$$\overline{\mathbf{v}} \cdot \nabla\zeta_T + \mathbf{v}_T \cdot \nabla\,(f + \overline{\zeta}) = \frac{4f}{p_0 - p_1}\overline{\omega}, \quad (5)$$

Again using the assumptions for the distribution of $\mathbf{v}(x, y, p)$ and $\omega(x, y, p)$ and the geostrophic approximations in the thermodynamic equation in steady state and eliminating $\overline{\omega}$ from it with equation (5), we have

$$\overline{\mathbf{v}} \cdot \nabla\zeta_T + \mathbf{v}_T \cdot \nabla(f + \zeta) = -\frac{Mg}{f}[c_1 Q_m - \overline{\mathbf{v}} \cdot \nabla h], \quad (6)$$

where $c_1 = \dfrac{R}{gc_p}\ln\dfrac{p_0}{p}$, $M = \dfrac{4f^2}{p_0 - p_1}\dfrac{1}{c_2 R\Gamma_p}$ and $c_2 = \dfrac{1}{2}\dfrac{p_0 + 3p_1}{p_0 - p_1} - \dfrac{4p_0 p_1}{(p_0 - p_1)^2}\ln\dfrac{2p_0}{p_0 + p_1}$. By introducing perturbation quantities and geostrophic approximation in equations (4) and (6) we obtain the two required differential equations in $h$ and $z$, where $z$ is the 500 mb perturbation height:

$$\overline{U}\nabla^2 z + \frac{\overline{U}_T}{3}\nabla^2 h + \beta\frac{\partial z}{\partial x} = -\frac{f^2}{gH}(\overline{U} - \overline{U}_T)\,\eta \quad (7)$$

$$\overline{U}\nabla^2\frac{\partial h}{\partial x} + \overline{U}_T\nabla^2\frac{\partial z}{\partial x} + \overline{U}\left(\frac{\beta}{\overline{U}} - M\right)\frac{\partial h}{\partial x} + M\overline{U}_T\frac{\partial z}{\partial x} = -Mc_1 Q_m, \quad (8)$$

where $\nabla^2 = \dfrac{\partial^2}{\partial x^2} + \dfrac{\partial^2}{\partial y^2}$ and $\beta = df/dy$. For simplicity the prime sign in the above equations is dropped. In these equations $\overline{U}$ is the speed of the basic current on 500 mb level and $\overline{U}_T$, the thermal wind in 1,000—500 mb layer.

Applying now the above differential equation to a rectangular region with a marginal cyclicity and a length equal to that of the latitudinal circle at 45°, the solution for $z$ may then be written as

$$z(x, y) = \frac{f^2}{gH}\frac{3\overline{U}(\overline{U} - \overline{U}_T)}{3\overline{U}^2 - \overline{U}_T^2}\int_0^{2\pi}\int_0^{2\pi}\eta(\alpha, \nu)\,\phi_\eta(x - \alpha, y - \gamma)\,d\alpha d\gamma + Mc_1\frac{\overline{U}_T}{3\overline{U}^2 - \overline{U}_T^2}\int_0^{2\pi}\int_0^{2\pi}Q_m(\alpha, \nu)\,\phi_q(x - \alpha, y - \gamma)\,d\alpha d\gamma \quad (9)$$

where the topographical influence function $\phi_\eta$ and the heating influence function $\phi_q$ are respectively given by

$$\phi_\eta(x, y) = \frac{1}{4\pi^2}\sum_{\lambda, k=-\infty}^{\infty}\sum \frac{M - \dfrac{\beta}{\overline{U}} + \lambda^2 + k^2}{\left[(\lambda^2 + k^2)^2 + 2M(\lambda^2 + k^2) - \dfrac{3M}{2}\dfrac{\beta}{\overline{U}}\right]}e^{i(\lambda x + ky)}, \quad (10)$$

$$\phi_q(x, y) = \frac{1}{4\pi^2}\sum_{\lambda, k=-\infty}^{\infty}\sum \frac{i(\lambda^2 + k^2)}{\lambda\left[(\lambda^2 + k^2)^2 + 2M(\lambda^2 + k^2) - \dfrac{3M}{2}\dfrac{\beta}{\overline{U}}\right]}e^{i(\lambda x + ky)}. \quad (11)$$

These series may easily be transformed into other forms which converge very rapidly.

With a time unit of one day and a length unit of the radius of 45° latitude circle we use for the winter case $\overline{U} = 0.287$, $\overline{U}_T = 0.245$ (corresponding $\overline{U} = 15$ m/s, $\overline{U}_T = 13$ m/s) $M = 231$ and $\beta/\overline{U} = 21.9$. Fig. 3a is the 500 mb flow pattern due to topographical effect only ($Q_m = 0$). In this figure we see that the position of the major trough and ridge is correctly presented. But the intensity of the southern part of the trough and ridge is much stronger than in the actual case. Further the band of

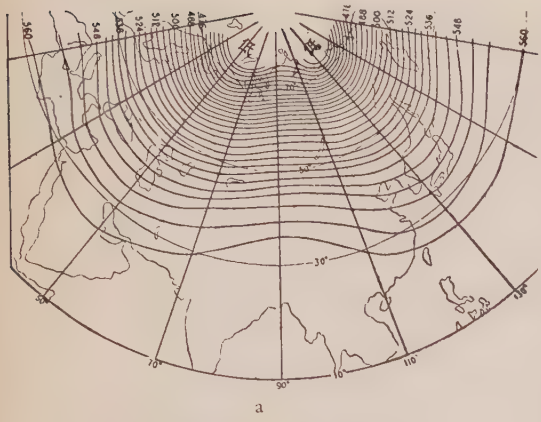

a

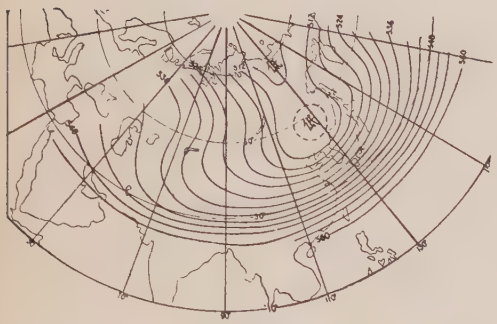

b

Fig. 3. Steady 500 mb flow pattern produced by the effect of (a) Tibetan Plateau and its adjacent mountains and (b) heat sources and sinks in the westerlies.

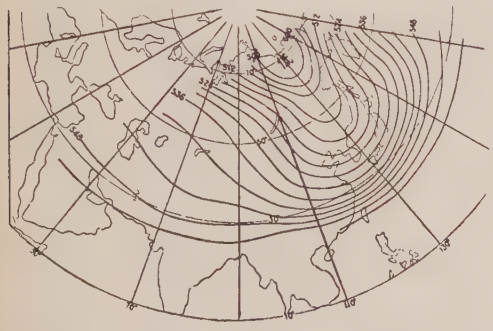

Fig. 4. Steady 500 mb flow pattern produced by the combined effect of mountains and heat sources and sinks in the westerlies.

strong westerlies is too much to the north of the observed position. Fig. 3b is the 500 mb topography due to large-scale heating only ($\eta = 0$). This figure also gives a correct position of the Asiatic major trough, but the ridge over Tibet and its adjacent plateau does not appear. The overall pattern of fig. 3a is better (i.e. nearer to the observed one) than that of fig. 3b. But in fig. 3b the strong Asiatic Jet is correctly shown. The combined effect of topography and large-scale heating on the flow pattern over the Far East is presented in fig. 4. Comparing this figure with fig. 1 of (I) we find that the computed trough and ridge as well as the jet check with the observed one fairly well.

The above investigation is based on small perturbation theory. To go one step further we attempted to discuss the dynamics of topographically produced perturbations of finite amplitude in a three-dimensional baroclinic current. Eliminating $\omega$ between the steady state vorticity equation and the thermodynamic equation in spherical coordinates $(\lambda, \Theta, p)$ we find

$$J\left(\frac{\nabla^2\phi}{f} + \frac{f}{\sigma}\frac{\partial^2\phi}{\partial p^2} + 2\Omega\cos\Theta, \phi\right) = 0 \qquad (12)$$

where $J(A, B) \equiv \dfrac{\partial A}{\partial q}\dfrac{\partial B}{\partial \lambda} - \dfrac{\partial A}{\partial \lambda}\dfrac{\partial B}{\partial q}$, $q = \cos\Theta$;

$$\nabla^2 \equiv \frac{1}{R^2 \sin\Theta}\left[\frac{\partial}{\partial\Theta}\left(\sin\Theta\frac{\partial}{\partial\Theta}\right) + \frac{1}{\sin\Theta}\frac{\partial^2}{\partial\lambda^2}\right];$$

$\lambda$ is the longitude; $\Theta$, the co-latitude; $R$, the earth's radius; $\Omega$, angular speed of the earth's rotation; $\sigma \equiv -\dfrac{1}{\varrho}\dfrac{\partial \ln\Theta}{\partial p}$, the static stability factor assumed to be constant; and $\phi$, the geopotential. The general solution of equation (12) is

$$\frac{\nabla^2\phi}{f} + \frac{f}{\sigma}\frac{\partial^2\phi}{\partial p^2} + 2\,\Omega\cos\Theta = F(\phi) \qquad (13)$$

where $F(\phi)$ is an arbitrary function of $\phi$. Under the assumption that the perturbation $\phi'$ vanishes in the vicinity of the poles and that the angular speed of the basic current is only a linear function of $p$, $F(\phi)$ may be determined as

$$F(\phi) = -\frac{2\,(\bar{\dot{\lambda}} + \Omega)}{f R^2 \bar{\dot{\lambda}}}\phi. \qquad (14)$$

Neglecting $\bar{\dot{\lambda}}$ against $\Omega$ we finally obtain a differential equation for a finite perturbation $\phi'$

$$\frac{\partial^2\phi'}{\partial P^2} + \frac{1}{R^2\sin\phi}\left[\frac{\partial}{\partial\Theta}\sin\Theta\frac{\partial\phi'}{\partial\Theta} + \frac{1}{\sin\Theta}\frac{\partial^2\phi'}{\partial\lambda^2}\right] + \frac{2\Omega}{R^2\bar{\dot{\lambda}}}\phi' = 0. \qquad \left(P = \frac{\sqrt{\bar{\sigma}}}{f}p\right) \qquad (15)$$

The upper boundary condition is taken as

$$\phi' = 0 \text{ at } p = 0. \tag{16}$$

The lower boundary condition may be formed from the thermodynamic equation which on the earth's surface $p = p_0$ $(\lambda, \Theta)$ is written as

$$J\left(\frac{\partial\phi}{\partial p}, \phi\right)\Big|_{p=p_0} = f R^2 \sigma \varrho_0 g w_0,$$

$$w_0 = \frac{1}{R^2 f} J(\eta, \phi_0) \tag{17}$$

where the geostrophic assumption is used.

Neglecting the variation of $\varrho_0$, the general solution of equation (17) is:

$$\frac{\partial\phi}{\partial p}\Big|_{p=p_0} - \sigma \varrho_0 g \eta = G(\phi_0) \tag{18}$$

where $G(\phi_0)$ is an arbitrary function of $\phi_0$ which may similarly be found as $F(\phi)$ in the following form

$$G(\phi_0) = -\frac{\bar{\lambda}_p}{\bar{\lambda}_0}\phi_0 \quad \left(\bar{\lambda}_p = -\frac{d\bar{\lambda}}{dp} > 0\right)$$

Finally the lower boundary condition is obtained as

$$\frac{\partial\phi'}{\partial P} + c\phi' = H(\lambda, \Theta) \quad \text{at } P = P_0(\lambda, \Theta) \tag{19}$$

where $c = f\bar{\lambda}_p/\sqrt{\bar{\sigma}}\,\bar{\lambda}_0$, $H(\lambda, \Theta) = f\varrho_0 g\sqrt{\bar{\sigma}}\eta(\lambda, \Theta)$.

The differential equation (15) is to be solved under the boundary conditions (16) and (19). It gives

$$\phi'(\lambda, \Theta, p) = f\varrho_0 g\sqrt{\bar{\sigma}} \sum_{n=1}^{\infty}\sum_{m=1}^{n} \frac{e^{-\frac{1}{2}(\xi-\xi_0)}\left[\psi_1(\xi_1)\psi_2(\xi) - \psi_2(\xi_1)\psi_1(\xi)\right]}{2k\triangle} \times \left[h_n^m \cos m\lambda + h'^m_n \sin m\lambda\right] P_n^m(\cos\Theta) \tag{20}$$

where $\xi = \frac{2k\sqrt{\bar{\sigma}}}{f\bar{\lambda}_p}\left[\bar{\lambda}_0 + \bar{\lambda}_p \frac{f}{\sqrt{\bar{\sigma}}}(P_0 - P)\right]$,

$$\xi_0 = \frac{2k\sqrt{\bar{\sigma}}\,\bar{\lambda}_0}{f\bar{\lambda}_p}, \quad \xi_1 = \frac{2k\sqrt{\bar{\sigma}}}{f\bar{\lambda}_p}\left(\bar{\lambda}_0 + \bar{\lambda}_p \frac{f}{\sqrt{\bar{\sigma}}} P_0\right)$$

$$\triangle = \begin{vmatrix} \left[\frac{d\psi_1}{d\xi} - \left(\frac{1}{2} + \frac{c}{2k}\right)\psi_1\right]_{\xi=\xi_0} & \left[\frac{d\psi_2}{d\xi} - \left(\frac{1}{2} + \frac{c}{2k}\right)\psi_2\right]_{\xi=\xi_0} \\ \psi_1(\xi_1) & \psi_2(\xi_1) \end{vmatrix}, \text{ and } k^2 = \frac{n(n+1)}{R^2}$$

$P_n^m(\cos\Theta)$ is the associated Legendre function and $h_n^m$ and $h'^m_n$ are coefficients of the spherical harmonic series expressed for the mountain function $\eta(\lambda, \Theta)$. $\psi_1$ and $\psi_2$ are the two fundamental solutions of the confluent hypergeometric equation

$$\frac{d^2\psi}{d\xi^2} - \frac{d\psi}{d\xi} + \frac{r}{\xi}\psi = 0, \text{ where } r = \Omega/kR^2\bar{\lambda}_p \frac{f}{\sqrt{\bar{\sigma}}}$$

They are given by CHARNEY (1947).

$$\psi_1 = \frac{\sin\pi a}{\pi}\left\{a\,\xi\,M(a+1, 2, \xi) \times \left[\ln\xi + \frac{\Gamma'(a)}{\Gamma(a)} - 2\frac{\Gamma'(1)}{\Gamma(1)}\right] + 1 + \sum_{n=1}^{\infty} Bn \frac{a(a+1)\cdots(a+n-1)}{(n-1)!\,n!}\xi^n\right\},$$

and $\psi_2 = \xi M(a+1, 2, \xi)$. Here $a = -r$, $B_n = \sum_{\nu=0}^{n-1}\left(\frac{1}{a+\nu} - \frac{2}{1+\nu}\right) + \frac{1}{n}$, $M(a, b, \xi) = 1 + \frac{a}{1\cdot b}\xi + \frac{a(a+1)}{2!\,b(b+1)}\xi^2 + \cdots$, and $\Gamma(a)$ is the Gamma function.

Numerical computation is carried out with $\sqrt{\bar{\sigma}} = 0.128$ m mb$^{-1}$ sec$^{-1}$, $\bar{\lambda}_0 = 0.63 \times 10^{-6}$ sec$^{-1}$, and $\bar{\lambda}_p = 0.68 \times 10^{-8}$ sec$^{-1}$ mb$^{-1}$. With these constants the series $\psi_1(\xi)$ and $\psi_2(\xi)$ computed by CHARNEY (1947) may be used. The flow over the northern hemisphere on 850 mb, 700 mb, 500 mb and 300 mb is computed. Fig. 5 is the 700 mb topography. From this figure we see that the position of the major troughs and ridges over the eastern world is in good agreement with observation, but there is a discrepancy between the computed and observed intensity of these systems. As in the theory of small perturbation the intensity of the computed troughs and ridges is too strong to the south.

The computed flow pattern over the western world is not in good agreement with the observed. It is because the flow over North America without friction is too much influenced by the Tibetan Plateau which has

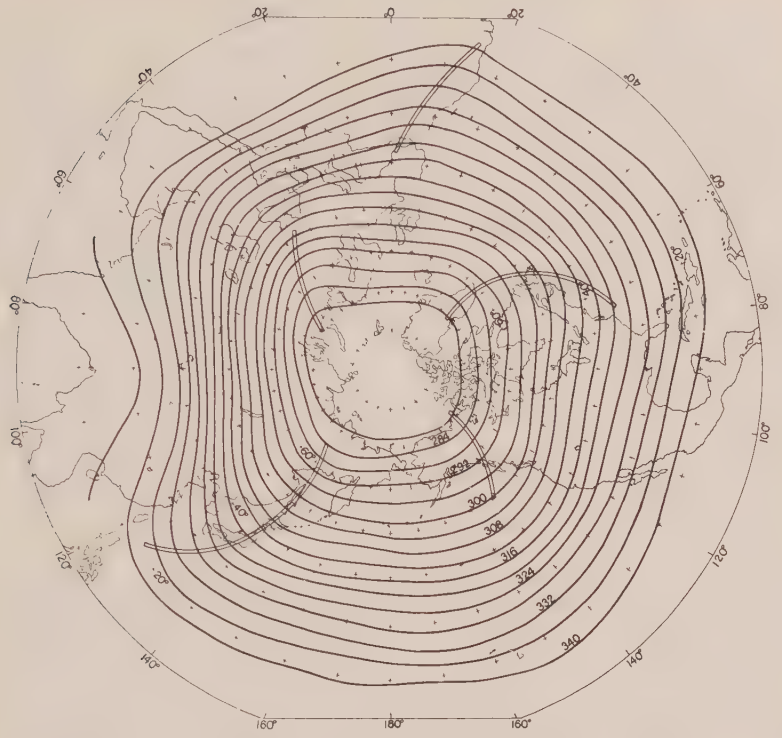


Fig. 5. 700 mb flow pattern produced by the earth's topography over the northern hemisphere.

much larger dimension than the Rocky Mountains. Considering these mountains alone the computed flow (figure not presented) over North America is in better agreement with the actual one.

It is also worth to point out that the axes of the computed troughs and ridges are vertical and the amplitude decreases quickly with increasing height. The former fact may also be shown in the foregoing theory of small perturbation. It is believed that this is due to the neglection of friction.

2. *The dynamic influence of the orography on the daily weather systems*

In the above we have tried to discuss the dynamics of the formation of mean flow pattern over Asia. Here in this section we shall attempt to discuss the dynamic influence of the orography on the development and movement of the daily weather systems over Eastern Asia and see how far the fact mentioned in (I) can be explained in this way.

In (I) it is pointed out that most of the troughs fill and most of ridges intensify on the wind side of Tienshan-Altai mountain ranges while Lake Baikal is the site for the development of the troughs and weakening of the ridges. These phenomena will be understood from the computations of tendencies due to orographical disturbance in a barotropic model. The vorticity equation in this model may be written as

$$\nabla^2 \frac{\partial z}{\partial t} = J\left(\frac{g}{f}\nabla^2 z + f, z\right) + \frac{f^2}{g\varrho}\frac{\partial \varrho w}{\partial z}. \quad (21)$$

Here the vorticity has been substituted by the geostrophic one. Because of the linearity of the equation with respect to $\frac{\partial z}{\partial t}$, the tendency due to orography may be calculated separately by the following differential equation.

$$\nabla^2 \frac{\partial \bar{z}}{\partial t} = -\frac{f^2}{g\bar{H}} w_0. \quad (22)$$

Here $\partial\bar{z}/\partial t$ may be considered as the rate of height change of 500 mb surface, $w_0 = \mathbf{v}_0 \cdot \nabla\eta$

a b

Fig. 6. The barotropic tendency on 500 mb due to orographical disturbance over China (unit: dm/day) (a) with $u_0=10$ m/s, $v_0=0$, (b) with $v_0=-5$ m/s, $u_0=0$.

and $H=p_0/\varrho_0 g$ is the height of homogenous atmosphere.

The approximate solution (FJØRTOFT, 1952) of the difference equation corresponding to (22) is

$$\frac{\partial \bar{z}}{\partial t}=\frac{d^2}{4gH}\left(\frac{f^2}{m^2}w_0+3\left[\frac{f^2}{m^2}w_0\right]\right),\quad 4d<\lambda<8d. \tag{23}$$

Here the brackets represent the mean over the four surrounding grid-points with grid length $d$, $m$ being the magnification factor of the map projection and $\lambda$ being the wave length of the motion suitable for the above equation. With a Lambert projection of scale $1:2\times10^7$ (latitude 30° and 60° being standard parallels) and $d=2.75$ cm (equal to the length of 5° longitude at along 70° N),

$$\frac{\Delta \bar{z}}{\Delta t}=1.05\times10^{-3}\left(\frac{f^2}{m^2}w_0+3\left[\frac{f^2}{m^2}w_0\right]\right) \tag{24}$$

$\Delta\bar{z}/\Delta t$ in unit of 10 geopotential meter per day and the physical quantities on the right of (24) in c.g.s. units.

With (24) and the smoothed topography of Eastern Asia (averaged over 2 degree latitude square) we have computed the tendencies on 500 mb due to orographical disturbance in a westerly current of 10 mps and in a northerly current of 5 mps (fig. 6a, b).

Fig. 6a shows negative tendencies in the regions of Kansu, SW Sinkiang and North China. These are just the regions where the troughs usually develop or form. West of Sinkiang are positive tendencies. These are just the regions where troughs usually fill. Fig. 6b indicates that in a north current there will be positive tendencies over Kansu. Thus during NW current, troughs are not apt to develop or form over this area. This agrees well with our synoptic experience. Further it is to be noted that under the same condition the tendency (positive or negative) computed here is about twice as large as that over the Rockies computed by BOLIN and CHARNEY (1951). Thus the dynamic effect of the plateau over Asia is more pronounced than that of the Rockies.

Because the development of the troughs over North China has special interest for us, we have made a further investigation on it. With $d=300$ km we have computed by relaxation method the surface tendencies due to orographical disturbances over North China in a barotropic atmosphere in a NW current of 10 mps (fig. 7). The negative tendencies shown in the figure agree quite well in position and magnitude with the development or formation of the 'North China Trough' formed at the beginning of the outbreak of northwesterlies. In general fine weather is associated with this type of troughs (fig. 8). This is different from the situation associated with other types of troughs in this region. This is because this type of trough is formed dynamically in a descending current.

Though we have some success with a barotropic model, yet there are two defects in this model: Firstly in general actual $\mathbf{v}_0$ is much smaller than that used for computation, therefore the computed tendency is much smaller than that observed if actual $\mathbf{v}_0$ is used. Secondly the computed tendency does not change with height in a barotropic model while in actual cases the upper current seems to be less disturbed by the mountain. In a stratified baroclinic atmosphere the result of similar computations will be free from the above defects. Actually the upward decrease of orographical perturbation in this atmosphere has been shown in the foregoing discussion. From the first law of thermodynamics and equation of vorticity we may obtain

$$\nabla^2\omega + \frac{f^2}{\sigma}\frac{\partial^2\omega}{\partial p^2} = 0. \qquad (25)$$

Equ. (25) is to be solved under boundary conditions $\omega(p_0) = \omega_0 = -g\varrho_0\mathbf{v}_0 \cdot \nabla\eta$ and $\omega(0) = 0$. Then from

$$\nabla^2\frac{\partial z}{\partial t} = \frac{f^2}{g}\frac{\partial\omega}{\partial p} \qquad (26)$$

we may compute $\partial z/\partial t$ at any level.

By this method we calculated the tendency on 300 mb, 500 mb, 700 mb and 900 mb produced by Tienshan-Altai mountain ranges with surface westerlies of 5 mps. $\eta$ is averaged over 5° latitude square, $\sigma = 2 \times 10^2$ cm$^2$ sec$^{-2}$ mb$^{-2}$, horizontal grid length being 390 km and the vertical grid length being 100 mb. Equation (25) has been solved by three-dimensional relaxation method with irregular stars at the boundary.

The results of the computation show that the perturbations produced by the large-scale topography in a stably stratified atmosphere decreases rapidly with height. On the wind side of the Tienshan-Altai mountain ranges the positive tendency at 300 mb is around

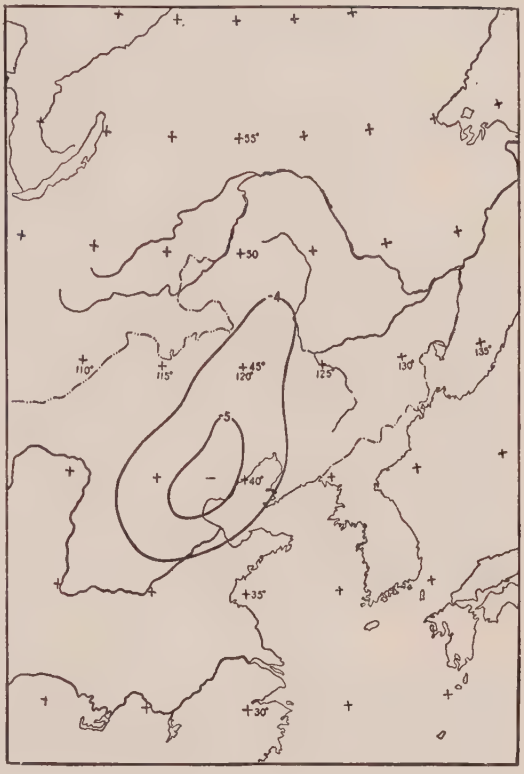


Fig. 7. The barotropic sea level tendency due to orographical disturbance over North China with surface NW wind of 10 m/s (unit: mb/day).

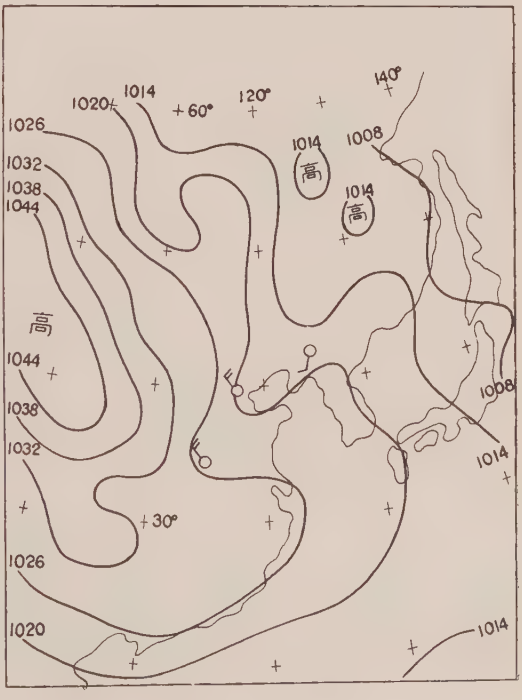


Fig. 8. Typical case of 'North China Trough' (surface chart Jan. 10, 1956, 18 z), notice the clear weather in the trough.

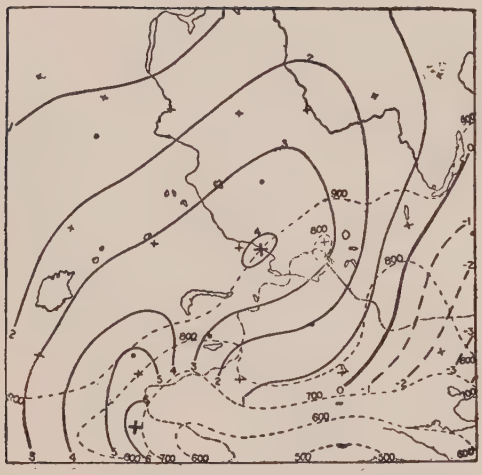

Fig. 9. The 700 mb tendency due to orographical disturbance of Tienshan-Altai mountain ranges in a stratified atmosphere (unit: dm/day). Thick lines: lines of equal tendency, thin dash lines: lines of equal pressure height (in mb) of earth's topography.

Fig. 11. Observed 24 hr tendency for 700 mb surface in decameters (from Jan. 26 (03 z) to 27 (03) 1957).

20 m/12h, but on 500 mb it is around 30 m/12h, on 700 mb, 40—60 m/12h and on 900 mb it reaches 60—80 m/12h. The distribution on 700 mb is shown as an example in fig. 9

From above it is seen that in the lower troposphere the orographical perturbation in a stratified atmosphere is about 4 times as big as that in a neutral atmosphere under the same condition. Further we may conclude from this that in the forecast of flow pattern in the lower troposphere around the Tibetan Plateau the dynamics of topography must be taken into consideration.

As an illustration of anticyclogenesis on the wind side of Tienshan-Altai mountain ranges we may give the following example. On Janu-

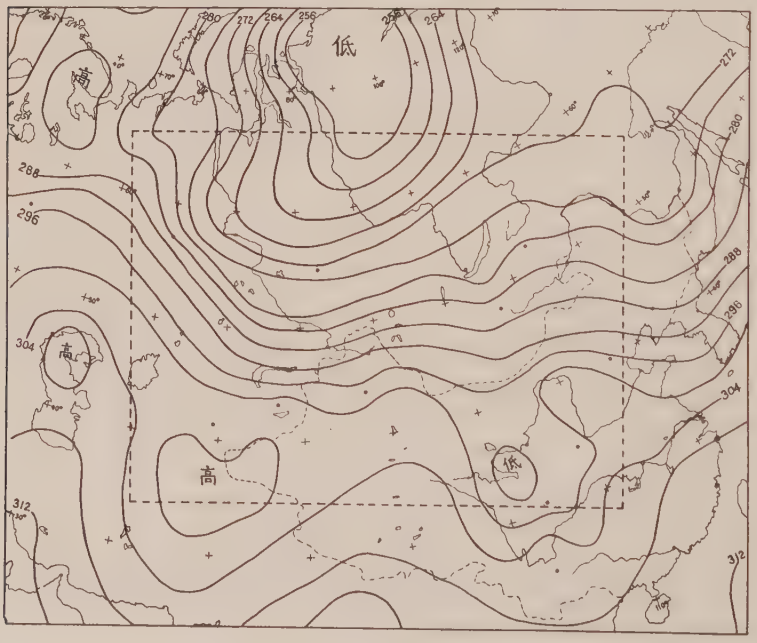


Fig. 10. 700 mb chart, Jan. 26, 1957 (15 z). Isohypes labelled in decameters.

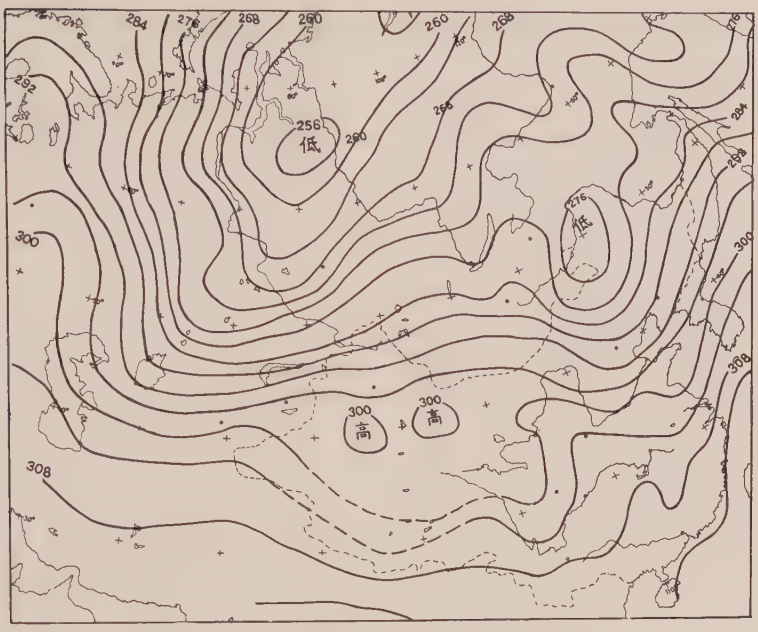


Fig. 12. 700 mb chart Jan. 25, 1957 (15 z).

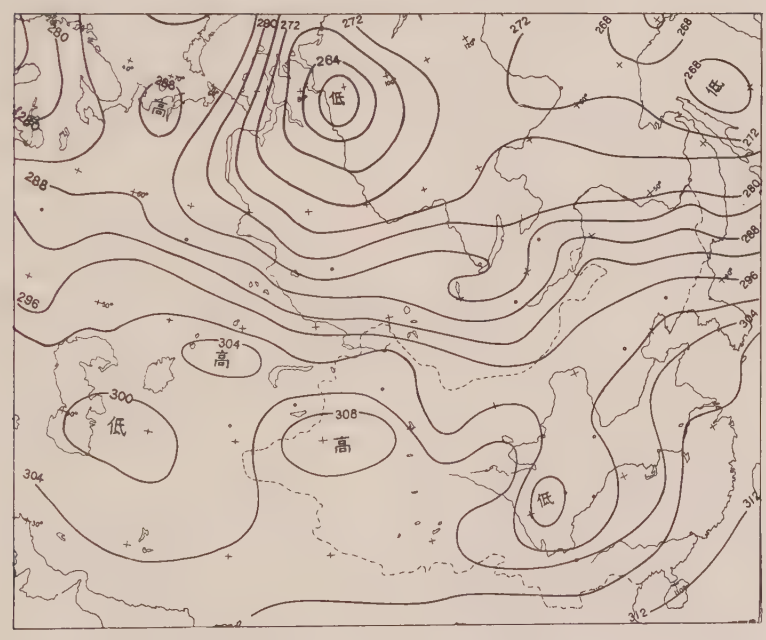


Fig. 13. 700 mb chart Jan. 27, 1957 (15 z).

ary 26, 1957 there is a flat trough on 500 mb (1 500 Z) moving to NW China (fig. 10). The observed 24 hour (12 hours before and 12 hours after the map time) height change on 700 mb reaches 80 meters over Balkhask (fig. 11). On the wind side of these mountain ranges we may observe rapid anticyclogenesis on 700 mb (fig. 12—13) and even more clearly on the surface map. Using half of the actually observed geostrophic wind as $\mathbf{v}_0$,

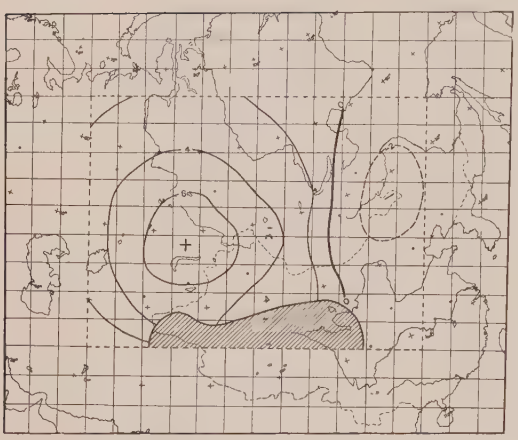

Fig. 14. Calculated tendency for 700 mb surface Jan. 26, 1957 (15 z) due to orographical disturbance, in dm/24 hr. (Shaded area: Plateau with pressure altitude higher than 700 mb.)

Fig. 15. Computed 24 hr tendency for 700 mb surface.

we computed the tendencies due to orographical disturbances (fig. 14). The maximum tendency reaches 70 m/24 hr. Beside this we also computed the distribution of the tendencies on different levels due to the advection of vorticity and the "free" vertical motion. We find that the distribution of the sum of these two 24 hour tendencies on 700 mb (fig. 15) agrees fairly well with the observed one. It is, however, to be noted that the positive height change associated with low level anticyclogenesis on the wind side of the mountain range is almost entirely contributed by the mountain. Thus the development or genesis of certain anticyclones in this region seems largely due to dynamic effect of orography.

Computation of the rapid filling of the troughs on the wind side of Tienshan-Altai has also been made. The results also show that the computations with consideration of the dynamics of topography check better with observations than that without topography being considered.*

Besides the development the movement of the weather systems may also be influenced by topography. It is our experience that the movement of the weather systems is faster on the north than on the south of Tibetan Plateau though the general steering current is stronger on the south side. It is easy to understand that on the northern (southern) slope prevails horizontal convergence (divergence) associated with the downward motion in the southerly current in front of a trough while there is divergence (convergence) in front of a ridge. Thus under the same general situations the systems would move faster on the northern slope than on the southern slope.

Let us take an ideal mountain $\eta = a\,(1 - |\gamma|/b)$, the origin of $\gamma$ being placed on the mountain ridge. Assuming that $\omega$ decreases linearly with $p$ and $\omega(0) = 0$ then $\omega(p) = \omega_\eta \frac{p}{p_\eta} \cong -\frac{g}{RT_\eta}\frac{\partial \eta}{\partial \gamma} v_\eta p$, the subscript $\eta$ indicating values on the mountain. In small motion the equation of continuity and vorticity equation are respectively

$$\frac{\partial u'}{\partial x} + \frac{\partial v'}{\partial \gamma} = \frac{g}{RT_\eta}\frac{\partial \eta}{\partial \gamma} v_\eta \qquad (27)$$

and

$$\left(\frac{\partial}{\partial t} + U\frac{\partial}{\partial x}\right)\left(\frac{\partial^2 v'}{\partial x^2} - \frac{\partial^2 u'}{\partial x \partial \gamma}\right) + \frac{\partial v'}{\partial x}\beta = f\frac{\partial}{\partial x}\left(\frac{\partial w}{\partial p}\right) \qquad (28)$$

* It may also be of interest to point out that according to our computation for a case (January 15, 1950) the formation of a Vb cyclone may be explained by the dynamic effect of the Alps. In the example used the upper air cut-off low was formed after the surface Vb cyclone. Thus PALMÉN'S (1949) mechanism does not account for the formation of a surface Vb cyclone, in this example at least.

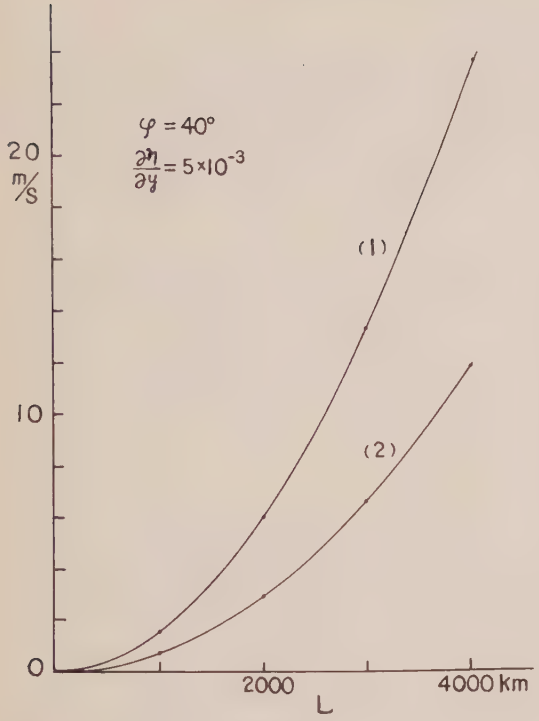


Fig. 16. Change of phase velocity (in m/s) as a function of wave length (in 1,000 km).
[1]) $L = 2\pi/k$, (motion independent of $y$)
[2]) $L = 2\pi/k = 2\pi/\mu$

Eliminating $u'$ and assuming $v_\eta = v'$ we obtain

$$\left(\frac{\partial}{\partial t} + U\frac{\partial}{\partial x}\right)\left(\frac{\partial^2 v}{\partial x^2} + \frac{\partial^2 v}{\partial y^2} - \alpha\frac{\partial v}{\partial y}\right) + \beta'\frac{\partial v}{\partial x} = 0, \tag{29}$$

the prime on $v$ being dropped and $\beta' = \beta + \alpha f$, $\alpha \equiv \frac{g}{RT_\eta}\frac{\partial \eta}{\partial y}$. Assuming a solution $v \alpha e^{i(kx+\mu y - \nu t)}$ we have

$$c = \frac{\nu}{k} = U - \frac{\beta'}{(k^2+\mu^2)^2 - (\alpha\mu)^2}[k^2 + \mu^2 + i\alpha\mu]. \tag{30}$$

Assuming the motion to be independent of $y$, we have

$$c = U - \frac{L^2}{4\pi^2}\left(\beta + \frac{fg}{RT_\eta}\frac{\partial \eta}{\partial y}\right) \tag{31}$$

Evidently

$$C \gtrless U - \frac{\beta U^2}{4\pi^2} \quad \begin{matrix} \text{north slope.} \\ \text{south slope.} \end{matrix}$$

The change of phase velocity due to orography is a function of wave length. Their relation, for $\varphi = 35°$ N and $\partial\eta/\partial y = 4 \times 10^{-3}$ (roughly equal to the slope of Tibetan Plateau), is given in fig. 16. For $L = 3 \times 10^8$ cm this velocity reaches several mps.

## Concluding remarks

Above we have sketched part of our research work in recent years on the general circulation over Eastern Asia. Through these studies we get a better understanding of the structure, variation and dynamics of the circulation over this part of the world. But we are aware that there are many important synoptic, aerological or dynamic problems we have not touched upon or not even thought of. However, in our next Five Year Plan our pibal and sounding stations become denser and denser and a rawin net is also going to be established. With the observations from this network of stations we would be able to do more work.

This third part of our report is a summary of the following papers:

Chao Jih-ping, 1956: A preliminary study of the distribution of heat source over Eastern Asia in winter computed from the flow pattern. *Acta Meteorologica Sinica*, **27**, 167—180 (in Chinese).

— 1957: On the dynamics of orographically produced finite perturbations in baroclinic westerlies. *Acta Meteorologica Sinica*, **28**, 303—314 (in Chinese).

Chu Pao-chen, 1957: The steady state perturbations of the westerlies by the large-scale heat sources and sinks and earth's orography (I). *Acta Meteorologica Sinica*, **28**, 122—140 and (II) ibid, 198—224 (in Chinese).

— 1957: A note on the orographical effect on the formation of the mean temperature field. *Acta Meteorologica Sinica*, **28**, 315—319 (in Chinese).

Liu Jui-chih and Koo Chen-chao, 1957: On the formation of North China Trough. *Acta Scientiarum Naturalium Universitatis Pekinesis*, **3**, 113—117 (in Chinese).

Koo Chen-chao and Chen Yung-san, 1957: The perturbation tendency due to the dynamical disturbance of Tienshan-Altai mountains in a stratified atmosphere. *Ke Hsueh T'ung Pao (Scientia)*, no. 12, 379—380 (in Chinese).

Koo Chen-chao and Chao Ming-tza and Chih Li-jen, 1957: Tendency computations for synoptic cases showing strong dynamical disturbance by Tienshan-Altai mountain ranges. (Manuscript.)

Koo Chen-chao and Chow Shao-ping, 1957: The influence of the slope of a plateau on the movement of troughs and ridges (in preparation).

Koo Chen-chao and Yeh Tu-cheng (see reference of I and II).

Yeh Tu-cheng, Lo Szu-wie and Chu Pao-chen (see reference of (I)).

## REFERENCES

Bolin, B., and Charney, J. G., 1951: Numerical tendency computation from the barotropic vorticity equation. *Tellus*, **3**, 248—257.

Charney, J., 1947: The dynamics of long waves in a baroclinic westerly current. *J. Met.*, **4**, pp. 125—162.

Fjørtoft, R., 1952: Numerical method of integrating the barotropic vorticity equation. *Tellus*, **4**, 179—194.

Palmén, E., 1949: On the origin and structure of high-level cyclones south of the maximum westerlies. *Tellus*, **1**, 22—31.

Sawyer, J. S., and Bushby, F. H., 1953: A baroclinic model-atmosphere suitable for numerical integration. *J. Met.*, **10**, 54—59.

# Some Comments on the Numerical Integration of the Vorticity Equation and Related Equations

By GEORGE S. BENTON, Johns Hopkins University[1], Baltimore, Maryland

(Manuscript received September 9, 1957)

*Abstract*

It is shown that if the streamfunction is specified over an Eulerian region $R$ $(x, y)$ at $t=0$, and on the boundaries of $R$ $(x, y)$ at $t > 0$, a solution of the vorticity equation which satisfies certain conditions of continuity will be unique. If vorticity is also specified at the inflow boundary, such a solution is excluded. In the latter case, an internal discontinuity propagates into the region along a material surface, and in principle solutions should be obtained separately for each sub-region and "matched" kinematically and dynamically at the interface. The associated analytical or numerical problems are prohibitive.

The problem of obtaining stable methods of numerical integration, specifying only the stream function on the boundary, is considered. Numerical integrations of a non-linear first order differential equation indicate that such stable methods may exist, in contradiction to linear theory.

The integration of the vorticity and associated equations for the first time-step is also considered. A method is presented which is not only simple to apply, but also maintains the same accuracy as succeeding time-steps for which centered difference techniques are used.

## 1. Introduction

In recent years, the numerical integration of non-linear partial differential equations has played an increasingly important role in scientific research. This is, perhaps, particularly true of meteorology. Since the early studies of CHARNEY, FJÖRTOFT, and VON NEUMANN (1950) numerical methods have been extensively used not only in meteorological research but also in operational forecasting.

The equations to be integrated have taken various forms, depending on the physical "model" to be studied and the degree to which simplifying assumptions are introduced. Nevertheless, many of the equations – and in particular the barotropic models – can be placed in the form:

$$\triangle\psi_t = g\left(\psi, \partial^n\psi/\partial x^m \partial y^{n-m}\right) \quad \begin{matrix} 0 \leq m \leq n \\ n = 1, 2, \ldots, k \end{matrix} \qquad (1)$$

where $\triangle$ is Laplace's operator, and the dependent variable $\psi$ is a streamfunction or a quasi-streamfunction which determines or is closely related to the field of fluid motion. It is to be noted that (1) includes as a special case the unsteady state, two dimensional vorticy equation for a homogeneous fluid:

$$\triangle\psi_t = -J\left(\psi, \triangle\psi\right) + \nu\triangle^2\psi \qquad (2)$$

where $\nu$ is the kinematic viscosity and $J$ represents the Jacobian with respect to an orthogonal cartesian coordinate system in the plane.

The numerical integration of equations of this class involve many mathematical problems which are at present only imperfectly understood. For example, the accumulation of truncation errors, and the associated problem of numerical stability, have not been adequately treated for these non-linear systems. A host

[1] The research reported in this article has been sponsored by the Geophysics Research Directorate, Air Force Cambridge Research Center, under Contract No. AF 19 (604)—916.

of additional unsolved problems could be mentioned.

In the present paper three problems in particular will be discussed. First, a statement of sufficient boundary conditions will be developed for the uniqueness of solutions to differential equations of class (1). In order to simplify the notation, the derivation will be presented in terms of the vorticity equation for a perfect fluid (i.e., (2) without the viscous terms). This equation is, of course, of fundamental importance in many fields of fluid dynamics. However, it must be emphasized that the method of proof developed for the vorticity equation can be applied with only trivial modification to most equations of class (1) as well as to certain systems of such equations.

A second problem considered involves a definition and discussion of overspecification in numerical integration. It will be shown that in recent meteorological research, boundary conditions have been overspecified. Some of the consequences are considered; the relation between overspecification and numerical stability is discussed; and two possible means of avoiding overspecification are proposed, one in terms of an Eulerian and one in terms of a Lagrangian analysis.

The third problem investigated is the error in the first time step of a numerical integration, given the value of the dependent variable $\psi$ in a region $R$ $(x, y)$ at time $t=0$. It is pointed out that the conventional method of using an uncentered difference for the first time step involves an error one order of magnitude larger than for all subsequent time steps. An alternative procedure is advanced which is simple to apply and which eliminates this increased error.

Throughout the text, numerical examples are included. For this purpose it is desirable to use a simplified non-linear partial differential equation for which the analytical solution is known. One convenient equation is:

$$u_t + uu_x = 0 \tag{3}$$

This equation, which has the solution:

$$u = \phi\,(x - ut) \tag{4}$$

provided $J\,(x - ut,\ t)$ is not zero, is of a type thoroughly discussed by LIGHTHILL (1955). Numerical integrations of (3) have been used to illustrate the effects of certain types of overspecification and of uncentered differences in the numerical procedure.

## 2. A Definition of "Overspecification" and of "Admissible Solution"

The concept of "overspecification" is so fundamental to the discussion which follows that it seems desirable to clarify its meaning at the outset. This concept is essentially related to the solution of differential equations, for which the dependent variables are to be determined everywhere within a specified region. Although it is possible to extend the meaning to difference equations, this will be deferred to a later section. In the discussion which immediately follows, the mathematics of continuous rather than of discrete systems is at issue.

It is interesting to note that even with regard to differential equations, there is much confusion in the literature concerning what constitutes "overspecification". Of course, "overspecification" occurs when the system of the differential equation and boundary conditions has no admissible solution. However, the fact has frequently been overlooked that to determine when a system is "overspecified", it is necessary to define "admissible solution". Usually, an "admissible solution" must satisfy not only the differential equation and the boundary conditions, but also additional restrictions as well.

This can be illustrated by a simple example. Consider the ordinary differential equation: $dy/dx = 1$. Most of us would agree, almost without thinking, that it would be an overspecification to demand that the solution pass through the two points: $x=0$, $y=0$; and $x=1$, $y=3$. Yet such a solution – in fact, an infinite number of such solutions – can be found provided we are willing to allow the dependent variable $y$ to be multi-valued in $x$. Figure 1 a shows such a solution: namely, $(y-x-1)^2=1$. Furthermore, an additional infinite set of solutions can be found provided we are willing to allow the dependent variable to be discontinuous (i.e. provided we are willing to let $dy/dx=1$ except at one or more points where the derivative is not defined). An example of a single-valued solution of this type is shown in Figure 1 b. Even in this

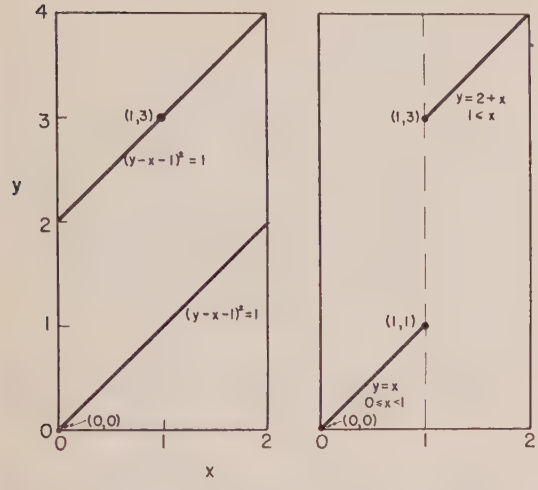


Fig. 1. Multivalued and discontinuous solutions of $dy/dx = 1$ passing through the points (0,0) and (1,3)

simple example, then, we can say the boundary conditions overspecify the differential equation *only* if we set up the arbitrary restriction that admissible solutions must be single-valued, continuous functions of $x$. Whether this limitation is a useful one or not depends upon the objectives of the investigator. Perhaps this is why the term "overspecification" appears so infrequently in mathematics, but is found so often in the literature of applied science.

In most physical problems, solutions are required in which the dependent variables are single-valued, continuous functions of the independent variables. This is not invariably the case, however. Obvious exceptions occur when the dependent variables are defined in a multiply connected region: e.g. the potential of the electromagnetic force field set up by current flowing in a wire of finite diameter. In other cases, dependent variables are deliberately allowed to be discontinuous on a given surface: e.g. the discontinuity in density and tangential velocity component at the interface between two homogeneous fluids, as in Helmholz waves. In the latter example, however, other requirements must be satisfied – namely, the kinematic and dynamic boundary conditions for the surface of internal discontinuity. In general, when discontinuity surfaces (in the dependent variables or their pertinent derivatives) occur within the region under consideration, solutions must be obtained independently for the regions on either side of the surface, and the solutions must then be "matched" in some suitable manner. We will have occasion to refer to this procedure in more detail below.

With these preliminary remarks in mind, let us return to differential equations of class (1). In meteorology, equations of this type are of primary interest in initial value problems. Values of the dependent variable $\psi$ are specified over a region $R\ (x, y)$ at a time $t=0$. The task is to determine what additional boundary conditions (if any) are necessary and sufficient to determine a unique admissible solution for the dependent variable $\psi\ (x, y, t)$ within $R\ (x, y)$ over a certain time interval $0 \leq t < \tau$.

Before this question can possibly be answered, it will be necessary to decide what additional restrictions are to be imposed in the definition of "admissible solution". In this, we must be guided by the nature of the physical problem and by the objectives of the investigation. In the following paper it will be assumed that an admissible solution $\psi\ (x, y, t)$ satisfies the differential equation over the region $R\ (x, y)$ within the time interval $0 \leq t < \tau$, and also meets the following requirements:

(1) The function $\psi\ (x, y, t)$ must be a single-valued, continuous, real function of the independent variables. This assumption is justified since we shall generally be interested in regions $R\ (x, y)$ which are simply connected. In addition, if a "shock" develops (i.e. if $\psi$ becomes multiple-valued within the region at $t=\tau$) the solution ceases to have physical validity. In such cases, no admissable solution of the differential equation may exist for $t \geq \tau$.

(2) The derivatives of $\psi$ that appear in the differential equation are defined everywhere an admissible solution exists. This restriction is justified since we shall not generally be interested in the propagation of surfaces of discontinuity within the region $R\ (x, y)$. We shall, therefore, be permitted to solve the differential equation over the entire region, without matching solutions at some moving internal boundary.

(3) An admissible solution $\psi\ (x, y, t)$ can be expanded in a convergent power series in time. For every point with $R\ (x, y)$ and for $-\varepsilon \leq t < \tau;\ \varepsilon > 0$:

$$\psi\ (x, y, t) = \sum_{n=0}^{\infty} t^n \phi_n\ (x, y) \qquad (5)$$

The desirability of this restriction is by no means as obvious as the first two. However, it will be useful to investigate solutions which are very well behaved. The effect of relaxing the requirement that (5) be valid will be considered in a later section.

With the above definition of "admissible solution" we are now in a position to attack equations of class (1). Unfortunately, it has not been possible to determine the boundary conditions which are necessary and sufficient for a unique solution to exist. Nevertheless, if we assume an admissible solution exists over some range, sufficient boundary conditions for uniqueness can be established.[1]

### 3. Sufficient Conditions for the Uniqueness of Solutions to the Vorticity Equation

The following proof will be developed for the two-dimensional vorticity equation for a perfect fluid:

$$\triangle\psi_t = -J(\psi, \triangle\psi). \tag{6}$$

The proof can, however, by a trivial modification be extended to most equations of class (1). *It will be assumed* that the following boundary conditions are specified: (a) the value of $\psi$ over $R(x, y)$ at $t = 0$; and (b) the value of $\psi$ at the boundaries of $R(x, y)$ for $0 \leq t < \tau$. *It will be shown* that there exists no more than one admissible solution which satisfies these boundary conditions. In other words, the boundary conditions are sufficient to establish uniqueness.

The proof is straightforward. Assume two solutions $\psi'$ and $\psi''$ which are admissible. Define a function $\Theta \equiv \psi' - \psi''$. Then $\Theta$ is zero over $R(x, y)$ at $t = 0$, and also is zero at the boundaries of $R(x, y)$ for $0 \leq t < \tau$. Substituting $\psi'$ and $\psi''$ in (6):

$$\begin{aligned} \triangle\psi'_t &= -J(\psi', \triangle\psi') \\ \triangle\psi''_t &= -J(\psi'', \triangle\psi'') \end{aligned} \tag{7}$$

Or, subtracting:

$$\triangle\Theta_t = -J(\psi', \triangle\psi') + J(\psi'', \triangle\psi'') \tag{8}$$

The right hand side of (8) is identically zero over $R(x, y)$ at $t = 0$. In addition, $\Theta_t = 0$ at the boundary of $R(x, y)$ at $t = 0$. Therefore, from a well known theorem concerning Laplace's Equation, it follows that $\Theta_t = 0$ over the entire region $R(x, y)$ at $t = 0$. In addition differentiation of $\Theta_t$ with respect to $x$ and $y$ leads to the requirement:

$$\frac{\partial(\psi')^{n+1}}{\partial x^{n-m}\partial y^m \partial t} = \frac{\partial(\psi'')^{n+1}}{\partial x^{n-m}\partial y^m \partial t} \quad \begin{matrix} \text{over } R(x, y) \text{ at } t = 0 \\ 0 \leq m \leq n \\ 0 \leq n \leq 3 \end{matrix} \tag{9}$$

Equations (7) can now be differentiated with respect to time, and the difference again taken. This leads to the relationship:

$$\begin{aligned} \triangle\Theta_{tt} = &-J(\psi'_t, \triangle\psi') - J(\psi', \triangle\psi'_t) + \\ &+ J(\psi''_t, \triangle\psi'') + J(\psi'', \triangle\psi''_t) \end{aligned} \tag{10}$$

However, from (9) the right hand side of this equation is again identically zero over $R(x, y)$ at $t = 0$, and in addition $\Theta_{tt} = 0$ at the boundary of $R(x, y)$. Therefore, $\Theta_{tt} = 0$ over the region $R(x, y)$ at $t = 0$.

Repeating the above process, it can be shown that $\partial^p\Theta/\partial t^p = 0$ over $R(x, y)$ at $t = 0$, for all integral values of $p$. However, from (5) $\psi'$ and $\psi''$ can be expanded in a Maclaurin Series in time. Thus, for any point $X, Y, T$ within $R(x, y)$ where $0 \leq T < \tau$:

$$\begin{aligned} \Theta(X, Y, T) = &\Theta(X, Y, 0) + T\Theta_t(X, Y, 0) + \\ &+ \frac{T^2}{2!}\Theta_{tt}(X, Y, 0) + \ldots . \end{aligned} \tag{11}$$

All terms on the right hand side of (11) have been shown to be zero. Hence $\Theta(X, Y, T) = 0$ and $\psi'$ is identically equal to $\psi''$ within the region and time limits considered. If a solution exists which meets the specified conditions, this solution must be unique.

### 4. Meteorological Implications of the Uniqueness Theorem

The implications of this uniqueness proof are of particular meteorological interest. In considering the problem of numerical integration of the equations for large scale atmospheric motions, CHARNEY ET AL. (1950) discussed

[1] Note that (5) is not equivalent to requiring that $\psi(x, y, t)$ be analytic, since the functions $\phi_n(x, y)$ are not necessarily analytic. A simple example of a non-analytic solution which satisfies the above conditions follows. Consider the linear equation $\psi_t + \psi_x + \psi_y = 0$, where $\psi$ is to be determined in the region $0 \leq x \leq 1$, $0 \leq y \leq 1$. One solution is given by equation (5) where: $\phi_n = (-1)^n (n!)^{-1} (x - y)^{3/2} \exp[(x + y)/2]$. Note that the second and all higher space-derivatives of $\psi$ are not defined along the line $x = y$, which bisects the region $R(x, y)$. The solution is clearly not analytic throughout the region, yet it is "admissible" according to the above definition.

the vorticity equation and on the basis of a heuristic argument concluded that the vorticity $\triangle\psi$ must be specified on those portions of the boundary along which the fluid was moving into the region under consideration (the socalled "inflow" boundaries). This argument has generally been accepted in subsequent literature dealing with problems or large scale atmospheric motions. In fact, some authors refer to this heuristic argument as a "proof" – presumably of the sufficiency and necessity of specifying the vorticity along the inflow boundaries. Yet it is clear from the discussion in the previous section that if a well-behaved solution exists, which is admissible according to the definition of Section 2, this solution will in general be excluded by specifying the vorticity on the inflow boundaries. In other words, the system will be overspecified.

This dilemma can be avoided in one of two ways. First, the boundary conditions can be reduced by assuming only the value of the stream function $\psi$ on the boundaries of the region $R\ (x, y)$ at $t > 0$. If a solution exists over a region $0 \leq t < \tau$ which is admissible according to the definition of Section 2, this solution will then be unique. Alternatively, the definition of admissible solution can be relaxed in some specified manner – for example, the first two limitations of Section 2 could be retained, but (5) could be relaxed and the solution could be required to satisfy some less restrictive continuity requirement. A solution of the differential equation may then exist which satisfies not only the assumed values of $\psi$ at the boundaries of $R\ (x, y)$, but also the assumed values of $\triangle\psi$ at inflow boundaries.

These alternatives can be illustrated by considering the simple non-linear differential equation:

$$u_t + uu_x = 0 \tag{12}$$

This equation can be written in the form $du/dt = 0$, and in this sense is analogous to the vorticity equation $d\ (\triangle\psi)/dt = 0$. In this one dimensional problem, we will assume that $u$ is specified along a segment of the $x$-axis, $R\ (x)$, at $t = 0$. The value of $u$ is to be determined within $R\ (x)$ for $0 \leq t < \tau$.

Let us first consider a solution which is well-behaved, according to the definition of Section 2. It is not difficult to show by an obvious extension of the method of the previous section that if solutions are sought for which $u, u_x$, and $u_t$ are single-valued and continuous, and for which $u$ can be expanded as a power series in time, no additional boundary conditions should be specified. In particular, neither $u$ nor its time variation should be specified along the inflow extremity of $R\ (x)$. Let us present a specific example. Let $u = 1.0 + 0.5 \cos x$ at $t = 0$ for $-\pi/2 \leq u \leq +\pi/2$. The unique admissible solution, applying the definition of Section 2, is: $u = 1.0 + 0.5 \cos\ (x - ut)$, and $u$ and its derivatives are finite, single-valued, and continuous within the segment $R\ (x)$ for $0 \leq t < .9\pi$. At $t = .9\pi$ a "shock" enters the region. Beyond the shock line the solution is not admissible, since in such regions the dependent variable $u$ becomes multi-valued. This inadmissibility corresponds to a lack of physical reality, since fluid velocity cannot have two or more values at a single point. This solution is shown in Figure 2 a. The straight lines are characteristics, of slope $1/u$, along which the velocity $u$ is conserved.

Les us now consider solutions of (12) which can be obtained by specifying additional boundary conditions, and by relaxing in an appropriate manner the definition of an admissible solution. First, let us require a solution for which $u$, $u_x$, and $u_t$ are defined and single valued in the region $R(x)$. Note that the restriction corresponding to (5) has been eliminated; however, the differential equation is valid everywhere in the region and an internal "matching" of dynamic or kinematic boundary conditions can be avoided. With this less restrictive definition of admissible solution, additional boundary conditions must be specified for uniqueness to exist. One possibility is to define $u$ at inflow boundaries for $t > 0$. However, this must be done in a very particular manner: such that $u_x$ and $u_t$ are always defined at the characteristic passing through the lefthand extremity of $R(x)$. In the particular example considered previously, this would require that:

$$u_t = \frac{0.5\ u \sin\ (x - ut)}{1 - 0.5\ t \sin\ (x - ut)}$$
$$u_x = \frac{-\ 0.5 \sin\ (x - ut)}{1 - 0.5\ t \sin\ (x - ut)} \tag{13}$$

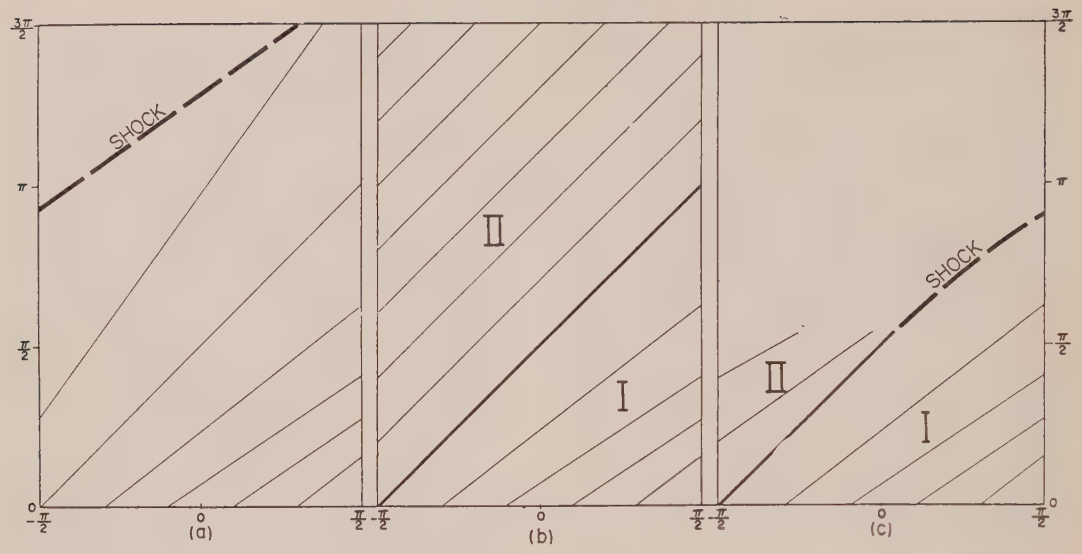


Fig. 2. Characteristic lines for three solutions of $u_t + uu_x = 0$, when $u(0, t) = 1.0 + 0.5 \cos x$ for $-\pi/2 \leq x \leq +\pi/2$. Value of $u$ at inflow boundary obtained: (a) from analytical extension; (b) by setting $u_t = 0$; (c) by setting $u_t = 1$.

along the characteristic $x = x_0 + u_0 t$, where $x_0$ and $u_0$ are the values of $x$ and $u$ at the left-hand extremity of $R(x)$. Finding a distribution of $u$ at the inflow boundary which satisfies (13) – and which differs from the result of Figure 2 a – is not difficult. One simple example is obtained by adding a function $(x - x_0 - u_0 t)^n$, $n > 1$, to the previous analytical solution, and by evaluating the result at $x = 0$ to obtain $u(0, t)$. However, the particular function selected for an additional boundary condition is not at issue. The major points to be made are: (1) if the differential equation is to be valid everywhere in the region over an appreciable time interval, the choice of the dependent variable at the inflow boundary is limited in a rigid manner, and (2) it is virtually impossible to meet these limitations *a priori* if the analytical solution is unknown.

The choice of $u$ at the inflow boundary becomes simple *a priori* only when the definition of "admissible solution" is further relaxed so that $u_x$ and $u_t$ may be undefined at some internal boundary. In this case one has considerable freedom in specifying $u$ at the inflow extremity. An obvious choice is to let $u_t$ be zero at the inflow boundary for all $t > 0$. Such a solution to the previous example has been presented in Figure 2 b. Note that $u_x$ and $u_t$ are discontinuous along the characteristic passing through $x = -\pi/2$, $t = 0$, which has been entered as a heavy line. The differential equation is, of course, not satisfied along this characteristic. The solution in Sub-Region I (restricted to the fluid within the segment $R(x)$ at $t = 0$) is, as before, $u = 1.0 + 0.5 \cos(x - ut)$; the solution in Sub-Region II (fluid which entered the segment at $t > 0$) is $u = 1$. These two solutions are matched kinematically at the characteristic line passing through the inflow extremity. Note that in this case no shock phenomenon occurs.

The importance of the choice of $u_t$ on the boundary is indicated in Figure 2 c. In this case it was assumed that $u_t$ was a non-zero constant at $x = -\pi/2$: namely, $u_t = 1$. A shock forms rather quickly, as indicated. Before the shock forms (as $t$ less than about $\pi/2$) the solution may again be divided into two sub-regions separated by the characteristic passing through the inflow extremity. At $t > \pi/2$, the kinematic boundary condition can no longer be satisfied at the surface of discontinuity and the dependent variable $u$ becomes multi-valued at that point.

The implications of the above discussion with regard to the vorticity equation are evident. The alternatives are: (1) to specify only the streamfunction on the boundary of $R(x, y)$ at $t > 0$, to assume a solution exists according

to the definition of admissibility of Section 2, and to attempt to obtain this unique solution by some acceptable procedure; or (2) to specify in addition the value of the vorticity at the inflow boundary, and to relax the definition of admissibility. The latter alternative will in general mean that derivatives of the vorticity will not exist along an internal surface: namely, the boundary between the fluid originally within the region at $t=0$, and the fluid which moves into the region at a subsequent time. This discontinuity will propagate into the region, and at a later instant will define the boundary of two sub-regions. To solve the system analytically, solutions of the vorticity equation should be obtained separately for each sub-region, and the solutions should be matched along the material boundary so that the kinematic and dynamic boundary conditions are satisfied. In this process, the equation $f(x, y, t) = 0$ of the material boundary on which the discontinuities occur must be determined. The associated analytical problem – or its numerical analogue – is formidable.

These questions can be avoided by accepting the definition of an "admissible solution" presented in Section 2. Fortunately, this poses no difficulties in meteorological problems, for the dependent variable and its derivatives are not subject to control at $t > 0$, and can only be estimated for use as boundary conditions by subjective means at best. Certainly if the techniques of solving large scale meteorological equations were analytical rather than numerical, there would be nothing to gain and much to lose by arbitrarily introducing internal discontinuities. Unique solutions could be obtained by specifying the streamfunction at all boundaries; the vorticity would not be specified either at inflow or outflow boundaries for $t > 0$. Whether these conclusions need be modified when numerical methods are applied will be considered in the following sections.

## 5. Boundary Conditions for Numerical Integration

When differential equations are translated into difference equations, and solutions are attempted by numerical means, it is found that a variety of methods of integration can be devised – each of which will yield a specific numerical result. Furthermore, these methods can be adapted to all sorts of different boundary conditions. Thus, in the case of the vorticity equation, methods of integration can readily be developed for which the vorticity is specified at all boundaries at $t > 0$, at only the inflow boundary, or at no boundary at all. In the sense that each of these procedures leads to a particular answer, the methods can easily be made unique.

For this reason, the concept of necessary and sufficient boundary conditions for the existence and/or uniqueness of an admissible solution has meaning in the numerical problem only in terms of the differential equation we are attempting to solve by approximate methods. We can therefore arbitrarily define "overspecification" of a system of difference equations as a statement of boundary conditions which would constitute overspecification in the continuum, as the grid spacing approaches zero. Similarly, "necessary" or "sufficient" conditions can also be defined in terms of the associated differential equation. This terminology will be followed below.

One additional fact must be pointed out. Since numerical methods are an attempt to obtain approximate solutions to a differential equation, the integration procedures devised must not be in conflict with theory applicable to the continuum. This is of importance in the present discussion in connection with the occurrence of discontinuity surfaces propagating into the region $R(x, y)$. We have already seen that in solving the differential equation under such circumstances, solutions must be obtained separately in each sub-region and matched at the moving surface of discontinuity. If numerical methods are applied under similar conditions, an equivalent procedure should in principle be followed. This would, of course, be extremely difficult to do – especially since the discontinuity is a Lagrangian surface moving in a finite Eulerian grid.

In practice, the discontinuity introduced by specifying vorticity on the inflow boundary has been ignored. The discontinuity cannot be detected with a finite grid, and application of a differencing procedure across the discontinuity results in an arbitrary "smearing". Although such a process can possibly be rationalized on purely pragmatic grounds, little theoretical justification exists. When we integrate numerically across discontinuities

along which the differential equation (and hence the difference equation) is not valid, we have no way of knowing what errors are introduced. If numerical methods are to achieve an adequate scientific basis, such arbitrary procedures must be carefully avoided.

In the numerical integration of the vorticity equation, therefore, it is extremely desirable to develop a method which will not require the specification of vorticity on either the inflow or the outflow boundaries at $t > 0$. Another problem must be faced, however. To be useful, such a method must be simple to apply; must not accumulate errors too rapidly; and must remain numerically stable.

The latter two requirements have so far proved to be a substantial stumbling block. According to PLATZMAN (1954) two methods of estimating vorticity at the outflow boundary were used by the research group at the Institute for Advanced Study at Princeton. The first method involved setting the vorticity at an outflow point equal to the vorticity at the first interior grid point; the second involved a linear extrapolation from two interior grid points. These methods were used only at the outflow boundaries, the vorticity on the inflow boundaries being specified in accordance with the conclusions of CHARNEY ET AL. (1950). Nevertheless, a rapid accumulation of errors occurred near the outflow boundary, and (in some cases at least) numerical instability resulted.

An analysis of this behavior must involve an investigation of truncation error and stability criteria in non-linear systems. This is beyond the scope of the present paper. However, it is certainly not proper on the basis of these experiences to take the negative point of view that overspecification is necessary if instability is to be avoided. Certainly, some numerical methods may exist which do not overspecify and which are not unstable. One (a Lagrangian approach) is discussed in Section 7; a second possible procedure (in Eulerian form) is presented in Section 8. Neither of these procedures may at present be feasible for operational forecasting. Each will have value as a research procedure.

## 6. A Numerical Example

In order to provide a partial check on the effect of non-linearity on stability and truncation error, a numerical solution of a first order equation ($u_t + uu_x = 0$) was undertaken. The investigation of PLATZMAN (1954) on the linear form of this equation ($u_t + ku_x = 0$ where $k$ is constant) made the attempt particularly interesting. Platzman found that complete overspecification (i.e. assigning the value of $u$ at both inflow and outflow extremities of the segment $R$ $(x)$) assured numerical stability, while either of two methods of computing the value of $u$ at the outflow extremity resulted in numerical instability. It is important to determine whether these surprising conclusions are applicable to the non-linear model.

The non-linear equation ($u_t + uu_x = 0$) assures the formation of shock phenomena somewhere in the $x-t$ plane if $u_x$ is not everywhere positive. An example was therefore chosen for which the analytical solution showed all shocks occurred downstream from the segment $R$ $(x)$ considered. Numerical integrations are therefore unaffected by multiple-valued solutions of the differential equation.

The solution chosen was:

$$u = {}^1/_2 \exp\,[(x-ut)^2 \ln 0.2/144]. \quad (14)$$

The distribution of $u$ at $t=0$ was in the form of an error function. The initial values were computed on the $x$-axis at unit intervals for $-12 \leq x \leq 12$; the time increment was set equal to unity. At $t=0$, $u$ was 0.1 at each

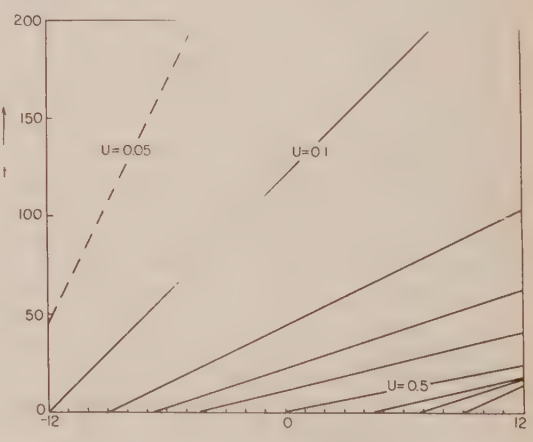


Fig. 3. Graphical solution of $u_t + uu_x = 0$. Straight lines are characteristics along which $u$ is conserved. The distribution of $u$ at $t=0$ is an error function with maximum at $x=0$.

extremity and 0.5 at the origin. The characteristic solution of (14) is shown in Figure 3.

Numerical integrations were performed using five different procedures:

(1) $u$ was held constant at both inflow and outflow boundaries.
(2) $u$ was held constant at the inflow boundary, and was computed at the outflow boundary using a quadratic extrapolation from two interior points. (This is a "first order" procedure as defined below.)
(3) $u$ was computed at both inflow and outflow boundaries using a quadratic extrapolation from two interior points. (A "first order" procedure.)
(4) $u$ was computed at both boundaries during the integration, using values of $u_x$ on the boundaries obtained from interior values of $u$. (A "second order" approximation, discussed below.)
(5) $u$ was computed at both boundaries using a somewhat different "second order" procedure, described below.

At the inflow boundary in Method 2, and at both boundaries in Method 3, the following equations were used:

$$\begin{aligned} u_{12} &= 2\,u_{11} - u_{10} + \Theta(\alpha^2) \\ u_{-12} &= 2\,u_{-11} - u_{-10} + \Theta(\alpha^2) \end{aligned} \tag{15}$$

where $\alpha$ is the increment in $x$, and $\Theta(\alpha^2)$ indicates that terms involving $\alpha^2$ and higher have been dropped from the appropriate Taylor Expansions. Note that although (15) is accurate to $\alpha^2$, this is a first order procedure since $u_x$ is the quantity actually used in the numerical integration, and the corresponding values of $u_x$ at first interior points are:

$$\begin{aligned} (u_x)_{11} &= \frac{u_{11} - u_{10}}{\alpha} + \Theta(\alpha) \\ (u_x)_{-11} &= \frac{u_{-10} - u_{-11}}{\alpha} + \Theta(\alpha) \end{aligned} \tag{16}$$

Methods 4 and 5 involve second order approximations for $u_x$. The respective relationships near the outflow boundary are:

$$\text{Method 4: } (u_x)_{12} = \frac{4u_{11} - 3u_{12} - u_{10}}{2\alpha} + \Theta(\alpha^2) \tag{17}$$

$$\text{Method 5: } (u_x)_{11} = 2(u_x)_{10} - (u_x)_9 + \Theta(\alpha^2)$$

The first expression can be derived from Taylor Expansions about $x = 12$. Similar expressions are used near the inflow boundary.

Integrations were carried out for 20 time steps, and for $t = 1$, 5, 10 and 20 the root-mean-square difference between each numerical solution and the analytical solution was evaluated and expressed as a percentage of the average value of $u$. The results are presented in Table I. In general, there is not too much difference between Methods 2, 3 and 4. However, one second order procedure (Method 5) shows signs of accumulating errors near the boundaries. The strongly overspecified procedure (Method 1) is definitely inferior to all others, with an average error of 35 % at the end of 20 iterations. Strong corrugations appear near the outflow boundary, and the maximum value of $u$ has increased from 0.50 to 0.85 (clearly an error, since the value of $u$ should be conserved). At this stage it appeared that a moderate extension of the computation would result in the onset of numerical instability in Method 1, although if Platzman's conclusions were applicable to the non-linear system this should have been the only stable method of the group.

To see whether instability would develop, the numerical integrations were extended to 200 iterations for Methods 1, 2, 3 and 4. The second order procedure (Method 4) became unstable after about 110 iterations. Interestingly enough, the other three methods remained stable, although in Method 1 the maximum value of $u$ exceeded unity for 21 consecutive iterations (from $t = 22$ through $t = 42$). The

**Table 1. Root-Mean-Square Errors for five methods of numerical integration, expressed as percentage of mean value of dependent variable**

| | Method of Numerical Integration | | | | |
|---|---|---|---|---|---|
| $t$ | 1. | 2. | 3. | 4. | 5. |
| 1 | 0.3 | 0.4 | 0.5 | 0.2 | 0.2 |
| 5 | 1.3 | 0.8 | 0.5 | 0.3 | 0.3 |
| 10 | 3.3 | 1.5 | 0.9 | 0.6 | 1.3 |
| 20 | 34.9 | 3.7 | 3.0 | 3.5 | 11.7 |

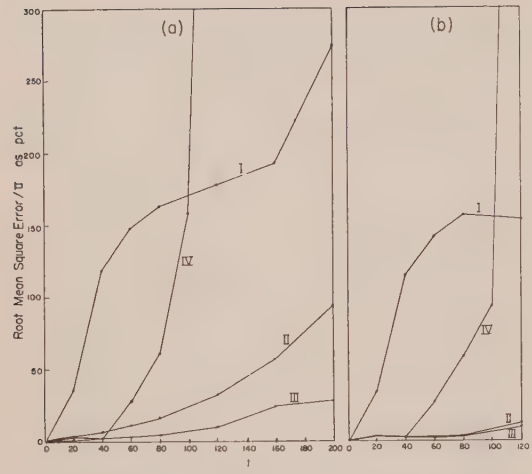


Fig. 4. Average root-mean-square errors of four methods of numerical integration of the equation $u_t + uu_x = 0$, expressed as percent of average value of dependent variable $u$. Time scale is normalized: $t$ equals number of iterations.

root-mean-square errors for each method are shown in Figure 4: (a) for the entire set of 25 points; and (b) for those points occupied by fluid originally within the region $R$ $(x)$. The latter graph is terminated at $t = 120$, since beyond this most of the original fluid has left the Eulerian region. Method 3 remains amazingly accurate, while Method 2 has greater limitations. As a result of numerical "smoothing" across a surface that is an internal discontinuity in the continuum, Method 2 is slightly less accurate than Method 3 even for the portions of the $x-t$ plane where the analytical solutions are identical. This is shown in Figure 4 (b). On the other hand, Method 1 is so inaccurate as to be virtually useless after about 20 iterations. By $t=80$, corrugations of wave length two extend throughout the entire set of 25 points. Method 4 starts out well, but is unstable and becomes virtually useless after about 55 iterations.

Obviously, not too many conclusions should be drawn on the basis of a single example. Nevertheless, several points are evident. First, the stability criteria developed by PLATZMAN (1954) for a linear system cannot be applied to a non-linear system. The method of integration which showed earliest signs of instability was the one which (according to linear theory) should have been the only stable procedure. Furthermore, the best method was one which (according to linear theory) should have been unstable. Second, increased stability cannot be assured by higher order difference approximation near the boundaries. This is not too surprising, since after a large number of iterations the truncation error may be extremely large compared to the differencing error. Third, using a first order approximation the dependent variable was successfully computed at both inflow and outflow points, and this method was definitely superior to the one which involved overspecification at the inflow boundary.

These results may not, of course, be applicable to third order differential equations in two dimensions. Nevertheless, when considered in connection with the theoretical results of earlier sections, they indicate a careful re-evaluation of current practices is in order.

## 7. A Lagrangian Method of Integration

The discussion of sufficient boundary conditions would not be complete without mention of a Lagrangian solution. The difficulties in the Eulerian methods arise from the propagation into the region $R$ $(x, y)$ of a material surface, separating the fluid within the region at $t = 0$ from the fluid which enters at a later time. These difficulties can, of course, be avoided by conducting the numerical integration in terms of a Lagrangian grid. In the case of the vorticity equation, this approach completely removes one question of overspecification, since the vorticity is known throughout the Lagrangian region at all time.

In terms of three dependent variables ($x$, $y$, and $\psi$) the vorticity equation of a perfect fluid becomes:

$$x_t = J(\psi, x)$$

$$y_t = J(\psi, y)$$

$$f(a, b) = J(x_t, x) + J(y_t, y) \tag{18}$$

$$= \psi_{aa}(x_b^2 + y_b^2) + 2\psi_{ab}(x_a x_b + y_a y_b) + \psi_{bb}(x_a^2 + y_a^2) - \psi_a(x_a x_{bb} - x_b x_{ab} + y_a y_{bb} - y_b y_{ab}) - \psi_b(x_b x_{aa} - x_a x_{ab} + y_b y_{aa} - y_a y_{ab})$$

Here $J$ is the Jacobian in terms of the independent variables $(a, b)$ – where $(a, b)$ are the values of $(x, y)$ at $t=0$. Use has been made of the Lagrangian equation of continuity: $J(x, y)=1$. The function $f(a, b)$ is the known distribution of vorticity at the initial time. It is important to note that the third equation is always elliptic, with constant characteristic slopes $\pm 2i$. Thus, if the streamfunction is specified at the boundary points at all time, and if the coefficients remain finite, a unique single-valued solution exists in the interior.

Equations (18) can be re-written in difference form for numerical integration without difficulty. The procedure for integration is as follows:

(1) Values of $x_t$ and $y_t$ are computed everywhere in the interior at $t = t_0$.
(2) From this, values of $x$ and $y$ are computed at each interior grid point $(a, b)$ at $t_1 = t_0 + \gamma$, where $\gamma$ is the time increment. Values of $x$ and $y$ are computed at boundary points using an equation of the form (15).
(3) The coefficients of the third equation of (18) are evaluated at $t_1$ using centered differences in the $(a, b)$ grid.
(4) The elliptic equation is solved for the streamfunction at all points.
(5) The above procedure is repeated.

In addition to theoretical advantages, such a numerical solution will yield particle trajectories, since the position $(x, y)$ of a particle $(a, b)$ is explicitly evaluated as a function of time. Difficulties include the increased storage to carry the values of three dependent variables, possible increase in truncation error, and problems in converting to an Eulerian system for purposes of plotting weather charts. However, with continued improvements in high speed computers, at least some of these difficulties are becoming less serious. Until Eulerian integrations can be conducted on a hemispheric scale, the Lagrangian system offers many unique advantages.

### 8. The First Time Step in Numerical Integration

One additional problem will now be considered: the errors introduced in integrating from $t=0$ to $t=\gamma$ (where $\gamma$ is the time increment in the integration). The conventional method employs a forward (uncentered) difference for the first step. This introduces an error of the order of $\gamma^2$ in $\psi$, whereas all subsequent steps in centered time difference form introduce errors of the order $\gamma^3$. For:

$$\begin{aligned} \psi_{i,j}^{(1)} &= \psi_{i,j}^{(0)} + \gamma\,(\psi_t)_{i,j}^{(0)} + \Theta(\gamma^2) \\ \psi_{i,j}^{(k+1)} &= \psi_{i,j}^{(k-1)} + 2\gamma\,(\psi_t)_{i,j}^{(k)} + \Theta(\gamma^3) \end{aligned} \qquad (19)$$

One immediate consequence of this increased error can be noted. In the vorticity equation in Eulerian form:

$$\triangle\psi_t = -J(\psi, \triangle\psi) \qquad (20)$$

the Jacobian is zero at maxima and minima of the streamfunction field (i.e. at centers of cyclones and anticyclones). If a forward time difference is employed, the vorticity at these important points cannot change in the first time step, although in actuality a significant variation may occur. This difficulty would be avoided by a higher order approximation, since even though $\triangle\psi_t$ were zero, the vorticity could pass smoothly through a maximum or minimum at $t=0$.

Various methods have been suggested for avoiding the increased error of a forward difference in the first time step, but none have been generally accepted because of their difficulty of application. The method suggested below, however, is very simple to apply and requires a minimum of additional programming.

Let us differentiate the vorticity equation with respect to time. Then:

$$\triangle\psi_{tt} = -J(\psi_t, \triangle\psi) - J(\psi, \triangle\psi_t). \qquad (21)$$

A program of computation can now be devised which only makes use of centered differences and higher order Taylor Expansions:

(1) From (20) compute $\triangle\psi_t$ at each interior grid point at $t=0$.
(2) Given (as boundary conditions) $\psi_t$ on the boundary of $R(x, y)$, compute $\psi_t$ at each grid point.
(3) From (21) compute $\triangle\psi_{tt}$ at each interior grid point at $t=0$. In this step it will be necessary to evaluate first space derivatives of $\triangle\psi_t$ at first interior grid points using a method analogous to (16).
(4) Given (as boundary conditions) $\psi_{tt}$ on the boundary of $R(x, y)$, compute $\psi_{tt}$ at each grid point.

(5) Using the values of $\psi_t$ and $\psi_{tt}$ from steps (2) and (4) compute $\psi$ at $t=\gamma$ using a Taylor Series expansion:

$$\psi_{i,j}^{(1)} = \psi_{i,j}^{(0)} + \gamma\,(\psi_t)_{i,j}^{(0)} + \frac{\gamma^2}{2!}\,(\psi_{tt})_{i,j}^{(0)} + \Theta\,(\gamma^3) \qquad (22)$$

Note that this method results in the same accuracy in the first time step as in each succeeding step. The procedure will be simple to program, since steps (1) and (2) are used throughout the entire computation, and the relaxation (or matrix inversion) in step (4) is identical in procedure to that in step (2). The method can be generalized easily to any equation in which only first time derivatives appear.

In order to check the improvement resulting from the application of this method, the simplified equation ($u_t + uu_x = 0$) was again considered. Six examples were considered, with $u$ chosen as sine waves of various wave lengths and amplitudes at $t=0$. An interval of $2\pi$ on the $x$-axis was selected, in order that cyclic continuity would be preserved and no errors would be introduced at the boundaries of the segment. Numerical integrations were carried through ten time steps, using two methods. Method (a) used forward difference at $t=0$; Method (b) solved numerically the equations:

$$\begin{aligned} u_t &= -\,uu_x \\ u_{tt} &= -\,uu_{xt} - u_t u_x = 2\,uu_x{}^2 + u^2 u_{xx} \end{aligned} \qquad (23)$$

in centered difference form at $t=0$, and used a Taylor expansion similar to (22). At all later time steps, identical procedures were employed for both methods. Differences between the results could therefore be attributed entirely to the first step.

After 1, 2, 5 and 10 iterations, the root-mean-square error was computed for each method, using the analytical solution as a standard. The average results, normalized in terms of the error in the first time step for Method (b), are shown in Figure 5. The error in Method (b) increased regularly with time. The error in the first time step of Method (a) was about five times as great as in Method (b). Some recovery occurred at the second iteration, but beyond that the error curves became parallel, and the difference between the two curves remained essentially constant

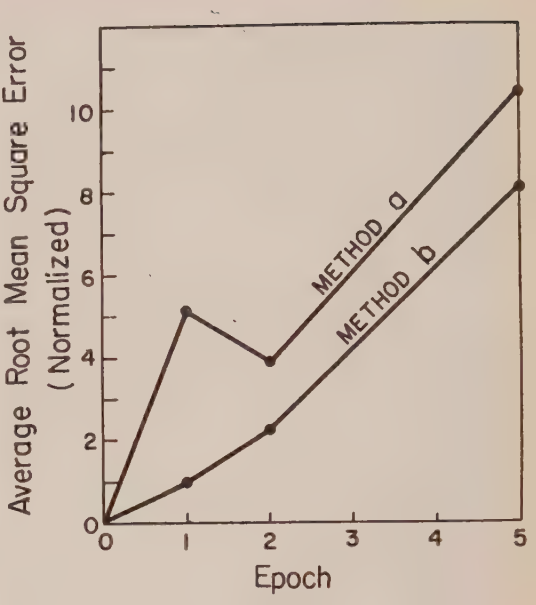


Fig. 5. Average root-mean-square errors of two methods of numerical integration of the equation $u_t + uu_x = 0$. Method b is identical to Method a, except that a higher order forward difference is used at $t=0$.

through the tenth iteration. At $t = 5\gamma$, the average error in Method (a) was about 30 % greater; at $t = 10\gamma$, it was about 15 % greater. In view of the small additional effort required to achieve this increase in accuracy, it is believed the method is worthy of routine application.

One final possibility suggests itself. Equations (20) and (21) can be used at any stage of the integration to the same order of accuracy as the centered difference form. This may not be operationally profitable, since two relaxations or matrix inversions are required at every time step. However, there are certain advantages which make this method of interest for research purposes. Thus, as (23) shows for the simplified equation, a certain "smoothing" is introduced by terms of the form $u^2 u_{xx}$ in the expression for the higher order time derivative. This should make the numerical integration more stable, while not causing the result to change appreciably from the analytical solution (which identically satisfies both equations in (23)).

This idea was tested using the numerical example of Section 6. Equations (23) were integrated through 200 iterations, using the

**Table 2. Root-Mean-Square Errors for two methods of numerical integration, expressed as a percentage of mean value of dependent variable**

| | Entire Region | | Original Fluid | |
|---|---|---|---|---|
| $t$ | Method 3 | Method b | Method 3 | Method b |
| 20 | 3.0 | 2.0 | 2.8 | 0.6 |
| 40 | 2.3 | 1.3 | 1.9 | 0.2 |
| 60 | 2.7 | 2.0 | 1.8 | 0.2 |
| 80 | 4.0 | 2.6 | 2.8 | 0.2 |
| 120 | 10.3 | 3.9 | 9.6 | 0.2 |
| 160 | 23.9 | 5.0 | 20.2 | 0.2 |
| 200 | 28.4 | 6.1 | 21.5 | 0.3 |

Method (b) discussed above at *each* time step. The root-mean-square errors are compared in Table II with Method 3 of Section 6, which was by far the best procedure previously tested over this extended period. It is interesting to note that Method (b) was definitely superior, both in the region occupied by the original fluid and over the entire set of 25 grid points.

In addition, absolutely no sign of instability appeared in Method (b), even after 200 iterations. Careful examination of the results show that centered difference estimates of $u_x$, $u_t$, $u_{xx}$, and $u_{tt}$ remain consistent in sign from one grid point to the next (except at appropriate maxima and inflection points). On the other hand the results of Method 3 show oscillations in sign of $u_{tt}$ after the second iteration; in $u_{xx}$ after 16 iterations; in $u_x$ after 17 iterations; and in $u_t$ after 27 iterations. These oscillations persist, although they do not grow to substantial magnitude. The results seem to indicate clearly that the new method may have research value in numerical integrations for which stability is difficult to achieve.

It is important to emphasize that this method is equally applicable to the full vorticity equation. If the results of the non-linear first-order equation are any guide, it should be possible to use this method to integrate the vorticity equation for an Eulerian grid, without overspecification. Such an integration – and comparison of the results with the overspecified system – will throw more light on the effect of the current practice of assuming vorticity on the boundary of a fixed region.

## 9. Acknowledgements

The author is indebted to Dr. Robert R. Long for many helpful and stimulating discussions of the problems of numerical integration. He is also indebted to Dr. George Platzman, who was kind enough to read the manuscript and offer his comments.

## REFERENCES

Charney, J. G., Fjörtoft, R., and Neumann, J. von, 1950. Numerical Integration of the Barotropic Vorticity Equation. *Tellus*, **2**, pp. 237—254.

Lighthill, M. J., and Whitham, G. B., 1955. On Kinematic Waves Part I, *Proc. Royal Society London, Ser. A*, **229**. pp. 281—316.

Platzman, G. W., 1954. The Computational Stability of Boundary Conditions in Numerical Integration of the Vorticity Equation, *Archiv für Met., Geoph., und Bioklim., Ser. A*, **7**, pp. 30—40.

# On the Relation Between Pressure and Wind, with Particular Reference to a Vortex.[1]

By JULIÁN ADEM, Instituto de Geofísica, Universidad Nacional de México and Instituto Nacional de la Investigación Científica, México, D.F.

(Manuscript received May 8, 1957, revised March 20, 1958)

*Abstract*

It is shown that if the boundary conditions to solve the vorticity and balance equations are prescribed independently, then the primitive equations of motion are not satisfied.

Given the wind field of a symmetrical vortex embedded in a resting atmosphere, analytical expressions for the pressure and wind tendency are derived. A numerical example is worked out and the results are used to obtain information regarding the effect of the boundary conditions and of the variation of the Coriolis parameter in a forecast with a barotropic model.

The barotropic non-divergent flow is defined by the following equations:

$$\frac{dv}{dt} + fu = -\frac{\partial \phi}{\partial y} \tag{1}$$

$$\frac{du}{dt} - fv = -\frac{\partial \phi}{\partial x} \tag{2}$$

$$\frac{\partial u}{\partial x} + \frac{\partial v}{\partial y} = 0 \tag{3}$$

where $d/dt \equiv \partial/\partial t + u\partial/\partial x + v\partial/\partial y$, $u$ and $v$ are the components along the $x$- and $y$-axes, respectively of the horizontal wind, the $x$-axis points to the east and the $y$-axis to the north, $f$ is the Coriolis parameter; and $\phi = p/\varrho$, where $\varrho$ is the density and $p$ the pressure.

Let $u = -\partial\psi/\partial y$ and $v = \partial\psi/\partial x$, then (3) is automatically satisfied and we only have to deal with equations (1) and (2).

By differentiating (1) with respect to $x$ and (2) with respect to $y$ and subtracting we obtain the well-known vorticity equation that contains only the stream function as dependent variable:

$$\nabla^2 \frac{\partial \psi}{\partial t} = J(\nabla^2 \psi,\ \psi) - \beta \frac{\partial \psi}{\partial x} \tag{4}$$

Differentiating (1) with respect to $y$ and (2) with respect to $x$ and adding we get

$$2[\psi_{xy}{}^2 - \psi_{xx}\,\psi_{yy}] - f\nabla^2\psi - \nabla\psi \cdot \nabla f + \nabla^2\phi = 0 \tag{5}$$

which gives a relation between wind and pressure. (The pressure field is given by $\phi\varrho$, where $\varrho$ is constant; we shall, however, refer to $\phi$ as the pressure.) This equation has been used by BOLIN (1955, 1956) and CHARNEY (1955) in an attempt to improve numerical forecasting by removing the geostrophic assumption.

[1] This research was started at the International Meteorological Institute in Stockholm, while the author was there. Part of the material is based on an unpublished manuscript, in which the late Prof. C.-G. Rossby was co-author.

Given the pressure field $\phi$ in a region $A$ enclosed in a boundary $C$ where we prescribe $\psi$, if we assume, for the sake of simplicity, that equation (5) is of the elliptic type, we can obtain the stream function $\psi$ by solving this equation (Bolin, 1956, p. 2).

When one substitutes in the primitive equations of motion the given pressure field and the $\psi$ computed using (5), they determine, except for an arbitrary constant, a unique solution for $\partial\psi/\partial t$ in the whole region $A$ and its boundary $C$.

It follows therefore that we cannot choose arbitrary boundary conditions to solve the vorticity equation, because when solving it to determine $\partial\psi/\partial t$ we must obtain the same solution as by solving the primitive equations. In other words, by prescribing $\phi$ in $A$ and $\psi$ and $\partial\psi/\partial t$ in $C$ arbitrarily independent to solve (4) and (5) we obtain a solution that does not necessarily satisfy the primitive equations.

Similarly, if we prescribe in the region $A$ the stream function, we cannot prescribe both the tendency and the pressure at the boundary in order to solve equations (4) and (5).

The above consideration shows that the problems of finding the pressure-wind relation and formulating the best boundary conditions are closely connected; and that these two problems in numerical forecasting are not independent and need to be investigated from a unified viewpoint.

In the present stage of numerical forecasting, the arbitrariness of the boundary conditions cannot be avoided, and the following questions can be formulated in connection with the above considerations:

1. In what type of problems is it essential to use consistent boundary conditions to solve (4) and (5)?

2. How can one choose the boundary conditions to solve equations (4) and (5) in order that the solution be also the solution of the primitive equations of motion?

The answers to these two questions are not given here, but they will be the subject of further research.

In the remaining part of this paper we shall deal with one example in which an analytical solution to equations (4) and (5) can be found which, because of its simplicity, lends itself to comparative studies and discussions.

We introduce a polar coordinate system $(r, \Theta)$ and prescribe at $t=0$ the stream field $\psi$ as a function of $r$ at $r \leq r_0$ and $\psi=0$ at $r \geq 0$. We assume that $\psi$ and its three first derivatives are continuous differentiable functions. This stream function represents a vortex.

Assuming $f = f_0 + \beta y$ where $f_0$ and $\beta$ are constants, we can compute the tendency field and the pressure field from the Poisson equations (4) and (5) (Adem, 1956, p. 365). We get:

$$\left(\frac{\partial\psi}{\partial t}\right)_{t=0} = -\frac{\beta x}{r^2}\int_0^r \psi r dr + xC_1 \qquad (6)$$

$$\phi = f\psi + \int_0^r \frac{1}{r}\left(\frac{d\psi}{dr}\right)^2 dr - \frac{\beta y}{r^2}\int_0^r \psi r dr + yC_2 + C_3 \qquad (7)$$

where $C_1$, $C_2$ and $C_3$ are arbitrary constants to be determined from the boundary conditions. We have retained only the arbitrary harmonic solutions pertinent to our discussion, and all others are zero. If we prescribe that the normal velocity is zero at the boundary $r = R_0$, then $(\partial\psi/\partial t)_{t=0} = 0$ at $r = R_0$, and we get

$$C_1 = \frac{\beta}{R_0^2}\int_0^{R_0} \psi\, r dr$$

On the other hand substituting (6) and (7) in (1) and (2) we see that our solution satisfies the primitive equations if $C_1 = -C_2$. Therefore the specification of $\partial\psi/\partial t$ at $r=R_0$ is enough to determine the arbitrary constant $C_2$ in (7). In other words, as stated above, one cannot prescribe both the pressure and the tendency at the boundary. If one prescribes the boundary conditions to solve the vorticity equation (4) one has no freedom to choose boundary conditions for the balance equation (5) and vice-versa. Finally the arbitrary constant $C_3$ is irrelevant and can be taken as zero.

Substituting the values of the arbitrary constants in (7) we obtain

$$\phi = f\psi + \int_0^r \frac{1}{r}\left(\frac{d\psi}{dr}\right)^2 dr - \frac{\beta \sin \Theta}{r}\int_0^r \psi r dr - \frac{\beta r \sin \Theta}{R_0^2}\int_0^{r_0} \psi r dr \qquad (8)$$

This formula gives the pressure field of a vortex of radius $r = R_0$ enclosed in a concentric circular region of radius $r = R_0$. We have only assumed that the normal velocity is zero at $r = R_0$.

In this formula the term

$$\int_0^r \frac{1}{r}\left(\frac{d\psi}{dr}\right)^2 dr$$

is due to the centripetal acceleration of the vortex and corresponds to the term $2(\psi_{xx}\psi_{yy} - \psi_{xy}^2)$ in equation (5).

The term

$$\beta \sin \Theta\left[r\psi - \frac{1}{r}\int_0^r \psi r dr - \frac{r}{R_0^2}\int_0^{r_0} \psi r dr\right]$$

corresponds to the variation of the Coriolis parameter.

It is interesting to note that at $r \geqq r_0$ where $\psi = 0$ (wind field zero) a pressure field, due entirely to the variation of the Coriolis parameter, exists and is given by

$$\phi = -\beta \sin \Theta\left[\frac{1}{r} + \frac{r}{R_0^2}\right]\int_0^{r_0} \psi r dr$$

From the primitive equation (1) we can compute, by multiplying by $\varrho$ and integrating over a circle of radius $r$, the resultant net force on a horizontal slice of unit height and with an area equal to the circle of radius $r$:

$$R = \varrho\int\int \frac{dv}{dt}\, dA = -\beta\varrho\pi\left[\int_0^r \psi r dr - \frac{r^2}{R_0^2}\int_0^{r_0} \psi r dr\right] \qquad (9)$$

In this integration, the contribution from integrating the term $-fu$ is

$$F = -\varrho\iint fu dA = \beta\varrho\pi\left[r^2\psi - 2\int_0^r \psi r dr\right] \qquad (10)$$

while that from integrating $-\partial\phi/\partial y$ is

$$P = -\varrho\int\int \frac{\partial\phi}{\partial y}\, dA =$$

$$= \beta\varrho\pi\left[\int_0^r r\psi dr - r^2\psi + \frac{r^2}{R_0^2}\int_0^{r_0} \psi r dr\right] \qquad (11)$$

This last term represents the resultant pressure force on the material line of radius $r$ and could be obtained directly from (8) by integrating at such line.

When $r = r_0$

$$(R)_{r=r_0} = -\beta\varrho\pi\left[1 - \frac{r_0^2}{R_0^2}\right]\int_0^{r_0} \psi r dr \qquad (12)$$

and if $R_0 \gg r_0$ we get the relations

$$(R)_{r=r_0} = \frac{1}{2}(F)_{r=r_0} = -(P)_{r=r_0}$$

showing that the net resultant force on the vortex is reduced by one half due to the pressure resultant. In a preliminary computation, Rossby (1948) neglected the resultant pressure force, but as pointed out by him afterwards (Rossby, 1949) and as shown by these computations the net force is decreased by one half if the resultant pressure force is included.

The net resultant is directed northwards in the case of a cyclone and southwards in the case of an anticyclone.

It is of interest to point out that the last term of the second member of (8), which represents the pressure field due to the boundary effect, tends to zero when the boundary $R_0 \to \infty$. However, as shown by (11), the integrated pressure resultant at $r = R_0$ does not go to zero and accounts for the necessary balance of forces implied by the primitive equations.

Let $\psi = \psi_0\ [1 - (r/r_0)^2]^4$ when $r \leq r_0$ and $\psi = 0$ when $r \geq r_0$.

This stream function represents a cyclone if $\psi_0 < 0$ and an anticyclone if $\psi_0 > 0$.

The maximum velocity $v_{max} = (d\psi/dr)_{max}$ is at $(r/r_0)^2 = 1/7$ and $\psi_0$ is given as a function of the radius and of the maximum velocity by

$$\psi_0 = -\,0.525\ r_0\ (d\psi/dr)_{max}$$

Let us consider a cyclone with maximum velocity $v_{max.} = 30$ m/s and $r_0 = 1{,}000$ km. Let $f_0 = 0.9 \times 10^{-4}$ sec$^{-1}$, $\beta = (1.7) \times 10^{-13}$ cm$^{-1}$ sec$^{-1}$. The results of the computation using this data to evaluate the different terms in expression (8) for the pressure field are shown in Table 1. Column I gives the values of $f_0\psi$ for different values of $r/r_0$. Columns II and III give the values of the terms due to the variation of the Coriolis parameter for $\sin\Theta = 1$. Column IV gives the values of the term due to the centripetal acceleration of the cyclone.

To get the actual quantities from Table 1, one has to multiply the values of the table by $(\psi_0)\ 10^{-4}$ and the results will then be given in cm$^2$ sec$^{-1}$.

For an anticyclone the sign of Columns I, II and III has to be changed, but the sign of IV remains unchanged, showing that for a cyclone the terms I and IV have to be added and that for an anticyclone they have to be subtracted. This fact shows that a negligible pressure field can be associated with a strong wind field in the case of an anticyclone, and that given a cyclone and an anticyclone of the same wind intensity and at the same latitude, the pressure field associated with the cyclone is always stronger than the one corresponding to the anticyclone (in the northern hemisphere).

**Table 1. Values of the different terms of the pressure field in a cyclone.**

The stream function is $\psi = \psi_0\,[1 - (r/r_0)^2]^4$. $v_{max} = 30$ m/s, $r_0 = 1{,}000$ km, $f_0 = 0.9 \times 10^{-4}$ sec$^{-1}$ and $\beta = (1.7) \times 10^{-13}$ cm$^{-1}$ sec$^{-1}$.

| | I | II | III | IV |
|---|---|---|---|---|
| $r/r_0$ | $f_0\psi$ | $r\beta\psi$ | $-\beta/r\int_0^r r\,dr$ | $\int_{r_0}^{r} \frac{1}{r}\left(\frac{d\psi}{dr}\right)^2 dr$ |
| 0 | —.900 | 0 | 0 | —.720 |
| .2 | —.764 | —.029 | .016 | —.541 |
| .4 | —.448 | —.034 | .025 | —.212 |
| .6 | —.151 | —.017 | .025 | —.032 |
| .8 | —.015 | —.002 | .021 | —.006 |
| 1.0 | 0 | 0 | .017 | 0 |
| 1.2 | 0 | 0 | .014 | 0 |
| 1.4 | 0 | 0 | .012 | 0 |
| 1.6 | 0 | 0 | .011 | 0 |
| 1.8 | 0 | 0 | .010 | 0 |
| 2.0 | 0 | 0 | .009 | 0 |

It is of interest to see how the values in this table vary when one varies $v_{max}$, $r_0$, $f_0$ and $\beta$. Column I is proportional to $f_0$, Columns II and III are proportional to $r_0$ and $\beta$, and Column IV is proportional to $v_{max}/r_0$.

The following conclusions regarding the importance of the $\beta$-term in the balance equation (5) are worth mentioning:

The $\beta$-term of equation (5) is locally small compared with the other terms. However, its integrated effect can be important.

The $\beta$-term increases proportionally with the dimensions of the disturbances to be forecasted; and, therefore, if it is of significance, its effects should appear mainly in forecasting large scale motions.

The tendency of the stream field is given by

$$\left(\frac{\partial\psi}{\partial t}\right)_{t=0} = -\frac{\beta x}{r^2}\int_0^r \psi r\,dr + \frac{\beta x}{R_0^2}\int_0^{r_0} \psi r\,dr \qquad (13)$$

If $R_0 \gg r_0$, we see by comparison with (8) that except for a shift of 90° it is the same field as the term of the pressure field responsible for the pressure resultant on the vortex. The tendency outside the vortex for $r \ll R_0$ is proportional to the net resultant force on the vortex, as is shown by comparison of (13) with (12).

From the analytical expressions for the pressure and wind tendency given by equations (8) and (13) we see that the boundary effect is due entirely to the variation of the Coriolis parameter and that if we vary in our example the boundary $r = R_0$ its effect is proportional to $1/R_0^2$. On the other side, for a fixed boundary $r = R_0$ the boundary influence at a given point is proportional to the distance between the point and the center of the vortex.

## REFERENCES

ADEM, J., 1956: A series solution for the barotropic vorticity equation... Tellus **8**, pp. 364—371.

BOLIN, B., 1955: Numerical forecasting with the barotropic model. Tellus **7**, pp. 27—49.

BOLIN, B., 1956: An improved barotropic model... Tellus **8**, pp. 1—15.

CHARNEY, J., 1955: The use of the primitive equations of motion in numerical prediction. Tellus **7**, pp. 22—26.

ROSSBY, C.-G., 1948: On displacements and intensity changes of atmospheric vortices. J. Marine Research **7**, pp. 175—187.

ROSSBY, C.-G., 1949: On a mechanism for the release of potential energy in the atmosphere. J. Meteor. **6**, pp. 178.

# Statistical Forecasting Operators Based on Dynamical Equations

By DUANE S. COOLEY, Air Force Cambridge Research Center

(Manuscript received August 19, 1957, revised February 14, 1958)

*Abstract*

Statistical forecasting operators are derived on the basis of a simple two-parameter model of the atmosphere. In the course of this investigation, the predictability of pressure-height changes due to the various physical processes specified by this dynamical model is investigated. It is found that the contribution of the non-linear processes to the 12 and 24 hr predictability is small.

## 1. Introduction

In recent years, dynamical forecasting by the numerical integration of partial differential equations describing the fluid motion in certain simplified models of the atmosphere has become a common practice. Among the many mathematical models which have been investigated is that expressed by the equations of thermotropic flow as derived by THOMPSON and GATES (1956). A statistical study of the physical processes expressed by these equations has been undertaken with a view to deriving suitable statistical forecasting operators based directly on the dynamical equations and also with a view to examining the importance of these physical processes for prediction purposes. By this procedure, a forecasting technique is synthesized from the statistical and the dynamic approaches. The statistical approach is similar to those discussed by WIENER (1949), WADSWORTH (1951), WHITE and PALSON (1955), MALONE (1955) and MILLER (1956). The form of the statistical solution to this prediction problem will be shown to be loosely analogous to that of the solution of the dynamic equations by Green's method.

## 2. The Dynamic Equations

The thermotropic equations derived by THOMPSON and GATES (1956) characterize a two-parameter model of atmospheric flow. In this model along with the usual assumptions of hydrostatic, adiabatic and geostrophic flow, the vertical shear of the horizontal wind, or the so-called thermal wind, is assumed to remain constant with height. For flat terrain the equations take the form

$$\nabla^2 \frac{\partial \overline{\psi}}{\partial t} + J(\overline{\psi}, \nabla^2 \overline{\psi}) + \beta \frac{\partial \overline{\psi}}{\partial x} + K J(\overline{\varphi}, \nabla^2 \overline{\varphi}) = 0 \qquad (1)$$

$$\nabla^2 \frac{\partial \overline{\varphi}}{\partial t} + J(\overline{\psi}, \nabla^2 \overline{\varphi}) + J(\overline{\varphi}, \nabla^2 \overline{\psi}) + L J(\overline{\varphi}, \nabla^2 \overline{\varphi}) + \beta \frac{\partial \overline{\varphi}}{\partial x} - \mu^2 \left[ \frac{\partial \overline{\varphi}}{\partial t} + J(\overline{\psi}, \overline{\varphi}) \right] = 0 \qquad (2)$$

where the bar represents an average with respect to pressure in the vertical, $\psi = gzf^{-1}$, $\varphi = RTf^{-1}$, $J$ is the Jacobian operator, $\nabla^2$ is

the Laplacian operator, $K$ and $L$ are functions of pressure only, $\mu^2$ is a positive constant determined by the static stability, $R$ is the gas constant for air, and $g$, $z$, $T$, $f$ and $\beta$ have their usual meanings. In solving these equations numerically, $\bar{\psi}$ is taken as proportional to the 500 mb height and $\bar{\varphi}$ as proportional to the 500—1,000 mb thickness. These equations were solved numerically for a square grid of points about 280 km apart over the United States and Canada. For details of the work, see THOMPSON and GATES (1956).

The solution of partial differential equations (1) or (2) could, presumably, be carried out by Green's method (HILDEBRAND, 1952). Let equation (1) be represented as

$$L\frac{\partial z}{\partial t} + F(x, y) = 0 \qquad (3)$$

Then the solution to the equation at any point $x$, $y$ can be represented formally as

$$\frac{\partial z}{\partial t}(x, y) = \int_{y_1}^{y_2}\int_{x_1}^{x_2} F(\xi, \eta)\, G(x, y; \xi, \eta)\, d\xi\, d\eta \qquad (4)$$

where $G$ is the Green's function for the problem, $\xi$ and $\eta$ are dummy variables of distance in the $x$ and $y$ directions respectively. If the integral solutions are obtained in finite difference form over $q$ grid points on the earth, one may write $\{\underline{X_D}\} = \underline{A}\,\{\underline{F}\}$ (5) where $\{\underline{X_D}\}$ is the column vector of the tendencies $\left(\frac{\partial z}{\partial t}\right)_i$ in this dynamic model at the $q$ grid points, $\{\underline{F}\}$ is the column vector of the values of $F$ at each point and $A$ is the matrix of coefficients representing finite-difference forms of the appropriate Green's function for the problem. In the equations (5) the boundary values of $\frac{\partial z}{\partial t}$ have been incorporated in $F$ for convenience.

### 3. The Statistical Equations

Consider the prediction of $\frac{\partial z}{\partial t}$ by statistical means. It may be treated as a linear least squares multiple regression problem in the multiple time series of $\frac{\partial z}{\partial t}$ and $F$ at the $q$ grid points. For simplicity we will consider that $\frac{\partial z}{\partial t}$ is a deviation from its mean value. For a given point $i$, $\left(\frac{\partial z}{\partial t}\right)_i$ can be approximated by

$$\left(\frac{\partial z}{\partial t}\right)_i = \sum_{j=1}^{q} b_{ij} F_j + e_i \qquad (6)$$

The regression coefficients $b_{ij}$ in (6) are to be determined from $n$ ($\geq q+1$) simultaneous observations of $\left(\frac{\partial z}{\partial t}\right)_i$ and $F_j$'s in such a manner as to minimize the error sum of squares at point $i$ given by

$$\sum_n e^2{}_i = \sum_n \left[\left(\frac{\partial z}{\partial t}\right)_i - \sum_{j=1}^{q} \partial_{ij} F_j\right]^2 \qquad (7)$$

where $\sum_n$ denotes the summation over $n$ observations. When $\sum_n e^2$ is minimized with respect to $b_{ij}$, the following general equation for the coefficients $b_{ij}$ is obtained:

$$\sum_{j=1}^{q} b_{ij} \sum_n F_{ij} F_k = \sum_n F_k \left(\frac{\partial z}{\partial t}\right)_i \quad k = 1.2 \ldots q \qquad (8)$$

This can be written as

$$\sum_{j=1}^{q} b_{ij} \overline{F_j F_k} = \overline{F_k \left(\frac{\partial z}{\partial t}\right)_i} \quad k = 1.2 \ldots q \qquad (9)$$

where the bar indicates an average over the $n$ observations and the barred terms now represent covariances. This system of linear equations can be solved for the $b_{ij}$ by inverting the matrix of covariances $[\overline{F_j F_k}] = A$ and multiplying by the covariance vector $\left[\overline{F_k \left(\frac{\partial z}{\partial t}\right)_i}\right] = P$.

The predicted values of $\frac{\partial z}{\partial t}$ at the $q$ grid points are simply given by the set of equations

$$\{\underline{X_s}\} = \underline{B}\,\{\underline{F}\} \qquad (10)$$

where $\{\underline{X_s}\}$ is the vector of the predicted tendencies $\frac{\partial \hat{Z}}{\partial t}$ in the statistical model at the $q$ grid points, $\{\underline{F}\}$ is the vector of predictor

functions and $\underline{B}$ is the matrix of regression coefficients.

Equation (10) is a statistical analogue of equation (5). The matrix $A$ of the coefficients of equation (5) representing a set of theoretical Green's functions is determined by the form of the equation governing the model and the characteristics of the grid system used. All mathematical models used for weather prediction are highly idealized representations of the true atmosphere. They usually do not include the effects of heating, accelerating wind fields, topography, etc. Those physical processes which are represented by the model cannot be evaluated accurately due to a lack of data over large areas of the globe or due to insufficient accuracy of the available observations. To some extent, statistical prediction suffers from the same inaccuracies and incompleteness of information.

The matrix $B$ of the coefficients $b_{ij}$ in the matrix equation (10) represents a set of empirical Green's functions. Because of its empirical nature, it results from the effects of all physical processes acting on or in the atmosphere. The effects of physical processes which are linearly related to the function $F$ of the initial conditions will be included. This is a result of the fact that in the least-squares sense the procedures by which the $b_{ij}$ were derived result in the best linear combinations of the function $F$ obtainable from the data used.

In actual practice it is necessary to stretch the analogy between the systems represented by the equations (5) and (10). This is because instantaneous values of the contour height tendencies are not available to derive the truly analogous empirical Green's functions of equation (10) and $\frac{\partial z}{\partial t}$ must be approximated by finite height changes over 12 or 24 hours. The Green's functions derived here were not intended primarily for preparing routine forecasts but for studying the relative importance of certain linear and non-linear information about the lower troposphere in making predictions.

## 4. Procedures

The effects on predictability of pressure-height changes due to the physical processes

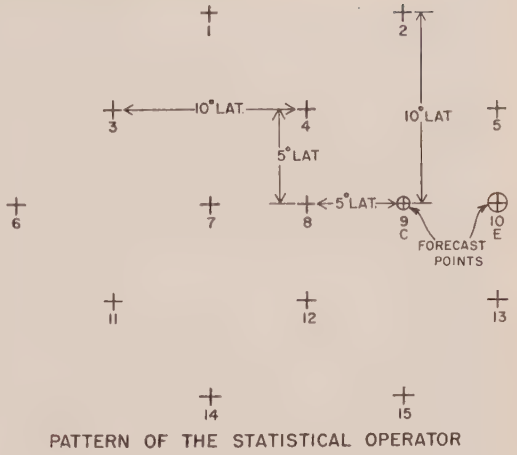


Fig. 1. Grid of 15 points at which values of the predictors were observed.

represented by certain non-linear terms of equations (1) and (2) were studied from the evaluations of finite difference approximations to these terms. First, the predictability of heights obtainable from certain linear combinations of heights was determined. Then in various ways the linear combinations of heights were used jointly with the non-linear functions as predictors and differences in predictability were noted.

The predictor functions $F$ were evaluated over a grid of 15 points of the form shown in fig. 1. The positions of the predictand points are circled. The data were gathered for various positions of the grid over the United States and southern Canada. However, the relative positions and orientations of the grid points were maintained.

The predictor functions $F$ at the 15 grid points were of the following form:

$F_1$ through $F_{15}$ : $Z_5$, 500 mb height
$F_{16}$ through $F_{30}$ : $Z_{10}$, 1,000 mb height
$F_{31}$ through $F_{45}$ : $J_1 \equiv J(Z_5, \nabla^2 Z_5)$
$F_{46}$ through $F_{60}$ : $J_2 \equiv J[(Z_5-Z_{10}), \nabla^2(Z_5-Z_{10})]$
$F_{61}$ through $F_{75}$ : $J_3 \equiv J(Z_{10}, \nabla^2 Z_{10})$
$F_{76}$ through $F_{90}$ : $J_4 \equiv J(Z_5, Z_5-Z_{10})$

These represent geostrophic approximations to the terms appearing in equations (1) and (2). $J_1$ expresses the advection of the vorticity of the 500 mb geostrophic wind by the 500 mb geostrophic wind. It is an approximation to the term representing the vorticity advection

in a barotropic model. $J_2$ is a measure of the advection of the vorticity of the thermal wind from 1,000 to 500 mb by this thermal wind. $J_3$ expresses the advection of the vorticity of the geostrophic wind at 1,000 mb by the 1,000 mb geostrophic wind. Finally, $J_4$ is a measure of the vertically averaged temperature advection in the lower troposphere. It is evaluated from the 500 to 1,000 mb thickness gradient and the 500 mb geostrophic wind.

Statistical operators were derived for the prediction of the 12 and 24-hour contour height changes at 1,000 and 500 mb. Calculation of the linear regression equations and the associated multiple correlation coefficients was performed using data provided by the Joint Geophysics Research Directorate—Air Weather Service Numerical Prediction Project. These data were abstracted from sixty weather maps at the 1,000 and 500 mb levels, 0300 and 1500 GCT, 1 to 31 January 1953. Five or six sets of observations were taken from each of the maps, making a sample size of 336 observations. Dr. W. L. Gates made available his IBM 701 EDPM program for computing the initial values of the Jacobian terms of equations (1) and (2).

If the regression analysis were carried out using all of the predictors, a $90 \times 90$ predictor covariance matrix would have to be inverted. Because of the limitations of the machine storage capacity and the cost of such calculations, and also for reasons of statistical stability, no more than 60 predictors were used simultaneously. The following combinations of predictors were used:

| | | |
|---|---|---|
| 1) : $Z_5$, $Z_{10}$ | Linear case, | 30 predictors |
| 2) : $Z_5$, $J_1$ | Barotropic case, | 30 predictors |
| 3) : $Z_5$, $Z_{10}$, $J_1$ | | 45 predictors |
| 4) : $Z_5$, $Z_{10}$, $J_1$, $J_2$ | | 60 predictors |
| 5) : $Z_5$, $Z_{10}$, $J_1$, $J_3$ | | 60 predictors |
| 6) : $Z_5$, $Z_{10}$, $J_1$, $J_4$ | | 60 predictors |

If the covariance matrix of any particular combination of predictors is designated as $A_s$ then equation (9) can be expressed in simple matrix form as

$$A_s B = P \tag{11}$$

where $B$ is the matrix of regression coefficients and $P$ is the predictor and predictand covariance matrix. Then as indicated previously, the coefficients in $B$ can be obtained by inverting $A_s$, since

$$B = A_s^{-1} P \tag{12}$$

The basic matrix inversion program used (employing the von Neumann—Goldstine method of matrix inversion, 1947) was capable of inverting 50th order matrices. Since three of the matrices ($A_4$ to $A_6$) are of 60th order, it was necessary to use a partitioning procedure and to obtain the inverse matrices by the escalator method (HOUSEHOLDER, 1953).

## 5. Results

The predictability of the dependent variables as a function of the various predictor combinations is readily measured by the percent reduction of the variance of the predictands as determined from the sample of data studied. (This percent reduction of the variance explained in the dependent data is equal to the square of the multiple correlation coefficient $R$ between all the predictors and the predictand and will henceforth be designated as $R^2$.) From such comparisons we can deduce information about the relative importance of physical processes described by the terms of the thermotropic equations as they affect the statistical predictions.

The percent reductions of the variances of the forecast height changes at the central forecast point (point 9 in fig. 1) using various combinations of predictors are listed in Table 1. Comparison of the first two lines of this table indicates that the linear terms $Z_5$, $Z_{10}$ yield better predictions of the 500 mb height changes than does the combination of information from $Z_5$ and the non-linear barotropic term $J_1$. The suggestion here is that linear baroclinic information is more important than non-linear barotropic information in predicting 500 mb height changes. When the predictors $Z_5$, $Z_{10}$, $J_1$ are combined as in $A_3$ some improvement in the 500 mb forecast is obtained indicating that the non-linear barotropic vorticity advection term does appear to add some useful information to that obtainable from the simple linear combination of heights at two levels.

In the fourth line of Table 1 are shown the effects of adding 15 values of $J_2$, the term representing the advection of the vorticity

**Table 1. Reduction of variance ($R^2$, percent, where $R$ is the multiple correlation coefficent) of predicted height changes at the central forecast point using various predictors.**

| | Predictands | | | |
|---|---|---|---|---|
| Predictors | $\triangle_{12}Z_5$ | $\triangle_{24}Z_5$ | $\triangle_{12}Z_{10}$ | $\triangle_{24}Z_{10}$ |
| $A_1 : Z_5, Z_{10}$ | 72 | 69 | 68 | 70 |
| $A_2 : Z_5, J_1$ | 66 | 58 | 50 | 51 |
| $A_3 : Z_5, Z_{10}, J_1$ | 75 | 72 | 72 | 72 |
| $A_4 : Z_5, Z_{10}, J_1, J_2$ | 77 | 73 | 73 | 73 |
| $A_5 : Z_5, Z_{10}, J_1, J_3$ | 76 | 72 | 73 | 73 |
| $A_6 : Z_5, Z_{10}, J_1, J_4$ | 78 | 76 | 79 | 77 |

of the thermal wind from 1,000 to 500 mb by the thermal wind in that layer, to the 45 predictors used in the third line. This term appears to add very little to the prediction of the 500 mb height changes. As might be expected, the term $J_3$, the advection of the 1,000 mb vorticity by the 1,000 mb geostrophic wind, which was used in arrangement $A_5$ contributed almost nothing to the prediction. The best set of 60 predictors appears to be that in the sixth row. The added predictors in $A_6$ are the values of the $J_4$ term which measure the advection of the mean virtual temperature in the lower troposphere by the 500 mb geostrophic wind.

The prediction of the 1,000 mb height changes as shown in the third and fourth columns of Table 1 follows a similar pattern for the most part. However, the predictors $Z_5$ and $J_1$ do quite poorly at the 1,000 mb level as might be expected, since they include information only from the 500 mb level. There does not appear to be the marked difference in predictability between 500 and 1,000 mb height changes usually found in numerical forecasting results (THOMPSON and GATES, 1956). Thus, the two non-linear terms which appear to contribute some information over and above that given by linear combinations of the heights of the two pressure surfaces are the barotropic vorticity advection term $J_1$ and the temperature advection term $J_4$.

Actually, higher values of $R^2$ were obtained for predictions of height change at the easternmost forecast point of the network, indicating that this grid point arrangement relative to the central forecast point did not include enough information from the west. For the eastern predictand the level of accuracy reaches 84 percent using the predictors in $A_6$.

An attempt was made to test the significance of the improvement gained by additional predictors. Since the sample of 336 observations of each predictor was obtained from 60 consecutive weather maps at 12 hour intervals, the observations are not independent in either time or space. Because of this, the tests of significance applied must be considered as necessary but not sufficient conditions for establishing the reality of the difference in predictability.

Table 2 shows the improvement in $R^2$ obtained by increasing the number of predictors and the values of the $F$ ratio calculated from the following formula given by ANDERSON and BANCROFT (1952):

$$F = \frac{R_r^2 - R_k^2}{\left(1 - R_r^2\right)\frac{r-k}{n-r-1}} \qquad (13)$$

Using this, one can determine whether the last $r-k$ of the total of $r$ variates made a significant contribution to $R_r^2$, the percent reduction of the variance of the predictand, above the percent reduction $R_k^2$ due to the first $k$ variates. The $F$ ratio then is used to test the null hypothesis that each of the last $r-k$ regression coefficients is equal to zero. Here $n$ is the sample size and $r-k$ would be the number of degrees of freedom of the numerator, the increase in variance. The quantity $n-r-1$ is the number of degrees of freedom of the unexplained variance, $1-R_r^2$, in the sample.

On the basis of this test, it would appear that the only combination of 30 linear and 30 non-linear predictors which makes a significant contribution toward improvement of the $R^2$ of the predictands at the central forecast point over all smaller combinations of predictors is that designated by $A_6$ (columns 7 to 9 of Table 2). For 11 of these 12 tests involving $A_6$, the calculated $F$ ratio indicates that the additional $r-k$ predictors make a significant contribution to the reduction at better than the 1 percent level.

The regression coefficients for the simple linear case for a 24 hour forecast of the 500 mb and 1,000 mb height changes are shown in fig. 2. Note in the upper left, the empirical influence function relating the 500 mb height to the height change. As might be expected, the greatest influence on the forecast point (circled) is from the height at that point itself.

**Table 2. $F$ ratios as measures of significance of improvement ($\triangle R^2$) of per cent reduction of variance of predicted height changes at the central forecast point using various arrangements of predictors. 5 and 1 per cent significance levels of $F$ are given at foot of table.**

| | | Predictors | | | | | | | | | | |
|---|---|---|---|---|---|---|---|---|---|---|---|---|
| | | 1 | 2 | 3 | 4 | 5 | 6 | 7 | 8 | 9 | 10 | 11 |
| | | $A_4$ vs. $A_1$ | $A_4$ vs. $A_2$ | $A_4$ vs. $A_3$ | $A_5$ vs. $A_1$ | $A_5$ vs. $A_2$ | $A_5$ vs. $A_3$ | $A_6$ vs. $A_1$ | $A_6$ vs. $A_2$ | $A_6$ vs. $A_3$ | $A_3$ vs. $A_1$ | $A_3$ vs. $A_2$ |
| $\triangle_{12}Z_5$ | $\triangle R^2$ | 5.3 | 10.9 | 1.7 | 4.5 | 10.1 | 0.9 | 6.8 | 12.4 | 3.1 | 3.6 | 9.3 |
| | $F$ | 2.11 | 4.34 | 1.33 | 1.73 | 3.89 | 0.68 | 2.87 | 5.25 | 2.66 | 2.83 | 7.22 |
| $\triangle_{24}Z_5$ | $\triangle R^2$ | 3.9 | 15.1 | 1.5 | 3.2 | 14.4 | 0.8 | 7.2 | 18.4 | 4.7 | 2.4 | 13.6 |
| | $F$ | 1.32 | 5.14 | 0.99 | 1.06 | 4.77 | 0.50 | 2.78 | 7.12 | 3.68 | 1.66 | 9.28 |
| $\triangle_{12}Z_{10}$ | $\triangle R^2$ | 4.3 | 23.0 | 1.3 | 4.3 | 23.0 | 1.2 | 10.3 | 29.0 | 7.2 | 3.0 | 21.7 |
| | $F$ | 1.46 | 7.76 | 0.87 | 1.43 | 7.72 | 0.82 | 4.44 | 12.52 | 6.26 | 2.06 | 14.76 |
| $\triangle_{24}Z_{10}$ | $\triangle R^2$ | 3.4 | 22.6 | 1.3 | 3.4 | 22.7 | 1.4 | 7.5 | 26.7 | 5.5 | 2.0 | 21.3 |
| | $F$ | 1.15 | 7.76 | 0.92 | 1.18 | 7.80 | 0.97 | 3.03 | 10.85 | 4.43 | 1.39 | 14.66 |
| | $F_5$: | 1.66 | 1.66 | 2.10 | 1.66 | 1.66 | 2.10 | 1.66 | 1.66 | 2.10 | 2.10 | 2.10 |
| | $F_1$: | 2.06 | 2.06 | 2.91 | 2.06 | 2.06 | 2.91 | 2.06 | 2.06 | 2.91 | 2.91 | 2.91 |

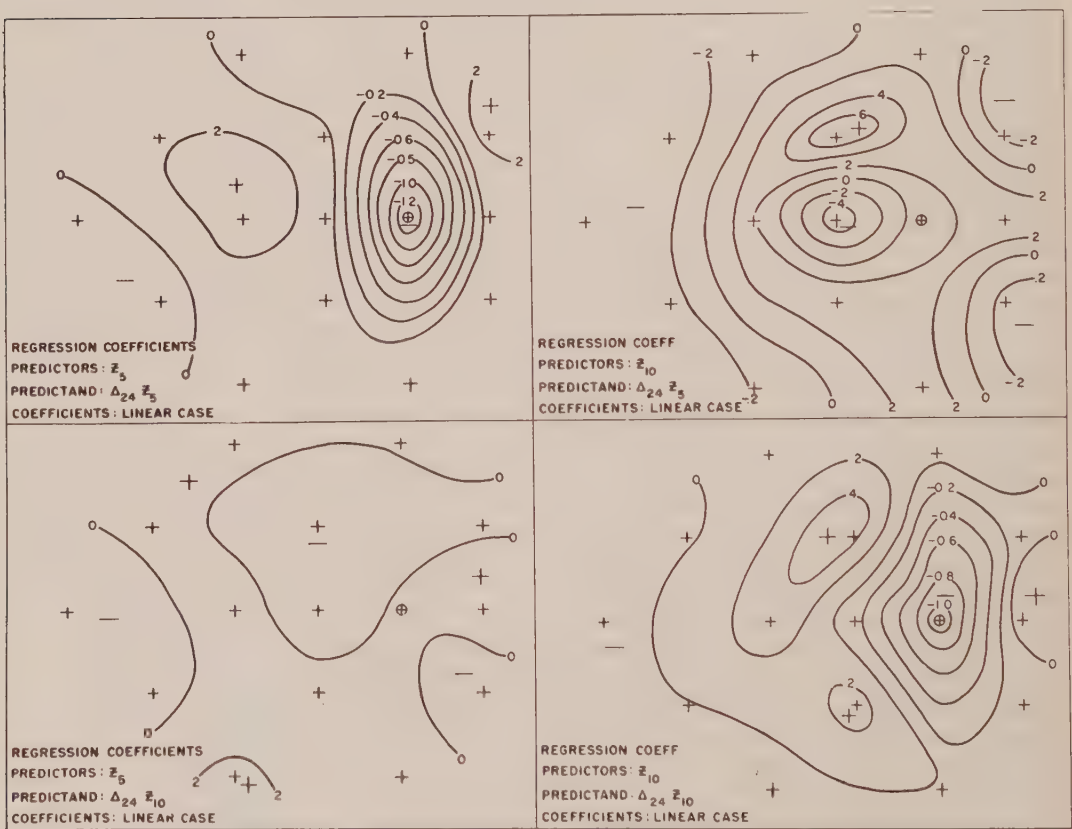


Fig. 2. Regression coefficients for the simple linear case for a 24 hour forecast of the 500 and 1,000 mb height changes using 15 values each of 500 mb and 1,000 mb height as predictors. The forecast is made for the circled point.

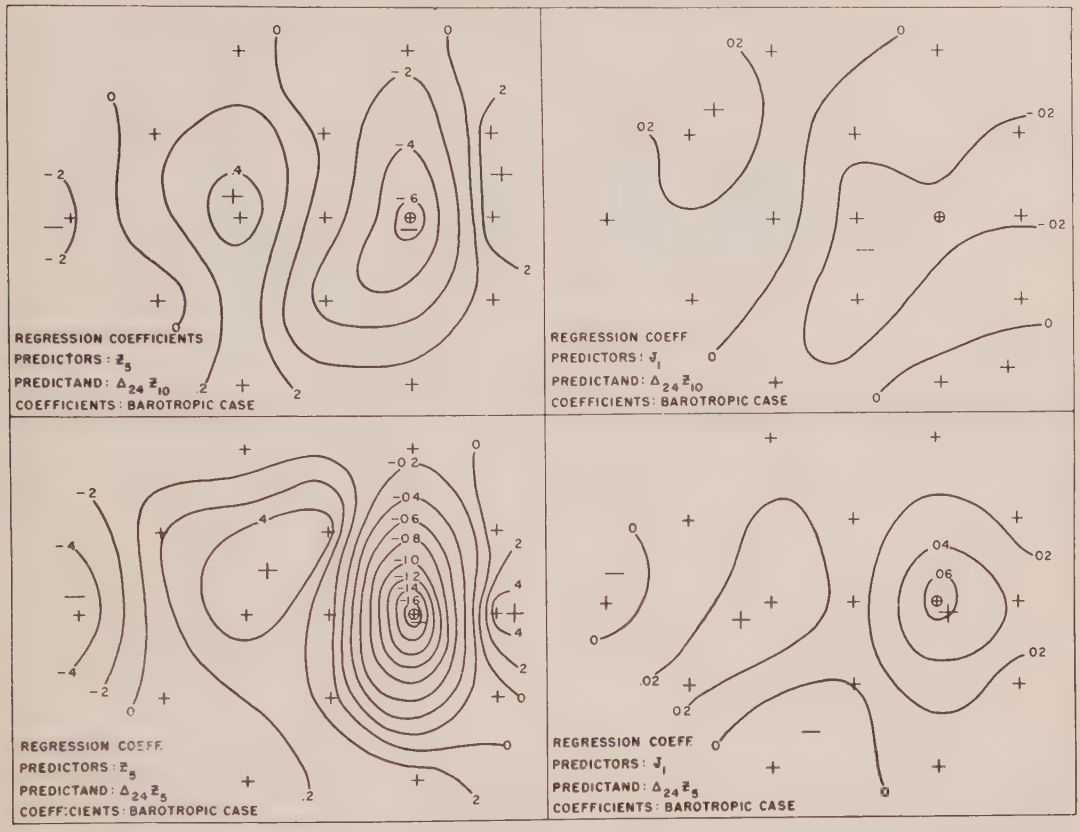


Fig. 3. Regression coefficients for the barotropic case for a 24 hour forecast of the 500 and 1,000 mb height changes using 15 values each of $Z_5$ and $J_1$ as predictors. The forecast is made for the circled point.

If the height is above normal, the tendency is for a negative change. But it can be seen from the upper right of fig. 2 that the influence of the 1,000 mb surface is quite important in predicting the 24-hr 500 mb height change. These empirical influence functions are of course more irregular than the Green's functions derived from the partial differential equations. In fig. 3, the maps show the regression coefficients for the case we have referred to as the barotropic case. Again the greatest weight is attached to the forecast point itself, but the barotropic vorticity advection term $J_1$ appears to affect the forecast only slightly.

Fig. 4 shows the coefficients for the forecast of $\triangle_{24} Z_5$ using 60 predictors which are values of the four variables $Z_5$, $Z_{10}$, $J_1$ and $J_4$. In fig. 5, the coefficients for forecasting $\triangle_{24} Z_{10}$ are shown using the same predictors as in fig. 4.

An example of a forecast made from the best 60-term operators is shown in fig. 6. In this forecast for 0300 GCT, 22 January 1953, over the eastern United States the agreement with observed changes is fairly good both at 500 and 1,000 mb. The correlation between forecast and observed 24-hour height changes at 500 mb is 0.91 and at 1,000 mb is 0.77.

## 6. Critical Comments

Some critical comments should be made with regard to the interpretation of the foregoing results.

1. In the process of solution of the partial differential equations, the field of the instantaneous height tendency $\frac{\partial z}{\partial t}$ is calculated and the values are assumed constant for a short time period, perhaps one hour. Using

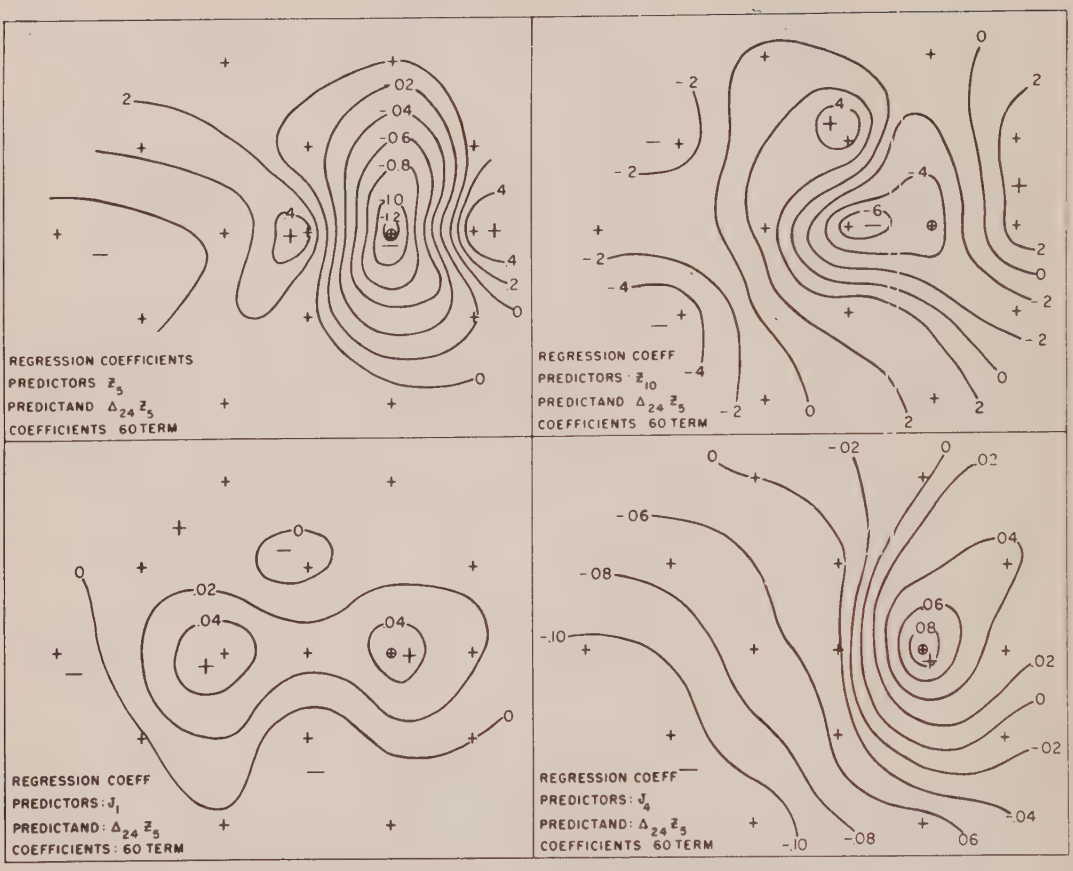


Fig. 4. Regression coefficients for a 24 hour forecast of the 500 mb height change using 15 values each of $Z_5$, $Z_{10}$, $J_1$ and $J_4$ as predictors. The forecast is made for the circled point.

these height changes, a new height field is obtained and the process is iterated to determine the height field at some later time. In the statistical process, the initial fields of the predictors $F$ are related directly to the 12 or 24 hour height changes. Because of this difference, the conclusions drawn from the results of the statistical study do not permit one to make fully conclusive inferences about the effectiveness of non-linear terms in numerical weather prediction by purely dynamical methods.

2. It is of interest to speculate on the small increase of predictability due to the non-linear terms. Presumably, if a set of values of one of the non-linear terms were used alone as a predictor, it would give a significantly good prediction of the height change. But this prediction might not be significantly better than one could obtain from a linear combination of the heights. This implies that much of the information contained in the quadratic terms is already included in the linear terms. Since the non-linear terms involving the Laplacian are computed from third order differences of heights or thicknesses, errors in the data could be amplified and cause large errors in these terms so that they fail to aid the prediction significantly. This point may be illustrated by the fact that in this study the simplest Jacobian, $J_4$, gave more significant results than the Jacobians representing higher order differences.

3. If the statistical operators are applied to

independent data it can be expected that the percent reduction will be reduced. A discussion of the expected reduction of $R^2$ is given by LORENZ (1956).

4. The significance tests applied as described above must be considered as necessary but not sufficient conditions for establishing the reality of the differences in predictability. Since the 336 observations of each variable came from only 60 weather maps at each level and the maps are 12 hours apart, correlations among the predictor data must be rather high in both space and time. Consequently, the number of degrees of freedom used in the significance tests is not realistic and the high significance indicated for some of the cases is seriously questionable.

Although this study indicates that the non-linear terms add only slightly to the linear statistical prediction, one should not infer directly that their value is small in dynamical forecasting. However, it is not believed that the statistical and dynamical forecasting techniques are so greatly different that there are not some serious implications about the relative importance of these non-linear terms for dynamical forecasting also.

## 7. Acknowledgments

The writer is indebted to Dr. Robert M. White for his considerable advice throughout the course of this work. Thanks also go to Mrs. Florence A. Mulkern who assisted in the

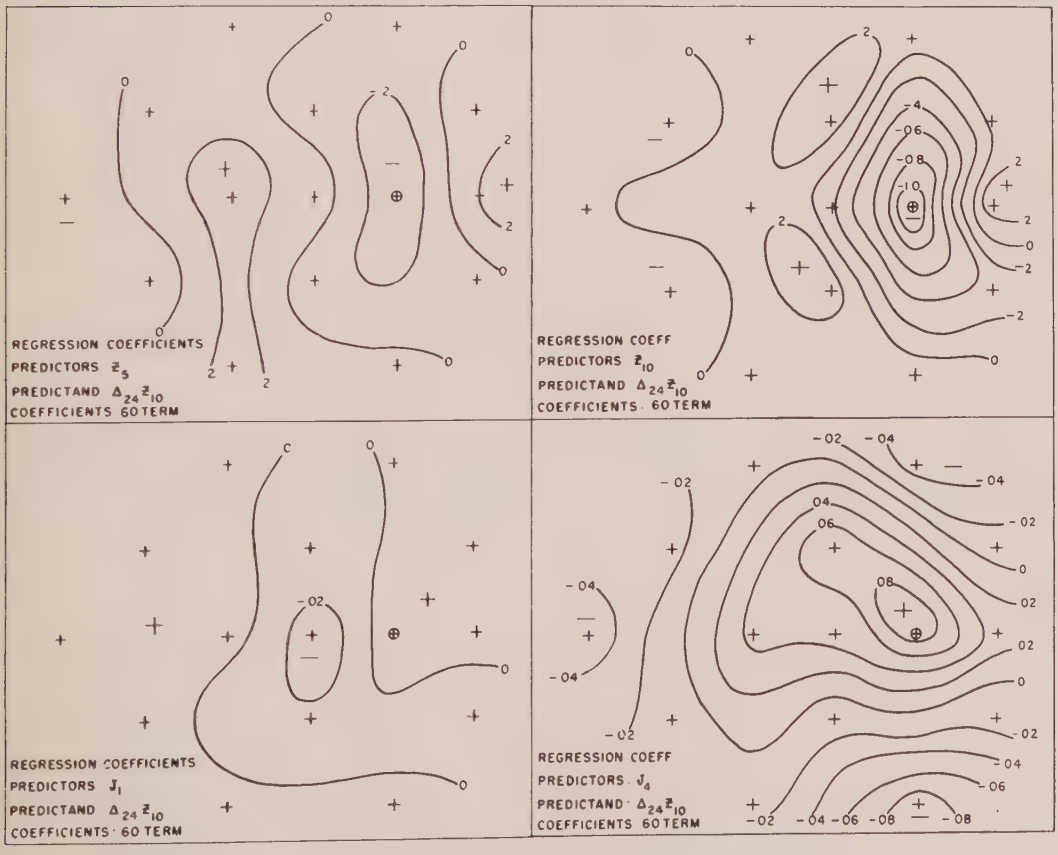


Fig. 5. Regression coefficients for a 24 hour forecast of the 1,000 mb height change using 15 values each of $Z_5$, $Z_{10}$, $J_1$ and $J_4$ as predictors. The forecast is made for the circled point.

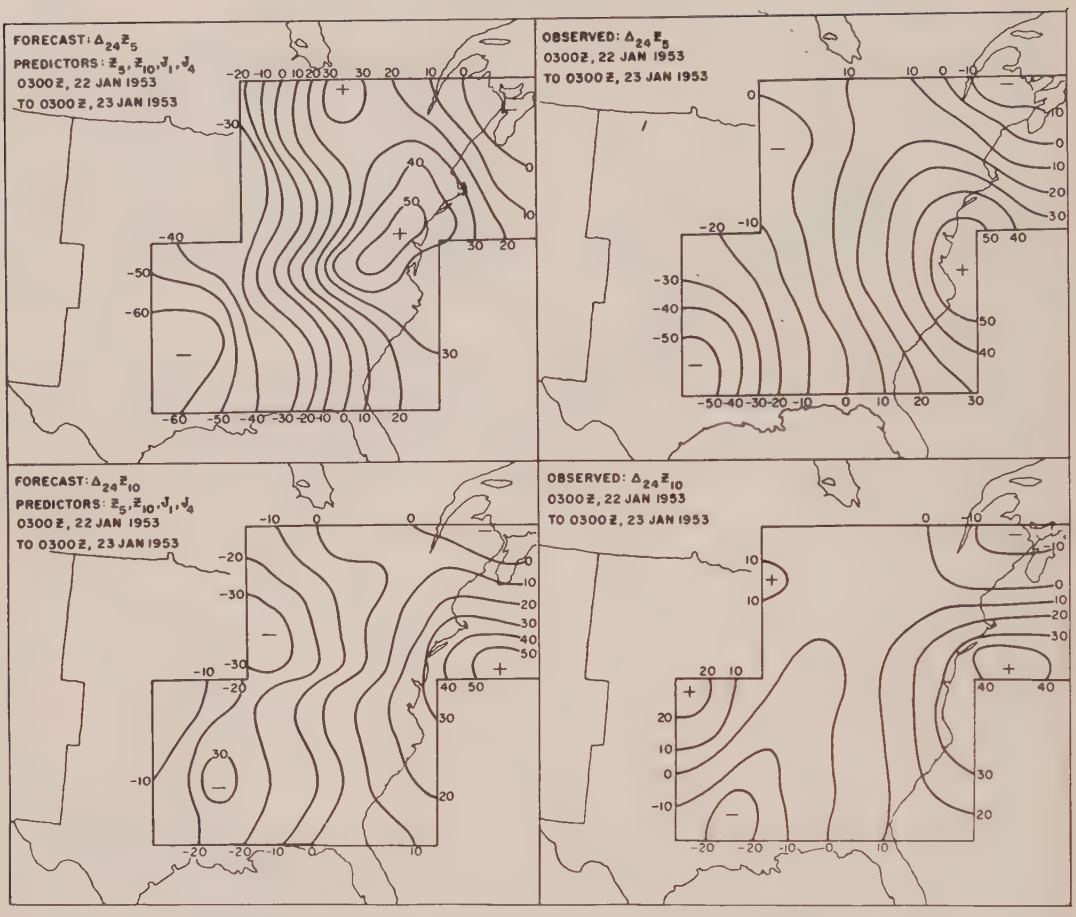


Fig. 6. Forecast and observed 24 hour height changes for the period ending 0300 GCT 23 January 1953. 500 mb above and 1,000 mb below. Forecasts were made using the best 60-term regression equations.

program preparation and in the production of computations on the IBM model 701 computer. Calculations were performed on an IBM 701 EDPM at International Business Machines Corporation in New York and on the IBM 701 at the Joint Numerical Weather Prediction Unit, U.S. Weather Bureau, Suitland, Maryland.

## REFERENCES


Anderson, R. L., and Bancroft, T. A., 1952: *Statistical theory in research*, New York, McGraw-Hill, pp. 168—172.

Hildebrand, F. B., 1952: *Methods of applied mathematics*. New York, Prentice-Hall, pp. 388—461.

Householder, A. S., 1953: *Principles of numerical analysis*. New York, McGraw-Hill, 274 pp.

Lorenz, E. N., 1956: *Empirical orthogonal functions and statistical weather prediction*. Scientific Rep. No. 1, Contract AF 19(604)-1566, Cambridge, Massachusetts Institute of Technology, 49 pp.

Malone, T. F., 1955: Application of statistical methods in weather prediction. *Proc. Nat. Acad. Sci.*, **41**, 806—815.

Miller, R. G., 1956: Statistics and the predictability of weather. Abstract in *Bull. Amer. Meteor. Soc.*, **35**, 495—496.

Thompson, P. D., and Gates, W. L., 1956: A test of numerical prediction methods based on the barotropic and two-parameter baroclinic models. *J. Meteor.*, **13**, 127—141.

von Neumann, J., and Goldstine, H. H., 1947: Numerical inverting of matrices of high order, *Bull. Am. Math. Soc.*, **53**, pp. 1021—1099.

Wadsworth, G. P., 1951: Application of statistical methods to weather forecasting. *Compendium Meteor.*, Boston, Amer. Meteor. Soc. 849—855.

White, R. M., and Palson, Jr., W. C., 1955: On the forecasting possibilities of empirical influence functions. *J. Meteor.*, **12**, 478—485.

Wiener, N., 1949: *Extrapolation, interpolation and smoothing of stationary time series*. Cambridge, Technology Press, Massachusetts Institute of Technology, 163 pp.

# On Pyrheliometric Measurements

By ANDERS ÅNGSTRÖM, Meteorological and Hydrological Institute of Sweden, Stockholm

(Manuscript received February 5, 1958)

## *Abstract*

Pyrheliometric measurements are now introduced in the meteorological practice to an extent which makes a condensed survey over the present status desirable.

In the following I have combined the main content of the survey on the pyrheliometric scales, given by the International Radiation Commissions, with a description of the present modernized type of the Ångström Pyrheliometer. I have added a critical examination of its function and the sources of error which ought to be avoided at its operation. A detailed survey of its construction seems justified by the fact that it is the only standard instrument at present available in the market, where institutes can easily determine its physical constants, thus controlling the basis for *absolute measurements* of solar radiation. I have added an Annex containing a simple theory of the "edge effect" in the pyrheliometer. The main content of the annex coincides practically with the theory I gave already in 1914, but I repeat it here with some minor corrections together with a discussion of the factors influencing the effect and also of the results of practical experiments.

The important result is derived, that the edge correction is to some extent dependent on the internal convection within the pyrheliometer, and may from this reason vary between about 1.3 and 3.8 percent of the measured radiation. In the new constructions, now available in Sweden, this error is eliminated.

## I. Pyrheliometric scales

In meteorological services and institutes radiation measurements have normally been standardized by one of two types of instrument, the Abbot Silver disc pyrheliometer or the Ångström compensation pyrheliometer. The silver disc instrument is calibrated by reference to a calorimeter maintained by the Astrophysical Observatory of the Smithsonian Institution, the sun being used as a source. The Ångström compensation pyrheliometer is now calibrated at Stockholm at the Meteorological and Hydrological Institute by reference to a standard Ångström instrument, earlier used for such calibrations at the Physical Institute at Uppsala. The calibration is checked and controlled in every special case by comparison with the instrument factor obtained by measuring the physical constants of the sensitive part of the instrument (see description given below).

### *1. The Smithsonian Pyrheliometric Scale*

The history of the Smithsonian scale of radiation may be studied in the publications, especially the annals, of the Astrophysical Observatory of the Smithsonian Institution. It is important to note that in 1932, following the introduction of an improved calorimeter, the Institution announced that the Scale of 1913 has an error, measurements in this Scale being high by 2.5 percent; this has been confirmed in 1934, 1947 and 1952. Nevertheless, the Smithsonian Institution has continued to standardize instruments in terms of the Scale of 1913 in order to preserve continuity in series of measurements and particularly in the publication of its solar constant

determinations. The correction of −2.5 % has, as far as is known, not been applied in meteorological practice. For further details see especially Annals of the Astrophysical Observatory of Smithsonian Institution, Vol. 7, 1954, p. 25.

*2. The Ångström pyrheliometric Scale*

The Ångström Scale is based on the compensation pyrheliometer constructed as to its main principle, by K. Ångström in 1893 and recommended in 1905 by the International Meteorological Organization for meteorological radiation measurements. The Scale is, and has been, embodied in a small group of specimen instruments, other instruments being substandards, not used absolutely. (As regards *absolute* measurements with the Ångström pyrheliometer, see description below.) When the Ångström instrument is used absolutely it is necessary to apply a certain correction to the readings, mainly on account of the so-called "edge effect" (A. Ångström 1914). The present estimate, following recent measurements in Stockholm by F. Lindholm (Lindholm 1958) of the magnitude of the required correction, is slightly above 2 percent, measurements on the uncorrected scale being too low. This correction has never been applied when substandard instruments have been calibrated in Sweden; in meteorological practice measurements have always been referred to the original Ångström scale, before the new international scale of 1956 was introduced.

*3. Comparison of the existing pyrheliometric Scales*

There have been frequent intercomparisons of the Ångström and Smithsonian scales, through substandard instruments representing either scale. Many comparisons of substandard instruments have been made with the sun as source. The advantage of such comparisons lies in the fact that they are referred to the same source as the one which is the object of the field measurements. The difficulty of such comparisons is that different areas of circumsolar sky are covered by the different instruments, and the intensity of radiation therefrom is widely variable with time and place, so that the silver disc and the Ångström instrument are not strictly comparable if the sun is used as source. As the circumsolar sky radiation is generally increasing with an increase in the scattering power of the atmosphere, one would expect that the difference between two radiometers, of which the one has a wider opening than the other, would vary with the scattering. A variation in the percentic difference with turbidity, airmass and height of the station above sea-level must therefore occur. As the difference due to these causes generally must be rather small in the case of the relation between readings with the Silver disc and the Ångström instrument respectively, the field measurements have not, however, given a clear indication of it.

The difficulty introduced by the circumsolar sky radiation is eliminated in laboratory comparisons with a lamp as a source, but other difficulties are here introduced, especially in the case of the Silver disc, e.g. it is not easy to maintain an even distribution of radiation over the comparatively large sensitive surface.

*4. Summary of results of the comparisons*

The generally accepted mean difference between measurements of solar radiation by instruments standardized by the Smithsonian Institution on the 1913 scale and by instruments standardized on the uncorrected Ångström scale may be expressed by the relation:

$$\frac{\text{SI}}{\text{Å}} = 1.035$$

Individual determinations show, however, considerable scatter. The mean of laboratory determinations, on artificial sources, give:

$$\frac{\text{SI}}{\text{Å}} = 1.028$$

A single laboratory determination of the difference between the (British) National Physical Laboratory (NPL) standard Scale of radiation and a substandard representing the uncorrected Ångström Scale shows readings on the latter Scale to be the lower in the relation:

$$\frac{\text{NPL}}{\text{Å}} = 1.005$$

A series of intercomparisons at Davos (1934) between a substandard Ångström instrument

and a Potsdam absolute pyrheliometer (PAP) of calorimeter type, using the sun as source, show a relation:

$$\frac{\text{PAP}}{\text{Å}} = 1.010$$

The Smithsonian Institution considers the 1913 scale to give too high values in the relation.

$$\frac{\text{SI}}{\text{True Scale}} = 1.025$$

Let us designate the Smithsonian Scale of 1913, less 2.5 percent the corrected Smithsonian Scale. On the other hand the edge effect seems to demand a correction of about +2 percent to the Ångström Scale. Let us designate the uncorrected Ångström Scale multiplied by the factor 1.02, the Ångström corrected Scale. The comparison of substandard instruments using the sun as source suggests that readings on the Ångström corrected Scale are in the mean 1.0 percent higher than on the Smithsonian corrected scale. Comparison on laboratory sources suggests that this figure is 1.7 percent. The single comparison of Guild suggests that measurements on the Ångström corrected Scale are 1.5 percent higher than measurements on the N.P.L. Scale. The Potsdam comparisons show that measurements on the Ångström corrected Scale are 1 percent higher than those referred to the Potsdam absolute pyrheliometer. The mean difference of 0.7 percent between comparisons using the sun and those using laboratory sources is of the magnitude to be expected from considerations of the apertures of standard and substandard instruments and an average distribution of circumsolar radiation.

*Conclusions.* In view of the facts and consideration given above the International Radiation Commissions at a meeting at Davos, September 1956

*Recommended the adoption of a new pyrheliometric Scale to be known as the International Pyrheliometric Scale 1956. Measurements made according to the original Ångström Scale should be increased by 1.5 percent. As the difference between the Smithsonian Scale of radiation as revised in 1913, and the original uncorrected Ångström Scale has been found to be 3.5 percent on the average for measurements of solar radiation, measurements made according to the Smithsonian Scale of 1913 should be reduced by 2.0 percent.*

## II. Present construction and use of the K. Ångström compensation pyrheliometer

1. *General principle*

The receiver of the instrument consists of two thin strips of manganin, made as identical in every way as possible. One strip is exposed to the sun radiation, while the other one is screened from the sun. Through the screened strip an electric current is passed, the intensity of which is regulated so that heating of the two strips is the same.

To secure this thermojunctions connected through a sensitive galvanometer are attached to the central points at the back side of the two strips. A current through the screened strip is adjusted, so that the galvanometer shows no deflection.

Let $q$ be the radiation per second per square centimeter, $a$ the width of the strips, $\beta$ the absorbing power of their blackened surface, $r$ their resistance in ohm per unit of length, and $i$ the intensity of the compensation current in ampere.

We then have:

$$a\beta q = \frac{ri^2}{4.186} \qquad (1)$$

from which:

$$q = \frac{ri^2}{4.186 \cdot a \cdot \beta} \text{ gram calories/second} \qquad (2)$$

or

$$Q = \frac{60ri^2}{4.186 \cdot a \cdot \beta} \text{ gram calories/minute} \qquad (3)$$

If the intensity of radiation be expressed in watts per square centimeter, we have

$$q' = \frac{ri^2}{a \cdot \beta} \qquad (4)$$

In order to measure the radiation we have to determine $\beta$, $a$ and $r$, a determination which can be made once for all. As the radia-

tion is generally given in gram calories per square centimeter and minute, we put:

$$\frac{60 \cdot r}{4.186 \cdot a \cdot \beta} = K \qquad (5)$$

where $K$ is "the constant" of the instrument. Knowing the constant we may, through measuring the compensation current, obtain the radiation from the equation:

$$Q = Ki^2 \qquad (6)$$

As the strips are exposed in practically the same way to the air and have the same temperature, corrections for cooling and convection are in this method eliminated. (On a slight influence of convection on the edge correction see the annex.)

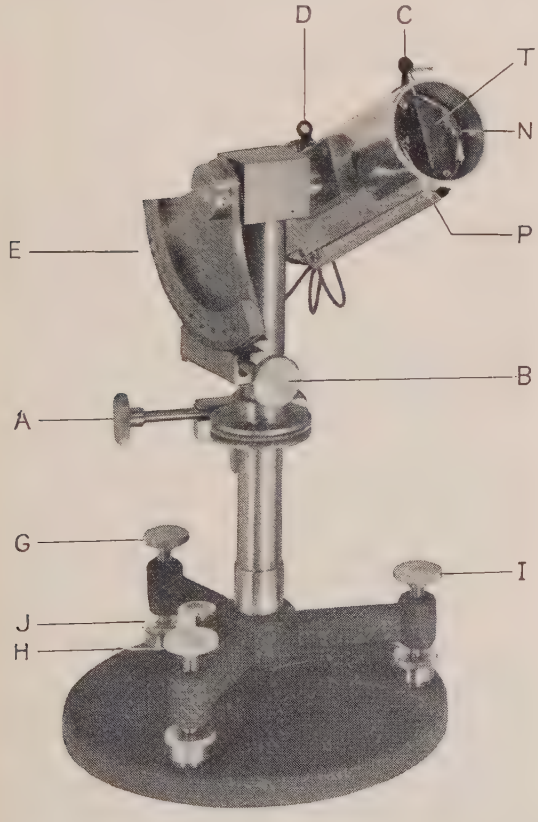


FIG. 1. FRONT VIEW OF PYRHELIOMETER. FILTER HOLDER REMOVED.

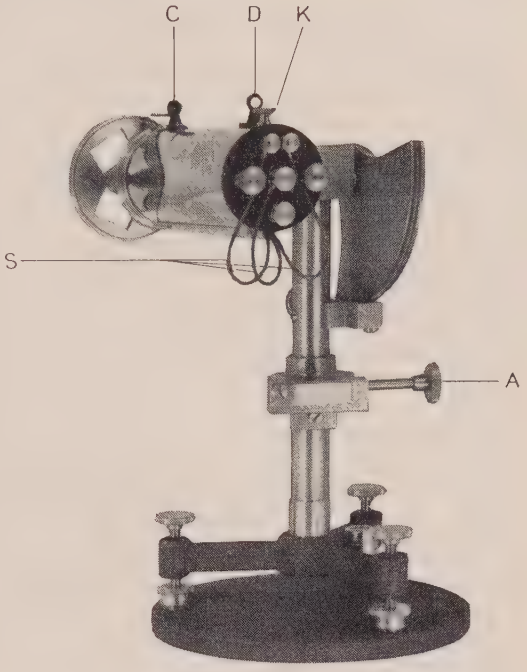


FIG. 2. BACK VIEW OF PYRHELIOMETER WITH FILTER HOLDER IN PLACE.

2. *Details of construction*

The instrument consists of a cylindrical metal tube – see Figs. 1 and 2 – in the rear of which the manganin strips are mounted on a strip-holder. The tube itself is mounted on a holder and can by means of the two knobs (A) and (B) be directed against the sun. The right direction is controlled by means of the diopters (C) and (D). The height angle of the sun may be read to a tenth of a degree on the scale (E). A condition for obtaining a correct height angle is that the whole instrument has been adjusted to the horizontal plane by means of the screws (G, H, I) and the libel (J).

The stripholder at the back of the tube can be removed for inspection by loosing the screw (K) and decoupling the three wires (S) (see fig. 2).

The three wires (S) are connected to the screen (T) by which the strips can be screened from the sun, in such a way that by the alternate screening of the strips *the current is auto-*

*matically passed through the strip which is in shadow.*

On the back side of the two manganin strips, two thermocouples (Q) and (R) of copper-constantan, electrically isolated from the strips, are mounted. The thermocouples are connected with two contact screws on the back side of the strip holder. To these same screws the wires to the sensitive galvanometer shall be connected. Two other screws on the back side of the strip holder serve as connections for the wires of the circuit which includes electric cells, milliammeter and slide resistance.

3. *Auxiliary instruments*

a) *The sensitive galvanometer* which serves to show the temperature difference between the strips, is used as a zero instrument. It shall be able to indicate whether temperature differences larger than about 0.01 of a degree C occur, but we are not concerned with the absolute value of its sensitiveness. Its inner resistance ought not to be too large. A sensitiveness of $1 \cdot 10^{-8}$ to $5 \cdot 10^{-8}$ amperes pro division, and an inner resistance of about 10 ohms are suitable. For many conditions a so called "light spot" galvanometer (for instance the type Norma, delivered by Philips) can be recommended. The pointer of the common ammeter type is here replaced by a small light spot crossed by a fine dark line, the position of which can be read on the scale. A number of other types can be used provided the sensitiveness is what has been suggested.

b) *The milliammeter* which serves to measure the compensation current through the screened strip is a highly important instrument. From the equation (6) we obtain:

$$\frac{dQ}{Q} = \frac{2di}{i} \qquad (7)$$

which shows that if we wish to measure the radiation correctly on half a percent we must measure the current correctly within a quarter of a percent. Most milliammeters of high quality enable us to do that. A frequent source of error, not always payed sufficient attention to, is *the temperature dependence of the milliammeter*. The instruments of the highest quality are practically free from a temperature dependence, but often one is forced to work

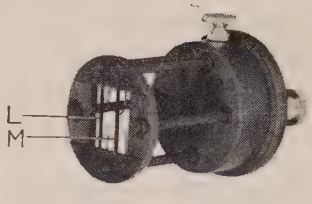


3A FRONT VIEW.

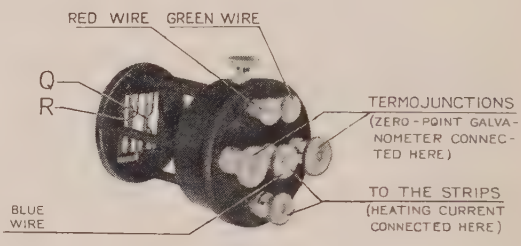


3B BACK VIEW.

FIG. 3 STRIP HOLDER.

with more simple instruments. Especially in such cases it is important not to subject the ammeter to large variations of temperature. This can to some extent be avoided if the instrument is kept in shadow. Further one has the possibility to determine the temperature coefficient and apply a correction for it.

*It is equally important to control, not too seldom, the accuracy of the milliammeters used with compensation pyrheliometers as to control the pyrheliometers themselves.*

The milliammeter ought to be able to measure currents up to about 0.4 ampere.

c) *The slide resistance*. When the compensation current is closed, it is of importance that we begin with a rather high resistance and slowly change it to a value which brings the galvanometer deflection back to zero. With an inner resistance of the milliammeter of about 10 ohm, the resistance of the slide resistance ought to be variable within the interval 10 to about 100 ohm. As variations can be obtained also by using smaller electromotive force in the circuit, one need not to be too strict about these limits. It is important,

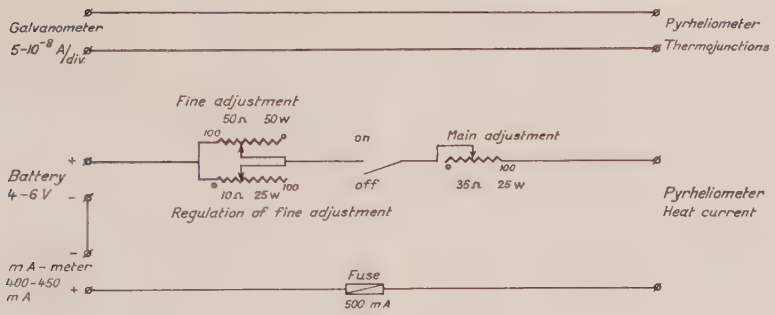


Fig. 4A *Circuit diagram*

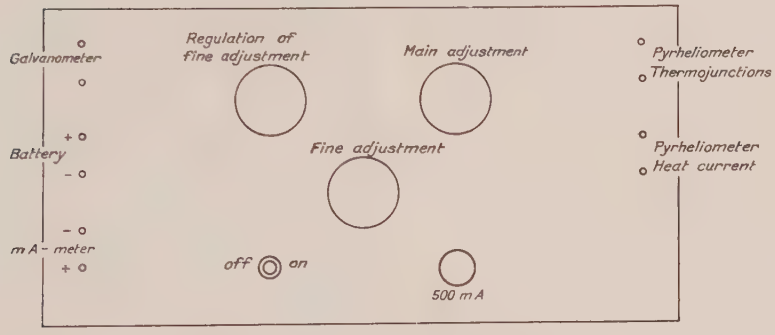


Fig. 4B. *Switchboard drawing*

however, that resistance and electromotive force are balanced in such a way that the maximum current which can be obtained is not so high that the strips are burned by heating.

It is important that the slide resistance is such that smooth variations can be obtained. A combination of two resistances, parallel or in series, is advisable, one for a coarse, the other for fine regulation of the current.

4. *Determination of the constant K*

Before the delivery the constant $K$ of every instrument is determined through comparison with a standard or substandard instrument. The constant of the standard pyrheliometer has been determined through measuring the quantities $r$, $a$ and $\beta$ defined above. As the instruments are expected to give readings which are correct within less than 0.5 percent, the accuracy of the determination of $r$, $a$ and $\beta$ for the standard should for every one of these factors be correct within about 0.1 percent.

The strips are cut off in a dividing engine and their width given on its scale. The width is also controlled under the microscope. The resistance between two knife edges resting at a distance apart, which has been measured, is determined. As the resistance of the manganin varies with less than 0.1 percent for a temperature difference $-40°$ to $+50°$, no regard needs to be taken to the temperature of the strips. The constant $K$, may therefore be regarded as independent of temperature, and no correction needs to be introduced on its account.

Direct observations by K. Ångström at the original construction and also by others have shown that the absorbing power $a$ of the surface blackened by the method of Crova, as described above, may be put equal to 0.980, with an accuracy, probably, of $\pm$ 0.2 percent.

The constant $K_s$ of the standard being com-

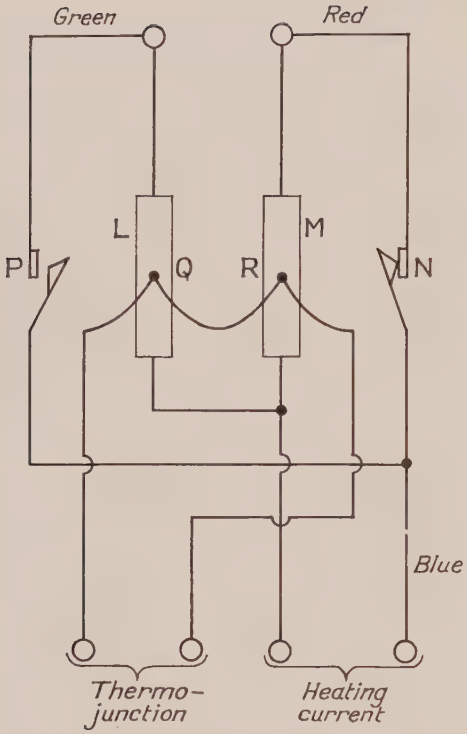


Fig. 5. *Electric circuit diagram of Pyrheliometer (when strip M is shaded)*

puted on the basis of these measurements, the constant $K_n$ of an individual instrument is determined from the equation:

$$K_s\, i_s^2 = K_n\, i_n^2 \qquad (8)$$

from which:

$$K_n = K_s \left[\frac{i_s}{i_n}\right]^2 \qquad (9)$$

where $i_s$ is the current measured in using the standard, $i_n$ the current measured in using the instrument, the constant of which is to be determined. From obvious reasons it is of advantage to use the same milliammeter for both determinations, provided the sun radiation is not so variable that simultanity of the both observations is to be given priority. In general $K_n$ is determined from several series of alternating measurements of $i_s$ and $i_n$. Every single computation of $K_n$ is in general made from mean values of $i_s$ and $i_n$, and the finally adopted value of $K_n$ is itself a mean value of several such computations of $K_n$.

At the constant determinations made at the Swedish Meteorological and Hydrological Institute, the constant of the individual instrument is always determined also in a second way, namely on the basis of measurements of $a$ and $r$, while $\beta$ is assumed to be equal to the absorption of the strips of the standard instrument, viz. equal to 0.980. In this way a constant $K_v$ is obtained. It serves as a control of the correct functioning of the instrument. This is as a rule approved for delivery only if $K_v$ does not differ from $K_n$ with more than 1 percent. The same rule was applied at earlier constant determinations at the Physical Institute of Uppsala (prior to 1922). But in all cases the value of $K_n$ is given priority. *It is the comparison with the standard instrument or with certain substandards, which determines the value of the constant to be accepted.*

### 5. *Correction to the constant experimentally determined*

Already in 1914 it was pointed out by the present author (A. ÅNGSTRÖM 1914), that a small correction ought to be applied to the readings with the Ångström compensation pyrheliometer, on account of the fact that in the standard instrument at Uppsala and also in the secondary instruments, which were then copies of the standard, the strip illuminated by the sun is not heated by the sun radiation to its whole length, as is, on the other hand, the strip heated electrically. The diaphragm screenes off the edges of the illuminated strip to an extention of about 1.5 to 2.0 mm at both ends. The consequence of this is that it takes less current energy per unit length of the strip to heat the screened strip to the same temperature as the illuminated one, than it would take if the sun radiation was allowed to fall on the whole length of the strip. At that early time I gave a simple theory, showing the error to be expected. It is

presented in Annex I together with some new applications.[1]

The edge effect has after 1914 been subjected to a number of investigations among which the ones of MARTEN (1916) and LINDHOLM (1958) may be especially mentioned. For an instrument used by myself at Algeria (No. 158) I found experimentally an edge effect of 1.3 percent, Marten gives a value as high as 2.8 and recent measurements by Lindholm seem to support the last named value. If one would consider the edge effect as the only cause of a deviation from a true scale, one would consequently have to apply a correction of + 2 percent or even slightly more to the constant $K_n$ determined as described above. There are however probably also some other small sources of error working in an opposite direction. On the bases of all comparisons made between the Ångström and Smithsonian Scales, and especially with reference to the laboratory experiments at the National Physical Laboratory, London, the International Radiation Commission recommended (1956) that for all measurements given in the uncorrected Ångström Scale a correction of +1.5 percent should be applied after the 1st of January 1957. This implies that to constants $K_n$ determined through comparisons with the standards in Stockholm according to the procedure described in § 4 of the present paper, this same correction ought to be applied.

All certificates on pyrheliometer constants issued by the Meteorological and Hydrological Institute at Stockholm are now (after January 1 st, 1957) in agreement with this recommendation.

### 6. *Operation of K. Ångström compensation pyrheliometer*

The instrument is adjusted against the sun by aid of libel and diopters. The screen is put straight forward allowing radiation to fall simultaneously on the both strips. No heating current is then applied to either strip. Take the reading of the galvanometer connected to the thermo-couple as *zero position*. Now turn the screen 90°, for instance to the left so that the left strip is shadowed, the right one exposed to the sun. At the same time the contact to the left strip is automatically closed. The intensity of the current is regulated as to bring back the galvanometer deflection to the zero position. When that has been made, the intensity of the current is read at the milliammeter. Next turn the screen 180°, in order to shadow the right strip. Automatically the current is switched over to that strip. The current is regulated for no deflection on the galvanometer and a new reading of its intensity is taken. Finally the screen is turned to the left again and the procedure of regulating and reading repeated. If the readings are $L_1$, $R$ and $L_2$, respectively, the current $i_m$ is determined from the equation:

$$i_m = \frac{L_1 + L_2 + 2R}{4} \qquad (10)$$

and the radiation computed from:

$$Q = Ki_m^2 \qquad (11)$$

where $K$ is the constant given in the certificate. If the certificate does not state that the constant refers to the International Pyrheliometric Scale of 1956, but is issued earlier and given in the Ångström Scale, add 1.5 percent to the constant in order to reduce it to the international Scale.

The height of the sun is obtained to a tenth of a degree from the scale attached to the instrument.

When high accuracy is demanded the solar height $h$ should be computed from the true local time according to the equation:

$$\sin h = \sin \varphi \sin \delta + \cos \varphi \cos \delta \cos t \qquad (12)$$

where $\varphi$ is the latitude of the station, $\delta$ is the declination of the sun and $t$ is the local time angle. At the time $1^h$ p.m. for instance the time angle is $\frac{360^\circ}{24} = 15^\circ$,

It is desirable that the indications on the elevation scale are controlled now and then through computations according to equation (12).

Under all circumstances it is important that the time is read at the same moment as

[1] In my previous paper I used a value for the heat conductivity of manganin taken from Smithsonian Physical Tables (1910). This value is ten times too large. The correct value is now introduced.

pyrheliometer readings are taken. At high sun elevations it may in general be sufficient to read the watch, when the reading $R$ is made at the ammeter. In general the time ought to be given in hours and minutes.

*Comparison of instruments.* When comparisons are made for the purpose of controlling the constants or for new standardizations it is especially important that they are made under the most favorable conditions as regards installment of the instruments and as regards sky and sun conditions. An exceptionally clear sky is desirable, mostly because the radiation is then, for solar heights above 30°, rather constant, with only a regular and slow variation. It is also desirable that the solar height is not very low. Solar heights below about 20° are not suited for standardization purposes.

At all installments of actinometric instruments for general purposes the neighbourhood of smoke creating industries ought to be avoided. The milliammeter and slide resistance ought if possible be placed within an observatory or in the shadow of some shelter; not only for protecting them against excessive heating but also to avoid as much as possible the heating of the contact connections of the electric wires.

I am indebted to my successor as Director of the Meteorological and Hydrological Institute of Sweden for the permission to use a number of figures included in the Institute's instruction for the use of the Ångström pyrheliometer.

## ANNEX

### On the edge effect at the Ångström compensation pyrheliometer.

By ANDERS ÅNGSTRÖM

The so called "edge effect" involves a correction to the readings of the Ångström compensation pyrheliometer. The correction is of the order of about 2.0 per cent in the case of the standard pyrheliometer, used to define the Ångström Pyrheliometric Scale. It arises through certain features of the construction, involving that the manganin strip exposed to the sun is not illuminated to its whole length but that the strip to a length of about 1.5—2.0 mm from the edges is screened by a diaphragm, while the other strip, which is in shadow, is heated by the electric current to its whole length. The consequence of this is that it takes less energy per unit length of the strip to heat it by the electric current, than corresponds to the heating by the sun radiation for the same temperature at the centre of the strips.

It is easy to give for an idealized case, which corresponds to the essentials of the actual conditions, a theory of the energy and temperature distribution at the two strips. The advantage of such a theory is that it clearly shows what order of size may be expected as regards the correction and also that it gives a very clear idea about the factors which influence the correction and about the variations to which it may be subjected under various conditions of exposure.

We make the assumption that the strips are perfectly absorbing, with a width $a$, a thickness $b$ and a conductive power for heat $c$. We further assume the strips to be soldered to great metal blocks, the temperature of which are independent of the temperature of the strips. The strips have the total length $2\,l$ and the strip illuminated by the sun is in shadow to a length $d$ from the edges. I further assume that the temperature $t_0$ at the centre of the strip is measured, and that this temperature is uninfluenced by the measuring device. Let it also be assumed that the thickness $b$ of the strips is negligible in comparison with $l$ and $a$ and that the temperature in every cross-section of the strip is the same.

We further assume that the convection and radiation to the surroundings from the different parts of the heated strips can be expressed through the cooling law of Newton, viz, it is proportional to the temperature difference between the surroundings and the part of the strip, which we consider. The temperature of the surroundings we assume equal to the temperature of the blocks to which the strips are soldered. To simplify we let this

temperature be the zero-point of our temperature scale. Then the convection from various parts of the strip is expressed by the quantity $kt$, where $t$ is the variable temperature and $k$ a cooling constant.

Some of these assumptions represent an idealization. The blocks to which the strips are soldered may to some extent adopt a temperature slightly above the "surroundings", the conduction of heat through the wires of the thermojunction influences to some degree the temperature distribution in the strips, and finally it seems probable that $k$ is to some extent variable along the strip in a way which probably is dependent on a number of external conditions. This, however, does not worry us so much, as the chief aim of the theory is to make clear what factors are involved and what is the order of size of their influence. There are no reasons to suppose that their influence in the practical case will be very different from what it is in the idealized one.

Let us investigate the variation of temperature of the strip as a function of the distance $x$ from the centre of the strip.

If the energy produced by the current is $W$ per unit area of the screened strip we get:

$$W a\, dx = k \cdot t \cdot a \cdot dx - a \cdot b \cdot c \frac{d^2t}{dx^2} dx \qquad (1)$$

from which

$$\frac{d^2t}{dx^2} - \frac{k}{b \cdot c} \cdot t + \frac{W}{b \cdot c} = 0 \qquad (2)$$

The general solution has the form

$$t = Ae^{+\mu x} + Be^{-\mu x} + S \qquad (3)$$

where we have

$$S = \frac{W}{k}, \text{ and } \mu = \sqrt{\frac{k}{b \cdot c}} \qquad (4)$$

The constants $A$ and $B$ are determined by the conditions:

$$t = 0 \text{ for } x = l; \text{ and } \frac{dt}{dx} = 0 \text{ for } x = 0$$

the last condition following simply from symmetry.

We thus get

$$A = B = -\frac{S}{e^{+\mu l} + e^{-\mu l}} \qquad (5)$$

For the temperature $t_0$ at the centre, where $l = 0$, we get from (3) and (5)

$$t_0 = \frac{W}{k}\left[1 - \frac{2}{e^{+\mu l} + e^{-\mu l}}\right] \qquad (6)$$

This temperature $t_0$ is equal to the temperature $t_{01}$ at the centre of the illuminated strip.

For the illuminated part of that strip we have:

$$t_1 = A_1 (e^{+\mu x} + e^{-\mu x}) + S_1 \text{ where} \qquad (7)$$

$$S_1 = \frac{Q}{k} \qquad (8)$$

where $Q$ is the radiation per unit surface of the illuminated strip.

For the shadowed part of the exposed strip we have:

$$\frac{d^2t_2}{dx^2} - \frac{k}{b \cdot c} \cdot t_2 = 0 \qquad (9)$$

which gives

$$t_2 = Me^{+\mu x} + Ne^{-\mu x}$$

$A_1$, $M$ and $N$ shall fulfill the conditions:

$$t_2 = 0 \text{ for } x = l;\ t_2 = t_1 \text{ for } x = l - d$$

and

$$\left(\frac{dt_1}{dx}\right)_{x = l - d} = \left(\frac{dt_2}{dx}\right)_{x = l - d}$$

This gives us for the temperature of the illuminated part of the exposed strip:

$$t_1 = -\frac{S_1}{2}\left[\frac{e^{+\mu d} + e^{-\mu d}}{e^{+\mu l} + e^{-\mu l}}\right](e^{+\mu x} + e^{-\mu x}) + S_1 \qquad (10)$$

and for the temperature at the centre:

$$t_{01} = \frac{Q}{k}\left(1 - \frac{e^{+\mu d} + e^{-\mu d}}{e^{+\mu l} + e^{-\mu l}}\right) \qquad (11)$$

We have $t_{01} = t_0$ and by dividing (11) by (6) we get:

$$\frac{Q}{W} = \frac{\psi(l) - 1}{\psi(l) - \psi(d)} \qquad (12)$$

where

$$\psi(l) = \frac{e^{+\mu l} + e^{-\mu l}}{2}$$

and similar for $\psi(d)$

For $\mu$ we had the expression $\mu = \sqrt{\frac{k}{b \cdot c}}$

In the case of the type of the Ångström pyrheliometer, to which most *measurements* of the edge correction refer, the value of $b$ is 20 microns; for $c$ we have measurements, for instance by Jäger and Dieselhorst, giving a value of 0.0519 gram calories per second and square centimeter for a temperature gradient of 1° per cm, at a temperature of 18°. At 100° the value is considerably larger namely 0.0631. A change of $c$ with about 8 percent for a temperature difference of 30° seems probable, which evidently means a change in $\mu$ of about 4 percent for the same interval of temperature.

The factor, the evaluation of which involves the greatest difficulty is $k$. The combined cooling effect of radiation and convection is without doubt variable within rather wide limits, dependent on the wind velocity, which must to some extent influence the air circulation within the pyrheliometer tube. Mac Farlane gives a value for $k$ of 0.000287 at 18° C (gram calories per square centimeter and second) with an increase to about 0.000319 at a temperature of 40°. This value, however, refers to the cooling of a black sphere placed in the centre of a spherical enclosure which has a blackened surface, the medium between the surfaces being moist air. The air was not ventilated, and aside from the thermal convection it must have been mainly at rest. The value of Mac Farlane is therefore probably smaller than the value of $k$ corresponding to the conditions within the pyrheliometer. If, in spite of that, we introduce the values of $b$, $c$ and $k$ given above and corresponding to a temperature of 18°, we find, allowing for the convection and the radiation from front and back surface of the strip ($= 2\,k$), a value for $\mu$ of 2.35. As the ratio $\frac{k}{c}$ enters into $\mu$, it may be assumed that the value of $\mu$ is much less dependent on the temperature than $c$ and $k$. The temperature dependence may therefore here be neglected. On the other hand it seems probable that the value of $\mu$ in our actual case is different from 2.35, especially on account of $k$ being different from what has been assumed.

Accurate measurements of the edge correction have now in fact been carried out by MARTEN after my first article on the subject was published in 1914. In the case of the pyrheliometer Nr 140 III, then belonging to the Meteorological Observatory at Potsdam, MARTEN determined $d$ to be equal to 0.2 cm, and found, by changing the length of the shadowed part of the strip from 0.1 to 0.4 cm mean values on the edge correction, given in the Table I, under $\delta^{obs}$. Here $\delta$ is defined through:

*Table 1*

| $d$ | $\delta$obs | $\delta$comp |
|---|---|---|
| 0.1 | 0.7 | 0.65 |
| 0.2 | 2.8 | 2.65 |
| 0.3 | 6.5 | 6.3 |
| 0.4 | 11.9 | 12.1 |

$$\delta = \left[\frac{Q}{W} - 1\right] \cdot 100 \qquad (13)$$

or

$$Q = W\,(1 + 0.01\,\delta) \qquad (14)$$

From (12) and (13) we get:

$$0.01\;\delta^{comp} = \frac{\psi\,(l) - 1}{\psi\,(l) - \psi\,(d)} \qquad (15)$$

If we in this formula introduce a value on $\mu$ equal to 2.4, we get the values of $\delta^{comp}$ given in the last column of Table I.

The variation of $\delta^{comp}$ with $d$ (in centimeter) is also demonstrated by fig. 6 through a full drawn line. The measured values of Marten are represented by crosses. The value for $k$ found

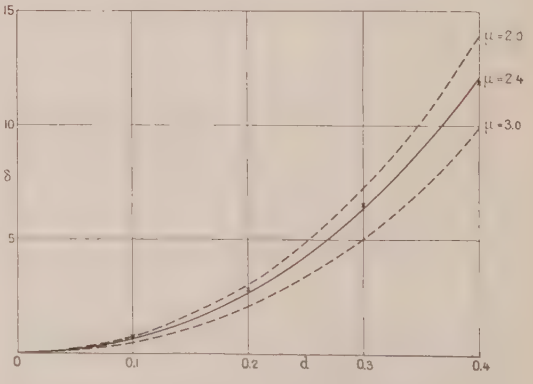


Fig. 6. Edge correction $\delta$ in per cent in its dependence of shadowed length $d$ ($\mu = 2.4$, $\mu = 2.0$, $\mu = 3.0$). Curves according to theory, crosses according to measurements by Marten.

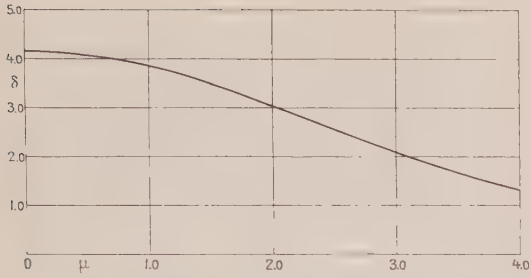


Fig. 7. Dependence of edge correction $\delta$ on convective constant $\mu$ ($d = 0.2$ cm, $l = 1.0$ cm).

through introducing the measured values of Marten into our formula seems, with regard to what has been stated earlier, to be a reasonable one. It is rather astonishing to find how well the theoretical formula then represents the actual conditions. This gives us reason for assuming that the formula may also give a trustworthy idea of the dependence of the edge correction on other variables than $d$, especially then on the dependence of $\delta$ on $k$.

This seems at present to constitute a rather important question. Can $\delta$ for a given instrument, where $d$ is keeping a fixed value of let us say 0.2 cm be regarded as practically constant? For all determinations of the difference between the Ångström and the Smithsonian Scale this is a rather fundamental question. Fig. 7 now gives the values of $\delta$ computed from my formula for different values of $\mu$, under the assumption $d = 0.2$, $l = 1.0$.

The limit value $\delta_{\mu=0}$ is computed from the formula and given by:

$$0.01\ \delta_{\mu=0} = \frac{l^2}{l^2 - d^2} - 1 = \frac{d^2}{l^2 - d^2} = 0.0415$$

It must here be emphasized that the zero-value of $\mu$ is quite imaginary, in the respect that $\mu$ can not be reduced below the value corresponding to radiation alone. In fact $k$ is composed of a radiation term and a convection term. It seems to be reason to assume that the cooling is to about two third due to convection. But even the convection can not be reduced below the value corresponding to the free convection due to the rise of the air from the heated strip on account of differences in density. It therefore seems probable that $\mu$ can under no conditions of ventilation be below about 50 percent of its normal value, viz. not below about 1.0.

The important result to be derived from the formula now is that $\delta$ can only be regarded as a constant for the case that $\mu$ does not vary between too wide limits. Already the measurements of Marten showed that in his different series, $\delta$, for $d = 0.2$, varied between the limits 2.6 and 3.2 percent. But it seems rather probable that in practical field work the variation of $k$, and consequently also of $\mu$, is such, that much greater variations can occur. Let us assume that under extreme conditions $\mu$ takes on values as low as 1.0, and as high as 4.0, viz. about the half and the double of the normal value. This gives us a variation of the edge correction from 3.85 at the minimum value of $\mu$, to 1.31 for the maximum, which means a difference of almost 2.5 percent in the measured radiation value. Such a variation may well be produced if the pyrheliometer in the first case is well screened against wind and in the second is openly exposed to a wind blowing directly into the tube. It seems rather probable that we have here an explanation to the rather large differences obtained by, for instance, Courvoisier in comparing substandards of the two standard Scales. In general one has, at observatories, much better opportunities to get installments of pyrheliometers, where the wind influence is reduced to a minimum than at field measurement in the open. This may mean a difference of more than $\pm 1$ percent in extreme cases.

What here has been said emphasizes the importance of reducing the edge correction to a minimum. For $d$ equal to 0.05 cm, and technically such a reduction of $d$ seems practicable, the edge correction for $\mu = 2.4$ is only 0.2 percent and its variation corresponding to extreme values of $\mu$ seems then to be reduced to less than $\pm 0.2$ percent. In general it may only be a fraction of this value.

At the construction of new instruments by A. Lindblad[1] or at the Swedish Meteorological and Hydrological Institute, attention is now payed to the conditions which here have been analysed. In the instrument of recent construction the screened edges of the illuminated strip are less than 0.2 mm in length. This means that the edge correction is practically eliminated.

[1] Address of A. Lindblad: Kungstensgatan 38, *Stockholm*, Sweden.

## REFERENCES


Abbot, G. G., 1911: The silver disk pyrheliometer. *Smithsonian Misc. Coll.*, Vol. **56**, No. 19.

Albrecht, F., 1935: Kalorische Messmethoden In: E. Kleinschmidt: Handbuch der Meteorologischen Instrumente und ihrer Anwendung, pp. 109—185, Berlin.

Aldrich, L. B., 1949: The Abbot silver disk pyrheliometer. *Smithson. Misc. Coll.*, Vol. **111**, No. 14.

Aldrich L. B. and W. H. Hoover, 1954: Pyrheliometry in *Annals of the Astrophysical Observatory*, Vol. **7**, pp. 99—104.

Ångström, Anders, 1914: Das Ångströmsche Kompensationpyrheliometer und die pyrheliometrische Skala. *Meteor. Zscht*, H. **8**, pp. 369—373.

— 1914: The Ångström Compensation Pyrheliometer and the pyrheliometric scale. *Astrophysical Journal*, Vol. **XL**, No, 3.

— 1919: Comparisons between pyrheliometers and on the difference between the Ångström and the Smithsonian Standard. *Monthly Weather Rev.*, Vol. **47**, pp. 798—799.

Ångström, Knut, 1893: Eine elektrische Kompensationsmethode zur quantitativen Bestimmung strahlender Wärme. *Nova Acta Reg. Soc. Sc. Ups.*, Ser. III, **16** (Transl.: Phys. Rev. Vol. **I**, 1894).

— 1899: The absolute determination of the radiation of heat with the electrical compensation pyrheliom eter with examples of the application of this instrument. *Astropys. Journ.*, Vol. **9**, p. 332.

— 1900: Intensité de la radiation solaire à differentes altitudes. *Nova Acta Reg. Soc. Sc. Ups.*, Ser. III, pp. 1—46.

— 1903: Energie dans le spectre visible de l'etalon Hefner. *Nova Acta Reg. Soc. Sc. Ups.*, Ser. III, pp. 1—12.

Bäcklin, E., 1925: Bestimmung von Pyrheliometerkonstanten am Physikalischen Institut der Universität Uppsala. *Arkiv för Mat. Astr. Fys.* utgivet av Kungl. Svenska Vetenskapsakademien, Bd. 19, H. 2.

— 1925: Ueber die Konstanz der Ångströmschen Pyrheliometerskala. Ibidem.

Courvoisier, P., 1957: Contributions to Standard Pyrheliometry (with an introduction by A. Ångström and W. Mörikofer). *Sveriges Meteor. och Hydrolog. Inst. Communications Series B, No. 13.*

Lindholm, F., 1958: On the Ångström Absolute Pyrheliometric Scale. Tellus **10**, pp. 249—255.

Marten, W., 1922: Zur Frage der absoluten pyrheliometrischen Skala. *Met. Zscht* **57**, pp. 342—345.

IGY Instruction Manual Part VI, Radiation Instruments and Measurements. Pergamon Press. 1957. London, New York, Paris.

# The Release of Latent Heat in Tropical Storms Due to the Fall-Out of Sea-Salt Particles

By A. H. WOODCOCK

Woods Hole Oceanographic Institution[1], Woods Hole, Massachusetts

(Manuscript received August 12, 1957 revised April 1, 1958)

*Abstract*

Observations of atmospheric sea salt in a hurricane are used to estimate the weight of salt in the clear air at cloud levels. These quantities are then used to determine the rate of release of heat in the moist air layers below, due to condensation on this salt as it falls from the relatively dry air at higher levels. This rate is found adequate to alter significantly the distribution of heat and water vapor in the cloud-layer air and to explain much of the observed potential temperature increase in the lower air converging upon the central regions of hurricanes.

## 1. Introduction

In meteorology computations involving the release of latent heat of vaporization of water assume that no significant amount of condensation occurs in the atmosphere until the relative humidity reaches 100 per cent. In fact the assumption of dry-adiabatic conditions in well-mixed sub-saturated air below cloud base is sometimes used as a basis for judging the probable accuracy of temperature measurements made in this air (JORDAN, 1952). In air containing certain quantities of hygroscopic particles, this assumption is probably not valid. The author has shown that condensation on sea salt particles in ascending air can bring about a significant release of latent heat in the sub-cloud layer at relative humidities less than 100 per cent (WOODCOCK, 1950).

The previous attempt to use measurements of sea-salt particles to estimate the role of the salt in the release of latent heat in the sub-cloud layer was not very conclusive. This was due primarily to uncertainty about the maximum amounts of salt to be expected in storms at sea, and to a failure to realize that salt falling from higher levels might also be important. Recently developed techniques (WOODCOCK, 1950a, 1952) (WOODCOCK and SPENCER, 1957), designed to sample the larger salt particles, have shown the presence in strong winds of particles having a weight of nearly $10^{-6}$ grams. These measurements have also shown that the glass slide technique averages quantities of salt, in one to ten kilometer sampling lengths over the sea, which may vary by a factor of two to ten within these lengths. Thus for this and other reasons (see section 8), one need not regard the averaged hurricane data used here as limiting quantities, since they result from application of the older glass-slide sampling

[1] Contribution No. 920 of the Woods Hole Oceanographic Institution. Work supported by the Office of Naval Research, under contract Nonr-798(00) (NR-082-124).

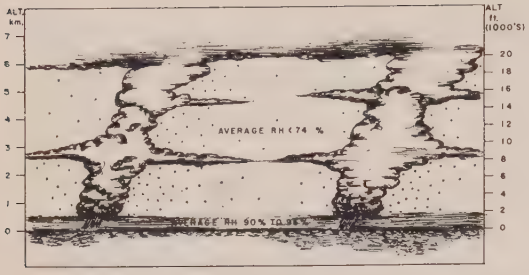


Fig. 1. Diagram illustrating the idea of the fall-out of large salt particles associated with clouds. This figure is intended to represent a cross-section normal to two cloud lines. It is assumed that the average relative humidity in the clear air at cloud levels above 5,000 feet is less than 74 per cent.

technique. No new measurements have thus far been made in these storms using the new techniques, but for present purposes the earlier observations are useful.

The current interest in expanding our knowledge of tropical storms and the improved facilities for doing so caused the author to hazard a second attempt to show that the quantity of airborne sea-salt is important in these storms. The primary purpose of the present paper is to discuss the role of salt which is carried upward by the clouds, in subsequently altering the distribution of heat and water vapor as it falls back towards the sea. It is hoped that hurricane-research aircraft will be able to test some of the conclusions of this study through direct measurements.

Byers (1944, p. 432) and Riehl (1951 and 1954) have discussed the near-isothermal expansion of the sub-cloud air flowing in towards the central low-pressure areas of tropical cyclones. Riehl emphasized the basic role of this phenomenon in altering the stability of the atmosphere in the central areas of hurricanes (Riehl, 1954, p. 313—316). Both of the above authors assumed that the sensible heat required to compensate for the adiabatic cooling as the pressure falls in the converging air (roughly 1° C per 10 mb of pressure decrease), is derived from the greatly agitated sea surface waters.

The following sections of this paper are intended to show that a large part of this heat can come from latent heat released by condensation of water vapor on salt particles. It is pictured that these particles, which are produced by bursting bubbles at the sea surface (Blanchard, Woodcock, 1957) (Kientzler et al., 1954) are carried up in the clouds, are distributed laterally by shear and turbulence and fall into or are mixed into the relatively clear air between the clouds. Here the particles will alter the vapor and heat distributions as they fall in and out of layers of air having different relative humidities on their way down towards the sub-cloud layer, as suggested by Figure 1. In falling from an area where the RH averages < 74 per cent, to one in which the average RH is 90 per cent or 96 per cent, condensation releases heat at a rate which is sufficient to account for the observed warming of the air flowing into tropical cyclones, if one assumes a salt fall-out of a certain average intensity over the whole area of the observed isothermal expansion.

## 2. Preliminary description of the model proposed

The purpose here is the initial clarification of the primary problem, which is to demonstrate that the transport of salt between the sea, the sub-cloud and cloud layers can result in a sensible heating of the sub-cloud air through the release of latent heat.

The spray particles entering the atmosphere from the sea can be divided, for present purposes, into two groups: 1), those particles which fall back into the sea without being carried out of the sub-cloud air, and 2), those which return to the sea after ascending in clouds and falling through relatively dry regions of the cloud-layer atmosphere.

Group one particles will produce a net cooling of the sub-cloud air due to evaporation. The amount of this cooling will be directly related to the difference in the salinity of the droplets which are ejected into the air from the bubbles in the sea and their salinity upon falling from the air and re-entering the sea. The relative humidity over spray droplets of sea water is about 98 %. Since surface-air relative humidities of 90 % and 96 % are assumed in the discussion below, the spray droplets will evaporate to some extent (see Fig. 2) before returning to the sea. Thus evaporation from these group one spray particles will tend to stabilize thermally the lower part of the sub-cloud layer, which

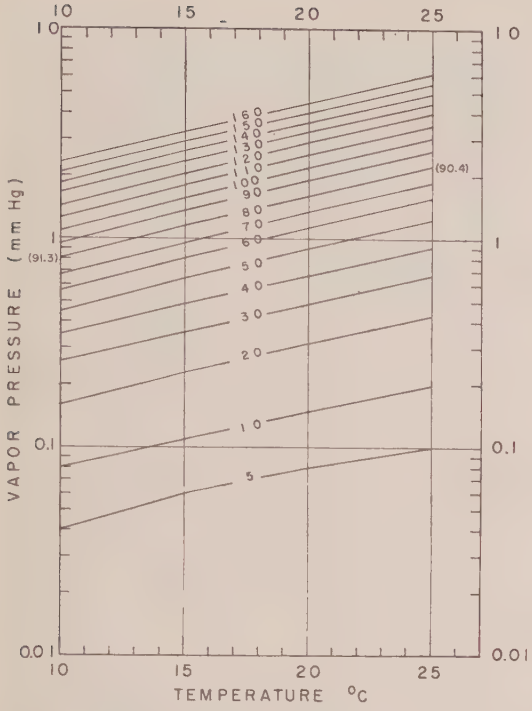


Fig. 2. Vapor pressure lowering over concentrated sea water at various temperatures and salt concentrations. Concentrations represent chloride in parts per thousand, by weight. (From ARONS and KIENTZLER, 1954).

contains the dryest air in this usually well-mixed section of the trade-wind or hurricane atmospheres (BUNKER et al. 1949) (RIEHL, 1954). The sensible heat required for this evaporation is assumed to come from the sea surface.

Group two particles are carried upwards into the clouds through the sub-cloud layer. They are assumed to enter cloud base having a salinity equal to that existing when they were ejected from the sea (i.e. equilibrium at RH 98 %). From the time of their production to the time when they enter cloud base, this group of particles could thus cause no net change in the total heat of the sub-cloud air. After being carried upwards to various altitudes in the clouds, the particles are mixed or fall into the dryer inter-cloud air and eventually fall back into the sub-cloud layer as relatively dry salt particles. The heat required to vaporize the water from the group-two particles is thus derived from high in the cloud-layer air. The quantity of latent heat released in the sub-cloud layer by condensation as these particles re-enter the layer, will be inversely proportional to their salinity as they subsequently fall into the sea or re-enter the clouds. In this cycle of vertical motions group-two particles will cool the cloud layer air and will warm the sub-cloud air, adding to the instability of each.

With the above model in mind, the author will now try to show that the range of increase of potential temperature observed in converging lower air in hurricanes may be computed, at least in part, from the quantities of salt found in these storms.

### 3. Sea salt in lower air

During the tropical storm which passed near Miami, Florida on September 22, 1949, the author made measurements of the average weight and number of the salt particles of certain size ranges present at an altitude of 40 meters above the sea at Hillsboro Lighthouse (WOODCOCK, 1950). Fig. 3, curve 12, shows the number and size of the salt particles found, presented as a cumulative-number distribution curve. For comparison other observations are shown which were made from aircraft at cloud levels in trade-wind

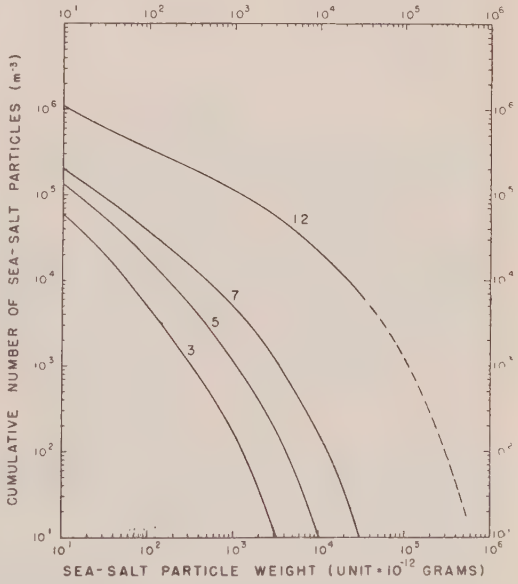


Fig. 3. Cumulative number distribution curves for averaged observations during wind forces 3, 5, 7 and 12.

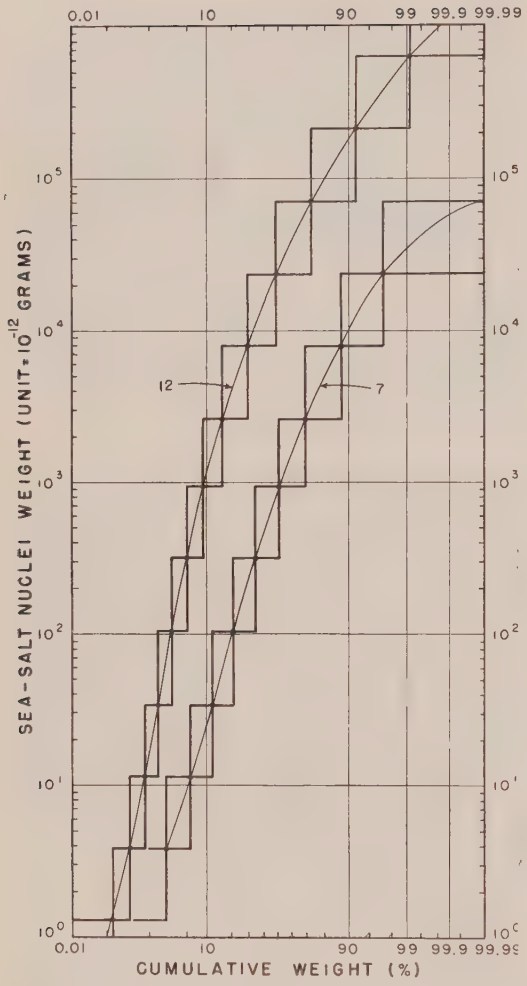


Fig. 4. Averaged cumulative per cent weight distribution of sea salt particles. Curve 12 represents hurricane conditions, and is taken from the measurements averaged in curve 12 of Figure 3. Curve 7 represents the averaged force 7 wind data given on line 7 of Figure 3. The rectangular areas are interpreted as follows: the range between 8,000 and 24,000 $\mu\mu$ gram particles (curve 12) contains about 20 per cent of the total weight in all of the particles measured. The curved lines are drawn through the points which represent the weight limits of each weight range. (See text for further discussion.)

areas under more moderate wind conditions. The broken portion of curve 12 is a reasonable extrapolation, based upon the author's wide experience in salt-aerosol sampling.[1]

[1] The hurricane samples were unfortunately taken prior to the development by the author of the "multi-strip sampling" technique (Woodcock, 1952). This sampling method which utilizes the low sampling efficiency of wide slides or "ribbons" (Langmuir, 1945), makes it possible to selectively sample the large sparsely distributed nuclei, despite the presence in the air of great numbers of the small nuclei. See the discussion section of this paper for further remarks about salt in hurricane winds.

The cumulative number distribution curve, which was originally derived from thirty-one size range measurements, was divided into fourteen weight ranges in accordance with the convenient size steps of the Porton eyepiece graticule (May, 1945). The product of the total number in each weight range and the median-number weight, approximates the weight of salt in each range. The ratios of these individual weights to their sum were used to derive the cumulative per cent weight distribution values shown on Figure 4. The sum of weights of sea salt represented by the force 12 curves on Figures 3 and 4 is 1.2 mg $m^{-3}$. As a test of the accuracy of this weight estimate, a further division of each of these fourteen steps into five, making a total of seventy size ranges, increased this value by only 0.1 mg $m^{-3}$. Thus curve 12 of Figure 4 is, for present purposes, a close approximation of the total salt represented by curve 12 of Fig. 3.

On Table I, column 1 shows the particle weights represented by curve 12 of Figure 3, divided into 20 weight range categories. Each of these weight ranges contains about 5 per cent of the total mass of sea salt present in all of the particles. The particle weights were taken from curve 12, Figures 3 and 4 as follows: Note on curve 12, Figure 4, that the salt particles in the weight range of about 320 to 1,200 $\mu\mu$ grams contain about 5 per cent of the total salt. In this weight range the cumulative number distribution curve (on Figure 3) crosses the mid-point of this selected 5 per cent interval at the nuclei weight of about 600 $\mu\mu$ grams. This and other similarly derived nuclei weights are shown in column 1 of Table I. Columns 2, 3 and 4 of Table I give the radii and the rates of fall of these nuclei as relatively dry salt particles.

Amounts of salt near cloud-base altitudes have been found to be about the same as those a few hundred feet over the sea surface, under a wide range of wind conditions. On the assumption that a similar mixing of

TABLE 1

**The sea-salt particle distribution represented by curve 12, Figure 3, divided into 20 equal weight categories. The nuclei weights given in column 1 are those of the median number particle and are used to compute the distribution of salt and condensed water at severals levels in the atmosphere. Inital weight of salt in each 5 % interval is 60 $\mu$ gms m$^{-3}$. See the text for more information.**

| Sea-salt nuclei as crystalline particles near sea surface | | | | Sea-salt nuclei as droplets upon arrival at cloud base | | | | |
|---|---|---|---|---|---|---|---|---|
| Weight $10^{-12}$ g | Radius $\mu$ | Fall Rate cm sec$^{-1}$ | Amount of salt falling $\mu$gms.m$^{-2}$ sec$^{-1}$ | Radius $\mu$ | Fall Rate cm. sec$^{-1}$ | Amount of salt & water falling $\mu$ gms.m$^{-2}$ sec$^{-1}$ | | Wt. of salt in each size range $\mu$gms. m$^{-3}$ |
| | | | | | | salt | water | |
| 1 | 2 | 3 | 4 | 5 | 6 | 7 | 8 | 9 |
| 50 | 1.8 | 0.084 | 0.05 | 9 | 1.0 | 0.6 | 36 | 60.5 |
| 600 | 4.0 | 0.42 | 0.25 | 17 | 3.5 | 2.2 | 74 | 61.9 |
| 1,750 | 5.8 | 0.86 | 0.52 | 22 | 5.8 | 3.7 | 90 | 63.0 |
| 3,200 | 7.0 | 1.27 | 0.76 | 26 | 8.0 | 5.2 | 113 | 64.5 |
| 4,800 | 8.0 | 1.63 | 0.98 | 29 | 9.7 | 6.3 | 128 | 65.4 |
| 7,100 | 9.2 | 2.15 | 1.29 | 32 | 11.4 | 7.5 | 137 | 66.0 |
| 9,900 | 10.2 | 2.72 | 1.63 | 35 | 13.4 | 9.0 | 147 | 66.8 |
| 13,100 | 11.2 | 3.25 | 1.95 | 37 | 15.0 | 10.2 | 155 | 68.2 |
| 16,700 | 12.2 | 3.85 | 2.31 | 40 | 17 | 11.8 | 170 | 69.5 |
| 21,800 | 13.3 | 4.50 | 2.70 | 42 | 19 | 13.4 | 177 | 70.7 |
| 28,000 | 14.5 | 5.45 | 3.27 | 45 | 22 | 15.6 | 196 | 72.3 |
| 36,000 | 15.7 | 6.40 | 3.84 | 48 | 24 | 17.7 | 210 | 73.9 |
| 44,000 | 16.8 | 7.30 | 4.38 | 51 | 26 | 20.0 | 224 | 75.6 |
| 54,000 | 18.0 | 8.40 | 5.04 | 54 | 29 | 22.4 | 244 | 77.4 |
| 68,000 | 19.4 | 9.70 | 5.82 | 57 | 32 | 25.4 | 257 | 79.5 |
| 88,000 | 21.2 | 11.6 | 6.9 | 61 | 36 | 29.9 | 293 | 83.0 |
| 114,000 | 23.1 | 13.8 | 8.3 | 65 | 40 | 33.8 | 307 | 85.6 |
| 152,000 | 25.4 | 16.7 | 10.0 | 70 | 44 | 39.2 | 331 | 89.0 |
| 223,000 | 29.0 | 22.0 | 13.2 | 77 | 50 | 46.7 | 345 | 93.5 |
| 410,000 | 35.4 | 33.0 | 19.8 | 90 | 63 | 68.5 | 441 | 108.7 |
| | | | 93.0 | | | 379.1 | 4,075 | 1,495.0 |

aerosols exists in hurricanes, the quantity of salt derived above can be used to estimate amounts carried upwards by clouds.

### 4. Transport of salt by ascending clouds

Using a reasonable average rate of rise of air in the cumulus clouds of 4 m sec$^{-1}$ (Malkus) and a weight of salt at cloud base altitudes of 1.2 mg m$^{-3}$, the estimated ascent of salt is 4.8 mg m$^{-2}$ sec$^{-1}$.

What proportion of a storm area contains such actively growing cumuli? Wexler found in a study of numerous radar (PPI) scope photographs of hurricane spiral rain bands, that the width of these bands was about the same as the width of the spacing between them (Wexler, 1947). If these rain bands roughly delineate the size of the areas of major ascent of moist cloud air, one might estimate that the areas of ascent are about the same size as the areas between.

It seems excessive to suppose however that one-half of a storm area contains actively ascending cloud material. A more conservative ratio of active cloud area to relatively clear inter-cloud area of one to ten is tentatively used. Sea salt ascending in the clouds at a rate of 4.8 mg m$^{-2}$ sec$^{-1}$ will, on this assumption, be sufficient to produce an average fall over ten square meters of 0.48 mg m$^{-2}$ sec$^{-1}$.

What proportion of this salt is subtracted from the cloud layer air, by the various rain mechanisms (Miyake, Suguira, 1950) (Woodcock, 1952) (Woodcock, Blanchard, 1955) which cause the salt particles to be carried back to the sea in solution in the falling raindrops? Miyake and Suguira (1954) have shown that the rate of precipitation of chloride during the passage of typhoon "Kitty" in Japan ranged

TABLE 2

**Rates of fall of sea salt in hurricane at equilibrium concentration at different relative humidities.* Quantities of salt taken from Table I, column 1 and from Figure 4.**

| Wt. of sea salt in particles $10^{-12}$ g | RH 90 % | | | RH 96 % | | | RH 98 % | | |
|---|---|---|---|---|---|---|---|---|---|
| | Particle radii $\mu$ | Particle fall rate cm $sec^{-1}$ | Sea salt falling $\mu$ gms $m^{-2}$ $sec^{-1}$ | Particle radii $\mu$ | Particle fall rate cm $sec^{-1}$ | Sea salt falling $\mu$ gms $m^{-2}$ $sec^{-1}$ | Particle radii $\mu$ | Particle fall rate cm $sec^{-1}$ | Sea salt falling $\mu$ gms $m^{-2}$ $sec^{-1}$ |
| 50 | 4.2 | 0.3 | 0.2 | 5.3 | 0.4 | 0.2 | 7.0 | 0.6 | 0.4 |
| 600 | 9.6 | 1.3 | 0.8 | 12.1 | 1.9 | 1.1 | 15.8 | 3.0 | 1.8 |
| 1,750 | 13.6 | 2.5 | 1.5 | 17.4 | 3.9 | 2.3 | 22.6 | 6.0 | 3.6 |
| 3,200 | 16.7 | 3.7 | 2.2 | 21.2 | 5.7 | 3.4 | 27.7 | 8.8 | 5.3 |
| 4,800 | 19.0 | 4.8 | 2.9 | 24.3 | 7.4 | 4.4 | 31.8 | 11.3 | 6.8 |
| 7,100 | 21.7 | 6.1 | 3.7 | 27.6 | 9.3 | 5.6 | 36.2 | 14.5 | 8.7 |
| 9,900 | 24.2 | 7.6 | 4.6 | 31.0 | 11.5 | 6.9 | 40.5 | 17.8 | 10.7 |
| 13,100 | 26.6 | 9.0 | 5.4 | 34.0 | 13.6 | 8.2 | 44.5 | 21.0 | 12.6 |
| 16,700 | 28.8 | 10.4 | 6.2 | 37.0 | 15.0 | 9.0 | 48.3 | 24.5 | 14.7 |
| 21,800 | 31.5 | 12.4 | 7.4 | 40.0 | 18.2 | 10.9 | 52.5 | 28.5 | 17.1 |
| 28,000 | 34.2 | 14.5 | 8.7 | 44.0 | 21.5 | 12.9 | 57.5 | 32.7 | 19.6 |
| 36,000 | 37.2 | 17.0 | 10.2 | 47.5 | 25.0 | 15.0 | 62.5 | 37.0 | 22.2 |
| 44,000 | 39.8 | 18.8 | 11.3 | 51.0 | 28.5 | 17.1 | 66.6 | 41.0 | 24.6 |
| 54,000 | 42.6 | 21.6 | 12.9 | 54.5 | 31.7 | 19.0 | 72.0 | 46.0 | 27.6 |
| 68,000 | 46.1 | 25.0 | 15.0 | 59.0 | 36.0 | 21.6 | 77.5 | 51.0 | 30.6 |
| 88,000 | 50.2 | 29.0 | 17.4 | 64.0 | 40.0 | 24.0 | 84.0 | 57.5 | 34.4 |
| 114,000 | 54.7 | 33.0 | 19.8 | 69.8 | 46.0 | 27.6 | 92.0 | 65.0 | 39.0 |
| 152,000 | 60.3 | 39.0 | 23.4 | 76.5 | 53.0 | 31.8 | 102.0 | 74.5 | 44.7 |
| 223,000 | 68.5 | 46.5 | 27.9 | 87.5 | 63.0 | 37.8 | 113.0 | 84.0 | 50.4 |
| 410,000 | 83.9 | 62.0 | 37.2 | 110.0 | 84.0 | 50.4 | 140.0 | 108.0 | 65.0 |
| | | | 217.7 | | | 308.2 | | | 439.8 |

* It is assumed here that the amount of salt is constant as the RH is varied. The original data (WOODCOCK, 1950, p. 398) are inadequate to test this assumption. Sampled amounts of salt differed by a factor of 2.4, while the RH varied from 82 % to 91 %. These RH values are thought to be too low however, due to the necessity to expose the thermometers inside the lighthouse enclosure (with several windows open). Thermometers exposed outside were immediately coated with a briny film, thus making the readings uncertain.

from about 0.003 to 0.08 mg $m^{-2}$ $sec^{-1}$, with an average of about .02. This range of values agrees very well with one estimated from the average rainfall in moving storms (RIEHL, 1954, p. 295) and from the chloride concentration in typhoon and hurricane rains (MIYAKE, SUGUIRA, 1954) (HARRISON, WILLIAMS, 1897).

Thus the estimated fall-out of chloride transported up in the clouds (about 0.27 mg $m^{-2}$ $sec^{-1}$) exceeds by a factor of more than ten the average observed rate of chloride fall in rains.

If, for the moment, one assumes that within the storm area sufficient salt has been carried up in the clouds to establish a steady state, then the average fall of briny particles through the relatively clear inter-cloud air ($S_f$) is simply derived as follows:

$$S_f = \frac{S_a - S_r}{10} \qquad (1)$$

where $S_f$ = sea salt falling (mg $m^{-2}$ $sec^{-1}$)
$S_a$ = sea salt ascending in clouds (4.8 mg $m^{-2}$ $sec^{-1}$)
$S_r$ = sea salt carried down in rains (0.04 mg $m^{-2}$ $sec^{-1}$)

Using equation (1) it is found that a fall-out of salt aerosols from the inter-cloud air of about 0.44 mg $m^{-2}$ $sec^{-1}$ should occur. (It will be noted that this quantity is very similar to the fall of salt computed on Table 2 from the observed values. This similarity is presumably due to a realistic choice of variables in estimating fall-out from the inter-cloud air.)

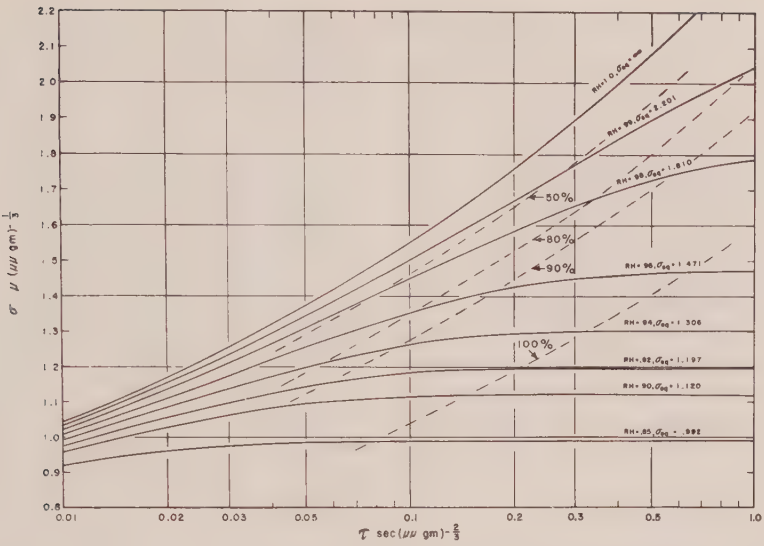


Fig. 5. Sea-salt particle-growth curves at various fractional humidities and a temperature of 25 C. Multiplication of $\tau$ by the cube root of nucleus mass, and of $\sigma$ by the nucleus mass raised to the 2/3 power, converts coordinates to droplet radius in microns and time in seconds (from KEITH and ARONS, 1954). The dashed lines have been added by the present author to estimate the time required to establish various fractions of the equilibrium volume of the droplets.

When the salt particles fall from the relatively dry inter-cloud air into the moist sub-cloud air, condensation occurs and heat is released.

## 5. Heating of unsatured sub-cloud air by condensation on falling salt

The amount of water which will condense ($W_L$) as the falling salt particles enter the moist air, is computed from the equation

$$W_L = S_f \frac{I}{c} \qquad (2)$$

where $W_L$ is expressed as mg m$^{-2}$ sec$^{-1}$
$S_f$ = weight of salt falling (mg m$^{-2}$ sec$^{-1}$)
$c$ = concentration of sea salt in particles by weight fraction (from ARONS and KIENTZLER, 1954).

Utilizing the relationships given in equation (2) and the salt fall-out, the weights of condensed water were computed. The heating of the air resulting from this condensation was then derived as follows:

$$T = m_L / C_p \qquad (3)$$

where $T$ = temperature change (°C gm$^{-1}$ sec$^{-1}$)
$m$ = weight of water condensed (gms gm$^{-1}$ sec$^{-1}$)
$L$ = latent heat of vaporization of water (585 cal gm$^{-1}$)
$C_p$ = specific heat of moist air (0.245 cal gm$^{-1}$)

Assuming that 0.44 mg m$^{-2}$ sec$^{-1}$ of sea salt are falling from an air layer having a RH of < 74 per cent,[1] into regions where the RH is 90, 96 and 98 per cent, equation (2) is used to derive the amount of water condensed. In so doing the data on Figure 2 are used. It is found that water is condensed at a rate of 12.6 mg m$^{-2}$ sec$^{-1}$, if the moist layer RH is 98 per cent, 5.9 mg m$^{-2}$ sec$^{-1}$ if it is 96 per cent and 2.9 mg m$^{-2}$ sec$^{-1}$, if it is 90 per cent. This assumes that a steady state exists and that condensation on all particles proceeds to a

[1] In a recent series of temperature soundings by the Woods Hole Oceanographic Institution aircraft (August 1956), the relative humidity in the clear air above 5,500 feet was 72 per cent or less in several locations in the West Indian region. It is supposed that it is the more or less normal trade-wind air and clouds of this time of year which are drawn into tropical cyclones (see discussion of this point by Wexler, 1947).

state of vapor pressure equilibrium in the moist air. In the time required to fall 200 meters, most of these particles will reach more than 90 % of their equilibrium size at these relative humidities (see Fig. 5; GUNN and KINZER, 1949; and Stoke's law).

The computed heating of the moist layer of air resulting from the above amounts of condensed water, utilizing equation (3), is shown in Table 3 below. The degree of this heating in any given mass of air depends of course upon the average relative humidity there. The air-layer depths selected for tabulation[1] lie in the range of those reported for the sub-cloud layer in tropical storms. It is this layer which contains most of the air spirally converging upon the rain-area. The extent to which the assumed relative humidities of this air are realistic is uncertain. Similar high values have however been reported and utilized in other hurricane studies (see TANNEHILL, 1943, Fig. 10; SIMPSON, 1947, and RIEHL, 1954, Fig. 11–29).

Riehl has indicated the potential temperature as a function of surface pressure in hurricanes (RIEHL, 1954, p. 287). It is concluded from his study of available data that the average pressure drop is about 50 mb, and that the average amount of sensible heating of the converging air is about 4° C.

Using Hughes' Figure 8 (HUGHES, 1952), which shows the average trajectories and rates of convergence of surface air to a point within 0.5° latitude (30 nautical miles) of the moving storm center, it is estimated that the heating of this air occurs in from 12 to 22 hours, with an average of about 18 hours. In other words 4° C is the approximate temperature increase in the air within the range of time required for it to move into the 0.5° latitude point from a distance of 240 nautical miles out from the center. On Table 3 it can be seen that the latent heat released due to condensation upon salt particles produces temperature increases which range from about 0.5 to 9 °C, depending upon the time used, the average relative humidity of the sub-cloud layer and the thickness of this layer. It is assumed of course that the high relative humidities are maintained by evaporation from the sea surface. As a rough first approximation, the similarity of this range of heating computed from the salt fall-out, to the range given in Riehl's study (see RIEHL, 1954, p. 287), encourages further work in this direction.

[1] A cubic meter of air is assumed to weigh one kilogram. No corrections have been made in this paper for pressure effects upon particle distributions or fall rates, since the condensation processes discussed are thought to occur largely at low altitudes.

### 6. Effects of salt fall-out from undiluted aerosols

The fall-out of salt into the moist lower air from the cloud layer will not, of course, be in a steady state, since the clouds which transport most of the salt are so unsteady (KESSLER) (SIMPSON). In order to estimate the average heating effects of this salt fall upon the sub-cloud layer as a whole, it was necessary in the previous section to assume a steady state and a ten times dilution of the salt transported by the clouds. It is of interest to consider some effects, of shorter duration, which might arise in areas where the aerosol population might remain undiluted. In order to do this it becomes necessary to estimate the aerosol concentrations to be expected in inter-cloud areas near active cloud systems.

Below it will be shown that condensational growth of the salt nuclei in ascent to cloud base and within the clouds will result in a "compression" of their spacial distribution.

TABLE 3

**Computed air temperature increases, in layers of various vertical thickness, due to condensation on falling salt**

| Height of layer Meters | Air temperature increase in 18 hours (°C) | | |
|---|---|---|---|
| | RH 90 | RH 96 | RH 98 |
| 200 | 1.0 | 2.9 | 9.4 |
| 400 | 0.5 | 1.5 | 4.7 |

The largest increase in concentration occurs as the nuclei fall from the clouds into relatively dry inter-cloud air. The cloud and its local environment thus become an area of concentration of salt.

a) *Ascent of salt-laden air to cloud base.* Columns 5 through 9, Table I, show the changes which occur as a result of the lifting of air from near the surface up to cloud base.

The radii in column 5 are taken from the sea-salt nuclei growth measurements of Kieth and Arons, and they represent the sizes of the salt particles of column 1 at cloud base, assuming dry adiabatic ascent at a rate of one meter per second (see Figure 6).[1] The rates of fall of individual particles, which are given in column 6, are taken directly from Stoke's law and, for the larger particles, from the measurements of Gunn and Kinzer (1949). The amounts of sea salt which are falling, are given in column 7, and are the product of the fall rate (column 6) and the quantity of salt in the size ranges concerned (column 9). The amounts of water falling are a product of the amounts of salt falling (column 7) and their concentration, expressed as grams per gram. (These rates of fall of salt and water represent fall relative to the air.) Finally, column 9, which indicates an increased amount of salt in the air, is a product of the initial amount of salt passing unit area per second and the quantity one over the rate of ascent of the air minus the rate of fall of the particles.

More definitely expressed, this relationship becomes:

$$W = w' \frac{1}{v - u} \qquad (4)$$

where $W$ = wt. of sea salt $m^{-3}$ of air
$w'$ = wt. of sea salt crossing each $m^{-2}$ per second ($\mu$ gms)
$v$ = rate of ascent of air (m $sec^{-1}$), and
$u$ = rate of fall of the particles (m $sec^{-1}$).

In each case $w'$ is fixed, in any column of air ascending at a steady rate, by the initial quantity of salt of each size range in the air as it rises from near the sea surface, by the fall rate of the particles and by the rate of rise of the air. This means that within an ascending column of air the weight of salt passing each square meter of horizontal surface, which is fixed in reference to the ground, is constant. It is assumed here that there is a horizontal homogeneity in the salt aerosol population.

Thus it seems, from the results in column 9, that the adiabatic ascent of moist air containing salt particles, will cause a concentration or a compression of the particle distribution. This compression is due to the condensational growth of the particles and to their consequent increased fall rate (in Table I, compare columns 2 and 3 to columns 5 and 6). It can be seen in equation (4) that the changing relationships between the rates of rise of the air and of the particles, alter the salt particle concentration.

An increase in the amount of salt with increasing altitude in the sub-cloud layer of the trade-wind atmosphere was first reported

[1] The conditions assumed in deriving the droplet sizes given in Figure 6, are not strictly applicable to the present case. However the error, in computed particle size at cloud base, which results from these differences in conditions is not significant here.

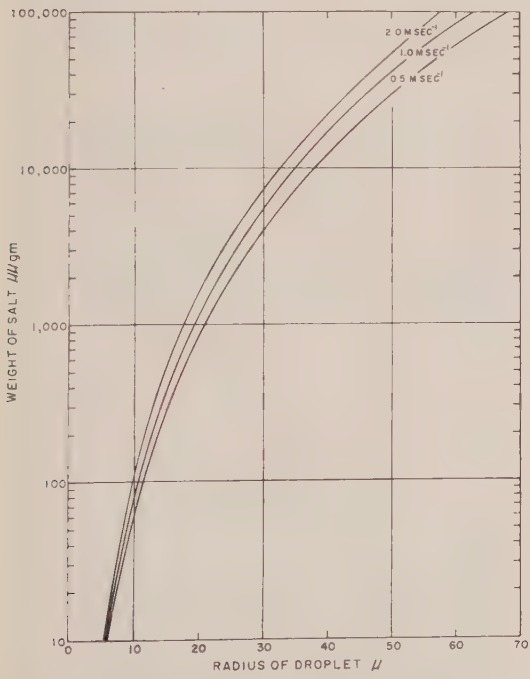


Fig. 6. Calculated radius of sea-salt droplets at cloud base (RH 100 per cent), as a function of nucleus mass and rate (taken from Keith and Arons, 1954).

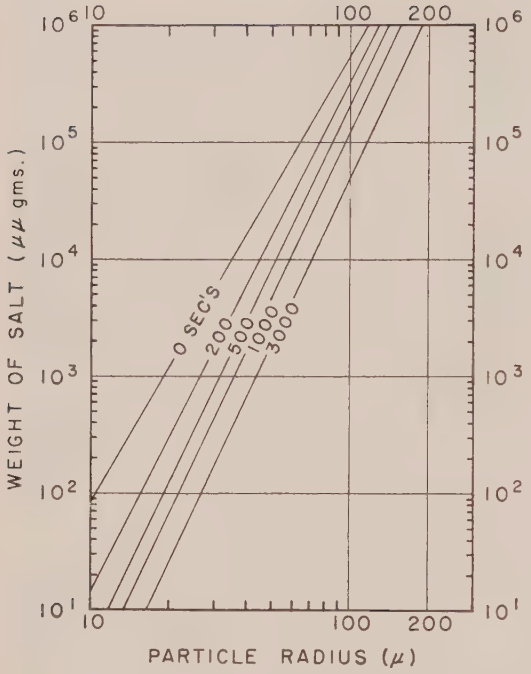


Fig. 7. Sizes of salt particles after given times in cloud:—including growth in coming to cloud base at 1 m/sec rise. (From KEITH and ARONS, 1954, see text).

by LODGE (1955) and has been subsequently occasionally observed by the author while making nuclei measurements for other purposes. These observations are not adequate to be used here as a test for the computed increase in salt with altitude. Such test measurements are planned in the future, using the recently developed airborne flame photometer (WOODCOCK, SPENCER, 1957) in conjunction with the glass-slide sampling method (WOODCOCK, 1952).

(b) *Ascent of salt-laden air in cumuli.* In the trade-wind areas the cumulus clouds are the major mechanism bringing about the transport of surface air from near cloud base altitudes upwards into the cloud layer (MALKUS, 1956) (RIEHL et al., 1951). We now assume that the clouds serve a similar role in the lower air spiraling into hurricanes, and determine the change in salt particle size and concentration as the air rises in these clouds and into the inter-cloud regions.

Figure 7 shows the radii of the various weights of sea-salt particles as a function of time of exposure in cloud air, assuming a relative humidity in the cloud of 100 per cent. These growth rates were derived for the author by C. H. Kieth, and are based upon his experimental determination of the condensation on sea-salt nuclei (KIETH, ARONS, 1954).

In Table 4, the droplet radii shown in column 2 are taken from the 1,000 second curve of Figure 7. At the rate of ascent assumed, this is about the time required for an air parcel to rise from cloud base to the top of a cloud of medium vertical development. Equation (4) is again applied to the different conditions in the cloud, in order to determine the additional "compression" of the particle distribution due to the changed relative motions. In this case, however, $W$ is determined by the quantity of salt in the air at cloud base and by the increased values for particle fall rate and rate of rise of the air in the cloud. The sums of the quantities in column 6 of Table 4, show that the calculated amount of salt per unit volume of air has again been increased by ascent in the cloud, as it was in ascending in the sub-cloud layer. Comparison of columns 4 and 5 of this table to columns 4, 7 and 8 of Table I, show that there has also been a marked increase in the rates of fall of salt and water with reference to the ascending air.

(c) *Fall-out of salt particles from cloud into clear air.* As the large salt-containing droplets in the cloud (column 2, Table 4) fall or are mixed into the clear environmental air, evaporation occurs and the resulting alteration of particle settling rate again compresses the distribution. This compression is derived as follows:

$$W' = W_c \frac{U}{U'} \qquad (5)$$

where $W'$ = wt. of sea salt in the clear air ($\mu$ gms m$^{-3}$) after evaporation to equilibrium has occurred

$W_c$ = wt. of sea salt in cloud (column 6, Table 4) in $\mu$ gms m$^{-3}$

$U$ = particle fall rate as droplet in cloud (column 3, Table 4), in cm sec$^{-1}$

$U'$ = particle fall rate after evaporation to equilibrium in clear air, in cm sec$^{-1}$

TABLE 4

**Alterations in the distribution of the salt particles represented by curve 12 figure 3, upon ascent in a cumulus cloud and upon falling out of the cloud into clear inter-cloud air.**

| Sea-salt nuclei as cloud droplets after 1000 seconds in cloud; R. H. 100 %; rise rate 4 m $sec^{-1}$ | | | | | | Droplets fall into clear air at cloud levels where R. H. < 74 % and evaporate to a crystal state | | |
|---|---|---|---|---|---|---|---|---|
| Weight of sea-salt particles $10^{-12}$ g | Cloud droplet radius $\mu$ | Cloud droplet fall rate cm $sec^{-1}$ | Amounts of salt and water falling $\mu$ gms. m $^{2}$ $sec^{-2}$ | | Wt. of salt in each size range $\mu$ gms. $m^{-3}$ | Salt particle radius $\mu$ | Particle fall rate cm. $sec^{-1}$ | Wt. of salt in each size range $\mu$ gms. $m^{-3}$ |
| | | | salt | water | | | | |
| 1 | 2 | 3 | 4 | 5 | 6 | 7 | 8 | 9 |
| 50 | 19 | 4.4 | 2.7 | 1,545 | 61 | 1.8 | 0.084 | 2,980 |
| 600 | 32 | 11.6 | 7.3 | 1,663 | 63 | 4.0 | 0.42 | 1,710 |
| 1,750 | 40 | 17.5 | 11.4 | 1,739 | 65 | 5.8 | 0.86 | 1,320 |
| 3,200 | 45 | 22.0 | 14.7 | 1,775 | 67 | 7.0 | 1.27 | 1,130 |
| 4,800 | 50 | 25.5 | 17.4 | 1,823 | 68 | 8.9 | 1.63 | 1,075 |
| 7,100 | 54 | 29.5 | 20.5 | 1,869 | 70 | 9.2 | 2.15 | 925 |
| 9,900 | 58 | 33.0 | 23.2 | 1,887 | 71 | 10.2 | 2.72 | 863 |
| 13,100 | 62 | 36.5 | 26.5 | 1,983 | 72 | 11.2 | 3.25 | 825 |
| 16,700 | 65 | 39.5 | 29.2 | 1,981 | 74 | 12.2 | 3.85 | 770 |
| 21,800 | 68 | 42 | 31.5 | 1,868 | 75 | 13.3 | 4.50 | 685 |
| 28,000 | 72 | 46 | 35.4 | 1,935 | 77 | 14.5 | 5.5 | 656 |
| 36,000 | 76 | 50 | 39.5 | 1,980 | 79 | 15.7 | 6.4 | 618 |
| 44,000 | 80 | 54 | 44.2 | 2,106 | 82 | 16.8 | 7.3 | 600 |
| 54,000 | 83 | 57 | 47.9 | 2,077 | 84 | 18.0 | 8.4 | 577 |
| 68,000 | 88 | 61 | 53.0 | 2,177 | 87 | 19.4 | 9.7 | 546 |
| 88,000 | 92 | 65 | 58.5 | 2,111 | 90 | 21.2 | 11.6 | 508 |
| 114,000 | 98 | 70 | 68.8 | 1,921 | 93 | 23.1 | 13.8 | 465 |
| 152,000 | 104 | 76 | 74.5 | 2,225 | 98 | 25.4 | 16.7 | 440 |
| 223,000 | 113 | 84 | 87.4 | 2,273 | 104 | 29.0 | 22.0 | 398 |
| 410,000 | 128 | 97 | 117.3 | 2,403 | 121 | 35.4 | 33.0 | 362 |
| | | | 811 | 39,341* | 1,602 | | | 17,453 |

* This fall rate, expressed in more familiar terms, is about 0.04 mm $hr^{-1}$, which is near the minimum measured within trade-wind orographic clouds (BLANCHARD, 1953).

Column 9 of Table 4 shows that a "compression" of salt concentration of about one order of magnitude would result if evaporation to a crystalline state in the clear air occurred with a continuous source of cloud particles allowing the establishment of a steady-state condition. The total rate of fall of salt in the clear air is the same as that in the cloud, for the product of the fall rate and the salt concentration, columns 8 and 9 of Table 4, can be seen to equal the values in column 4. In other words the conservation of mass principle is assumed to apply here, so that the number of particles falling into the top of a given column of air in a certain time interval must equal the number falling out at the bottom of this column in the same interval.

Thus the ascent of salt-laden air from near the sea surface to cloud base altitudes, its ascent in cumulus clouds and its final passage into the clear cloud-level air, tend in each case to increase the quantity of salt in the air.

As previously mentioned, an increase of salt with altitude is sometimes observed in the sub-cloud layer. Recent use of an airborne flame photometer in trade-wind clouds has indicated that the average salt (sodium) content of these clouds is sometimes higher than the average salt content of the air below cloud base (WOODCOCK, SPENCER, 1957). No data are available however on the nuclei present in the clear air at cloud levels at times or at places where an inter-cloud increase in salt might have been encountered. Observations aimed specifically at exploration of the salt nuclei gradients in the lower trade-wind atmosphere during storms are needed to test the above calculated gradients.

The computed and observed increase with altitude in the amount of salt particles in the air encourages some calculations concerning the possible effects of these particles in altering the distribution of water vapor and temperature as they fall, in undiluted concentration, from the higher levels towards the sea. For convenience in making the calculations of salt fall-out in inter-cloud air, it is assumed that the ascent of new masses or bubbles (SCORER, LUDLAM, 1953) of cloud materials is frequent enough to produce a relatively steady source of the larger salt particles, which supply the greatest amount of falling salt (see column 4, Table 4). With a markedly transient cloud source of the falling particles, the wide range of fall speeds present among these larger particles (see column 8, Table 4) would soon cause a diminishing concentration in the clear air as the larger particles fell away from the smaller.

Of course the droplet population of a significant volume of a cumulus cloud is not likely to have been exposed to saturated conditions for exactly 1,000 seconds as was assumed in Table 4. However, for the rate of rise assumed here, exposure times in ascending air parcels of about 500 to perhaps 1,500 seconds seems reasonable for the clouds concerned. On Figure 7 and Table 4 it can be seen that this range of exposure duration is not sufficient to cause droplet size differences, for any given particle weight, which would markedly alter the particle-concentration effects discussed here. The important requirements are that droplets of the approximate sizes given be present in the clouds and that they form on salt particles having weights approximating those given. No reference to measurements of the droplet size distribution of marine cumuli in tropical storms has been found in the literature. However, Squire's results in Australian and Hawaiian maritime clouds during moderate winds (SQUIRES, GILLESPIE, 1952) (SQUIRES, WARNER, 1957) are consistent with the computed drop size distributions given here. The effects of coalescence of droplets upon size distribution and in increasing rates of fall were not considered above. Introduction of these complicating effects would serve only to increase salt fall-out, which for present purposes is shown to be adequate.

The purpose of the above computations of the compression effects of ascent and growth upon salt particle concentration was to show, in the section to follow the local heating effects of fall-out of salt from areas of undiluted aerosol concentration. In estimating these effects in the sub-cloud layer as a whole, it will be remembered that, in section 5 above, a dilution of the cloud-borne salt by a factor of ten was assumed.

(d) *Altered vapor and temperature distribution in cloud layer.* When the particles fall from the cloud into the inter-cloud air having a relative humidity less than 74 %, evaporation to relative dryness will occur. The diminishing droplet size causes a sharp reduction in rate of fall of individual particles (see column 8, Table 4). However, the great increase in the salt concentration in the air, shown in column 9, will cause the total rate of fall of salt $m^{-2}$ $sec^{-1}$ in each weight range to remain the same as it was in the cloud – note for instance that the product of the fall rate and the weight of salt in each size range (columns 8 and 9 of Table 4) is equal to the quantities in column 4. The sum of these quantities can be seen to be 811 $\mu$ grams of sea salt falling per square meter per second.

If, in falling towards the sea, this mass of salt moves out of the dry air (RH < 75 per cent) and into a layer where the RH is 90 per cent, condensation will occur on the particles, heat will be released and water will be carried downward. Upon subsequently falling out of the moist layer and into a dry

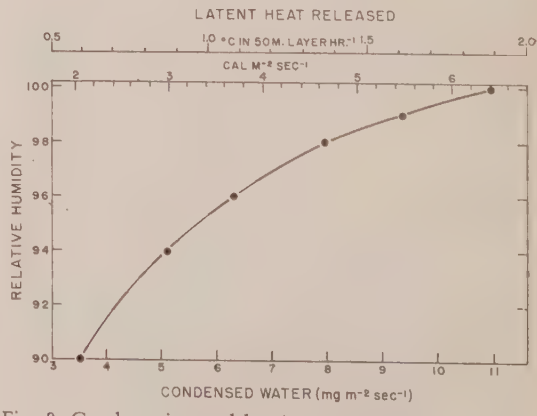


Fig. 8. Condensation and heating in moist layer of air of 50 m depth, during initial 100 seconds after entry into layer of salt particles falling from dry air. (See text for more information.)

TABLE 5

**Amounts of water condensed on salt particles 100 seconds after they fall into saturated air from dry air (RH < 74 %).**

| Sea-salt particle weight $10^{-12}$ g | Total amounts of salt falling $\mu$ gms $m^{-2}$ $sec^{-1}$ | Particle radius after 100 seconds $\mu$ | Particle fall rates after 100 seconds cm $sec^{-1}$ | Amount of water falling after 100 seconds $\mu$ gms $m^{-2}$ $sec^{-1}$ |
|---|---|---|---|---|
| 50 | 2.7 | 12.5 | 2.1 | 440 |
| 600 | 7.3 | 21.5 | 6.0 | 492 |
| 1,750 | 11.4 | 26.5 | 9.0 | 491 |
| 3,200 | 14.7 | 30.0 | 11.5 | 503 |
| 4,800 | 17.4 | 33.0 | 13.5 | 526 |
| 7,100 | 20.5 | 36.0 | 15.8 | 542 |
| 9,900 | 23.2 | 38.5 | 17.8 | 539 |
| 13,100 | 26.5 | 41.0 | 20.0 | 569 |
| 16,700 | 29.2 | 42.5 | 21.3 | 539 |
| 21,800 | 31.5 | 45.0 | 23.8 | 517 |
| 28,000 | 35.4 | 47.0 | 25.5 | 521 |
| 36,000 | 39.5 | 50 | 28.7 | 541 |
| 44,000 | 44.2 | 52 | 31.0 | 559 |
| 54,000 | 47.9 | 55 | 33.7 | 572 |
| 68,000 | 53.0 | 58 | 36.4 | 585 |
| 88,000 | 58.5 | 61 | 39.0 | 579 |
| 114,000 | 68.8 | 64 | 42.0 | 596 |
| 152,000 | 74.5 | 69 | 47.0 | 592 |
| 223,000 | 87.4 | 75 | 53.5 | 598 |
| 410,000 | 117.3 | 86 | 64.0 | 641 |
| | 811 | | | 10,942 |

layer, evaporation will occur, the dry layer will be cooled and water vapor added. Thus the passage of salt-bearing particles down through the atmosphere will act to warm and dry the moist layers and to cool and moisten the dry layers. The heat released and the water transported by this process is estimated as follows.

The particles represented by column 4, Table 4, upon falling from dry air into saturated air, will cause condensation of about 11 mg of water $m^{-2}$ $sec^{-1}$ during the first one hundred seconds of their fall through the moist air. This quantity was derived as shown in Table 5, using the information given in Figure 5. Other quantities were obtained in this manner for unsaturated air layers. The results are given in Figure 8.

Since the condensation in the first one hundred seconds will occur in an air layer of about 50 meters of vertical thickness, or less (see fall rates, Table 5), we can estimate the average heating of this layer. Using equation (3), it is found that the condensation rates given on the lower scale of Figure 8 will heat 50 kg of air by the amounts given on the upper scale. This range of rates of release of latent heat is equivalent to the wet-adiabatic lifting of the lower air at 3 to 10 cm $sec^{-1}$.

Thus fall-out of undiluted aerosols can produce greater amounts of local heating than those estimated for the sub-cloud layer as a whole (Table 3). It is suggested that this heating may be an important factor in the production of instability, especially in those cases where moist parcels of air are trapped by overlying layers of stable air.

Thus a significant transport of water and release of heat can occur at relative humidities of 100 per cent and less as sea-salt aerosols fall through layers of air of different relative humidities. Of course the actual amount of water condensed would be somewhat less, due to the slow lowering of the relative humidity of a moist layer, of specific vertical extent, as water is removed and latent heat released. It is supposed that such lowering of the relative humidity is, in many cases, reduced or prevented by ascent due to the heating of the air.

It may be useful to point out a further effect

of the fall-out of salt particles through the moist air of the cloud layer. Their tendency to establish vapor pressure equilibrium at each level should act to equalize the relative water vapor distribution. A trend towards constancy of relative humidity would result from the fact that in air over sea-salt solutions of constant salinity, the relative humidity changes very little with temperature. Note on Figure 2 for instance, that the relative humidity over a sea-salt solution, which is 80 ‰ chloride, is 91.3 % at ten degrees and 90.4 % at twenty-five degrees. Particles falling through air layers of differing relative humidity will add water to the relatively dry levels and subtract water from the relatively moist levels. The trend will always be towards a more constant droplet salinity and hence a more constant relative humidity. To what extent this effect is traceable in the trade-wind or tropical-storm atmosphere is as yet unknown.

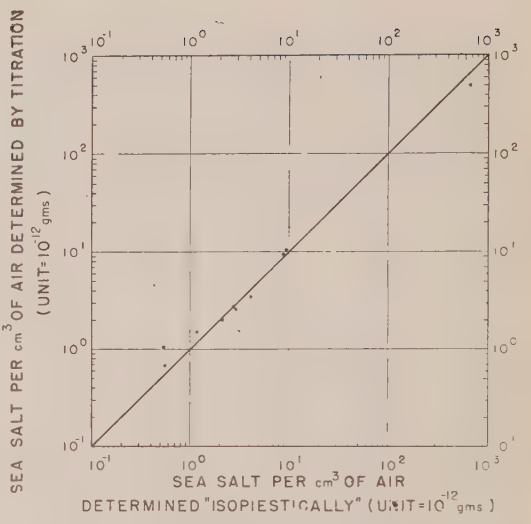
SEA SALT PER cm³ OF AIR DETERMINED BY TITRATION (UNIT=10⁻¹² gms)
SEA SALT PER cm³ OF AIR DETERMINED "ISOPIESTICALLY" (UNIT=10⁻¹² gms)

Fig. 9. The quantities of airborne salt collected by impingement on one mm wide strips and measured directly by precipitation with silver nitrate and indirectly by the equal pressure method.

### 7. Accuracy of measurement of salt particles

The isopiestic method (GLASSTONE, 1940) for measuring the weights of salts in solution in small droplets is considered sufficiently accurate as applied to the problems discussed here. Figure 9 shows several test comparisons of weights of chloride measured by titration, using a microburette to measure the silver nitrate solution, and by the isopiestic method (WOODCOCK, 1950) (WOODCOCK, GIFFORD, 1949). The error of the titration was less than plus or minus 10 per cent. TWOMEY (1954) has recently demonstrated the close correspondence of the individual salt particle sizes determined isopiestically and by the chemically sensitized film method of SEELY (1952). It should be noted that experimental application of the isopiestic method above a relative humidity of about 90 per cent apparently introduces an error which becomes increasingly significant as 100 per cent is approached (CROZIER, 1954).

### 8. Discussion

In evaluating and expanding upon the foregoing explanation for the relatively constant temperature of the surface air in hurricanes, consideration of the following questions seems useful at this time.

a) Will the fall speed of the salt particles in the inter-cloud air be sufficient to bring them down to the sub-cloud air before they are carried out of the storm area by radial winds?

The data on Table 1 show that the particles which contribute most to the salt fall-out, descend as crystalline nuclei (RH < 74 %) at rates of several hundreds to one thousand meters per hour. They will soon fall back from the inter-cloud to the sub-cloud layers, if they are not carried up into the regions of rapid out-flow at high levels. This conclusion is based upon RIEHL's evidence (1954, p. 303) that the radial wind speeds at intermediate altitudes are low, and vacillate between inflow and outflow. At the upper levels high outflow rates will probably carry the particles far out from their areas of origin. The question of the role of the fall-out of these dispersed particles in the release of heat in moist peripheral regions of storms, such as those in the lower atmosphere in advance of Edna and Ione (KESSLER, 1957), will be investigated in a later study.

b) Are observed rates of radial inflow of surface air adequate to replace the ascending air required to transport the salt up in clouds?

In section 2 of this paper it was simply assumed that cumulus clouds in a hurricane carry aloft sufficient surface air and aerosols to maintain a certain average or "steady state"

salt fall through the inter-cloud area. This assumption seems questionable however, if it is supposed that there is no interchange of air between the cloud and sub-cloud layers, and that each mass of rising air in the clouds is replaced by an equal mass of converging sub-cloud air. This question is elaborated in the following discussion.

Converging sub-cloud air in tropical storms is thought to equal in mass the air which ascends in the cumuli and which eventually flows radially outwards at higher levels (RIEHL, 1954). Observations of radially converging lower air, which might be compared to the above estimates of the amounts of ascending air needed to carry the load of salt aerosols, are not available for individual storms. However, in Hughes' study (HUGHES, 1952) of the pattern of low level winds (at about 1,000 feet) in Pacific tropical cyclones, averaged radial inflow was derived for 28 storms. From this inflow averaged ascent over the whole storm area of from 1 to 12 cm $sec^{-1}$ is derived, the greater and more rapid part of the ascent being in or near the central "rain area". In the present study of the role of salt particles in the release of latent heat, the best estimates of the range of rates of ascent of air required to carry a sufficient salt load lie between 10 and 100 cm $sec^{-1}$. This range of rates is computed, assuming that the salt load of the sub-cloud air varies from the average of my own measurements to a maximum which is about equal to the highest values reported in the literature (about 10 mg $m^{-3}$, RAU, 1956). Thus an overlap of the range of rates of ascent derived from Hughes' measurements, and the range of rates of ascent required to carry the salt load occurs, but a wide disparity in average magnitude exists.

It appears improbable from the above estimates that the radial inflow of the lower air is sufficient to carry the salt load required in the present study. A mass of ascending air several times that of the recorded average inflowing air is required. The question remains open however, for recent evidence indicates that the earlier observations of radial inflow are too low, and also that a considerable interchange of air between the cloud and sub-cloud layers occurs which is part of the normal growth mechanism of trade-wind cumulus clouds (MALKUS). This latter evidence shows that a part of the air ascending in cumuli can be regarded as "cyclic air", and that it is incorrect to assume that the amount of radially converging air necessarily equals the amount ascending in the cumuli.

c) Is it necessary to regard the amounts of salt observed in one hurricane as an upper limit of quantities to be expected in these storms? This problem is especially pertinent here, since the present study reveals somewhat marginal heating effects from salt amounts taken from available data.

The experience of sampling atmospheric salt particles under a wide range of conditions has convinced the author that the amount of salt represented by curve 12 of Figure 3 should not be considered an upper limiting quantity. The hurricane-aerosol data used here, which are the only available data, were obtained at a time when most of the storm was over land. The sampling position was the top of Hillsboro Lighthouse, on the Florida east coast, at Pompano. At the time of sampling, September 22, 1948, 2330, E.S.T. (WOODCOCK, 1950), the storm center or "eye" was over inland Florida, and the air from which the samples were taken had only recently passed from over land about 30 miles south of the station (see surface winds, Miami to Key West, N.W.R.C., Ashville, N.C.). Since the salt aerosol load of the air is a function of the fetch over the sea, as well as of wind force (WOODCOCK, 1954), this recent passage of the air from over land would result in a relatively low salt content when compared to this content if the entire cyclone had been over the sea. The author has little doubt that the salt load of the lower air in severe wind storms at sea commonly exceeds the amounts given here by a factor of ten or more. Such amounts would of course result in proportional increases in the heating of the sub-cloud air in the model proposed. However, the above hurricane sample serves the purpose here, which is to demonstrate that observed quantities of salt nuclei, upon ascent in clouds, will alter the distribution of water vapor and temperature as they fall back towards the sea. The magnitudes of these effects are certainly large enough to satisfy a first-approximation study.

It is perhaps not a coincidence that the weights of salt required to bring about the

release of latent heat discussed here, add little to the air density. The maximum quantity of airborne sea salt considered (i.e. about 10 mg $m^{-3}$) will produce a density increase, at ordinary surface pressures, about equal to the increase caused by a temperature decrease of 0.01 C in the usual air temperature range.

## 9. Conclusions and Recommendations

A mature hurricane at sea is a gigantic salt-aerosol generating and distributing mechanism. Fall-out from the aerosols carried aloft in the storm clouds, may liberate significant amounts of latent heat in the moist lower layers of the atmosphere. Thus the vast self-generated salt cloud in the atmosphere of these storms should be seriously considered as one of the properties influencing their stability. In the model proposed a moist lower layer and a relatively dry inter-cloud layer of air is required.

It is recommended that many measurements of the size distribution of sea-salt particles be made in the relatively clear air in various parts of tropical (and extra-tropical) marine cyclones. If these measurements reveal a salt fall-out of several milligrams per square meter per second into the air converging upon a storm center, the effects of this salt in adding to the internal temperature gradient become apparent. Riehl shows for instance (Riehl, 1954, p. 313—316) that the isothermal expansion of the converging sub-cloud air, results in temperature excesses of several degrees as this air ascends in the "rain area" of hurricanes.

## Acknowledgments

The author is especially grateful for the critical efforts of Dr. Arnold Arons, which resulted in a clarifying and unifying revision of the original form of this paper. He is also indebted to his associate, Mr. D. C. Blanchard and to Mr. W. V. Kielhorn for helpful suggestions.

## REFERENCES


Arons, A. B., and Kientzler, C. F., 1954: Vapor pressure of sea-salt solutions. Trans. Amer. Geophys. Union, **35**, 722—728.

Blanchard, D. C., 1953: Raindrop size-distribution in Hawaiian rains. Jour. Met., **10**, 457—473.

Blanchard, D. C., and Woodcock, A. H., 1957: Bubble formation and modification in the sea and its meteorological significance. Tellus, **9**, 145—158.

Bunker, A. J., Haurwitz, B., Malkus, J. S., and Stommel. 1949: Vertical distribution of temperature and humidity over the Caribbean Sea. Pap. Phys. Oceanogr. and Meteor., **XI**, No. 1, pp. 1—82.

Byers, H. R., 1944: General Mereorology, McGraw-Hill, New York.

Crozier, W. D., 1954: Errors in the "isopiestic" method for measuring masses of salt particles. Science, **120**, 840—841.

Glasstone, Samuel, 1940: Text-book of physical chemistry. D. Van Nostrand Co., Inc., New York, 1289 pp.

Gunn, R., and Kinzer, G, D., 1949: The terminal velocity of fall of water droplets in stagnant air. J. Meteor., **6**, 243—248.

Harrison, J. B., and Williams, John, 1897: The proportions of chlorine and nitrogen as nitric acid and as ammonia in certain tropical rainwaters. J. Amer. Chem. Soc., **19**, 1—9.

Hughes, L. A., 1952: On the low-level wind structure of tropical storms. Jour. Meteor., **9**, 422—428.

Jordan, C. L., 1952: On the low-level structure of the typhoon eye. Jour. Meteor., **9**, 285—290.

Kessler, Edwin III, 1957: Outer precipitation bands of hurricanes Edna and Ione. Bull. Amer. Met. Soc., **38**, 335—346.

Kientzler, C. F., et al., 1954: Photographic investigations of the projection of droplets by bubbles bursting at a water surface. Tellus, **6**, 1—7.

Kieth, C. H., and Arons, A. B., 1954: The growth of sea-salt particles by condensation of atmospheric water vapor. J. Meteor., **11**, 173—184.

Langmuir, I., and, Blodgett, K. B., 1945: A mathematical investigation of water droplet trajectories. Gen. Elec. Res. Lab. Rep., A.T.S.C. contract W-38-038-Ac-9131, 1—47.

Lodge, J. P., 1955: A study of sea-salt particles over Puerto Rico. J. Meteor., **12**, 493—499.

Malkus, Joanne Starr, 1956: On the maintenance of the Trade-Winds. Tellus, **8**, 335—350.

— Personal communication.

May, K. R., 1945: The Cascade Impactor: An instrument for sampling coarse aerosols. Jour. Sci. Inst., **22**, 187—195.

Miyake, Y., and Suguira, Y., 1950: The mechanism of the dissolution of the atmospheric chlorides into rain water. Pap. Meteor. Geophys., **I**, 222—226.

Miyake, Y., and Suguira, Y., 1954: Chemical studies of rain water accompanied by a typhoon. Geophys. Mag. Tokyo, **26**, 29—34.

Rau, Walter, 1956: Bestimmung der Grösse und Häufigkeit der chloridteilchen im maritimen Aerosol. Meteor. Rund., **9**, 210—214.

Riehl, H., Yeh, T. C., Malkus, J. S., and Laseur, N. E., 1951: The north-east trade of the Pacific Ocean. Q. Jour. Roy. Met. Soc., **LXVII**, 598—626.

Riehl, H., 1951: Aerology of tropical storms, Compendium of Meteorology, 902—913, Amer. Meteor. Soc., Boston, Mass.

— 1954: Tropical Meteorology, McGraw-Hill, New York.

Scorer, R. S., and Ludlam, F. H., 1953: Bubble theory of penetrative convection. Quart. J. Roy. Met. Soc., **79**, 94—103.

Seely, B. K., 1952: Detection of micron and submicron chloride particles. Analyt. Chem., **24**. 576—579.

Simpson, R. H., 1947: A note in the movement and structure of the Florida hurricane of October 1946. Mon. Wea. Rev., **75**, 53—58.

— Personal communication.

Squires, P., and Gillespie, C. A., 1952: A cloud droplet sampler for use on aircraft. Quart. J. Roy. Met. Soc., **78**, 387—393.

Squires, P., and Warner, J., 1957: Some measurements in the orographic cloud of the Island of Hawaii and in trade wind cumuli Tellus, **9**, 475—494.

Tannehill, I. R., 1943: Hurricanes. Princeton University Press, Princeton, New Jersey.

Twomey, S., 1954: The composition of hygroscopic particles in the atmosphere. J. Meteor. **11**, 334—338.

Wexler, Harry, 1947: Structure of hurricanes as determined by radar. Annals N.Y. Acad. Sci., **XLVII**; Art. 8, 821—844.

Woodcock, A. H., 1950: Sea salt in a tropical storm. J. Meteor., **7**, 397—401.

— 1954: Airborne sea salt as a function of altitude and wind force. J. Meteor., **10**, 362—371.

— 1952: Atmospheric salt particles and raindrops. Jour. Meteor., **9**, 200—212.

Woodcock, A. H., and Spencer, A. T., 1957: An airborne flame photometer and its use in the scanning of marine atmospheres for sea salt particles. J. Meteor., **14**, 437—447.

Woodcock, A. H., and Gifford, Mary M., 1949: Sampling atmospheric sea-salt nuclei over the ocean. J. Marine Research, **8**, 177—197.

Woodcock, A. H., and Blanchard, D. C., 1955: Tests of the salt-nuclei hypothesis of rain formation. Tellus, **7**, 437—448.

Woodcock, A. H., 1950 a: Impact deposition of atmospheric sea salts on a test plate. Proc. Am. Soc. Testing Mats., **50**, 1151—1166.

# The Spatial Variation of Liquid Water and Droplet Concentration in Cumuli

By P. SQUIRES, Division of Radiophysics, C.S.I.R.O., Sydney, Australia

(Manuscript received April 15, 1957)

*Abstract*

Measurements of liquid water content and droplet concentration in cumuli over path lengths of about one metre have been used to investigate the structure of these clouds. The measurements indicate that the cloud process is far from adiabatic, and that a dominating role is played by the admixture of drier air from outside the cloud. They suggest, further, that the main source of this dry air may be the region above the cloud top.

## 1. Introduction

Measurements of the properties of cumuli have led a number of investigators to the conclusions that the classical model of an adiabatically expanding parcel of air is inadequate, and that significant interaction must occur between the cloud and its environment. It is apparent that the processes involved in the life cycle of a cumulus are of great complexity, and the volume of data so far available does not seem to form an adequate basis for the construction of any complete theory.

Some measurements of droplet spectra have been made in cumuli, and certain aspects of these results, which appear relevant to the problem of interaction between the cloud and its surroundings, are discussed.

## 2. Observations

Cloud droplet spectra have been measured in various types of cloud, mostly cumuli, using the aircraft sampler described by SQUIRES and GILLESPIE (1952). Ten samples can be taken at one loading. The minimum interval between samples is about 3 seconds, corresponding to about 200 metres of travel.

The errors in the measurement of droplet concentrations arise from two sources: variations in the action of the exposing mechanism, and errors in air speed. The sampling device has been calibrated at intervals during the measurements, and has shown fluctuations amounting to 3 % in the exposure time of a given point on the sampling rod. Air speed indicators are reliable to about 5 %, and in cloud the aircraft speed changes at times by this amount from the mean value. It seems therefore that the droplet concentrations should have an accuracy of about 10 %.

Until 1952, a sampling layer of magnesium oxide was used. Subsequent investigation showed that this was unsatisfactory for the measurement of droplet diameters and since then a layer of soot has been used. The diameters of the holes made by droplet of a given size in the soot layer have been found by projecting, at aircraft speed, a small sampling piece coated with soot through a curtain of droplets, produced, in most cases, by a spinning disk. The ratio of hole diameter to drop diameter (d) is known with an accuracy which varies with droplet size; above $d = 20\ \mu$, the

probable error is under 5 %. Below $d = 20\,\mu$ it increases with decreasing drop size to about 15 % at $d = 5\,\mu$; this increase does not appear to be due to a lack of reproducibility in the ratio, but almost wholly to the difficulty of producing and measuring a group of uniform droplets in this size range. The accuracy of liquid water contents therefore depends on the sizes of the drops occurring in the cloud. Over the range of diameters $d > 10\,\mu$, which usually contributes most of the liquid water, the probable error in diameter does not exceed 10 %. It seems reasonable therefore to assign an overall accuracy of about 30 % to the measurements of liquid water content. However, the comparative accuracy of the measurements is probably better than this.

For this reason, the mean value of $n$ or $w$ found from the samples in one pass through a cumulus is not reliable. Thus, when the mean value of $w$ is plotted against $h$ for each cloud, the resulting graph is confused, and shows no clear trend of $w$ with height. Since WARNER (loc. cit.) has shown that $w$ begins to decrease one to two thousand feet below the cloud top, it is not satisfactory to lump together observations from several clouds of differing total depths. In the case of the ratio $w/w_a$, however, this is admissable, as this ratio decreases steadily with increasing height. The mean variation of $w/w_a$ with $h$ is shown in Table 1. This variation agrees with that shown by WARNER, but these values of $w/w_a$ are consistently smaller by about 0.1. This discrep-

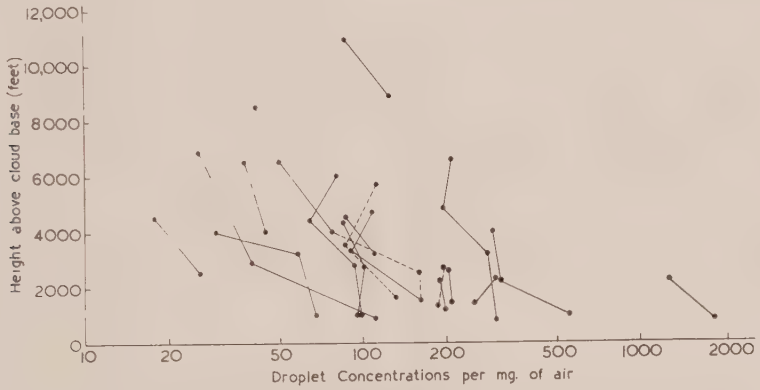


Fig. 1. The variation of droplet concentration with height above cloud base in individual clouds. Dashed lines are used in places for the sake of clarity.

### 3. Variations in the vertical

According to the extensive measurements of WARNER (1955) the liquid water content ($w$ g m$^{-3}$) in cumuli increases upwards to within one or two thousand feet below the cloud top. However, he found that at all levels it was less than the value which would have resulted from the adiabatic expansion of air which was just saturated at the level of the cloud base ($w_a$). He further showed that the ratio $w/w_a$ decreases with increasing height above the cloud base ($h$). The present measurements confirm some of these conclusions. As will be shown later by some examples, the characteristics of the droplet spectrum change erratically and indeed almost randomly when successive samples are spaced at about 200 m. ancy is not as serious as it seems, since the values of $w$ used here to give a mean value are measured at randomly distributed points, whereas WARNER used the "peak value" of $w$ from each traverse.

Both ZAITSEV (1950) and WEICKMANN and KAMPE (1953) have reported a rapid decrease in droplet concentration with increasing height. The present series of observations indicates a trend in this direction, although not so marked or consistent as that found by these authors. The mean droplet concentration per milligram of air ($N_h$) has been found for each pass through an isolated cumulus. When these mean values are plotted against the height above cloud base, it appears on the whole that $N_h$ decreases as $h$ increases; there are

**Table 1. The variation of the ratio $w/w_a$ with height above cloud base**

| Height above cloud base (feet) | No. of observations | Median value of $w/w_a$ |
|---|---|---|
| 0—1000 | 24 | 0.33 |
| 1000—2000 | 119 | 0.26 |
| 2000—3000 | 66 | 0.18 |
| 3000—4000 | 62 | 0.17 |
| 4000—5000 | 23 | 0.12 |
| 5000—6000 | 0 | — |
| 6000—7000 | 27 | 0.08 |

however exceptions. These exceptions may be real, or they may be due to the fact that, with the rapid and erratic variations in droplet concentrations, many more samples would have been needed to secure a fair average at each level. In order to smooth out these fluctuations, the data for each cloud have been grouped in height intervals of 2,000 feet ($h$ = 0 – 2,000; 2,000 – 4,000 etc.). For each interval of $h$, the mean value of $N_h$ has been found for the observations in each cloud, and in Fig. 1 this is plotted against the centroid of the $h$-values in the interval. This figure is based on 455 samples. Points referring to observations in a single cloud are connected by straight lines. Out of the 31 lines in the figure, 24 (about 77 %) indicate a decrease in $N_h$ with increasing $h$. Out of the eighteen clouds represented only two (11 %) showed an increase in droplet concentration from the lowest to the highest level plotted in Fig. 1. In both these cases the height interval was only about 1,000 feet, so that even if the rate of decrease of $N_h$ had been similar to that found in other clouds, the change between the two levels would have been small, and easily masked by random fluctuations.

Concentrations have been expressed for the present purpose in number per milligram of air instead of in the usual volume units. Thus the apparent trend for droplet concentrations to decrease upwards owes nothing to the mere expansion of the air as it rises. This decrease must therefore be due to some process which eliminates droplets from the cloud. Concentrations expressed in numbers per cm³ naturally show the same trend as is seen in Fig. 1, and to a slightly greater extent because of the upward decrease of air density.

The observations at the various levels were not, of course, simultaneous. However, the practice followed was to begin passes at the higher levels and work down. The droplet concentration in a cumulus is more likely to

**Table 2.**

Showing the random nature of the variation of droplet concentration per cm³ ($n$) and liquid water content ($w$ g m$^{-3}$) in samples spaced about 200 m apart in horizontal traverses through some cumuli: **n** in bold face, *w* in italics.

| Date | Height in feet of | | | Sample No. | | | | | | | | | |
|---|---|---|---|---|---|---|---|---|---|---|---|---|---|
| | Cloud base | Cloud top | Level of traverse | 1 | 2 | 3 | 4 | 5 | 6 | 7 | 8 | 9 | 10 |
| 23 Oct. 1954 ..... | 2,200 | 9,000 | 6,250 | **28** | **42** | **24** | **75** | **4** | **5** | | | | |
| | | | | *0.46* | *0.11* | *0.57* | *1.40* | *0.25* | *0.03* | | | | |
| 6 Nov. 1954..... | 800 | 6,000 | 1,800 | **63** | **43** | **55** | **133** | **117** | **74** | **82** | | | |
| | | | | *0.05* | *0.14* | *0.18* | *0.45* | *0.44* | *0.25* | *0.38* | | | |
| 26 Nov. 1954 ..... | 3,600 | 8,500 | 7,000 | **66** | **79** | **58** | **82** | **70** | **238** | **57** | **128** | **62** | **164** |
| | | | | *0.66* | *0.74* | *0.71* | *1.00* | *0.71* | *2.14* | *0.62* | *1.50* | *0.79* | *2.69* |
| 1 Dec. 1954 ..... | 2,500 | 6,500 | 5,600 | **107** | **19** | **19** | **14** | **10** | **15** | **6** | **14** | | |
| | | | | *1.29* | *0.20* | *0.25* | *0.11* | *0.10* | *0.26* | *0.06* | *0.05* | | |
| 13 Mar. 1956 ..... | 2,500 | 7,500 | 6,500 | **82** | **59** | **52** | **73** | **199** | **140** | **77** | **67** | **260** | |
| | | | | *0.15* | *0.13* | *0.13* | *0.17* | *0.63* | *0.41* | *0.13* | *0.17* | *0.80* | |
| 2 Nov. 1956..... | 7,200 | 12,000 | 9,800 | **24** | **231** | **141** | **505** | **117** | **270** | **127** | **177** | **165** | **549** |
| | | | | *0.02* | *0.15* | *0.15* | *0.74* | *0.17* | *0.35* | *0.19* | *0.26* | *0.21* | *0.73* |

**Table 3. The relative variation of droplet concentration on entering a cumulus (250 observations)**

| Sample number | Mean relative droplet concentration |
|---|---|
| 1 | 1.02 |
| 2 | 1.08 |
| 3 | 1.02 |
| 4 | 0.88 |
| 5 | 0.96 |
| 6 | 1.16 |
| 7 | 1.10 |
| 8 | 1.04 |
| 9 | 0.89 |
| 10 | 0.99 |

decrease with time than to increase; hence this lack of simultaneity would not contribute to the effect shown in Fig. 1, but rather would tend to mask it.

### 4. Variations in the horizontal

When successive samples taken on a single horizontal pass through a cumulus are compared, it is found that the variations in the droplet concentration per $cm^3$ ($n$) and in the liquid water content ($w$) are strongly correlated. This is illustrated in Fig. 2 by scatter diagrams for some individual passes. A regression line through the origin corresponds to a constant mean droplet volume. The corresponding mean radius $\bar{r}$ is entered on each diagram. It will be seen that the correlation is especially clear when this mean radius is small.

The scatter diagrams of Fig. 2 serve also to illustrate the magnitude of the fluctuations which occur in a horizontal traverse. As mentioned earlier, these fluctuations are nearly random. In order to illustrate this further, the values of $n$ and $w$ found in typical traverses through some cumuli are shown in Table 2.

Discussing his measurements of liquid water content, WARNER (loc. cit.) states that, in many clouds, the transition from clear air to dense cloud is abrupt. A similar conclusion is indicated by the present measurements. In order to investigate the variation of $n$ on entering a cloud, the mean value of $n$ for each traverse was found ($n_h$). The ratio $n/n_h$ was then computed for each sample. This was done for 26 traverses in which nine or ten samples were taken in uninterrupted succession at intervals of about 200 m. The mean value of the ratio $n/n_h$ was then found for all the first samples taken in the cloud, for all the second samples, and so on. These mean values are given in Table 3. In the majority of cases the samples, spread over some 2 km, represent nearly the whole width of the cloud, and in all cases at least half of it. The practice was to take the first sample one to two seconds after the aircraft entered the cloud. Cloud entry was judged by watching the wing-tip of the aircraft; this carried a black de-icer boot against which intervening cloud could be seen distinctly. Table 3 indicates that, beyond a point about 100 m inside the cloud, there is on the average no further increase in droplet concentration.

In the case of liquid water content, the volume of data available is much less, since $w$ cannot be found from the observations where a magnesium oxide layer was used. In

**Table 4. The relative variation of liquid water content on entering a cumulus (164 observations)**

| Sample number | Mean relative liquid water content |
|---|---|
| 1 | 0.99 |
| 2 | 0.71 |
| 3 | 0.88 |
| 4 | 1.22 |
| 5 | 0.89 |
| 6 | 1.16 |
| 7 | 0.74 |
| 8 | 1.02 |
| 9 | 1.16 |
| 10 | 1.02 |

**Table 5. Frequency table of values of the ratio $w/w_a$ (321 observations)**

| Range of $w/w_a$ | Percentage frequency |
|---|---|
| 0—0.1 | 23 |
| 0.1—0.2 | 31 |
| 0.2—0.3 | 19 |
| 0.3—0.4 | 8 |
| 0.4—0.5 | 6 |
| 0.5—0.6 | 4 |
| 0.6—0.7 | 3 |
| 0.7—0.8 | 2 |
| 0.8—0.9 | 0 |
| 0.9—1.0 | 2 |
| over 1.0 | 1 |

Fig. 2. Scatter diagrams illustrating the association between the fluctuations of droplet concentration ($n$ per cm$^3$) and liquid water content ($w$ g per m$^3$) in horizontal traverses through cumuli.

order to investigate the variation of $w$ on entering a cumulus, all traverses have been utilized where at least seven samples were taken. Otherwise the data have been handled in the same way as for $n$. The result is shown in Table 4. It will be seen that the total number of observations is smaller, and that this sequence is rather more irregular than that of Table 3; however it appears unlikely that $w$ increases on the average by more than 10 % from the first sample to the middle of the cloud and it is quite possible that there is no average increase.

## 5. The range of variation of the liquid water content

It is of some interest to consider the frequency of values of $w/w_a$, irrspective of position in the cloud; this is shown in Table 5. Since the sample is taken from a strip of air which is never more than 2 metres in length, and usually less than 1 metre, it may be considered as a point measurement of $w$. Table 5 indicates that $w$ exceeds $w_a$ only in about 1 % of the samples. The maximum value found for $w/w_a$ was 1.16; this exceeds unity by less than the possible error of the measurement. Even if it is assumed that the values of $w$ are consistently too low by 30 %, so that all values of $w/w_a$ greater than about 0.8 in Table 5 really correspond to $w \geq w_a$, it would appear that the adiabatic liquid water content was attained in only 3 % of the samples. It seems likely therefore that this happens only in a few percent of the volume of an average cumulus. The overall mean value of $w/w_a$ was 0.18.

Occasionally, completely null samples were found inside a cumulus. To all appearances, the aircraft was completely surrounded by cloud but it is possible that, in some cases, samples were taken in a clear space between two adjacent cumuli, or between two towers rising out of a common base. This was certainly not always the case. Out of nearly a thousand samples taken in cumuli, about 8 % were null, and rather more than half of these were isolated null samples; that is, the sample about 200 m away on each side of it showed cloud droplets. It is most unlikely that any large proportion of these isolated null samples were due to the kind of error described above. This means that, even in the interior of cumuli, the liquid water content is sometimes zero; in fact, $w$ is at least as likely to fall to a zero value as it is to rise to the adiabatic value, $w_a$.

## 6. Summary of results

Summarizing the results given above, some of which have already been reported by the authors mentioned, it has been found that:

(a) The liquid water content ($w$) of cumuli, even when measured over a path length of only about one metre, is nearly always less than the adiabatic value $w_a$. In the clouds observed, $w$ attained the value $w_a$ only over a few per cent of the volume of a cloud, on the average; it fell to a zero value, well inside the cloud, at least as often. The average value of $w/w_a$ was about 0.2.

(b) On the average, both the droplet concentration ($n$) and $w/w_a$ decrease upwards from the cloud base.

(c) On a horizontal traverse, the variations of $n$ and $w$ are large and erratic, but they rise and fall together. This association between the variations of $n$ and $w$ seems to be closer when the average droplet size is small.

(d) On entering a cumulus from the clear air the droplet concentration rises, on the average, to its mean value for the whole traverse within a distance of about 100 m from the cloud boundary. The liquid water content also rises sharply over this distance, but it is possible that there may be a slight remaining increase from this point towards the centre of the cloud, amounting to perhaps 10 %; the data are however not sufficient to decide whether this further increase occurs or not.

## 7. Discussion

The fact that $w$ is nearly always less than $w_a$ implies that an admixture of drier air occurs throughout all but a few percent of the volume of a cumulus. This dry air may enter from the sides or the top, but not from the bottom, since the almost horizontal base of a cumulus indicates that all air passing through this level is saturated; the variations in cloud base height correspond to variations in $w_a$ which are small compared with the observed values of the deficit of liquid water, $(w_a - w)$. At times the admixed air apparently can penetrate far into the cloud without becoming saturated,

for a region devoid of water can remain so only if the air is unsaturated, so that water droplets diffusing into it will evaporate. The upward decrease of the ratio $w/w_a$ implies that the effects of this admixture increase upwards.

It is plausible that this admixture of dry air is also the cause of the variation of droplet concentration, some of the smaller droplets evaporating when dry air mixes with cloud air. There is however the alternative possibility, that these variations are caused by the coalescence of droplets. DAS (1956) has computed numerically the evolution as a result of coalescence of several droplet spectra, some of them containing large droplets. His results show that over periods up to an hour the change in the droplet spectrum, and in droplet concentration, would be very slight. These calculations were based on an analysis similar to that of SCHUMANN (1940), using a value of unity for the collection efficiency. The calculations of PEARCEY and HILL (1957) indicate that for the small droplet sizes often found near the bases of cumuli, for which the Reynolds number is much less than 1, the collection efficiency is usually much less than unity.

It seems reasonable therefore to take the results of DAS as giving an upper limit for the effectiveness of gravitational coalescence in modifying the droplet spectrum as a whole. This negative result found by DAS has no bearing on the problem of the formation of a relatively small number of large drops or raindrops by coalescence, since he has excluded some droplets at both the upper and lower ends of the spectrum from his calculations; moreover, as TELFORD (1955) has shown, statistical fluctuations can be important in the formation of the relatively small number of raindrops.

It would appear therefore on purely a priori grounds that the variations in droplet concentration are not attributable to coalescence, but to the evaporation of some of the smaller droplets when dry air mixes with cloudy air. This view is clearly in agreement with the observational results given above. The variations of $w$ in a horizontal traverse cannot be due to coalescence; it is plausible, therefore, that the variations of $n$, which are strongly associated with those of $w$, are also due to the admixture of dry air. Clearly, droplets are more likely to be evaporated completely by mixing when the average drop size is small. Thus the fact that the association between the variations of $n$ and $w$ seems to be stronger when the average drop size is small also points in this direction. Finally, the mere erratic nature of the variations of $n$ across a cloud suggests that they are more likely to be due to a process like the turbulent admixture of dry air than to an internal process such as coalescence.

If it is true that the horizontal variations of $n$ are due to admixture, it seems plausible that the vertical variation, which is similar in magnitude to the erratic variations in the horizontal, could be due to the same cause. Like $w/w_a$, the droplet concentration per milligram of air, $N$, decreases upwards, and this too could be due to the increasing effects of the admixture of dry air in the higher parts of the cloud.

The admixture of drier air from outside the cloud would seem therefore to play an important part in the structure of cumuli. As for the source of this air, observations discussed so far indicate only that its effects increase upwards. On the other hand the data of Tables 3 and 4 give an indication which does not, on the face of it, accord well with the theory originated by STOMMEL (1947), according to which the departure of the observed lapse rate in cumuli from the wet adiabatic lapse rate is due to the lateral entrainment of dry air from around the sides of the cloud. If this were so, one would expect to find a marked gradient of $w$ and $n$ from the boundary of the cloud towards its centre. The examples given in Table 2 illustrate the fact that there is no consistent trend in this direction. Tables 3 and 4 show that, when data from a number of cumuli are averaged together, there is little or no increase in $n$ or $w$ beyond a point about 100 m inside the cloud boundary.

However, MALKUS (1949) has pointed out that as a result of vertical wind shear, cumuli are often asymmetrical. Since the traverses used in Tables 3 and 4 were made in directions which were randomly distributed with respect to the direction of the wind shear vector, this asymmetry could contribute to the apparent uniformity of average cloud properties along a traverse. Nevertheless, it

does not seem likely that asymmetry due to wind shear could so completely mask the central maximum of liquid water content and droplet concentration which the entrainment theory would imply.

In the light of these measurements, an alternative mechanism suggests itself. The sharp increase in $n$ and $w$ near the cloud boundary and the upward increase in the effects of admixed air are both explained readily if it is supposed that the dry air comes into the cumulus, not from the sides, but from the top. A parcel of dry air which is enveloped by the cloud during its growth, or which diffuses into the cloud top by turbulence, is in an unstable situation. It will be cooled by the inward diffusion of liquid water from all sides, and must subside through the cloud. Since the driving force is supplied by the evaporation of liquid water, this mechanism will be the more effective, the wetter the cloud. The increased turbulence found in cumuli derives its energy from density differences, and it is likely therefore that vertical mixing predominates over the horizontal mixing which is postulated in the entrainment theory.

On this view, a cumulus will contain some dry air at all stages of its growth, and at all levels. Its structure may be likened to that of a sponge, the spaces in which represent parcels of dry air. Some of these parcels may not have moved far from the positions they occupied when the growing cloud enveloped them; others may have subsided a considerable distance. Evidently this model offers a simple explanation also for the rapid fluctuations which are found when flying through cumuli, and the occasional presence of clear regions even well inside the cloud.

## 8. Conclusion

The specific conclusions concerning the spatial variations of the liquid water content and droplet concentration have been given in detail in Section 6 above. The discussion of Section 7 confirms the conclusions of other investigators that interaction between the cloud and its surroundings is of great importance; the fact that the liquid water content averaged only about one fifth of the adiabatic value shows that, in cumuli, the adiabatic model bears little resemblance to reality. The existence of regions inside the clouds where liquid water was completely absent also indicates very definitely that they must contain some air which could not have originated below the condensation level. At the most, only a few per cent of the volume of an average cumulus consists of unmixed air which has risen adiabatically from cloud base.

It appears that the values of the liquid water content, and the spatial variations of the properties of the cloud, can be qualitatively explained by postulating an admixture of dry air in a proportion which increases steadily from the base upwards. This postulate could be satisfied by several models, and in particular by that of the lateral entrainment of dry air; however, the results concerning the average variation of properties across cumuli do not seem to agree well with expectations based on this theory.

The measurements suggest that most of the dry air may enter by turbulent diffusion through the cloud top, both during the growing and mature phases. The mechanism by which such parcels of dry air could subside through the cloud is physically clear. The random variations which would result from the operation of this process throughout the cloud's life correspond well with the fine structure in turbulence, temperature, droplet concentration and liquid water content which is observed.

## 9. Acknowledgements

The author wishes to acknowledge the work of Mr. K. A. Davidson and Mr. E. Harting in the difficult task of calibrating the method of measuring droplet diameters, and their help in making the observations. Acknowledgement is due to the Aircraft Research and Development Unit of the Royal Australian Air Force which provided and flew the aircraft used.

## REFERENCES


Das, P. K., 1956: The change in the distribution of drops in a cloud. Indian J. of Meteor. and Geophys., **7,** 55—59.

Malkus, J. S., 1949: Effects of wind shear on some aspects of convection. Trans. Am. Geophys. Un., **30,** 19—25.

Pearcey, T., and Hill, G. W., 1957: A theoretical estimate of the collection efficiencies of small droplets. Quart. J. R. Met. Soc., **83,** 77—92.

Schumann, T. E. W., 1940: Theoretical aspects of the size distribution of fog particles. Quart. J. R. Met. Soc., **66,** 195—207.

Squires, P., and Gillespie, C. A., 1952: A cloud-droplet sampler for use on aircraft. Quart. J. R. Met. Soc., **78,** 387—393.

Stommel, H., 1947: Entrainment of air into a cumulus cloud. Pt. 1. J. Meteor., **4,** 9—94.

Telford, J. W., 1955: A new aspect of coalescence theory. J. Meteor, **12,** 436—444.

Warner, J., 1955: The water content of cumuliform cloud. Tellus, **7,** 449—457.

Weickmann, H. K., and Aufm Kampe, H. J., 1953: Physical properties of cumulus clouds. J. Meteor., **10,** 204—211.

Zaitsev, V. A., 1950: Water content and distribution of drops in cumulus clouds. *Glavaia Geofizicheskaia Observatoria, Trudy,* **19,** 122—132.

# Penetrative Downdraughts in Cumuli

By P. SQUIRES, C.S.I.R.O., Radiophysics Laboratory, Sydney, Australia

(Manuscript received October 1, 1957)

*Abstract*

Observations of cumuli have shown that the adiabatic model is quite inadequate, and that dry air must mix with the condensing upcurrent. Theories of the interaction between cumuli and their environment are discussed. The hypothesis that dry air enters these clouds chiefly from above is examined quantitatively. It is found that, as a result of evaporative cooling, such air could penetrate several kilometres into a growing cloud. This hypothesis accounts for the fine structure which is observed, and provides a natural and simple explanation for the fact that the lapse rate in cumuli is steeper than the wet adiabatic, and indeed approximates closely to that of the environment. Unlike alternative theories, it provides a means whereby the liquid water content may be automatically self-limiting, as the observations seem to require, for the motions which introduce dry air deep into the cloud depend for their energy supply on the presence of liquid water, and have velocities which are roughly proportional to its concentration.

## 1. Introduction

A wealth of evidence has been accumulated which shows that the properties of cumuli cannot be explained by the adiabatic expansion of air which was saturated at cloud base level. Measurements of temperature in cloud described by BUNKER et al. (1949) and by BARRETT and RIEHL (1948) indicate that the average lapse rate in cumuli is steeper than the wet adiabatic and approximates to that of the environment. Additional evidence is afforded by measurements of liquid water content ($w$ g m$^{-3}$). After reviewing the observations, WARNER and SQUIRES (1958) concluded that although the adiabatic liquid water content ($w_a$) sometimes occurs over a distance of the order of a metre, the average value of $w$ over some tens of metres ($\overline{w}$) seldom if ever equals $w_a$. The ratio $\overline{w}/w_a$ decreases rapidly with height and at 2 km above cloud base falls below 0.2, on the average. There is little evidence to suggest that $\overline{w}$ reaches much greater values in large clouds than in moderate ones; in all clouds, it seems rare for $\overline{w}$ to exceed 2 g m$^{-3}$, and it is usually less than 1 g m$^{-3}$. As regards distribution in the horizontal, there is a great wealth of fine structure, which becomes very striking when $w$ is measured over a distance of about 1 metre. There is no clear systematic variation from the cloud edges towards the middle. Contrary to the impression given by ZAITSEV (1950), the low values of $w$ appear to be distributed rather randomly, with no marked preference for the peripheral regions; the edge of a cloud is often very sharp.

These findings clearly require for their explanation a model of cumulus development which includes as a necessary concomitant of the cloud's growth a large scale mixing of dry air with the upcurrent.

## 2. Theories of interaction between the cloud and its environment

Since cumulus bases are typically flat, it seems impossible for dry air to enter the cloud from below, for in the present context, "dry" air means air which, if displaced adiabatically to the level of the cloud base, would arrive there unsaturated. The variations in cloud base height, which rarely exceed one or two hundred metres, are much too small to explain the observed deficiency of liquid water, $(w_a - w)$. Clearly, however, all air which originates from above the cloud base level will be "dry" in the sense defined. Thus there is room for three possibilities:

(a) The dry air may not have moved far from its original position, having mixed in situ with the saturated, cloudy air rising from below.

(b) It may have come in from around the sides of the cloud, mixing horizontally with the updraught.

(c) It may have originated from the region just above the growing cloud top, entering the cloud as downdraughts and mixing vertically with the updraught.

Model (a) is closely related to the bubble theory of convection advanced by SCORER and LUDLAM (1953), according to which the growth of a cumulus is the result of the arrival at condensation level of a succession of buoyant bubbles, each of which is steadily eroded as it rises. If other bubbles follow the same path through the air, they will penetrate further because the ambient air has been moistened by their predecessors; by this process a cumulus builds up in steps.

Model (b) was postulated by STOMMEL (1947) to explain the observed lapse rates in cumuli, and has been used as a basis for discussion by MALKUS (1949, 1952). The latter author has had considerable success in interpreting observations by means of a postulated entrainment. However, in these cases, there has been no independent evidence relating to the amount of entrainment, and it seems possible that some other mechanism which introduced dry air into the cloud in the required amounts could explain the observations equally well. Indeed, the only direct evidence of entrainment is provided by measurements of wind fields around large cumuli and thunderstorms made during the Thunderstorm Project. BYERS and HULL (1949) have described how the proportional rate of change in area of triangles formed by three balloons were used to compute horizontal divergence. The typical rate of entrainment into these large clouds was found to be 100 % in 4 km. By contrast, STOMMEL (loc. cit.) computed that, in order to explain the observed lapse rates in small trade wind cumuli, it was necessary to postulate an entrainment rate of 100 % in a height interval of 300 to 1,000 m. Again, BEST (1951) computed the liquid water content in large cumuli assuming entrainment of air of 70 % relative humidity at a rate similar to that found by BYERS and HULL, and found values of $w$ which far exceed those which have usually been observed in large cumuli; the corresponding values of $w/w_a$ exceed 0.5 at all heights. It therefore seems that, if the entrainment rates measured by BYERS and HULL are typical of cumuli in general, this source of dry air by itself is inadequate to explain the observed properties of such clouds.

Model (c) has been outlined elsewhere (SQUIRES, 1958) in an attempt to explain some of the observed characteristics of cumuli. A parcel of dry air which enters the top of a growing cloud by turbulent diffusion will be cooled by the evaporation of liquid water, and may subside into the cloud. The existence of a mechanism of this kind is suggested by measurements of vertical velocity, such as those of JONES (1954a), which have frequently revealed an intimate mixture of up-and-down-draughts of the same order of magnitude. Again, the downward motions often seen around the outsides of cumuli in lapse time records are commonly attributed to evaporative cooling consequent on mixing between the cloud and its dry environment. If this explanation is correct, it seems likely that the similar mechanism of model (c) could lead to deep penetration of a cloud by dry air parcels. This model, like (a) and (b), explains qualitatively the observation that the effects of the admixture of dry air increase upwards through the cloud, as shown by the decrease of $w/w_a$. It gives a picture of cloud development not unlike that of model (a). In both cases, the final result is a heterogeneous mixture of air from below condensation level with air which originally occupied, roughly,

the space now filled by cloud. The difference is that here, an active, penetrative role is assigned to the dry air. Thus a heterogeneous cloud with much fine structure could result even from a steady updraught.

Model (c) has certain advantages:

(i) The remarkable fact that lapse rates in cumuli do not differ much from that of the environment finds a simple explanation by means of the mechanism of penetrative downdraughts. If the cloud should become markedly warmer than the environment at the same level, an extremely unstable situation will exist at the top of the cloud; vertical interchange must take place between the cloud top and the clear air above it. Evidence of the existence of this kind of interchange is given by the observations of JAMES (1954) who measured the air temperature while flying some 150 m directly above small developing cumulus clouds, and found that there were regions about 100 m across in which the temperature was some 1.5° to 3° C colder than elsewhere; these regions were sharp-edged, and stood in strong contrast to the undisturbed temperature field normally found in the clear air above cloud base and well away from clouds. These cold regions may have resulted from the evaporation of cloud protuberances into the surrounding dry air.

Indeed, it seems likely that the protuberances at the top of growing cumuli may be taken as evidence of the existence of strong hydrostatic instability in the region of the cloud top; if so, there is little reason to doubt that downdraughts are entering the cloud mass with a vigour similar to that shown by the protuberances. But whereas cooling by evaporation tends to stabilize the cloud protuberances when they mix with the dry environment, it renders the dry air parcels more unstable as they mix with the surrounding cloud.

(ii) As mentioned in the Introduction, the measurements of liquid water content so far made indicate that, whatever the value of $w_a$, $w$ usually averages less than 1 g m$^{-3}$ over large volumes, and is unlikely to exceed 2 g m$^{-3}$ except in small regions. This suggests that there is some form of self-limiting mechanism at work, that is, that the admixture of dry air is greater in wet clouds than in dry ones. In both the bubble model (a) and the entrainment model (b), the admixture of dry air is not directly affected by the concentration of liquid water; in model (c), it is the liquid water itself which provides the driving force for the motions which give rise to mixing. As will be seen later, the subsiding speed of dry air parcels in cloud is roughly proportional to $w$.

(iii) It is a common observation that turbulence as observed from an aircraft is much stronger in clouds than in the clear air between them; according to BUNKER et al. (1949) by at least one order of magnitude. Now it is clear that the turbulence associated with clouds derives its energy from density differences, so that the turbulent motions must in the first place be vertical; cloud turbulence is likely to be far from isotropic, vertical mixing predominating strongly over horizontal mixing.

(iv) As mentioned in the Introduction there is no clear evidence for a gradient of properties from the cloud centre out towards the edges, as must be expected under model (b). The horizontal increase of $w$ on entering a cloud is often very rapid, and there is no counterpart here to the vertical gradient of $w$ which WARNER (1955) found to occur regularly in the uppermost 300 – 500 m of cumuli. This contrast reinforces the argument of (iii) above, indicating that vertical mixing plays a dominant role.

The hypothesis is therefore advanced that the mechanism of model (c) constitutes an important aspect of the interaction between cumuli and their environment. It remains now to investigate this model in a quantitative manner, that is, to determine whether the air in the dry layers which the growing cloud penetrates is itself capable of penetrating the cloud mass in a manner which is unorganized on the scale of the cloud. This penetration may be envisaged as occurring by the agency of more or less continuous downdraughts, for which there is some evidence (JONES, 1954 (b) and WARNER, 1955), or in the form of individual parcels. The latter view has been chosen in the interests of theoretical simplicity.

A penetrating dry parcel will obviously be subject to attrition and may at times be torn asunder. Thus a large parcel may enter the cloud, penetrate some distance, and then disintegrate, giving rise to two or more smaller ones which thereafter follow a more

or less independent course. As our purpose is merely to investigate whether the proposed mechanism is capable of introducing dry air into the interior of a cloud in a time interval comparable with the observed lifetime of cumuli, the subsiding parcels will be supposed to remain integral.

### 3. A physical model of the downdraught theory of interaction

The following postulates describe the physical model which is used for the purpose of computation:

(a) A parcel of dry air becomes immersed in the cloud top as a result of the erratic growth of cloud protuberances, or by turbulence reinforced by the increased hydrostatic instability which must tend to occur at the cloud top when the lapse rate of the environment is steeper than the wet adiabatic, as is usually the case.

(b) Mixing occurs between the parcel and its cloudy environment.

(c) Cloud droplets diffusing into the parcel by turbulence immediately evaporate and, as a result, the parcel is cooled. Cloud droplets immersed in unsaturated air, even at a relative humidity of 99 %, will evaporate to a diameter of a micron or so in some tens of seconds, unless they contain a giant condensation nucleus; these are relatively rare. Thus they will have lost practically all their mass within a time which is short compared with the periods considered.

(d) The resistance to the motion of the parcel through the cloud arises solely from eddy interchange of matter between the parcel and its environment. The disturbance of the pressure field in the environment consequent upon the motion of the parcel is neglected. This simplification is justified to some extent by the following consideration. No hypothesis is made as to the shape of the parcels, and they may be envisaged as quasi-spherical or, more plausibly, as being elongated in a vertical direction, so that they form short-lived downdraughts. In this case, the effect of the disturbance of the pressure field could well be small compared with that of eddy interchange between the parcel and the cloud.

(e) The parcel is envisaged as containing a constant mass of air. Following the method used by PRIESTLEY (1953) it will be assumed that, in unit time, a mass of air k is removed from each unit mass of air in the parcel and is lost to the surrounding cloud; this is replaced by an equal mass of cloudy air, which mixes with the parcel. The effect of the parcel on the cloud will be neglected in this calculation; obviously however the final effect of many such parcels will be to cool and dry the cloud, especially in its upper parts.

The mixing rate $k$ mentioned in (e) depends on the effectiveness of eddy diffusion in transferring matter from the cloud to the parcel and vice versa. For the moment it suffices to remark that $k$ varies inversely with parcel size; the relation between them will be discussed later.

In addition to these postulates, the following simplifications and assumptions are made:

(a) In computing the density difference between the parcel and its environment, temperatures, not virtual temperatures, are used. Since the parcel itself is close to saturation in the critical stages of its history, the neglect of the effect of humidity mixing ratio on the air density is not very serious. Moreover, this simplification results in an underestimate of the negative buoyancy of the parcel, and so reduces the computed downward speeds; it is therefore conservative.

(b) The computation begins at a point where the parcel is immersed in the cloud; it is at the same temperature as the cloud, and is at rest.

(c) The liquid water content of the cloud is taken as being constant throughout its depth.

(d) The cloud air is assumed to have uniform and constant upward velocity.

(e) The lapse rate in the cloud is taken as constant.

(f) The mixing ratio of water vapour in the cloud air is found assuming the air to be saturated and at a temperature determined by (e) above.

All these postulates seem reasonable for the purpose in hand except perhaps (c). This is quite contrary to the adiabatic model, which would indicate a steady decrease downwards to zero at the cloud base; however, it represents the observations at least as well as any other simple assumption.

WARNER (1955) shows typical curves of the variation with height of the peak value of liquid water content ($w_p$) found during an

aircraft traverse of a cloud. These curves indicate a rapid increase from zero at cloud base through the first 500 to 1000 m, and a rather more rapid decrease at cloud top. Between these two regions, the height variation of $w_p$ is different in different clouds, and no systematic average trend is apparent. The behaviour with height of the mean value of $w$, $(\overline{w})$, as distinct from the peak value $(w_p)$, depends on the shape of the $w$-traces obtained during the traverses. WARNER (private communication) states that in about half the clouds measured, $\overline{w}$ behaved similarly to $w_p$; in the remainder the height variation of $\overline{w}$ was even more erratic than that of $w_p$. Measurements by DAY and MURGATROYD (1953), WEICKMANN and AUFM KAMPE (1953) and SQUIRES (1958) give indications which are in agreement with these conclusions.

As so many variables are involved in the specification of the problem, and the solution of the equations is laborious, the calculations have been carried out for only one set of conditions, which have been chosen to represent a fairly well developed trade wind cumulus.

**4. Basic equations for an unsaturated parcel**

On the basis of the postulates described in the last section, and neglecting some terms which are small because the density of the parcel is little different from that of the cloud, the equation of motion of the parcel is:

$$\dot{v} = \left(\frac{\Delta}{\overline{\Theta}_c} - w_c\right) g - k\,(v + V) \qquad (1)$$

where $v$ is the downward velocity of the parcel, $V$ the speed of the cloud upcurrent, $\Delta$ the amount in degrees C by which the parcel is colder than the cloud at the same level, $\overline{\Theta}_c$ the mean absolute temperature of the cloud, and $w_c$ the liquid water content of the cloud in grams per gram of air. Since the overall variation of the absolute temperature of the cloud is only a few percent, no serious error is involved in using the mean temperature $\overline{\Theta}_c$ instead of the temperature at the level concerned.

The liquid water content of the cloud $(w_c)$ enters into this equation because the suspended liquid water increases the effective density of the cloud air.

The equation governing the temperature of the parcel is:

$$\dot{\Delta} = k\left(\frac{Lw_c}{c_p} - \Delta\right) - (\Gamma_d - \Gamma_c)\, v \qquad (2)$$

where $L$ is the latent heat of evaporation of water, $\Gamma_d$ the dry adiabatic lapse rate and $\Gamma_c$ the lapse rate in the cloud.

The humidity mixing ratio of the parcel varies according to the equation;

$$\dot{x} = k(x_c(z) + w_c - x) \qquad (3)$$

where $x$ is the mixing ratio of the parcel air and $x_c\,(z)$ that of the cloud air at the level $z$.

Differentiating (1) gives:

$$\ddot{v} = \frac{\dot{\Delta}}{\overline{\Theta}_c}\, g - k\dot{v}$$

and substituting for $\dot{\Delta}$ from (2) and for $\Delta$ from (1) gives a second order linear differential equation in $v$. Taking as boundary conditions $v = 0, \Delta = 0$ at $t = 0$, and defining the origin of $z$, measured downwards, as the position of the parcel at $t = 0$, the following expressions result:

$$\frac{\Delta}{w_c} = \overline{\Theta}_c \frac{bN}{mg}\, e^{-kt} \sin bt + \overline{\Theta}_c\left[1 + \frac{k}{g}\left(\frac{V}{w_c} + \frac{N}{m}\right)\right] (1 - e^{-kt} \cos bt) \qquad (4)$$

$$\frac{z}{w_c} = \frac{N}{m}t - \left[\frac{Nk}{m^2} + \frac{g}{m} + \frac{k}{m}\left(\frac{V}{w_c} + \frac{N}{m}\right)\right](1 - e^{-kt}\cos bt) + \left[\frac{kg}{mb} + \frac{k^2}{mb}\left(\frac{V}{w_c} + \frac{N}{m}\right) - \frac{Nb}{m^2}\right] e^{-kt} \sin bt \qquad (5)$$

where $b = \left[\frac{g}{\overline{\Theta}_c}(\Gamma_d - \Gamma_c)\right]^{1/2}$

$$N = \frac{gkL}{\overline{\Theta}_c c_p} - gk - \frac{k^2 V}{w_c}$$

and $\quad m = k^2 + \frac{g}{\overline{\Theta}_c}(\Gamma_d - \Gamma_c).$

TABLE 1

**Characteristics of the downward motion of dry air parcels through a cloud against a steady upcurrent of 1 m sec$^{-1}$.**

| Liquid water content of the cloud (g/kg) | 0.3 | | | | 1.0 | | | | | | 3.0 | | | | | | |
|---|---|---|---|---|---|---|---|---|---|---|---|---|---|---|---|---|---|
| Mixing Rate, $k$: $10^{-3}\times$ | 1.0 | 2.0 | 4.0 | 6.0 | 1.0 | 2.0 | 2.5 | 3.0 | 4.0 | 6.0 | 0.5 | 1.0 | 2.0 | 3.0 | 4.0 | 5.0 | 6.0 |
| Final R. H. % | 98.6 | 100 | 100 | 100 | 99.1 | 96.7 | 98.5 | 100 | 100 | 100 | 92.6 | 92.2 | 91.8 | 95.7 | 99.7 | 100 | 100 |
| "Absolute" Penetration (m) | 533 | 439 | 319 | 260 | 1852 | [1] 3000 | [1] 3000 | 1513 | 1024 | 866 | 2740 | [1] 3000 | [1] 3000 | [1] 3000 | [1] 3000 | 120 | 120 |
| Time Taken secs. | 3600 | 1646 | 823 | 478 | 3600 | 2999 | 2466 | 1115 | 650 | 435 | 3600 | 1983 | 1004 | 759 | 598 | 130 | 125 |
| "Relative" Penetration (m) | 4133 | 2085 | 1142 | 738 | 5452 | 5999 | 5466 | 2628 | 1674 | 1301 | 6340 | 4983 | 4004 | 3759 | 3598 | 250 | 245 |
| Final Temperature Deficit (°C) | 0.11 | 0.15 | 0.26 | 0.37 | 0.32 | 0.40 | 0.44 | 0.48 | 0.62 | 0.83 | 0.86 | 0.81 | 0.93 | 1.46 | 1.70 | 3.14 | 3.42 |
| Final Downward Velocity (m sec$^{-1}$) | 0.16 | 0.27 | 0.50 | 0.77 | 0.53 | 1.04 | 1.27 | 1.45 | 1.65 | 2.61 | 1.10 | 2.02 | 3.19 | 4.68 | 5.18 | 3.77 | 5.1 |

[1] i. e. To cloud base.

Using the values of $z$ as a function of $t$ given by (5), $x$ may be found numerically or graphically from the solution of (3):

$$x = x_0 e^{-kt} + ke^{-kt}\int_0^t e^{kt}(x_c\ (z) + w_c)\ dt \qquad (6)$$

where $x_0$ is the original mixing ratio of the parcel air. Saturation is reached when the value of $x$ found from (6) equals the saturation mixing ratio of air at the temperature and pressure of the parcel.

When the parcel becomes saturated, it will continue to subside for a time because of its temperature deficit and downward momentum. Consequently, some of the liquid water diffusing in must continue to evaporate if the parcel air is to remain saturated. In these circumstances the modified equations corresponding to (1), (2) and (3) above must be treated as simultaneous. The equation to which they lead, however, is non-linear, so that the computations become more complex than in the case of the unsaturated parcel. As will be seen, the penetration of unsaturated parcels is sufficient to establish the quantitative adequacy of the downdraught hypothesis. Consequently, the point where saturation is first reached is taken as the terminus.

The numerical evaluations have been carried out for a cloud based at 1 km (16° C) with its top at 4 km (−2° C). Thus $\Theta_c = 280°$ K, $\Gamma_c =$ 6° C per km. The parcel entering the cloud at the moment $t = 0$ is assumed to have an initial relative humidity of 50 %. With a pressure corresponding to 4 km (ICAN) and a temperature of −2° C, this gives $x_0 = 2.68$ g/kg. The speed of the updraught, V, is taken as 1 m sec$^{-1}$. Three values of liquid water content are used, 0.3, 1.0 and 3.0 g/kg. The first two values may reasonably be taken as representing average conditions in dry and wet clouds respectively (WARNER and SQUIRES loc. cit.); the last value is approximately the mean of the adiabatic value of this cloud, which varies from zero at the base to 6.2 g/kg at the top. It has been included in order to illustrate what rapid and deep penetrations would occur in a cloud of such high liquid water content. The vigour with which dry air parcels would penetrate it may explain why such high values of $w$ have so far been observed only in isolated regions of cumuli.

Calculations have been carried out on the basis of equations (4), (5) and (6). The results

of interest are shown in Table I. The calculations have been terminated either when the parcel saturates, or when it subsides 3,000 metres and so reaches cloud base, or after the lapse of an hour, which ever occurs first. The "absolute" penetration in Table I is the final depth of the parcel below its starting point. "Relative" penetration is the depth of cloud above it at the end of the calculation, assuming that the cloud top continues to rise at the speed of the updraught after the parcel enters the cloud; since dry air parcels may enter the top of a cloud equally well at any stage of growth this figure gives an idea of how deeply they may become buried in the cloud as a result of their own subsidence, and the cloud's growth. For each value of the cloud liquid water content, only those values of $k$ are shown which are necessary to illustrate the behaviour of parcels of varying size. As will be seen from equation (7) below, the parcel size varies inversely with $k$. Small parcels ($k > 6 \times 10^{-3}$) are strongly cooled and develop high downward speeds, but saturate quickly. Larger parcels ($k < 10^{-3}$) remain unsaturated for a long time, but, except in the unrealistic case $w = 3$ g/kg, they are only slightly cooled and subside relatively slowly through the updraught.

Table I indicates that parcels of a suitable size can penetrate deeply into growing cumuli in a period commensurate with the life-time of these clouds, especially when it is remembered that they can enter at all stages of growth ("Relative" penetration). The degree of cooling and the falling speed are both roughly proportional to the liquid water content of the cloud, and the values found for them are consistent with observed fluctuations in cloud, especially in the more realistic cases $w_c = 0.3$ and 1.0 g/kg.

An inspection of Table I will disclose some apparent anomalies – small changes in $k$ sometimes give rise to large changes in parcel behaviour. These discontinuities are due to the fact that both the temperature deficit of the parcel and its downward velocity have an exponentially decreasing sinusoidal component (Equations (4) and (5)). The relative humidity of the parcel shows a similar behaviour. For certain values of the parameters, the parcel approaches saturation quite closely early in its history – one of the peaks of the relative humidity curve reaches close to 100 % – but nevertheless it remains unsaturated for a considerable time afterwards. In these circumstances, a small change in the parameter $k$ may have the result that the peak exceeds 100 %, that is, the parcel saturates. This kind of discontinuity in the data of Table I does not necessarily imply an anomaly in the physical behaviour of the parcels. It is due to the arbitrary termination of the calculations at the point where saturation is first reached. Thus it seems likely that in a case like $w_c = 3$ g/kg, $k = 5 \times 10^{-3}$, where saturation is just reached at the first peak of the relative humidity curve, the parcel would in fact quickly dry out again and continue downwards for some distance before finally saturating.

It is impossible to give more than a very rough indication of the size of these parcels. However, it can be established that the optimal parcel size deduced from the calculations is not absurd in the physical context being discussed. Treating the eddy diffusivity, $K$, as constant, it is easily shown that

$$k = c\ K/R^2 \qquad (7)$$

where $c$ is a constant depending on the form assumed for the profile of properties across the parcel, and $R$ is the parcel "radius"; in the case of a vertically elongated parcel, R would be the radius of its horizontal cross section. Thus, in any one cloud, $k$ may be regarded as a measure of parcel size, and this remains valid even though the eddy diffusivity depends on the scale of the phenomenon, that is, the effective value of $K$ really depends on $R$. PRIESTLY (loc. cit.) has discussed the value of the constant c and has concluded that $c = 8$ is a reasonable choice. The correct value of $c$ is not likely to depart from this by more than a factor of 2. However, there seems to be no way of arriving at an appropriate value for $K$, even within an order of magnitude. The eddy diffusivity which is effective in causing mixing between the parcel and the cloud is that due to eddies significantly smaller than the parcel. It will be much less than that which might be deduced, for example, from an aircraft accelerometer record, assuming the turbulence to isotropic, for this would include the effects of the motion of the parcels themselves. On the other hand, it will evidently exceed the small-scale background turbulence

of the clear air outside the cloud, since the motion of the parcels, and of the upcurrent, will give rise to additional small-scale turbulence. It seems in any case unlikely that the appropriate value of $K$ should lie outside the range $10^2$ to $10^6$ cm$^2$ sec$^{-1}$. Taking $k = 2.10^{-3}$ as the optimal value, the resulting value of $R$ from (7) is found to be in the range 6 to 600 m. Thus the optimal parcel sizes deduced from equation (7) are plausible in relation to the phenomena under discussion.

Table 1 indicates that, for any one value of the effective eddy diffusivity, only a narrow range of parcel sizes are capable of achieving appreciable penetrations in a reasonable period of time. In actual clouds, the steady state assumed in deriving this result never occurs, and moreover the parcels must often be reduced in size by attrition or by disruption. A large parcel may enter the cloud early in its growth and, although incapble of subsiding far, may later act as a source of dry air for the region near cloud base. Thus no literal significance can be attached to the detailed values in Table 1. The calculations can be regarded only as showing that certain downdraughts (of a physically plausible size) are capable of achieving significant penetrations, so that the proposed mechanism for introducing dry air into a cloud is quantitatively adequate. There is, of course, nothing in the calculations themselves to indicate how often such downdraughts occur in clouds, but the physical arguments of Section 2 indicate that they are common.

## 5. Conclusions

Theories of the interaction between cumuli and their environment have been reviewed in the light of the existing observations. Physical arguments have been given which indicate that the region around the top of a growing cloud may be an important source of the dry air which mixes with the upcurrent. A theoretical model of the penetration of a cloud by dry downdraughts has been set up, and the calculations carried out for a cloud 3 km deep, with an upcurrent of 1 m sec$^{-1}$. As can be seen from Table 1, these calculations show that parcels of dry air can remain unsaturated while subsiding up to three kilometres (i.e. to cloud base) through the updraught in a time which is commensurate with the life-time of cumuli. Even after saturating, such parcels, being colder than the surrounding cloud, would continue to subside for some time as regions of relatively low liquid water content.

A large number of such parcels entering the cloud top at all stages of its growth would result in a wealth of fine structure in the distribution of liquid water content and other cloud properties, and would have the effect of reducing the liquid water content and of cooling the cloud, especially in its upper parts. Thus the hypothesis affords an explanation of the presence of fine structure and of the fact that the observed liquid water content is nearly always less than the adiabatic value. It also explains the upward decrease of the ratio $\bar{w}/w_a$, and the frequent occurrence of a cloud lapse rate steeper than the wet adiabatic.

On this view, the initial immersion of dry air parcels in the cloud is greatly accentuated when the cloud top becomes appreciably warmer than the environment. In addition, the deeper penetration which follows is achieved by motions which depend for their energy supply on the presence of liquid water, and which it appears have velocities roughly proportional to it. Thus a very wet cloud would be more susceptible to deep penetration than a dry one. The mechanism described therefore provides a type of automatic action which not only ensures that the lapse rate in the cloud shall not depart far from that of the environment, but also limits the concentration of liquid water. Both these aspects of the hypothesis accord well with the observations.

A corollary of the hypothesis is that there should be a radical difference in structure between convection in the clear air and in cloud; the presence of the liquid phase in cloud introduces an element of instability by providing a source of energy which is available to drive smaller scale motions. This situation has no analogue in the case of clear air convection.

## REFERENCES


Barret, E. W., and Riehl, H., 1948: Experimental verification of entrainment of air into cumulus. *J. Meteor.*, **5**, 304—307.

Best, A. C., 1951: The occurrence of high rates of ice accretion on aircraft. M.R.P. 610.

Bunker, A. F., Haurwitz, B., Malkus, J. S. and Stommel,, H., 1949: Vertical distribution of temperature and humidity over the Caribbean Sea. Papers in Phys. Ocean. and Meteor., Mass. Inst. Tech. and Woods Hole Ocean. Inst. XI No 1.

Byers, H. R., and Hull, E. C., 1949: Inflow patterns of Thunderstorms as shown by winds aloft. *Bull. Am. Meteor. Soc.* **30**, 90—96.

Day, G. J., and Murgatroyd, R. J, 1953: The cumulus cloud investigations made by the Meteorological Research Flight during the period August 4th—15th, 1952. M.R.P. 826.

James, D. G., 1954: Fine scale characteristics of the lowest 5,000 ft. of the atmosphere as observed from an aircraft. M.R.P. 875.

Jones, R. F., 1954 a: Five flights through a Thunderstorm belt. *Quart. J. Roy. Met. Soc.* **80**, 377—387.

— 1954 b: Radar echoes from and turbulence within cumulus and cumulo-nimbus clouds. Prof. Notes Met. Off., London, **7**, No. 109.

Malkus, J. S., 1949: Effects of wind shear on some aspects of convection. *Trans. Amer. Geoph. Un.* **30**, 19—25.

— 1952: Recent advances in the study of convective clouds and their interaction with the environment. *Tellus*, **4**, 71—87.

Priestley, C. H. B., 1953: Buoyant motion in a turbulent environment. *Aust. J. Phys.* **6**, 279—290.

Scorer, R. S., and Ludlam, F. H., 1953: The bubble theory of penetrative convection. *Quart. J. Roy. Met. Soc.* **79**, 96—103.

Squires, P., 1958: The spatial variation of liquid water content and droplet concentrations in cumuli. *Tellus.* **10**, 372—380.

Stommel, H., 1947: Entrainment of air into a cumulus cloud. *J. Meteor.* **4**, 91—94.

Warner, J., 1955: The water content of cumuliform cloud. *Tellus* **7**, 449—457.

Warner, J., and Squires, P., 1958: Liquid water content and the adiabatic model of cumulus development. *Tellus.* **10**, 390—394.

Weickmann, H. K., and Kampe, H. J. Aufm, 1953: The physical properties of cumulus clouds. *J. Meteor.* **10**, 204—211.

Zaitsev, V. A., 1950: Liquid water content and distribution of drops in cumulus clouds, Leningrad, Glavaya Geofizicheskaia Observatoriy, Trudy, 19 (81): 122—132.

# Liquid Water Content and the Adiabatic Model of Cumulus Development

By J. WARNER and P. SQUIRES
C.S.I.R.O., Radiophysics Laboratory, Sydney, Australia

(Manuscript received October 28, 1957)

## *Abstract*

The literature shows considerable disagreement concerning the liquid water contents found in cumuliform cloud and the relation of observed values to those deduced from the adiabatic model. The present paper describes some observations in which two methods of measuring liquid water have been used simultaneously and found to be in good general agreement. However, the two methods employed very different averaging periods, so that individual measurements were not strictly comparable. These results, and the observations of other workers, are discussed in relation to the general level of liquid water in cumuliform cloud and its variability in space.

## 1. Introduction

Some information concerning the structure and development of cumuliform cloud can be gained from a study of the spatial distribution of liquid water. While several observers agree that these clouds show a wealth of fine structure, there is no general agreement as to the general level and the overall pattern throughout the cloud. Both aspects – the fine structure and the general level and pattern – are relevant to theories of cumulus growth and interaction with the environment and to the theory of rain formation by the coalesence of droplets, a process which certainly occurs in warm clouds, and is likely to be important also in many clouds which reach far above the freezing level.

## 2. Discussion of previous measurements

Measurements of liquid water content have been made by a variety of means; the most important difference between them lies in the averaging time of the instruments. All the measurements give an average value over a narrow strip of cloud of finite length, but this length ranges from a few kilometres in some methods to about a metre in others.

### (a) *The general level of the liquid water content*

The earliest measurements in considerable numbers were made in connection with icing research. LEWIS (1951) has summarized these measurements: the averaging distance employed varied from 3 km upwards; in 342 observations taken in cumulus and cumulo-nimbus, the maximum value found was 1.71 g $m^{-3}$, and the median, 0.34 g $m^{-3}$. BEST (1951) also discussed these measurements and concluded that the observed values were ordinarily less than those deduced from the adiabatic model of cumulus development. In order to explain this deficiency, following STOMMEL (1947), he postulated a lateral entrainment of dry air into the cloud.

Zaitsev (1950) deduced the liquid water content from the size of a coloured spot made by depositing the collected water on filter paper. This method apparently averaged over a distance of about 100 m. Zaitsev's values are much higher than those found by most other observers. Indeed, in one of the two clouds for which he gives data, the measured value in the region of the central maximum exceeds the adiabatic liquid water content by a factor of about two; in the other, it is about equal to it.

Day and Murgatroyd (1953) and Day (1956 a) have measured the liquid water content of large cumuli with an icing meter and with heated cylinders. They gave the lag of the latter method as about 10 seconds and it may be assumed that their values represent averages over some 500 to 1,000 m. They quoted mean and maximum values for each traverse. In the measurements of Day and Murgatroyd the maximum value hardly ever reached 1 g $m^{-3}$, and the mean was usually less than 0.5 g $m^{-3}$. In Day's measurements, the maximum usually exceeded 1 g $m^{-3}$, and perhaps occasionally 2 g $m^{-3}$, but the instruments used were incapable of measuring values above about 1.8 g $m^{-3}$. The average value in this series hardly ever reached 1.0 g $m^{-3}$, and usually fell in the range 0.3 to 0.7 g $m^{-3}$. Comparing these mean values with the adiabatic model, it is found that the ratio of the mean observed to the calculated value, $\overline{w}/w_a$, never reaches 0.5; in the first series, its median value is about 0.08; in the second, about 0.2.

Day (1956 b) has recently made further measurements using a refrigerated icing disc, in order to avoid the loss of water which can occur at moderately sub-freezing temperatures when $w$ is large, as described by Ludlam (1951). In this series Day found maximum values of water content ($w_m$) appreciably higher than in his earlier work; in cumuli it exceeded 1.0 g $m^{-3}$ in a majority of cases. The maximum found was 4.2 g $m^{-3}$, and it seems that in some cases, $w_m$ may have exceeded $w_a$. Mean values were not given – these were no doubt much smaller.

Weickmann and Aufm Kampe (1953) deduced liquid water contents from measurements of the transmission of light. The values quoted by them are the highest in the literature, reaching over 6 g $m^{-3}$ in cumulus congestus. About a quarter of their values exceed that found on the adiabatic model. However, their technique has been criticized by Fritz (1954), who pointed out that with a given liquid water content, transmission could be greatly reduced if small droplets ($r \approx 1\ \mu$) were present in numbers reaching some thousands per $cm^3$. Eldridge (1957) has recently made infra-red transmissometer measurements on Mt. Washington, and deduced that at times some tens of thousands of such droplets were present, per $cm^3$. Day (1956 a) made measurements of visibility and drop size as well as liquid water content during his runs through cloud. He used a modified form of Trabert's formula due to Best (1953), to compute a value of visibility from his measured values of drop size and liquid water. The values obtained were about three times the observed values. Thus it seems possible that the water content values deduced by Weickmann and Kampe were too high.

A series of measurements has been made by Warner (1955) using an instrument in which the impacted cloud water changes the electrical resistance of a paper tape. This method yields an average over a distance of the order of 50 m. The absolute values are similar to those found by earlier observers, with the exception of Zaitsev (loc. cit.) and Weickmann and Kampe (loc. cit.) whose values are higher. Comparing the observed peak values for each traverse ($w_p$) with those calculated for the adiabatic model ($w_a$), it was found that the ratio $w_p/w_a$ was always less than unity; on the average it was about 0.5 near cloud base, and decreased upwards until at a level some 2,000 m above base it had fallen to about 0.2.

Liquid water contents have been deduced from measurements of droplet sizes by Squires using the imprints made on sooted glass slides. This method yields an average over a distance of about 1 m. The values found are in general agreement with those of Warner. The mean value of $w/w_a$ was found to decrease from cloud base upwards, in the same manner as reported by Warner (loc. cit.).

It is clear from this summary that there is no unanimity concerning the general level of the liquid water content. Zaitsev (loc. cit.) and Weickmann and Aufm Kampe (loc. cit.) found values which often exceed that expected

on the adiabatic model, and commonly reached several g $m^{-3}$. According to other observers, the average values for a traverse only occasionally reached 1 g $m^{-3}$, irrespective of the size of the cloud, and in those cases where the observations could be compared with the adiabatic model, it seems that $w$ was usually less than one quarter of $w_a$.

(b) *The fine structure*

A transmissometer record reproduced by Weickmann and Aufm Kampe (loc. cit.) gives clear evidence of the occurrence of large fluctuations over short distances. It shows that great changes can occur in a distance of a few metres so that only an instrument with a time constant of much less than a second could delineate the fine structure, even if no more is attempted than to record all the fluctuations which are comparable with the average value. Malkus et al. (1948) in testing an optical instrument designed to measure liquid water and cloud droplet sizes reached a similar conclusion.

Further supporting evidence of an indirect nature is afforded by observations made with a microwave refractometer in two cumuli by Bussey and Birnbaum (1953). Their record of refractive index shows major fluctuations occurring over distances of only a few metres. A common rapid fluctuation is equivalent to a change in water vapour content of 1 g $m^{-3}$, and it seems likely, on any hypothesis as to the origin of the inhomogeneities, that they would also appear to a marked extent in a sufficiently detailed record of the liquid water content.

The measurements of Warner (loc. cit.) give a direct indication of the variability of liquid water, averaged over a distance of the order of 50 m. There were large fluctuations during nearly all traverses; these were often in the nature of downward excursions from a rather characteristic peak level, to which the record returned when the fluctuation had been passed. Records of this nature could perhaps be interpreted as indicating the existence of a number of cells. The downward fluctuations, however, were randomly distributed across the visible cloud, and showed no systematic preference for the peripheral regions. The edge of the cloud was often quite sharp; the liquid water content apparently rose from zero to its peak value within ten or twenty metres in some cases.

In the measurements made by Squires (loc. cit.) the average value of the ratio $w/w_a$ was about 0.2, but occasionally the full adiabatic liquid water content was encountered. Out of some 300 spot measurements, this happened only four times. Rather more frequently, well inside clouds, a zero value was found. These measurements, usually spaced some 200 m apart, showed marked variation from one observation to the next. Superimposed on the trends which appear in Warner's records, there appears to be a still finer structure of almost equal amplitude.

### 3. A comparison between two instruments

In order to try to resolve the question of the general levels of liquid water content, and to investigate further the fine structure of cloud, a comparison has been made of the instruments described by Warner and Newnham (1952) and Squires and Gillespie (1952). These two methods, the general principles of which have been mentioned above, are fundamentally different in operation, and have very different averaging distances. It seemed therefore that if they were in agreement concerning the general level of liquid water content, it would be most unlikely that both should be wrong.

The comparisons were made by operating the two instruments simultaneously from one aircraft in two series of measurements: in the orographic cloud of Hawaii in 1954* and in cumuli in Eastern Australia in 1956. The results obtained on a series of runs through a cumulus cloud are shown in Fig. 1, which demonstrates the typical variability of liquid water found in cumulus with both instruments. It also shows that there is fair general agreement, although on a few occasions the two instruments are in very considerable disagreement. From what has been said above about the fine structure of clouds, and considering the difference in averaging distance of the two methods, this is not a matter for surprise. A scatter diagram showing the results of all the comparisons made on this day is shown in Fig. 2, which again shows the similarities and differences apparent from the individual records of Fig. 1. The mean water

* See Tellus, Project Shower, 9. (Editors note.)

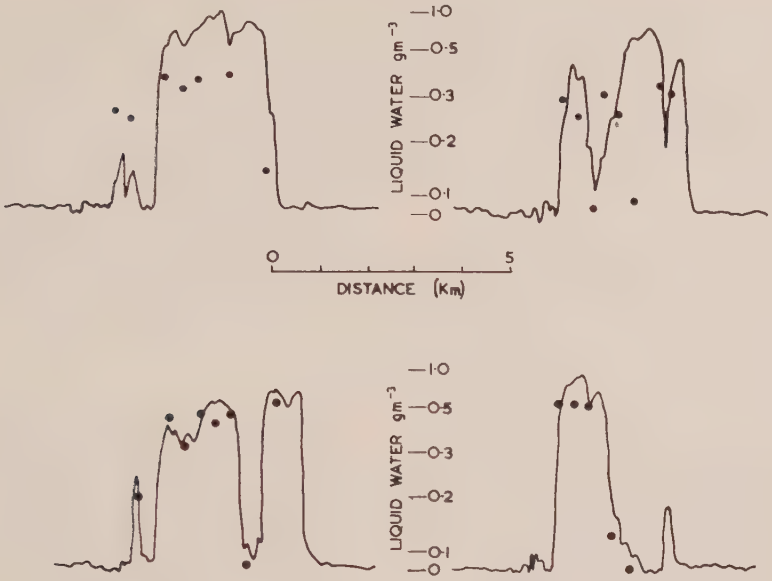


Fig. 1. Comparison of record of liquid water meter with values of liquid water deduced from droplet spectrum (circles) at various times during traverses through cumuli.

content deduced from droplet volumes in 155 samples in cumulus cloud in 1956 was 0.267 g $m^{-3}$; that obtained from the record of the water content meter at the times of sampling was 0.295 g $m^{-3}$, which is 1.11 times that deduced from the droplet volumes. The maximum values obtained on both instruments were near to 1 g $m^{-3}$. The modal drop diameter of the samples ranged from 7 to 26 microns with a mean of 17 microns. No

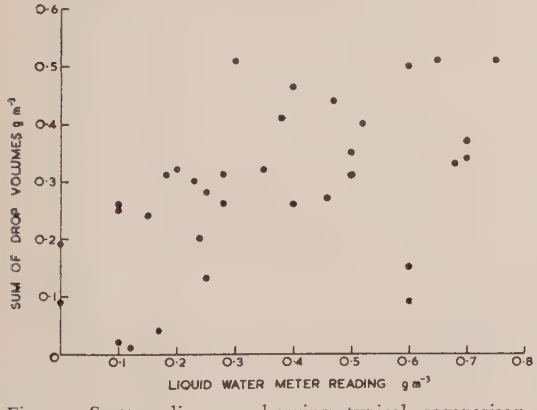


Fig. 2. Scatter diagram showing typical comparison between values of cloud water content deduced from liquid water meter and droplet spectrum (one day's observations).

significant correlation was found between the ratio of the measurements of the two instruments on a cloud sample and the modal droplet diameter of that sample, which suggests that the agreement is not a chance event depending upon some peculiar property of the droplet spectra.

Similar comparisons were made from the data of Squires and Warner (1957) relating to orographic cloud on the island of Hawaii. In this case, however, the degree of simultaneity of observations was not as great. The mean water content deduced from the droplet volumes in 92 samples was 0.349 g $m^{-3}$; that obtained from the record of the water content meter at the times of sampling was 0.280 g $m^{-3}$ which is 0.80 times that deduced from the droplet volumes. The modal drop diameter of the samples ranged from 7 to 104 microns with a mean of 32 microns. The ratio of the water content measurements was again independent of modal drop diameter of the sample.

Since the two instruments obtain their values of liquid water through two totally different techniques and the calibration procedures were also completely different, it must be concluded that both calibrations are prob-

ably correct to within about ± 20 %. However, it is clear that with these instruments or any others used for measurement of liquid water content both cloud structure and instrumental averaging time must be borne closely in mind in interpreting the observations.

## 4. Conclusion

From these comparisons and the observations discussed in Section 2, it seems that cumuliform cloud consists typically of a large number of regions of relatively high and low liquid water content, the horizontal extent of which apparently ranges upwards from a few metres. It appears that the full adiabatic liquid water content in cumuli is realized, if at all, only in regions which are of negligible size in relation to the cloud as a whole. In most cases the liquid water in the main body of the cloud is less than a quarter of the adiabatic value, and often considerably less.

## REFERENCES


Best, A. C., 1951: The occurrence of high rates of ice accretion on aircrafts. M.R.P. 610.

Best, A. C., 1953: A modified form of Trabert's formula. *J. Met.* **10**, 227—228.

Bussey, H. E., and Birnbaum, G., 1953: Measurement of variations in atmospheric refractive index with an airborne microwave refractometer. *J. Res. Nat. Bureau of Standards U.S.A.* **51**, 171—178.

Day, G. J., 1956 a: Further observations of large cumuliform clouds by the Meteorological Research Flight. M.R.P. 980.

Day, G. J., 1956 b: A refrigerated disc icing meter. M.R.P. 916.

Day, G. J., and Murgatroyd, R. J., 1953: The cumulus cloud investigations made by Meteorological Research Flight during the period August 4th—15th, 1952. M.R.P. 826.

Fritz, S., 1954: Small drops, liquid water content, and transmission in clouds. *J. Met.* **11**, 428—429.

Eldridge, R. G., 1957: Measurement of drop size distributions *J. Met.* **14**, 55—58.

Lewis, W., 1951: Meteorological aspects of aircraft icing. *Compendium of Meteorology*, American Meteorological Society, Boston, 1197—1203.

Ludlam, F. H., 1951: The heat economy of a rimed cylinder. *Quart. J. R. Met. Soc.* **77**, 663—666.

Malkus, W. V. R., Bishop, R. H., and Briggs, R. O.,, 1948: Analysis and preliminary design of an optical instrument for the measurement of drop size and free water in clouds. N.A.C.A. Tech. Note No. 1622.

Squires, P., 1958: The spatial variation of liquid water and droplet concentrations in cumuli. *Tellus* **10**, 372—380.

Squires, P., and Gillespie, C. A., 1952: A cloud droplet sampler for use on aircraft. *Quart. J. R. Met. Soc.* **78**, 387—393.

Squires, P., and Warner, J., 1957: Some measurements in the orographic cloud of the island of Hawaii and in trade wind cumuli. *Tellus*. Project Shower, **9**, 475—495.

Stommel, H., 1947: Entrainment of air into a cumulus cloud. *J. Met.* **4**, 91—94.

Warner, J., 1955: The water content of cumuliform cloud. *Tellus* **7**, 449—457.

Warner, J., and Newnham, T. D., 1952: A new method of measurement of cloud-water content. *Quart. J. R. Met. Soc.* **78**, 46—52.

Weickmann, H. K., and Kampe, H. J. Aufm, 1953: Physical properties of cumulus clouds. *J. Met.* **10**, 204—211.

Zaitsev, V. A., 1950: Liquid water content and distribution of drops in cumulus clouds. Glavna Geofizicheskaya Obseratoriya, Trudy **81**, 122—132.

# NOTES

## Eccentric Circumpolar Vortices in a Barotropic Atmosphere[1]

By EARL W. BARRETT, Department of Meteorology, University of Chicago

(Manuscript received May 29, 1957)

Recent investigations (La Seur, 1954) have shown that on many occasions the circulation of the middle troposphere possesses a marked eccentricity; i.e., the center of symmetry of the flow is found at a considerable distance from the geographic pole. At such times the intensity of the zonal component of the flow (calculated with respect to the geographic pole) is low, while the meridional component appears large. Harmonic analysis of the motion reveals that most of the energy of the meridional motion is concentrated in the first longitudinal harmonic (wavelength 360 degrees of longitude). If, on the other hand, the motion is analyzed with respect to the circulation pole (centroid of the streamline field), it is found that the purely zonal component in the coordinate system thus defined is often as great or even greater than in those cases where the motion is symmetric about the geographic pole. Thus the zonal index calculated in geographical coordinates may at times give a rather misleading picture of the character of the circulation; what appears to be a flow with a large meridional component may actually be a rather symmetric zonal vortex with respect to an eccentric pole.

As far as this writer is aware, no previous theoretical analyses of the behavior of eccentric vortices having a scale comparable to the planetary dimensions have been made. Rossby (1948, 1949) has treated the case of an axially symmetric vortex embedded in an atmosphere at rest with respect to a rotating earth; the model so arrived at is compatible with the observed behavior of cyclones and anticyclones with diameters small compared to the planetary diameter. In the Rossby model the vortex is subject to an acceleration equal to the area integral of the Coriolis force over the horizontal extent of the vortex divided by the mass of air bounded between two surfaces of this horizontal extent which are separated by unit height. This resultant Coriolis acceleration is not balanced by any pressure gradient in the resting environment and hence produces a meridional component of translation of the vortex as a whole. This approach is obviously unsuitable for the study of a vortex which occupies the entire sphere, since no pressure-gradient-free region can surround such a vortex.

The balance of the present paper is devoted to the derivation of an equation governing the behavior of eccentric circumpolar vortices covering the entire sphere which are initially purely zonal with respect to the circulation pole, and to a brief discussion of the resulting motions for a few simple cases. The flow is assumed to satisfy the two-dimensional nondivergent barotropic vorticity equation.

The circulation pole is assumed to lie initially at geographic latitude $\phi_0$ and geographic longitude $\lambda_0 = 0$. The stream function $\psi$ for the motion is taken to be a single pure zonal spherical harmonic; hence the motion at $t = 0$ is prescribed everywhere on the sphere by the equation

$$\psi = A + BP_n (\sin \varphi) \qquad (1)$$

[1] This paper is an extract from a dissertation submitted to the faculty of the Department of Meteorology of the University of Chicago in partial fulfillment of the requirements for the degree of Doctor of Philosophy.

where $A$ and $B$ are independent of position, $P_n$ is the zonal harmonic (Legendre polynomial) of order $n$ with argument $\sin \phi$, and $\phi$ is latitude measured with respect to the eccentric pole. The instantaneous zonal angular velocity of the flow is given by

$$\dot{\lambda} = a^{-2} \sec \phi \, \partial\psi/\partial\phi = a^{-2} \sec \phi \, BP_n^1 (\sin \phi) \quad (2)$$

One must now find solutions of the vorticity equation

$$\nabla^2(\partial\psi/\partial t) + \mathbf{v} \cdot \nabla(\nabla^2\psi + f) = 0 \quad (3)$$

which satisfy (1) as an initial condition at $t = 0$ and which are finite, single-valued and twice-differentiable over the sphere. It is possible to express the Coriolis parameter $f$ as a function of latitude and longitude in the eccentric system; this was, in fact, the first approach used by the writer. Such a solution is rather laborious, occupies excessive space in print, and is obtained in a form which masks the physical significance of the result. The same solution is obtainable much more simply by transforming (1) to geographic coordinates and solving (3) in the geographic system.

The transformation is readily accomplished by use of the "addition theorem" for zonal harmonics (JAHNKE and EMDE, 1943, p. 115). In the notation used in this paper, this theorem may be written

$$P_n(\sin\phi) = P_n(\sin\phi_g)\, P_n(\sin\phi_0) + 2 \sum_{m=1}^{n} \frac{(n-m)!}{(n+m)!} P_n^m(\sin\phi_0)\, P_n^m(\sin\phi_g) \cos m(\lambda_0 - \lambda_g) \quad (4)$$

where $\phi_0$ and $\lambda_0$ are the geographic coordinates of the eccentric pole from which $\phi$ is measured, and $\phi_g$, $\lambda_g$ are the geographic coordinates of any point on the sphere. Since $\lambda_0 = 0$ initially, the stream function equation in geographic coordinates becomes

$$\psi = A + BP_n(\sin\phi_0)\, P_n(\sin\phi_g) + 2B \sum_{m=1}^{n} \frac{(n-m)!}{(n+m)!} P_n^m(\sin\phi_0)\, P_n^m(\sin\phi_g) \cos m\lambda_g \quad (5)$$

Inspection of (5) shows that all zonal and tesseral harmonics in the streamline field possess the same lower index $n$. Such an ensemble of harmonic waves is of the type discussed by NEAMTAN (1946). The property of such a set of waves which is of major interest here is that the resultant streamline field is a pattern in which the isolines of relative vorticity always coincide with the streamlines. This follows from the fact that the relative vorticity $\nabla^2\psi_n^m$ of any tesseral-harmonic stream function component is given by the associated Legendre equation

$$\nabla^2 \psi_n^m + n(n+1)\, a^{-2} \psi_n^m = 0, \qquad \psi_n^m = B_{mn} P_n^m e^{im\lambda g} \quad (6)$$

so that, if $n$ is the same for all the $\psi_n^m$, the relative vorticity is given by

$$\nabla^2\psi = -n(n+1)\, a^{-2} \psi, \qquad \psi = \sum_{m=0}^{n} B_{mn} P_n^m(\sin\phi_g)\, e^{im\lambda g} \quad (7)$$

and is simply proportional to the value of $\psi$ at each point. From this it follows that the velocity vector of the flow is always tangent to a line of constant relative vorticity and hence the advection of relative vorticity vanishes everywhere. This implies that there can be no generation of new zonal or tesseral harmonics by interaction between the existing harmonics, hence $n$ can never take on any value different from the initial one. Thus the solution of the vorticity equation (3) for a set of waves of this type will be closed with respect to the index $n$ (and hence with respect to the upper index $m$ also), since the term $\mathbf{v} \cdot \nabla f$ does not introduce nonlinear interactions.

Substituting (7) into (3) and setting $\mathbf{v} \cdot \nabla(\nabla^2\psi) = 0$ and $\mathbf{v} \cdot \nabla f = 2\Omega a^{-2} \partial\psi/\partial\lambda_g$ gives the vorticity equation applicable to sets of harmonic waves of the type given in (5)

$$2\Omega \, \partial\psi/\partial\lambda_g - n(n+1)\, \partial\psi/\partial t = 0 \quad (8)$$

This is immediately recognizable as the equation for one-dimensional wave propagation in a linear non-dispersive medium. All harmonics propagate without change of amplitude in the negative $\lambda_g$-direction with the same angular speed $\omega = 2\Omega/n(n+1)$. The solution

of (8) which is satisfied by (5) as initial condition is

$$\psi = A + BP_n(\sin\phi_0)\,P_n(\sin\phi_g) + \\ + 2B\sum_{m=1}^{n}\frac{(n-m)!}{(n+m)!}P_n^m(\sin\phi_0)\,P_n^m(\sin\phi_g) \\ \cos m\,[\lambda_g + 2\Omega t/n\,(n+1)] \qquad (9)$$

But this is identical in form to (4) with $-\lambda_g$ replaced by $-[\lambda_g + 2\Omega t/n(n+1)]$. Hence (9) may be transformed back to an eccentric coordinate system with a *moving* pole located at geographic coordinates $\phi_0, \lambda_0 - 2\Omega t/n\,(n+1)$. The stream function in this coordinate system is the original one, $\psi = A + BP_n(\sin\phi)$, with $\phi$ being measured from the moving pole. It has thus been shown that an eccentric circumpolar vortex in a barotropic atmosphere, for which the stream function is expressible as a pure zonal spherical harmonic, retains its shape and intensity unchanged while the eccentric pole executes a retrograde precession about the geographic pole at an angular speed $2\Omega/n(n+1)$ which depends only upon the rotation speed of the planet and the number of wind speed maxima in the vortex. The sense of rotation of the vortex and the magnitude of the wind speed maxima (which are determined solely by the coefficient $B$) do not enter into the equation for the precession rate. In this respect the vortices considered in this paper differ markedly from those treated by Rossby in the previously-referenced papers; the sense and speed of the motion were major determining factors in the subsequent displacements of the vortices considered by Rossby. These differences are in no way surprising, since the physical models are highly dissimilar. It is of interest to note that the area integral of the Coriolis force over the entire sphere vanishes identically for the vortices treated in this paper.

The precession speeds and the latitudes and number of wind maxima are listed in Table I for the first few values of $n$. Directions of the wind are those obtained with negative values of $B$. Latitudes refer to the eccentric coordinate system.

**Table I. Properties of some Zonal Harmonic Eccentric Vortices.**

| n (No. Wind Maxima) | Latitudes and Directions of Maxima | Precession Period of Pole, Days |
|---|---|---|
| 1 | Equator, W. (Solid Rotation) | 1 |
| 2 | 45°, W; —45°, E. | 3 |
| 3 | ±59°, W; Equator, E. | 6 |
| 4 | 67°, W; 20.5°, E; —20.5°, W; —67°, E. | 10 |
| 5 | ±70°, W; ±34°, E; Equator, W. | 15 |

It is, of course, rather unlikely that the actual streamline field in the atmosphere can be fitted closely at any time by a single zonal harmonic. It is apparent from Table I that a zonal harmonic vortex gives a streamline field that is either an even or an odd function of latitude. In general in the atmosphere one expects a rough symmetry of the wind field with respect to the equator, hence the odd functions ($n$ even) are not too likely to be found in the real atmosphere. The even functions display the desired symmetry, but unfortunately always yield a wind maximum at the equator, in disagreement with the facts in the real atmosphere. It is therefore probable that more than one value of $n$ would be required to describe the actual zonal wind field. In such a case the vortices associated with each value of $n$ would interact nonlinearly to generate new harmonics. However, in cases of square-law nonlinearity (such as the relative-vorticity advection term in the vorticity equation) one always finds in the response function the same harmonics which would have been present in the absence of nonlinearity (although changed in amplitude) in addition to the new harmonics generated through the nonlinearity. Therefore one should expect to find evidence of eccentric circulations precessing at the indicated rates in the atmosphere even though they may be hidden in a mixture of other wave motions. For example, if a part of the total complex motion is a solid rotation about an eccentric axis ($n=1$), a diurnal wave in the stream function should be observable at each station. The corresponding variation in the geopotential is readily deducible by taking the divergence of the vector equation of motion so as to obtain the "balance equation" in the form

$$\eta\,\nabla^2\psi + \nabla\eta\cdot\nabla\psi = \nabla^2\left(G + {}^1/_2\mathbf{v}\cdot\mathbf{v}\right) = \nabla^2 Q \qquad (10)$$

where $\eta$ is the absolute vorticity and $G$ represents the geopotential (to avoid confusion with the symbol $\phi$ already used for the latitude). Substituting from (9) into (10), with $n=1$, yields a Poisson equation which is readily solvable for $Q$ since the lefthand side of (10) consists of a finite number of spherical harmonics. The geopotential is obtained by subtracting from $Q$ the squared-velocity term, yielding

$$G = K - B^2/3a^2 + [{}^2/_3 \Omega B P_1 \ (\sin \phi_0) - B^2/3a^2 \ P_2 \ (\sin \phi_0)] \ P_2 \ (\sin \phi_g) + [\Omega/3 \ BP^1{}_1 \ (\sin \phi_0) - B^2/9a^2 \ P^1{}_2 \ (\sin \phi_0)] \ P^1{}_2 \ (\sin \phi_g) \cos (\lambda g + \Omega t) - B^2/36a^2 \ P_2^2 \ (\sin \phi_0) \ P_2^2 \ (\sin \phi_g) \cos 2 \ (\lambda_g + \Omega t)$$

which shows that the oscillation of geopotential at a station possesses a diurnal and a semidiurnal component. It is well-known (Wilkes, 1949) that the surface pressure (or 1,000-mb geopotential) does in fact exhibit such oscillations, and that the semidiurnal component varies with latitude approximately in accordance with a $P_2^2$-distribution. These pressure oscillations are usually attributed to a tidal or thermal forcing and involve a divergent atmospheric model. The analysis in this paper indicates, however, that a non-divergent atmosphere with purely two-dimensional flow may also exhibit pressure oscillations with diurnal and semidiurnal periods. It is therefore reasonable to inquire whether or not the mechanism treated in this paper, i.e., a solid rotation of the atmosphere about a slightly eccentric pole, might contribute a part of the observed diurnal pressure variation.

The data indicate that the amplitudes of the diurnal and semidiurnal components of the "solar" pressure oscillation are of the same order of magnitude at most stations; the semidiurnal wave is usually somewhat the larger of the two. Substituting various values of $B$ into (11) shows that for all solid rotation angular speeds up to 100 deg long day$^{-1}$ the terms linear in $B$ are at least one order of magnitude larger than the quadratic terms (i.e., the motion is geostrophic to the extent of 90 per cent or more) and that therefore the semidiurnal amplitude factor is less than two per cent of the diurnal amplitude factor. It thus appears that the observed oscillations cannot be accounted for by an eccentric solid-rotation vortex unless the semidiurnal component is amplified by a factor of at least 100 through a resonance phenomenon. Such a resonance phenomenon involves a divergent atmosphere and hence falls outside the scope of the model used in this paper. However, it is imaginable that a divergence field might exist which is small enough to leave the two-dimensional flow pattern nearly unaffected while permitting the necessary resonant amplification.

Another factor must be considered, however. It is observed that the phases of the oscillations in the real atmosphere vary only slightly over the year with respect to solar time. Since the factor $\Omega$ appearing in the dynamical equations is the *sidereal* rotation rate of the earth, it follows that the periods of the pressure oscillations appearing in (11) are one sidereal day and one-half sidereal day respectively. The phases with respect to solar time of the oscillations described by (11) should therefore shift through 360 degrees during one solar year. Since only a small phase change during the year is actually observed, one must conclude that the contribution to the diurnal pressure variation from an eccentric vortex of solid rotation must be much smaller than the solar tidal or thermal influence.

The antisymmetric vortex with $n=2$ might conceivably play a part in the 20—30 km region. Evidence presented by Scherhag (1948) and Kochanski and Wasko (1956) supports the notion of a circulation at these levels which is anticyclonic in the summer hemisphere and cyclonic in the winter hemisphere. Eccentricity of this flow should give rise to a 3-day cycle in the stream function at these upper levels.

The symmetric case with $n=3$, with its associated 6-day cycle, is at best only a rough approximation to the flow in the middle troposphere, but might be present as one component of a more complex flow. The case $n=5$ (with sense opposite to that given in Table I) might possibly be found in the lower levels of the troposphere, where the eccentricity would give rise to a 15-day periodicity in the pressure or geopotential.

As already pointed out by La Seur (1954), it must be recognized that on many occasions when eccentricity is well-marked the circulation pole is quasi-stationary. Obviously such situations cannot be explained in terms of the simple model and must be regarded as the

result of orographic or thermal forcing, as discussed by FRENZEN (1956) and LA SEUR (1956).

It is of some interest to note that the analysis given above is not restricted to purely zonal spherical-harmonic streamline patterns but may be extended to include any wave pattern consisting of one or more tesseral-harmonic components plus one zonal-harmonic component in the eccentric coordinate system, provided that all of the harmonics have the same lower index. If the stream function in the eccentric system be written in the form

$$\psi = A + BP_n(\sin\phi) + \sum_{m=1}^{n} C_m P_n^m(\sin\phi)\, e^{im\lambda} \tag{12}$$

in which the $C_m$ may be complex, it is seen at once that this equation satisfies eq. (7). The direct transformation to geographic coordinates cannot be carried out on eq. (12) in a simple manner because the "addition theorem" of eq. (4) is not applicable to the associated Legendre polynomials. The author has been unable to locate or deduce the law of transformation for these functions. Fortunately, however, the proof of the extended analysis does not require the transformation but rests on the establishment of the invariance of certain quantities under the transformation.

It has just been stated that the stream function in eq. (12) satisfies the condition that

$$\nabla^2\psi = -n(n+1)\, a^{-2}\psi \tag{7}$$

Now $\psi$ is an absolute scalar field and hence $\nabla^2\psi$ is also an absolute scalar field; the numerical value of the Laplacian at each point is therefore independent of the choice of the coordinate system, as is the numerical value of the stream function itself. Therefore only the one value of the lower index $n$ may enter into the specification of the Laplacian, regardless of the coordinate system adopted. The geostrophic velocity vector $\mathbf{v}$ is an absolute vector, since it is computed from the surface gradient of the absolute scalar $\psi$. The quantity $\mathbf{v}\cdot\nabla(\nabla^2\psi)$ is therefore also an absolute scalar. Since it is clear from eq. (7) that this scalar vanishes in the eccentric coordinate system, and since it has been shown to be an absolute scalar, it must vanish in any other coordinate system. It has thus been proved that, whatever be the law of transformation of the associated Legendre polynomials, it cannot result in the introduction of polynomials with a lower index different from the value chosen for use in eq. (12). The scalar $\mathbf{v}\cdot\nabla f$ is likewise an absolute scalar, hence eq. (8) applies to the stream function of eq. (12) without modification. Since the conclusion regarding the precession rate of the pole is reached by (a) a coordinate transformation, followed by (b) solution of eq. (8) for the propagation velocity in the geographic system, and (c) performing the coordinate transformation which is the inverse of (a), the proof given above that eq. (8) is applicable to the set of harmonics in eq. (12) suffices; the law of transformation need not be specified.

The precession rate of the eccentric pole, $-2\Omega/n(n+1)$, is the same as the propagation speed relative to the geographical coordinates of harmonic waves with lower index $n$; hence the wave pattern is stationary in the eccentric system. The wave velocity as measured by an observer on the ground is seen to be unaffected by the choice of an eccentric coordinate system; only the amplitudes and phases of the various harmonics are altered by the choice of coordinates. The use of an eccentric pole may nevertheless be desirable on occasion in order to minimize the number and/or the amplitudes of the harmonic waves which might be involved in a particular computation.

## Acknowledgements

The writer gratefully acknowledges the suggestion of Prof. Herbert Riehl which led to the present study, and the assistance given by Prof. George W. Platzman during the course of the analysis.

## REFERENCES

FRENZEN, P., 1956: Criteria for the occurrence of an eccentric circumpolar vortex in the atmosphere inferred from model experiments. *J. Meteor.* **13**, 124—125.

FRENZEN, P., 1956: Additional remarks. *J. Meteor.* **13**, 126.

JAHNKE, E., and EMDE, F.: "Tables of Functions". Dover Publications, New York, 1943; 379 pp.

KOCHANSKI, A., and WASKO, P. E., 1956: Daily wind flow at the 50- and 25-mb levels. *Bull. Amer. Meteor. Soc.* **37,** 8—13.

LA SEUR, N. E., 1956: Reply. *J. Meteor.* **13,** 125—126.

LA SEUR, N. E., 1954: On the asymmetry of the middle-latitude circumpolar current. *J. Meteor.* **11,** 43—57.

NEAMTAN, S. M., 1946: The motion of harmonic waves in the atmosphere. *J. Meteor.* **3,** 53—56.

ROSSBY, C.-G., 1948: On displacements and intensity changes of atmospheric vortices. *J. Marine Res.* **7,** 175—187.

ROSSBY, C.-G., 1949: On a mechanism for the release of potential energy in the atmosphere. *J. Meteor.* **6,** 163—180.

SCHERHAG, R., "Neue Methoden der Wetteranalyse und Wetterprognose". Springer-Verlag, Berlin, 1948; 424 pp.

WILKES, M. V.: "Oscillations of the Earth's Atmosphere". Cambridge Monographs on Physics, University Press, Cambridge (England), 1949; 74 pp.

# Current Data on the Chemical Composition of Air an Precipitation XIV

(For further information see Egnér, H., Eriksson, E., *Tellus* **7**, pp. 134—139, **8**, p, 285 and 517)

| Code | mm | mg/m² S | Cl | $NO_3$–N | $NH_3$–N | Na | K | Mg | Ca | pH | $-\frac{\mu val}{HCO_3\ l}$ | $\frac{\varkappa \cdot 10^6}{\Omega \cdot cm}$ | µg/m³ (=kg//km³) S | Cl | $NH_3$–N | Na | K | Mg | Ca |
|---|---|---|---|---|---|---|---|---|---|---|---|---|---|---|---|---|---|---|---|
| | Precipitation May 1957 (D 705) | | | | | | | | | | | | Air May 1957 (L 705) | | | | | | |
| Ad | 27 | 14 | 29 | 18 | 54 | 19 | 12 | 8 | — | 5.6 | 0 | 35 | — | — | — | — | — | — | — |
| BL | 76 | 178 | 55 | 23 | 22 | 20 | 14 | 6 | 91 | 5.7 | 5 | 19 | 8.3 | 6.8 | 8.1 | 1.8 | 1.1 | × | 1.1 |
| | Precipitation Jan. 1958 (D 801) | | | | | | | | | | | | Air Jan 1958 (L 801) | | | | | | |
| Kn | 21 | 56 | 645 | 5 | 4 | 423 | 26 | 71 | 87 | 6.6 | 32 | 194 | 8.1 | 208.0 | 1.4 | 132.0 | 6.5 | 12.1 | 14. |
| Ri | 56 | 26 | 95 | 3 | 1 | 43 | 2 | 16 | 28 | 5.7 | 8 | 9 | 0.3 | 1.6 | 0.3 | 0.7 | 0.4 | 0.8 | 1.2 |
| Ki | 6 | 10 | 7 | 0 | 1 | 10 | 1 | 4 | 36 | 6.1 | — | 13 | × | × | × | × | × | × | × |
| Ar | 34 | 25 | 12 | 5 | 6 | 9 | 6 | 6 | 23 | 5.7 | 6 | 10 | 3.5 | 0.6 | 0.8 | 1.3 | 1.1 | 1.3 | 2.3 |
| Öj | 23 | 25 | 16 | 5 | 7 | 10 | 4 | 4 | 27 | 5.7 | 7 | 16 | × | × | × | × | × | × | × |
| Rö | 29 | 26 | 13 | 3 | 3 | 9 | 2 | 4 | 18 | 5.2 | 0 | 13 | 16. | 5.4 | 3.8 | 4.3 | 6.3 | 4.7 | 7.0 |
| Of | 23 | 31 | 30 | 5 | 5 | 17 | 6 | 7 | 16 | 5.2 | 0 | 19 | 4.0 | 0.9 | 1.7 | 2.1 | 2.1 | 1.5 | 4.1 |
| Br | 15 | 26 | 24 | 7 | 15 | 15 | 4 | 5 | 13 | 5.6 | 10 | 25 | 3.4 | 3.0 | 0.6 | 3.7 | 2.6 | 1.0 | 4.2 |
| ÅF | 20 | 18 | 49 | 1 | 3 | 29 | 3 | 6 | 12 | 5.8 | 4 | 17 | 11. | 12. | 3.2 | 6.3 | 3.1 | 2.5 | 15. |
| ÅH | — | — | — | — | — | — | — | — | — | — | — | — | — | — | — | — | — | — | — |
| Fö | 5 | 30 | 19 | 2 | 3 | 11 | 2 | 5 | 33 | 5.7 | 46 | 63 | — | — | — | — | — | — | — |
| Sv | 26 | 28 | 16 | 6 | 1 | 14 | 9 | 6 | 25 | 5.6 | 19 | 17 | — | — | — | — | — | — | — |
| Rä | 15 | 19 | 19 | 8 | 5 | 8 | 4 | 2 | 190 | 7.2 | 390 | 87 | 8.4 | 1.7 | 2.6 | 1.1 | 0.8 | 5.6 | 7.4 |
| Åm | 25 | 31 | 37 | 9 | 9 | 22 | 4 | 8 | 26 | 6.2 | 3 | 20 | 6.6 | 3.7 | 3.9 | 6.4 | 6.1 | 3.4 | 5.3 |
| Sa | 23 | 5 | 4 | 0 | 2 | 0 | 0 | 1 | 5 | 6.3 | 8 | 2 | 17 | 2.1 | 2.6 | 2.3 | 1.9 | 1.9 | 4.9 |
| Ul | 9 | 25 | 25 | 4 | 7 | 12 | 2 | 4 | 11 | 5.3 | 5 | 36 | 12 | 1.8 | 1.8 | 1.9 | 1.1 | 0.6 | 1.0 |
| Er | 17 | 24 | 26 | 8 | 6 | 16 | 3 | 6 | 17 | 5.3 | 1 | 21 | 8.0 | 1.2 | 1.9 | 2.0 | 1.6 | 1.5 | 1.8 |
| St | 6 | 20 | 36 | 5 | 7 | 20 | 11 | 5 | 32 | 6.1 | 53 | 67 | 9.0 | 1.1 | 2.2 | 1.2 | 0.5 | 0.8 | 2.3 |
| Fo | 11 | 18 | 18 | 4 | 2 | 11 | 3 | 5 | 21 | 5.6 | 10 | 24 | 6.6 | 2.3 | 2.0 | 2.5 | 2.0 | 0.9 | 2.3 |
| Kv 1 | 5 | 340 | 26 | 5 | 20 | 12 | 15 | 15 | 350 | 3.3 | 0 | 700 | 22 | 6.6 | 5.1 | 8.3 | 9.9 | 19. | 73 |
| Kv 7 | 6 | 23 | 29 | 5 | 8 | 17 | 3 | 18 | 21 | 4.7 | 0 | 72 | × | × | × | × | × | × | × |
| VK | 7 | 37 | 74 | 10 | 15 | 44 | 12 | 12 | 42 | 6.3 | 21 | 100 | 11 | 5.9 | 2.3 | 5.9 | 3.6 | 3.3 | 6.8 |
| La | 12 | 25 | 57 | 6 | 9 | 44 | 4 | 6 | 35 | 5.8 | 30 | 44 | 15 | 2.0 | 3.1 | 1.9 | 1.0 | 1.8 | 4.1 |
| Bo | 53 | 60 | 99 | 14 | 9 | 88 | 9 | 24 | 37 | 5.7 | 1 | 21 | 3.9 | 2.9 | 0.8 | 5.1 | 2.1 | 1.0 | 2.1 |
| Vi | 6 | 110 | 1550 | 19 | 8 | 990 | 25 | 150 | 69 | 4.3 | 0 | 1050 | 6.3 | 21 | 1.4 | 14 | 1.8 | 4.5 | 2.3 |
| Fa | 24 | 39 | 51 | 9 | 8 | 33 | 4 | 8 | 23 | 4.8 | 0 | 31 | 5.5 | 0.5 | 1.0 | 0.8 | 0.5 | 1.0 | 1.6 |
| Fl | 26 | 35 | 51 | 7 | 4 | 25 | 4 | 6 | 14 | 4.7 | 0 | 23 | 12 | 4.0 | 2.2 | 1.6 | 1.4 | 1.5 | 3.2 |
| Fi | 45 | 68 | 130 | 14 | 14 | 70 | 8 | 25 | 24 | 5.3 | 0 | 30 | — | — | — | — | — | — | — |
| Am | 49 | 48 | 54 | 15 | 7 | 40 | 7 | 13 | 22 | 4.8 | 0 | 22 | — | — | — | — | — | — | — |
| Si | — | — | — | — | — | — | — | — | — | — | — | — | — | — | — | — | — | — | — |
| Pl | 36 | 56 | 170 | 26 | 26 | 110 | 9 | 21 | 33 | 4.2 | 0 | 70 | 22 | 14 | 3.0 | 8.4 | 1.4 | 2.2 | 1.9 |
| Sö | 29 | 35 | 62 | 7 | 6 | 31 | 4 | 8 | 25 | 4.8 | 0 | 25 | — | — | — | — | — | — | — |
| Sm | 23 | 28 | 44 | 8 | 11 | 25 | 3 | 7 | 16 | 4.8 | 0 | 28 | 4.9 | 1.4 | 1.7 | 1.3 | 0.7 | 0.7 | 2.0 |
| Sy | 10 | 18 | 35 | 0 | 5 | 17 | 2 | 5 | 24 | 5.8 | 25 | 34 | 4.3 | 3.9 | 2.2 | 1.2 | 0.4 | 0.6 | 2.1 |
| BH | 57 | 53 | 99 | 18 | 22 | 58 | 7 | 14 | 21 | 4.6 | 0 | 27 | 1.3 | 1.3 | 0.2 | 0.1 | 0.9 | 0.9 | 1.0 |
| Sk | 31 | 66 | 140 | 18 | 33 | 88 | 6 | 16 | 23 | 4.4 | 0 | 52 | 17 | 23 | 3.0 | 13 | 2.0 | 2.4 | 5.6 |
| Al | 37 | 90 | 200 | 22 | 33 | 100 | 7 | 22 | 47 | 4.7 | 0 | 65 | 29 | 5.2 | 3.7 | 3.7 | 0.8 | 1.9 | 3.1 |
| Hi | 8 | 25 | 48 | 5 | 6 | 26 | 4 | 5 | 23 | 6.1 | 50 | 54 | — | — | — | — | — | — | — |
| Ta | 9 | 18 | 92 | 2 | 6 | 30 | 4 | 7 | 4 | — | — | 41 | — | — | — | — | — | — | — |
| An | — | — | — | — | — | — | — | — | — | — | — | — | — | — | — | — | — | — | — |
| Yt | 63 | 42 | 600 | 4 | 10 | 350 | 29 | 44 | 50 | 5.7 | 29 | 48 | — | — | — | — | — | — | — |
| Gj | 66 | 130 | 1 330 | 1 | 6 | 620 | 25 | 81 | 38 | 5.8 | 9 | 67 | — | — | — | — | — | — | — |
| Fn | 31 | 32 | 98 | 4 | 9 | 61 | 5 | 10 | 48 | 6.0 | 40 | 29 | — | — | — | — | — | — | — |
| Få | 43 | 21 | 34 | 3 | 4 | 22 | 5 | 6 | 21 | 5.6 | 8 | 10 | — | — | — | — | — | — | — |
| Vå | 11 | 9 | 8 | 2 | 4 | 6 | 1 | 4 | 20 | 6.5 | 83 | 22 | 6.8 | 6.1 | 4.8 | 1.3 | 0.6 | 1.0 | 4.2 |
| Tr | 13 | 10 | 23 | 5 | 4 | 7 | 4 | 2 | 7 | 5.5 | 0 | 15 | — | — | — | — | — | — | — |
| Ke | 7 | 16 | 9 | 5 | 5 | 6 | 0 | 1 | 19 | 5.8 | 38 | 29 | — | — | — | — | — | — | — |
| Sd | 10 | 140 | 960 | 8 | 16 | 510 | 23 | 71 | 52 | 5.6 | 0 | 44 | — | — | - | — | — | — | — |
| Da | 60 | 41 | 70 | 13 | 7 | 20 | 6 | 9 | 17 | 4.8 | 0 | 18 | — | — | — | — | — | — | — |
| Ås | 48 | 46 | 70 | 15 | 10 | 56 | 13 | 14 | 43 | 5.7 | 12 | 18 | 7.3 | 4.9 | 2.8 | 2.9 | 1.3 | 2.2 | 16 |

| Code | mm | mg/m² | | | | | | | | pH | $-\frac{\mu val}{l}$ $HCO_3$ | $\frac{\varkappa \cdot 10^6}{\Omega \cdot cm}$ | $\mu g/m^3 (= kg/km^3)$ | | | | | | |
|---|---|---|---|---|---|---|---|---|---|---|---|---|---|---|---|---|---|---|---|
| | | S | Cl | $NO_3$–N | $NH_3$–N | Na | K | Mg | Ca | | | | S | Cl | $NH_3$–N | Na | K | Mg | Ca |
| | | Precipitation Jan. 1958 (D 801) | | | | | | | | | | | Air Jan. 1958 (L 801) | | | | | | |
| Li | 70 | 140 | 1 670 | 35 | 31 | 1 530 | 65 | 210 | 110 | 4.4 | 0 | 16 | 3.5 | 14 | 2.1 | 9.6 | 1.0 | 2.5 | 1.9 |
| So | 2 | — | 6 | — | — | 2 | 1 | — | 4 | 5.7 | 0 | 35 | 0 | 13.4 | 13.1 | 2.7 | 2.7 | 3.5 | 10.7 |
| Ka | 12 | 6 | 15 | 2 | 2 | 3 | 4 | 3 | 29 | 6.6 | 10 | 22 | 10.0 | × | 6.4 | 1.3 | 2.1 | × | 17.4 |
| Ku | 30 | 19 | 17 | 5 | 12 | 6 | 9 | 1 | 15 | 4.8 | 0 | 13 | 7.0 | 38.0 | 8.1 | 0 | 3.8 | 5.5 | 3.8 |
| Jy | 36 | 36 | 74 | 6 | 4 | 48 | 4 | 5 | 29 | 6.7 | 89 | 21 | × | × | 9.6 | × | × | × | × |
| Pu | 12 | 12 | 8 | 3 | 2 | 2 | 2 | 0 | 11 | 4.9 | 0 | 16 | 3.6 | 5.4 | 10.3 | 1.2 | 1.2 | 2.0 | 1.2 |
| Tv | 11 | 27 | 74 | 6 | 4 | 41 | 5 | 6 | 13 | 4.4 | 0 | 49 | 0 | 6.6 | 0.5 | 0.8 | 0.8 | 1.1 | 1.5 |
| Rj | 75 | 12 | 2 700 | 1 | 1 | 1 587 | 31 | 220 | 82 | 5.4 | 7 | 15 | × | × | × | × | × | × | × |
| Vn | 14 | 83 | 262 | 6 | 12 | 149 | 28 | 24 | 87 | 5.9 | 0 | 121 | — | — | — | — | — | — | — |
| Gr | 51 | 122 | 364 | 15 | 30 | 203 | 29 | 30 | 74 | 4.4 | 0 | 63 | — | — | — | — | — | — | — |
| Öd | 46 | 58 | 330 | 20 | 48 | 180 | 14 | 25 | 40 | 5.1 | 0 | 50 | 17 | 2.2 | 3.1 | 2.0 | 1.0 | 1.5 | 5.0 |
| Bs | 54 | 88 | 579 | 11 | 21 | 337 | 24 | 43 | 35 | 4.8 | 0 | 57 | — | — | — | — | — | — | — |
| Ly | 45 | 138 | 198 | 20 | 28 | 104 | 15 | 21 | 89 | 4.2 | 0 | 67 | — | — | — | — | — | — | — |
| As | 49 | 84 | 500 | 18 | 38 | 260 | 12 | 35 | 39 | 4.5 | 0 | 65 | 2.1 | 4.8 | 5.4 | 3.9 | 1.5 | 2.9 | 24. |
| Vd | 58 | 144 | 380 | 22 | 90 | 217 | 27 | 29 | 59 | 4.9 | 0 | 52 | — | — | — | — | — | — | — |
| Bl | 30 | 70 | 250 | 12 | 22 | 135 | 12 | 24 | 36 | 4.6 | 0 | 61 | — | — | — | — | — | — | — |
| Ty | 37 | 110 | 240 | 20 | 52 | 150 | 9 | 25 | 48 | 6.1 | 23 | 52 | 19. | 11. | 5.2 | 6.3 | 1.2 | 1.4 | 8.6 |
| Hö | 48 | 110 | 902 | 12 | 22 | 502 | 29 | 53 | 81 | 4.6 | 0 | 91 | — | — | — | — | — | — | — |
| Ad | 49 | 98 | 245 | 19 | 39 | 137 | 15 | 23 | 56 | 4.8 | 0 | 49 | — | — | — | — | — | — | — |
| Lw | 181 | 720 | 9 580 | 36 | 33 | 6 273 | 235 | 776 | 192 | 7.0 | 250 | 220 | × | × | × | × | × | × | × |
| Ab | 78 | 89 | 620 | 13 | 15 | 400 | 25 | 73 | 150 | 6.1 | 120 | 60 | 7.5 | 5.7 | 3.9 | 3.4 | 2.9 | 4.7 | 10. |
| Ed | 51 | 64 | 280 | 6 | 14 | 170 | 10 | 28 | 59 | 6.4 | 28 | 34 | 11. | 9.7 | 1.9 | 6.0 | 0.7 | 1.8 | 3.3 |
| Es | 164 | 157 | 890 | 10 | 18 | 557 | 31 | 67 | 33 | 5.0 | 0 | 29 | 4.7 | 3.4 | 0.6 | 1.5 | 1.0 | 0.3 | 0.5 |
| Le | 72 | 100 | 440 | 17 | 78 | 170 | 23 | 36 | 53 | 4.4 | 0 | 61 | 48. | 6.7 | 5.6 | 3.5 | 4.0 | 6.1 | 30. |
| Ro | 60 | 41 | 160 | 11 | 13 | 71 | 10 | 18 | 51 | 4.5 | 0 | 33 | 24 | 11. | 3.5 | 4.2 | 1.0 | 1.9 | 5.3 |
| NA | 109 | 100 | 750 | 11 | 40 | 420 | 16 | 58 | 94 | 5.6 | 15 | 39 | 10 | 7.9 | 4.3 | 4.8 | 1.2 | 1.6 | 3.4 |
| Ca | 92 | 150 | 2 090 | 6 | 63 | 1 080 | 59 | 142 | 61 | 6.2 | 94 | 88 | 0.9 | 4.0 | 1.0 | 1.8 | 0.0 | 0.5 | 0.0 |
| Va | 212 | 297 | 5 088 | 28 | 106 | — | — | — | — | 6.0 | 2 | 89 | — | — | — | — | — | — | — |
| Sc | 54 | 200 | 650 | 12 | 39 | 329 | 25 | 46 | 68 | 4.4 | 0 | 70 | 44.5 | 40.7 | 7.8 | 26.8 | 4.1 | 4.8 | 6.0 |
| BV | 25 | 51 | 77 | 5 | 9 | 25 | 6 | 15 | 56 | 4.8 | 0 | 40 | 63.8 | 7.7 | 8.6 | 2.3 | 6.3 | 1.6 | 3.1 |
| Bn | 49 | 144 | 214 | 8 | 27 | 75 | 13 | 31 | 404 | 6.2 | 79 | 82 | 40.3 | 10.3 | 6.4 | 3.2 | 10.6 | 1.9 | 2.0 |
| Au | 70 | 145 | 100 | 31 | 41 | 41 | 14 | 19 | 68 | 4.6 | 0 | 29 | 42.9 | 9.7 | 8.2 | 1.2 | 1.6 | 2.7 | 1.0 |
| Fe | 75 | 133 | 160 | 20 | 28 | 100 | 17 | 19 | 30 | 4.5 | 0 | 28 | 2.7 | 2.7 | 1.2 | 0.3 | 0.7 | 1.7 | 2.7 |
| Ba | 87 | 89 | 45 | 3 | 6 | 20 | 12 | 7 | 24 | 4.8 | 0 | 14 | 34.8 | 29.7 | 13.5 | 4.4 | 13.5 | 4.4 | 12.8 |
| Ho | 55 | 94 | 34 | 12 | 17 | 12 | 42 | 14 | 84 | 5.3 | 0 | 23 | 32.7 | 10.0 | 4.0 | 1.8 | 6.7 | 1.5 | 2.2 |
| Rm | 27 | 37 | 71 | 9 | 2 | 27 | 6 | 8 | 296 | 6.7 | 320 | 90 | 11.9 | 8.5 | 5.8 | 4.3 | 0.8 | 0.8 | 4.5 |
| Et | 30 | 91 | 948 | 8 | 22 | 42 | 13 | 6 | 577 | 4.9 | 0 | 130 | 15.9 | 4.1 | 3.6 | 1.0 | 0.5 | 0.6 | 0.6 |
| He | — | — | — | — | — | — | — | — | — | — | — | — | — | — | — | — | — | — | — |
| Rz | 23 | 40 | 0 | 7 | 16 | 3 | 5 | 8 | 42 | 5.3 | 0 | 28 | 12.6 | 3.2 | 7.0 | 2.1 | 2.4 | 0.7 | 0.9 |
| Wi | 28 | 76 | 17 | 8 | 6 | 4 | 6 | 15 | 113 | 5.8 | 5 | 38 | 62.5 | 5.6 | 8.6 | 2.6 | 0.7 | 0.5 | 2.2 |
| Lz | 56 | 94 | 34 | 4 | 0 | 6 | 6 | 9 | 69 | 5.5 | 0 | 17 | 14.1 | 6.9 | 4.6 | 1.1 | 2.4 | 0.9 | 2.3 |
| Kl | 59 | 105 | 0 | 0 | 10 | 4 | 9 | 16 | 58 | 5.6 | 0 | 15 | 45.9 | 7.0 | 7.1 | 2.1 | 3.6 | 1.6 | 4.0 |
| BL | | | | | | | | | | | | | | | | | | | |
| DH | 86 | 320 | 9 116 | 38 | 17 | 5 435 | 180 | 671 | 211 | 4.0 | 0 | 336 | 2.3 | 6.1 | 1.8 | 3.2 | 0.4 | 1.6 | 0.3 |
| DB | 80 | 153 | 416 | 27 | 30 | 300 | 17 | 32 | 48 | 4.4 | 0 | 41 | 30.5 | 1.6 | 4.5 | 2.1 | 0.7 | 0.4 | 1.1 |
| W | 86 | 146 | 422 | 32 | 30 | 288 | 20 | 33 | 25 | 4.1 | 0 | 48 | 25.5 | 7.4 | 3.8 | 3.6 | 1.2 | 3.2 | 0.9 |
| SA | 63 | 164 | 242 | 24 | 36 | 158 | 15 | 19 | 35 | 4.2 | 0 | 51 | 29.0 | 6.3 | 6.6 | 1.9 | 1.6 | 0.3 | 1.2 |
| U | 61 | 133 | 141 | 25 | 24 | 89 | 12 | 14 | 39 | 4.1 | 0 | 42 | 58.5 | 4.7 | 5.0 | 2.0 | 1.8 | 0.7 | 1.8 |
| B | 154 | 175 | 292 | 61 | 59 | 255 | 38 | 25 | 69 | 4.6 | 0 | 25 | 17.5 | 2.7 | 1.6 | 2.4 | 0.8 | 0.0 | 0.7 |
| D | 48 | 59 | 137 | 17 | 7 | 108 | 8 | 13 | 29 | 4.6 | 0 | 29 | 26.6 | 10.3 | 4.4 | 4.0 | 0.8 | 0.6 | 0.9 |
| MH | 74 | 31 | 184 | 18 | 13 | 110 | 7 | 1 | 44 | 5.1 | 0 | 18 | 19.0 | 12.7 | 3.0 | 3.1 | 1.5 | 0.4 | 1.0 |
| Rs | 105 | 22 | 737 | 18 | 7 | 383 | 15 | 45 | 54 | 5.2 | 0 | 28 | 0.9 | 2.9 | 2.4 | 2.0 | 1.1 | 0.0 | 0.7 |
| LM | 88 | 18 | 150 | 19 | 12 | 110 | 6 | 15 | 46 | 5.4 | 0 | 10 | 12.4 | 11.9 | 11.3 | 3.3 | 1.4 | 0.7 | 0.8 |
| Lx | 106 | 67 | 53 | 29 | 13 | 53 | 5 | 8 | 39 | 5.3 | 0 | 9 | 15.6 | 80.7 | 72.4 | 59.5 | 20.3 | 1.2 | 2.9 |
| Bg | 51 | 6 | 125 | 20 | 18 | 60 | 7 | 9 | 49 | 5.6 | 4 | 19 | 7.8 | 26.1 | 13.0 | 24.7 | 4.3 | 3.7 | 3.9 |
| Ae | 71 | 8 | 85 | 41 | 12 | 43 | 5 | 8 | 94 | 6.2 | 21 | 20 | 23.2 | 4.5 | 11.3 | 2.7 | 2.1 | 0.0 | 2.5 |
| Za | — | — | — | — | — | — | — | — | — | — | — | — | × | × | × | × | × | × | × |

| Code | mm | mg/m² | | | | | | | | pH | $-\frac{\mu val}{l}$ | $\frac{\varkappa \cdot 10^6}{\Omega \cdot cm}$ | μg/m³(=kg/km³) | | | | | | |
|---|---|---|---|---|---|---|---|---|---|---|---|---|---|---|---|---|---|---|---|
| | | S | Cl | $NO_3$-N | $NH_3$-N | Na | K | Mg | Ca | | $HCO_3$ | | S | Cl | $NH_3$-N | Na | K | Mg | Ca |
| | Precipitation Febr. 1958 (D 802) | | | | | | | | | | | | Air Febr. 1958 (L 802) | | | | | | |
| Kn | 5 | 10 | 230 | 2 | 3 | 112 | 7 | 28 | 30 | 5.8 | 21 | 349 | 7.0 | 135 | 1.6 | 158 | 7.6 | 16.2 | 13. |
| Ri | 13 | 15 | 14 | 2 | 1 | 10 | 1 | 2 | 8 | 7.1 | 12 | 11 | × | × | × | × | × | × | × |
| Ki | 33 | 22 | 13 | 2 | 0 | 6 | 1 | 2 | 15 | 6.5 | 5 | 5 | × | × | × | × | × | × | × |
| Ar | 1 | 3 | 13 | — | — | 4 | 1 | 1 | 9 | — | — | — | 2.6 | 2.1 | 2.0 | 1.7 | 3.9 | 1.4 | 4.1 |
| Öj | 19 | 17 | 38 | 4 | 4 | 12 | 5 | 2 | 31 | 6.2 | 10 | 20 | 3.7 | 2.1 | 0.9 | 1.2 | 0.9 | 1.1 | 4.1 |
| Rö | 9 | 9 | 12 | 2 | 2 | 9 | 2 | 2 | 14 | 5.7 | 20 | 20 | 9.4 | 7.2 | 2.9 | 5.8 | 4.8 | 1.8 | 8.9 |
| Of | 21 | 8 | 8 | 4 | 0 | 10 | 3 | 3 | 11 | 5.4 | 26 | 16 | 3.9 | 1.8 | 1.0 | 1.0 | 0.5 | 0.8 | 0.8 |
| Br | 1 | — | 2 | — | — | 2 | — | — | — | — | — | — | 3.4 | 3.4 | 1.8 | 2.6 | 5.3 | 1.7 | 4.7 |
| ÅF | 31 | 23 | 20 | 2 | 1 | 16 | 3 | 4 | 14 | 6.2 | 14 | 10 | 12. | 3.1 | 2.5 | 1.8 | 2.2 | 1.5 | 9.9 |
| ÅH | 8 | 2 | 23 | 1 | 1 | 10 | 2 | 2 | 26 | 6.0 | 10 | 20 | — | — | — | — | — | — | — |
| Fö | 4 | 21 | 11 | 2 | 2 | 6 | 3 | 1 | 37 | 5.7 | — | 65 | — | — | — | — | — | — | — |
| Sv | 12 | 7 | 8 | 1 | 1 | 7 | 3 | 2 | 17 | 6.3 | 32 | 12 | — | — | — | — | — | — | — |
| Rä | 13 | 9 | 16 | 3 | 2 | 5 | 2 | 2 | 80 | 7.2 | 270 | 48 | 8.4 | 5.4 | 3.3 | 1.8 | 1.7 | 2.8 | 6.9 |
| Åm | 21 | 10 | 16 | 4 | 3 | 11 | 5 | 2 | 16 | 6.2 | 7 | 10 | 6.2 | 5.0 | 1.9 | 4.1 | 2.2 | 2.2 | 3.3 |
| Sa | 13 | 16 | 12 | 4 | 1 | 7 | 2 | 7 | 20 | 5.8 | 0 | 18 | 19. | 5.5 | 2.7 | 4.4 | 2.4 | 3.6 | 7.4 |
| Ul | 9 | 11 | 13 | 4 | 6 | 7 | 2 | 4 | 9 | 5.1 | 0 | 26 | 13. | 1.5 | 1.9 | 1.5 | 1.1 | 0.5 | 1.5 |
| Er | 6 | 9 | 8 | 2 | 1 | 6 | 2 | 3 | 10 | 5.2 | 0 | 27 | × | × | × | × | × | × | × |
| St | 17 | 22 | 24 | 6 | 6 | 16 | 5 | 4 | 32 | 6.4 | 31 | 24 | 9.6 | 1.3 | 2.6 | 0.7 | 0.3 | 0.3 | 2.3 |
| Fo | 37 | 18 | 18 | 4 | 2 | 10 | 3 | 4 | 22 | 5.9 | 6 | 8 | × | × | × | × | × | × | × |
| Kv 1 | 24 | 660 | 35 | 9 | 26 | 19 | 22 | 20 | 610 | 4.3 | 0 | 360 | 92. | 2.8 | 14. | 0.8 | 4.5 | 6.2 | 36. |
| Kv 7 | 51 | 46 | 27 | 11 | 14 | 14 | 4 | 6 | 34 | 5.5 | 0 | 18 | × | × | × | × | × | × | × |
| VK | 24 | 29 | 28 | 5 | 6 | 13 | 5 | 4 | 21 | 5.0 | 0 | 20 | 12. | 4.9 | 0.9 | 1.1 | 1.7 | 1.0 | 5.4 |
| La | 26 | 31 | 49 | 8 | 18 | 27 | 4 | 6 | 17 | 5.3 | 0 | 23 | 11. | 6.1 | 2.7 | 1.0 | 1.2 | 0.6 | 7.6 |
| Bo | 51 | 41 | 79 | 12 | 7 | 51 | 5 | 16 | 23 | 5.0 | 0 | 20 | 3.5 | 0.9 | 0.8 | 1.4 | 0.5 | 0.6 | 3.1 |
| Vi | 29 | 40 | 650 | 11 | 5 | 250 | 15 | 55 | 23 | 4.3 | 0 | 130 | 9.2 | 16. | 0.9 | 4.7 | 0.4 | 1.6 | 4.5 |
| Fa | 54 | 26 | 31 | 7 | 4 | 18 | 3 | 6 | 24 | 5.5 | 0 | 10 | 3.2 | 9.5 | 0.9 | 0.4 | 0.1 | 0.2 | 3.3 |
| Fl | 61 | 28 | 26 | 10 | 1 | 16 | 3 | 5 | 15 | 4.8 | 0 | 14 | 11. | 7.0 | 1.6 | 0.9 | 0.7 | 0.5 | 4.3 |
| Fi | 81 | 60 | 100 | 18 | 14 | 57 | 6 | 31 | 15 | 4.6 | 0 | 22 | — | — | — | — | — | — | — |
| Åm | 67 | 51 | 72 | 15 | 7 | 54 | 6 | 10 | 23 | 4.7 | 0 | 18 | — | — | — | — | — | — | — |
| Si | — | — | — | — | — | — | — | — | — | — | — | — | — | — | — | — | — | — | — |
| Pl | 65 | 80 | 200 | 26 | 28 | 115 | 10 | 19 | 18 | 4.3 | 0 | 43 | 8.0 | 2.5 | 2.5 | 1.0 | 0.0 | 2.6 | 1.4 |
| Sö | 53 | 41 | 26 | 15 | 7 | 22 | 5 | 9 | 46 | 4.6 | 0 | 22 | — | — | — | — | — | — | — |
| Sm | 38 | 31 | 47 | 12 | 9 | 13 | 3 | 6 | 9 | 4.7 | 0 | 24 | 5.8 | 2.4 | 1.6 | 0.4 | 0.2 | 0.9 | 1.2 |
| Sy | 32 | 25 | 35 | 12 | 13 | 19 | 5 | 6 | 20 | 4.8 | 0 | 22 | 5.6 | 7.9 | 2.3 | 0.9 | 2.0 | 1.3 | 5.4 |
| BH | 73 | 55 | 89 | 24 | 16 | 51 | 5 | 12 | 20 | 4.6 | 0 | 22 | 4.8 | 1.1 | 0.8 | 0.9 | 0.2 | 0.7 | 1.1 |
| Sk | 55 | 91 | 230 | 26 | 41 | 130 | 13 | 20 | 32 | 4.4 | 0 | 48 | 10. | 4.7 | 2.4 | 1.6 | 0.5 | 0.9 | 1.7 |
| Al | 70 | 83 | 160 | 19 | 18 | 86 | 8 | 20 | 36 | 4.4 | 0 | 36 | 20. | 5.4 | 3.2 | 1.4 | 0.5 | 1.2 | 3.0 |
| Hi | 31 | 46 | 66 | 12 | 9 | 22 | 4 | 7 | 26 | 4.7 | 0 | 30 | — | — | — | — | — | — | — |
| Ta | 24 | 25 | 110 | 3 | 12 | 52 | 5 | 10 | 13 | 5.7 | 0 | 36 | 4.9 | 2.8 | 2.6 | 1.5 | 1.1 | 1.0 | 2.1 |
| An | — | — | — | — | — | — | — | — | — | — | — | — | — | — | — | — | — | — | — |
| Yt | 28 | 22 | 290 | 3 | 11 | 160 | 22 | 21 | 20 | 5.9 | 40 | 53 | — | — | — | — | — | — | — |
| Gj | 103 | 77 | 1 310 | 3 | 8 | 540 | 35 | 96 | 53 | 5.7 | 7 | 58 | — | — | — | — | — | — | — |
| Fn | 18 | 14 | 22 | 3 | 4 | 24 | 3 | 5 | 38 | 6.7 | 110 | 27 | — | — | — | — | — | — | — |
| Få | 44 | 15 | 19 | 3 | 3 | 12 | 4 | 2 | 24 | 5.8 | 24 | 10 | — | — | — | — | — | — | — |
| Vå | 8 | 14 | 6 | 2 | 1 | 6 | 2 | 4 | 15 | 6.5 | 93 | 23 | 4.3 | 4.8 | 9.3 | 2.4 | 1.9 | 0.8 | 5.4 |
| Tr | 20 | 3 | 8 | 3 | 3 | 5 | 1 | 5 | 9 | 5.7 | 0 | 8 | — | — | — | — | — | — | — |
| Ke | 17 | 11 | 8 | 4 | 5 | 5 | 1 | 5 | 14 | 6.3 | 10 | 14 | — | — | — | — | — | — | — |
| Sd | 92 | 110 | 520 | 12 | 26 | 200 | 17 | 44 | 30 | 5.9 | 0 | 38 | — | — | — | — | — | — | — |
| Da | 41 | 21 | 14 | 3 | 1 | 9 | 4 | 4 | 12 | 5.6 | 0 | 6 | — | — | — | — | — | — | — |
| Ås | 44 | 30 | 31 | 9 | 6 | 27 | 7 | 6 | 20 | 5.3 | 0 | 14 | 7.0 | 3.9 | 1.8 | 0.9 | 0.7 | 1.6 | 4.0 |
| Li | 54 | 180 | 850 | 13 | 5 | 310 | 25 | 68 | 36 | 4.7 | 0 | 82 | 5.9 | 15. | 1.6 | 9.6 | 1.2 | 2.4 | 3.8 |
| So | 6 | 0 | 3 | 1 | 1 | 1 | 1 | 1 | 4 | 5.2 | 0 | 14 | 0 | 1.0 | 8.2 | 2.0 | 2.4 | 1.0 | 4.0 |
| Ka | 7 | 10 | 9 | 2 | 1 | 3 | 6 | 1 | 15 | 6.3 | 0 | 29 | × | × | × | × | × | × | × |
| Ku | 5 | 7 | 4 | 3 | 2 | 1 | 2 | 1 | 6 | 4.6 | 0 | 39 | 6.1 | 46.0 | 15.2 | 4.0 | 4.7 | 2.3 | 4.7 |
| Jy | 9 | 6 | 15 | 2 | 3 | 7 | 10 | 4 | 24 | 6.3 | 0 | 32 | × | × | × | × | × | × | × |
| Pu | 12 | 0 | 7 | 3 | 2 | 2 | 2 | 1 | 13 | 4.9 | 0 | 21 | 0 | 1.3 | 4.7 | 1.1 | 1.6 | 0.5 | 1.9 |
| Tv | 6 | 0 | 30 | 3 | 2 | 10 | 2 | 2 | 13 | 4.4 | 0 | 60 | 0 | 1.4 | 2.7 | 1.5 | 2.4 | 0.4 | 11.1 |

| Code | mm | mg/m² S | Cl | $NO_3$–N | $NH_3$–N | Na | K | Mg | Ca | pH | $-\frac{\mu val}{l}$ $HCO_3$ | $\frac{\varkappa \cdot 10^6}{\Omega \cdot cm}$ | µg/m³ (=kg/km³) S | Cl | $NH_3$–N | Na | K | Mg | Ca |
|---|---|---|---|---|---|---|---|---|---|---|---|---|---|---|---|---|---|---|---|
| | Precipitation Febr. 1958 (D 802) | | | | | | | | | | | | Air Febr. 1958 (L 802) | | | | | | |
| Rj | 23 | 16 | 200 | 2 | 2 | 100 | 5 | 23 | 8 | 5.3 | 0 | 37 | 9.2 | 9.5 | 1.4 | 7.3 | 0.7 | 1.8 | 3.7 |
| Vn | 42 | 63 | 163 | 11 | 19 | 111 | 16 | 16 | 41 | 4.9 | 0 | 35 | — | — | — | — | — | — | — |
| Gr | 49 | 84 | 208 | 15 | 33 | 110 | 26 | 16 | 57 | 4.5 | 0 | 46 | — | — | — | — | — | — | — |
| Öd | 54 | 70 | 180 | 16 | 29 | 100 | 10 | 16 | 32 | 4.9 | 0 | 31 | 17. | 12. | 5.8 | 5.2 | 2.5 | 2.2 | 8.5 |
| Bs | 72 | 106 | 564 | 20 | 27 | 327 | 33 | 43 | 39 | 4.6 | 0 | 48 | — | — | — | — | — | — | — |
| Ly | 64 | 134 | 118 | 25 | 29 | 79 | 18 | 26 | 35 | 4.2 | 0 | 51 | — | — | — | — | — | — | — |
| As | 103 | 31 | 460 | 28 | 56 | 170 | 17 | 34 | 35 | 4.4 | 0 | 42 | 18. | 4.3 | 3.6 | 1.1 | 0.4 | 1.1 | 5.8 |
| Vd | 93 | 137 | 113 | 17 | 72 | 102 | 24 | 21 | 26 | 4.8 | 0 | 26 | — | — | — | — | — | — | — |
| Bl | 70 | 109 | 124 | 18 | 27 | 93 | 18 | 22 | 51 | 4.5 | 0 | 34 | — | — | — | — | — | — | — |
| Ty | 58 | 110 | 200 | 26 | 59 | 78 | 12 | 23 | 58 | 5.2 | 0 | 38 | 6.3 | 10. | 4.3 | 5.4 | 2.0 | 2.8 | 7.0 |
| Hö | 70 | 97 | 503 | 25 | 28 | 282 | 31 | 40 | 49 | 4.8 | 0 | 51 | — | — | — | — | — | — | — |
| Ad | 59 | 87 | 99 | 18 | 27 | 78 | 17 | 24 | 20 | 4.7 | 0 | 34 | — | — | — | — | — | — | — |
| Lw | 55 | 366 | 6 317 | 11 | 26 | 3 767 | 154 | 451 | 169 | 6.7 | 115 | 432 | × | × | × | × | × | × | × |
| Ab | 78 | 100 | 580 | 10 | 3 | 310 | 26 | 45 | 110 | 6.5 | 66 | 47 | 13. | 2.9 | 2.6 | 1.8 | 1.1 | 4.1 | 6.8 |
| Ed | 51 | 34 | 72 | 9 | 15 | 65 | 21 | 5 | 37 | 5.3 | 0 | 23 | 13. | 4.6 | 1.4 | 3.1 | 0.2 | 1.2 | 2.0 |
| Es | 128 | 126 | 361 | 13 | 26 | 272 | 23 | 27 | 31 | 5.1 | 0 | 22 | 4.3 | 4.9 | 0.2 | 1.4 | 0.9 | 0.5 | 8.1 |
| Le | 72 | 120 | 230 | 20 | 30 | 86 | 12 | 26 | 53 | 4.2 | 0 | 48 | 31. | 8.7 | 3.9 | 1.4 | 0.6 | 5.5 | 24. |
| Ro | 59 | 4 | 260 | 15 | 12 | 130 | 16 | 22 | 43 | 4.4 | 0 | 51 | 32. | 22. | 2.9 | 11. | 1.9 | 2.9 | 17. |
| NA | 109 | 100 | 1 000 | 14 | 41 | 610 | 37 | 76 | 220 | 6.2 | 60 | 56 | 3.4 | 8.3 | 3.9 | 3.7 | 0.3 | 1.6 | 3.6 |
| Ca | 89 | 138 | 1 406 | 5 | 46 | 761 | 38 | 107 | 53 | 5.8 | 4 | 65 | 1.2 | 3.0 | 1.1 | 3.6 | 0.3 | 0.5 | 0.0 |
| DA | 102 | 173 | 408 | 9 | 23 | — | — | — | — | 5.2 | 0 | 30 | — | — | — | — | — | — | — |
| Va | 131 | 183 | 2 620 | 37 | 17 | — | — | — | — | 5.9 | 6 | 74 | — | — | — | — | — | — | — |
| Sc | 80 | 189 | 532 | 33 | 33 | 258 | 23 | 39 | 88 | 4.1 | 0 | 51 | 30.0 | 23.9 | 7.9 | 10.5 | 3.5 | 1.6 | 5.3 |
| BV | 53 | 206 | 226 | 18 | 19 | 98 | 25 | 33 | 168 | 4.4 | 0 | 52 | 39.6 | 10.0 | — | 1.4 | 1.0 | 1.5 | 4.9 |
| Bn | 73 | 246 | 117 | 23 | 35 | 43 | 16 | 37 | 580 | 5.9 | 0 | 53 | 114.0 | 31.4 | 5.2 | 2.4 | 2.0 | 1.3 | 7.7 |
| Au | 124 | 168 | 24 | 27 | 14 | 35 | 22 | 21 | 142 | 4.4 | 0 | 19 | 20.5 | 12.8 | 3.1 | 1.6 | 1.1 | 2.0 | 2.2 |
| Fe | 193 | 0 | 0 | 14 | 0 | 31 | 14 | 15 | 91 | 4.8 | 0 | 9 | 9.9 | 4.0 | 0.5 | 0.2 | 0.6 | 1.4 | 5.7 |
| Ba | 110 | 132 | 31 | 12 | 3 | 147 | 12 | 6 | 118 | 5.2 | 0 | 9 | 9.4 | 7.2 | 3.1 | 1.2 | 0.7 | 0.8 | 6.2 |
| Ho | 106 | 211 | 118 | 0 | 0 | 40 | 242 | 18 | 158 | 5.5 | 0 | 18 | 55.3 | 35.7 | 7.3 | 1.3 | 1.5 | 0.8 | 7.7 |
| Rm | 83 | 162 | 16 | 18 | 0 | 23 | 15 | 12 | 597 | 6.1 | 240 | 35 | 21.7 | 5.1 | 10.5 | 4.4 | 1.1 | 0.2 | 5.6 |
| Et | 81 | 122 | 7 | 11 | 0 | 15 | 20 | 15 | 72 | 4.7 | 0 | 17 | 15.3 | 5.5 | 7.0 | 10.0 | 0.6 | 0.4 | 2.0 |
| He | — | — | — | — | — | — | — | — | — | — | — | — | — | — | — | — | — | — | — |
| Rz | 20 | 59 | 6 | 13 | 12 | 10 | 4 | 7 | 64 | 5.6 | 0 | 29 | 13.9 | 4.2 | 4.2 | 2.5 | 1.0 | 0.4 | 3.2 |
| Wi | 51 | 105 | 0 | 23 | 46 | 18 | 8 | 17 | 188 | 5.0 | 0 | 25 | 35.5 | 7.1 | 8.1 | 2.2 | 1.2 | 0.4 | 4.3 |
| Lz | 130 | 136 | 61 | 25 | 7 | 32 | 22 | 26 | 235 | 5.7 | 28 | 16 | 11.7 | 3.6 | 6.5 | 2.0 | 3.9 | 0.7 | 5.5 |
| Kl | 57 | 86 | 0 | 6 | 17 | 6 | 7 | 16 | 65 | 4.9 | 0 | 15 | 51.5 | 8.5 | 9.1 | 7.3 | 3.1 | 0.8 | 5.7 |
| BL | | | | | | | | | | | | | | | | | | | |
| DH | 41 | 241 | 3 914 | 32 | 15 | 2 378 | 80 | 246 | 201 | 4.4 | 0 | 340 | 15.1 | 6.6 | 5.2 | 3.1 | 1.3 | 4.5 | 0.9 |
| DB | 52 | 120 | 271 | 40 | 44 | 151 | 12 | 24 | 47 | 4.3 | 0 | 56 | 15.9 | 13.2 | 5.6 | 12.6 | 2.2 | 2.8 | 2.7 |
| W | 69 | 44 | 303 | 36 | 44 | 183 | 12 | 28 | 35 | 4.3 | 0 | 49 | 34.3 | 72.9 | 5.2 | 37.9 | 2.6 | 6.2 | 3.1 |
| SA | 94 | 118 | 627 | 53 | 52 | 282 | 19 | 37 | 53 | 4.4 | 0 | 48 | 18.2 | 19.0 | 4.4 | 2.7 | 1.6 | 1.6 | 3.0 |
| U | 87 | 128 | 139 | 37 | 37 | 66 | 13 | 14 | 62 | 4.3 | 0 | 40 | 49.4 | 48.5 | 4.4 | 2.3 | 1.5 | 3.3 | 0.8 |
| B | 297 | 95 | 255 | 86 | 50 | 140 | 21 | 24 | 98 | 4.6 | 0 | 20 | 16. | 13.4 | 1.2 | 1.2 | 0.7 | 0.7 | 0.8 |
| D | 101 | 21 | 105 | 43 | 32 | 56 | 7 | 3 | 47 | 4.8 | 0 | 17 | 6.2 | 4.8 | 4.1 | 2.3 | 0.9 | 0.7 | 0.9 |
| MH | 83 | 76 | 87 | 25 | 7 | 6 | 5 | 12 | 51 | 4.8 | 0 | 19 | 20.6 | 12.4 | 2.8 | 6.6 | 0.6 | 0.7 | 1.0 |
| Rs | 107 | 61 | 684 | 12 | 1 | 353 | 15 | 45 | 31 | 5.0 | 0 | 29 | 5.1 | 4.2 | 2.6 | 1.8 | 0.2 | 0 | 1.0 |
| LM | 102 | 82 | 217 | 16 | 14 | 127 | 7 | 79 | 39 | 5.1 | 0 | 17 | 30.5 | 8.7 | 7.9 | 1.8 | 0.2 | 1.6 | 0.5 |
| Lx | 173 | 88 | 66 | 26 | 5 | 31 | 7 | 10 | 40 | 4.9 | 0 | 10 | 16.5 | 89.0 | 64.2 | 53.3 | 19.3 | 1.5 | 2.6 |
| Bg | 44 | 43 | 65 | 6 | 0 | 32 | 4 | 7 | 55 | 5.7 | 3 | 18 | 19.3 | 4.8 | 5.7 | 1.5 | 0.2 | 0.7 | 1.3 |
| Ae | 82 | 103 | 62 | 20 | 3 | 28 | 7 | 7 | 147 | 5.9 | 25 | 20 | — | — | — | — | — | — | — |
| Za | | | | | | | | | | | | | | | | | | | |
| | Precipitation March 1958 (D 803) | | | | | | | | | | | | Air March 1958 (L 803) | | | | | | |
| Kn | 8 | 16 | 320 | 2 | 4 | 211 | 9 | 39 | 41 | 6.1 | 24 | 304 | 6.3 | 143. | 1.7 | 152. | 7.1 | 12.0 | 11. |
| Ri | 8 | 11 | 76 | 2 | 4 | 33 | 10 | 4 | 42 | 6.7 | 74 | 54 | × | × | × | × | × | × | × |
| Ki | 7 | 4 | 5 | 0 | 0 | 4 | 2 | 2 | 13 | 6.0 | 45 | 14 | × | × | × | × | × | × | × |

| Code | mm | mg/m² | | | | | | | | pH | $-\frac{\mu val}{l}$ $HCO_3$ | $\frac{\varkappa \cdot 10^6}{\Omega \cdot cm}$ | $\mu g/m^3$ (= kg/km³) | | | | | | |
|---|---|---|---|---|---|---|---|---|---|---|---|---|---|---|---|---|---|---|---|
| | | S | Cl | $NO_3$–N | $NH_3$–N | Na | K | Mg | Ca | | | | S | Cl | $NH_3$–N | Na | K | Mg | Ca |
| | | Precipitation March 1958 (D 803) | | | | | | | | | | | Air March 1958 (L 803) | | | | | | |
| Ar | 11 | 22 | 6 | 1 | 1 | 5 | 3 | 3 | 16 | 6.1 | 34 | 15 | × | × | × | × | × | × | × |
| Öj | 25 | 24 | 7 | 4 | 8 | 6 | 3 | 3 | 17 | 5.1 | 0 | 17 | 3.7 | 1.2 | 1.8 | 0.7 | 1.4 | 2.4 | 5.2 |
| Rö | 10 | 17 | 7 | 2 | 2 | 11 | 6 | 14 | 14 | 5.3 | 7 | 18 | 3.3 | 4.6 | 2.7 | 3.0 | 2.3 | 1.1 | 11 |
| Of | 18 | 19 | 10 | 2 | 3 | 10 | 7 | 7 | 14 | 5.8 | 6 | 13 | 7.3 | 1.9 | 2.9 | 2.7 | 2.2 | 3.9 | 17 |
| Br | 7 | 7 | 6 | 1 | 2 | 8 | 3 | 2 | 12 | 5.7 | 15 | 17 | × | × | × | × | × | × | × |
| ÅF | 6 | 1 | 5 | 1 | 1 | 12 | 4 | 2 | 14 | 6.4 | 68 | 23 | 3.6 | 2.8 | 1.8 | 1.9 | 1.6 | 3.4 | 9.9 |
| ÅH | 2 | 18 | 7 | 2 | 2 | 5 | 2 | 3 | 8 | 4.3 | — | — | — | — | — | — | — | — | — |
| Fö | 6 | 21 | 4 | 2 | 1 | 9 | 6 | 2 | 0 | 5.1 | 0 | 34 | — | — | — | — | — | — | — |
| Sv | 25 | 21 | 9 | 0 | 1 | 7 | 6 | 6 | 0 | 6.0 | 18 | 12 | — | — | — | — | — | — | — |
| Rä | 5 | 17 | 13 | 3 | 2 | 4 | 5 | 2 | 68 | 7.3 | 450 | 100 | 9.6 | 2.4 | 2.7 | 1.0 | 1.8 | 0.1 | 5.1 |
| Åm | 30 | 33 | 30 | 5 | 12 | 20 | 10 | 6 | 25 | 6.2 | 0 | 18 | 7.7 | 0.3 | 0.3 | 0.0 | 0.4 | 0.1 | 2.5 |
| Sa | 7 | 20 | 11 | 1 | 0 | 6 | 6 | 6 | 24 | 6.1 | 34 | 38 | 15 | 6.7 | 2.3 | 2.0 | 1.8 | 1.5 | 6.0 |
| Ul | 16 | 22 | 12 | 4 | 6 | 9 | 3 | 5 | 9 | 4.8 | 0 | 28 | 9.1 | 0.4 | 2.2 | 1.3 | 1.9 | 0.1 | 1.0 |
| Er | 16 | 15 | 12 | 4 | 2 | 8 | 4 | 4 | 10 | 5.8 | 26 | 16 | — | — | — | — | — | — | — |
| St | 12 | 28 | 18 | 4 | 3 | 8 | 6 | 6 | 35 | 6.4 | 40 | 31 | 7.0 | 1.9 | 2.6 | 0.5 | 1.1 | 1.0 | 4.2 |
| Fo | 2 | — | 2 | — | — | 3 | — | — | — | — | — | — | 0.9 | 0.0 | 2.5 | 0.3 | 0.9 | 0.0 | 3.9 |
| Kv 1 | 13 | 120 | 12 | 6 | 22 | 10 | 17 | 14 | 610 | 4.5 | 0 | 290 | × | × | × | × | × | × | × |
| Kv 7 | 17 | 38 | 13 | 5 | 7 | 9 | 3 | 5 | 25 | 5.1 | 0 | 29 | 1.8 | 0.6 | 1.6 | 0.3 | 1.2 | 0.3 | 2.7 |
| VK | 8 | 26 | 20 | 6 | 7 | 14 | 9 | 4 | 14 | 5.9 | 0 | 43 | 2.2 | 1.9 | 3.5 | 1.8 | 5.6 | 1.7 | 5.5 |
| La | 5 | 7 | 21 | 4 | 4 | 11 | 2 | 3 | 16 | 5.6 | — | 50 | 7.3 | 2.2 | 2.3 | 0.2 | 1.2 | 0.2 | 9.3 |
| Bo | 3 | 3 | 74 | 3 | 2 | 18 | 3 | 7 | 15 | 6.6 | — | 74 | 4.7 | 3.3 | 2.0 | 4.1 | 2.1 | 1.0 | 9.3 |
| Vi | 4 | 39 | 180 | 5 | 4 | 120 | 7 | 46 | 11 | 4.7 | — | 220 | 4.5 | 7.2 | 1.0 | 2.9 | 0.8 | 0.8 | 3.9 |
| Fa | 49 | 43 | 4 | 8 | 7 | 23 | 10 | 6 | 21 | 5.2 | 0 | 19 | × | × | × | × | × | × | × |
| Fl | 19 | 22 | 23 | 4 | 2 | 9 | 3 | 4 | 11 | 4.5 | 0 | 24 | 1.2 | 0.6 | 1.4 | 0.7 | 1.4 | 0.3 | 0.8 |
| Am | 16 | 19 | 58 | 5 | 2 | 36 | 5 | 6 | 14 | 5.9 | 13 | 25 | — | — | — | — | — | — | — |
| Fi | 28 | 40 | 86 | 11 | 15 | 50 | 6 | 12 | 11 | 5.0 | 0 | 34 | — | — | — | — | — | — | — |
| Pl | 7 | 24 | 24 | 8 | 7 | 15 | 2 | 3 | 7 | 4.3 | 0 | 65 | 1.4 | 8.0 | 5.0 | 4.3 | 1.0 | 1.2 | 11 |
| Sö | 19 | 39 | 21 | 6 | 3 | 11 | 4 | 4 | 55 | 5.6 | 9 | 33 | — | — | — | — | — | — | — |
| Sm | 19 | 34 | 22 | 7 | 8 | 14 | 4 | 4 | 11 | 4.4 | 0 | 41 | 7.2 | 1.5 | 2.1 | 0.9 | 0.5 | 1.0 | 3.5 |
| Sy | 16 | 41 | 17 | 5 | 10 | 11 | 4 | 4 | 35 | 4.9 | 0 | 35 | 2.3 | 8.6 | 3.7 | 0.5 | 1.5 | 1.8 | 26 |
| BH | 8 | 17 | 28 | 5 | 4 | 17 | 3 | 9 | 12 | 4.4 | 0 | 48 | 8.1 | 0.6 | 2.2 | 0.0 | 0.5 | 1.1 | 7.9 |
| Sk | 11 | 36 | 52 | 12 | 23 | 31 | 3 | 6 | 15 | 4.4 | 0 | 65 | 1.0 | 2.2 | 2.8 | 4.0 | 1.9 | 1.6 | 1.4 |
| Al | 19 | 40 | 42 | 11 | 13 | 23 | 2 | 7 | 20 | 4.4 | 0 | 45 | × | × | × | × | × | × | × |
| Hi | 2 | — | 11 | — | — | 10 | — | — | — | — | — | — | — | — | — | — | — | — | — |
| Ta | 20 | 24 | 100 | 3 | 6 | 74 | 5 | 10 | 17 | 6.5 | 23 | 36 | × | × | × | × | × | × | × |
| An | — | — | — | — | — | — | — | — | — | — | — | — | — | — | — | — | — | — | — |
| Yt | 28 | 11 | 90 | 3 | 8 | 53 | 19 | 16 | 16 | 6.2 | 55 | 22 | — | — | — | — | — | — | — |
| Gj | 24 | 53 | 70 | 2 | 5 | 45 | 3 | 13 | 18 | 6.3 | 22 | 20 | — | — | — | — | — | — | — |
| Fn | 11 | 13 | 10 | 2 | 5 | 6 | 2 | 2 | 13 | 6.4 | 28 | 15 | — | — | — | — | — | — | — |
| Få | 9 | 13 | 140 | 6 | 22 | 50 | 41 | 2 | 25 | 6.8 | 390 | 120 | — | — | — | — | — | — | — |
| Vå | 3 | 7 | 5 | 1 | 3 | 6 | 3 | 3 | 19 | 7.0 | — | 36 | 1.5 | 0.0 | 4.7 | 0.2 | 1.1 | 0.9 | 5.9 |
| Tr | 3 | 4 | 5 | 1 | 1 | 2 | 2 | 2 | 4 | 6.0 | — | — | — | — | — | — | — | — | — |
| Ke | 0 | — | — | — | — | — | — | — | — | — | — | — | — | — | — | — | — | — | — |
| Sd | 57 | 40 | 160 | 3 | 7 | 120 | 9 | 16 | 23 | 6.2 | 20 | 18 | — | — | — | — | — | — | — |
| Da | 4 | 3 | 5 | 2 | 2 | 6 | 3 | 3 | 23 | 7.0 | — | 40 | — | — | — | — | — | — | — |
| Ås | 0 | — | — | — | — | — | — | — | — | — | — | — | 8.7 | 0.3 | 1.4 | 0.4 | 1.5 | 1.1 | 4.0 |
| Li | 13 | 58 | 210 | 8 | 4 | 170 | 6 | 21 | 14 | 4.9 | 0 | 91 | 15 | 12 | 2.5 | 6.4 | 3.0 | 2.3 | 13 |
| So | 4 | 5 | 3 | — | — | 2 | 0 | — | 8 | 4.9 | 0 | 21 | 5.5 | 0 | 1.8 | 0.8 | 0.6 | 0.5 | 0.3 |
| Ka | 21 | 8 | 20 | 3 | 2 | 5 | 11 | 2 | 28 | 6.0 | 0 | 14 | 6.7 | 1.1 | 8.2 | 1.3 | 1.6 | 1.2 | 3.8 |
| Ku | 8 | 0 | 3 | 2 | 0 | 1 | 4 | 1 | 7 | 5.1 | 0 | 15 | 0 | 2.0 | 9.3 | 3.1 | 11.0 | 2.4 | 15.0 |
| Jy | 14 | 0 | 91 | 3 | 4 | 5 | 7 | 2 | 14 | 5.9 | 0 | 20 | 0 | 10.0 | 1.8 | 1.3 | 1.7 | 0.5 | 9.5 |
| Pu | 14 | 0 | 2 | 2 | 1 | 1 | 1 | 1 | 10 | 4.7 | 0 | 18 | 7.5 | 0 | 1.7 | 0.3 | 0 | 0.3 | 2.1 |
| Tv | 10 | 19 | 8 | 2 | 1 | 3 | 4 | 2 | 8 | 4.7 | 0 | 23 | × | × | × | × | × | × | × |
| Rj | 27 | 59 | 580 | 4 | 7 | 390 | 22 | 61 | 27 | 5.2 | 0 | 110 | × | × | × | × | × | × | × |
| Vn | 3 | 7 | 29 | 1 | 7 | 20 | 2 | 9 | 2 | 5.9 | 0 | 72 | — | — | — | — | — | — | — |
| Gr | 6 | 24 | 41 | 4 | 7 | 24 | 4 | 12 | 14 | 4.7 | 0 | 82 | — | — | — | — | — | — | — |
| Öd | 11 | 30 | 65 | 6 | 9 | 52 | 4 | 10 | 25 | 6.1 | 33 | 57 | 11 | 3.6 | 3.8 | 1.1 | 0.9 | 1.0 | 3.6 |

| Code | mm | mg/m² | | | | | | | | pH | $-\frac{\mu val}{l}$ $HCO_3$ | $\frac{\varkappa \cdot 10^6}{\Omega \cdot cm}$ | μg/m³ (=kg/km³) | | | | | | |
|---|---|---|---|---|---|---|---|---|---|---|---|---|---|---|---|---|---|---|---|
| | | S | Cl | $NO_3$–N | $NH_3$–N | Na | K | Mg | Ca | | | | S | Cl | $NH_3$–N | Na | K | Mg | Ca |
| | | Precipitation March 1958 (D 803) | | | | | | | | | | | Air March 1958 (L 803) | | | | | | |
| Bs | 5 | 17 | 90 | 4 | 8 | 54 | 6 | 11 | 18 | 4.8 | 0 | 109 | — | — | — | — | — | — | — |
| Ly | 9 | 34 | 32 | 7 | 11 | 17 | 3 | 16 | 3 | 4.2 | 0 | 80 | — | — | — | — | — | — | — |
| As | 5 | 21 | 130 | 5 | 9 | 79 | 3 | 14 | 13 | 4.8 | 0 | 140 | 3.6 | 1.0 | 3.9 | 0.1 | 1.9 | 1.0 | 8.6 |
| Vd | 15 | 37 | 56 | 7 | 27 | 35 | 5 | 15 | 15 | 5.0 | 0 | 49 | — | — | — | — | — | — | — |
| Bl | 6 | 25 | 41 | 4 | 7 | 24 | 4 | 8 | 23 | 4.9 | 0 | 83 | — | — | — | — | — | — | — |
| Ty | 2 | 4 | 44 | 5 | 8 | 25 | 2 | 7 | 19 | 6.5 | — | — | 7.8 | 6.1 | 4.8 | 7.9 | 1.6 | 1.9 | 4.3 |
| Hö | 4 | 15 | 74 | 3 | 13 | 47 | 4 | 18 | 15 | 4.6 | 0 | 149 | — | — | — | — | — | — | — |
| Ad | 5 | 12 | 18 | 1 | 6 | 13 | 2 | 5 | 7 | 4.7 | 0 | 61 | — | — | — | — | — | — | — |
| Lw | 4 | — | — | — | — | — | — | — | — | — | — | — | 3.6 | 14.0 | 0.8 | 0.0 | 0.6 | 0.7 | 0.0 |
| Ab | 99 | 130 | 410 | 45 | 63 | 950 | 51 | 120 | 150 | 5.2 | 0 | 100 | 11 | 5.4 | 2.1 | 0.2 | 0.6 | 1.1 | 2.8 |
| Ed | 43 | 130 | 180 | 24 | 47 | 120 | 14 | 22 | 47 | 4.5 | 0 | 59 | 14 | 3.9 | 3,1 | 1.7 | 1.7 | 1.0 | 5.0 |
| Es | 33 | 79 | 95 | 18 | 21 | 63 | 3 | 11 | 17 | 4.2 | 0 | 53 | 19.2 | 2.4 | 1.6 | 1.8 | 0.9 | 0.5 | 8.5 |
| Le | 31 | 55 | 170 | 29 | 56 | 93 | 12 | 27 | 71 | 4.6 | 0 | 71 | × | × | × | × | × | × | × |
| Ro | 37 | 65 | 160 | 31 | 41 | 82 | 17 | 21 | 95 | 4.3 | 0 | 71 | 18. | 6.4 | 3.0 | 3.4 | 1.5 | 1.5 | 3.0 |
| NA | 41 | 130 | 800 | 39 | | 470 | 26 | 62 | 130 | 5.3 | 0 | 120 | 16. | 27. | 5.3 | 17. | 1.5 | 3.1 | 4.1 |
| Ca | 70 | 134 | 1 089 | 18 | 25 | 629 | 24 | 87 | 56 | 4.6 | 0 | 73 | 11.8 | 1.4 | 1.8 | 3.1 | 0.6 | 0.3 | 0.0 |
| Bt | 87 | 148 | 1 723 | 30 | 6 | — | — | — | — | 6.1 | 16 | 85 | — | — | — | — | — | — | — |
| DA | 23 | 133 | 614 | 46 | 3 | — | — | — | — | 4.9 | 0 | 189 | — | — | — | — | — | — | — |
| Va | 133 | 109 | 865 | 13 | 13 | — | — | — | — | 5.4 | 0 | 33 | — | — | — | — | — | — | — |
| Sc | 9 | 37 | 116 | 8 | 9 | 53 | 5 | 9 | 34 | 4.2 | 0 | 96 | 19.9 | 15.2 | 6.2 | 4.5 | 2.3 | 0.8 | 1.8 |
| BV | 10 | 45 | 94 | 17 | 5 | 16 | 7 | 16 | 172 | 4.4 | 0 | 177 | 40.7 | 14.7 | 7.0 | 1.2 | 1.0 | 0.6 | 1.8 |
| Bn | 26 | 50 | 104 | 35 | 29 | 39 | 20 | 19 | 320 | 6.0 | 60 | 13 | 42.5 | 17.3 | 6.8 | 2.3 | 1.7 | 1.8 | 1.5 |
| Au | 26 | 72 | 59 | 14 | 15 | 19 | 12 | 10 | 57 | 4.4 | 0 | 38 | 25.5 | 9.2 | 6.4 | 1.3 | 1.8 | 2.5 | 3.8 |
| Fe | 55 | 103 | 0 | 16 | 38 | 29 | 24 | 6 | 25 | 4.3 | 0 | 32 | 9.2 | 1.1 | 1.3 | 1.7 | 1.1 | 2.3 | 5.4 |
| Ba | 31 | 41 | 40 | 13 | 18 | 18 | 9 | 3 | 62 | 5.6 | 28 | 21 | 22.9 | 8.7 | 4.9 | 1.8 | 0.9 | 0.7 | 1.4 |
| Ho | 63 | 137 | 38 | 7 | 6 | 15 | 63 | 22 | 91 | 5.1 | 0 | 22 | 29.4 | 4.4 | 4.0 | 0.9 | 0.8 | 0.6 | 1.2 |
| Rm | 17 | 22 | 29 | 13 | 2 | 12 | 6 | 4 | 171 | 6.5 | 208 | 88 | 12.2 | 3.4 | 3.6 | 2.7 | 0.5 | 0.3 | 1.8 |
| Et | 19 | 53 | 40 | 11 | 12 | 15 | 12 | 5 | 57 | 5.2 | 0 | 38 | 35.3 | 8.5 | 8.3 | 3.5 | 1.0 | 1.0 | 4.6 |
| He | — | — | — | — | — | — | — | — | — | — | — | — | — | — | — | — | — | — | — |
| Rz | 15 | 36 | 5 | 8 | 4 | 4 | 2 | 3 | 33 | 5.0 | 0 | 26 | 16.0 | 2.5 | 3.5 | 1.9 | 0.8 | 0.3 | 1.0 |
| Wi | 71 | 115 | 35 | 8 | 11 | 25 | 20 | 13 | 113 | 5.4 | 0 | 18 | 50.9 | 9.8 | 7.6 | 2.3 | 0.9 | 0.3 | 0.8 |
| Lz | 46 | 109 | 14 | 21 | 18 | 15 | 10 | 13 | 98 | 5.7 | 12 | 25 | 34.6 | 6.5 | 5.0 | 0.8 | 0.9 | 0. | 0.7 |
| Kl | 33 | 62 | 10 | 7 | 15 | 6 | 5 | 8 | 41 | 5.2 | 0 | 19 | 23.9 | 5.3 | 3.5 | 1.4 | 0.9 | 0.3 | 0.6 |
| BL | | | | | | | | | | | | | | | | | | | |
| DH | 27 | 127 | 363 | 31 | 21 | 213 | 12 | 105 | 69 | 4.2 | 0 | 110 | 37.1 | 26.1 | 5.2 | 9.1 | 0.7 | 42.8 | 2.4 |
| DB | 27 | 88 | 122 | 8 | 1 | 76 | 6 | 13 | 46 | 4.4 | 0 | 61 | 34.9 | 14.8 | 6.9 | 8.1 | 1.0 | 15.3 | 2.2 |
| W | 24 | 88 | 96 | 7 | 1 | 60 | 10 | 12 | 42 | 4.3 | 0 | 65 | 25.6 | 14.6 | 7.1 | 7.1 | 0.9 | 12.5 | 2.0 |
| SA | 22 | 112 | 73 | 16 | 6 | 44 | 10 | 9 | 44 | 4.6 | 0 | 67 | 15.3 | 1.7 | 3.7 | 4.5 | 0.2 | 0.3 | 1.0 |
| U | 23 | 88 | 75 | 19 | 14 | 39 | 9 | 11 | 66 | 4.6 | 0 | 58 | 57.6 | 10.8 | 2.7 | 4.6 | 0.5 | 0.8 | 1.0 |
| B | 67 | 171 | 136 | 54 | 30 | 60 | 16 | 19 | 100 | 4.4 | 0 | 49 | 23.7 | 6.5 | 3.7 | 0.9 | 0.3 | 5.1 | 0.8 |
| D | 16 | 58 | 57 | 15 | 4 | 40 | 3 | 8 | 30 | 4.8 | 0 | 53 | 20.4 | 8.4 | 4.6 | 1.7 | 0.6 | 8.8 | 1.7 |
| MH | 27 | 63 | 71 | 21 | 19 | 30 | 16 | 8 | 65 | 5.9 | 36 | 37 | 35.7 | 22.0 | 4.6 | 2.4 | 1.2 | 0.0 | 0.9 |
| Rs | 86 | 59 | 362 | 24 | 6 | 175 | 9 | 25 | 31 | 5.0 | 0 | 17 | 19.2 | 4.1 | 2.6 | 2.5 | 0.6 | 0.0 | 6.0 |
| LM | 47 | 43 | 60 | 20 | 5 | 39 | 3 | 8 | 59 | 5.1 | 0 | 17 | 10.2 | 2.2 | 3.8 | 3.5 | 1.0 | 0.2 | 59.8 |
| Lx | 57 | 53 | 63 | 25 | 7 | 26 | 64 | 12 | 25 | 5.9 | 14 | 17 | 18.0 | 9.1 | 3.4 | 2.4 | 1.1 | 0.1 | 7.7 |
| Bg | 56 | 69 | 73 | 20 | 11 | 33 | 6 | 7 | 104 | 5.5 | 0 | 20 | 15.7 | 2.9 | 4.6 | 1.8 | 1.2 | 0.0 | 10.4 |
| Ae | 113 | 24 | 58 | 31 | 16 | 20 | 9 | 8 | 159 | 5.7 | 11 | 12 | — | — | — | — | — | — | — |
| Za | 54 | 26 | 27 | 15 | 25 | 20 | 7 | 19 | 120 | 6.3 | 49 | 28 | — | — | — | — | — | — | — |

# $CO_2$-values in Scandinavia February—April 1958

(Cf. FONSELIUS, KOROLEFF: *Tellus* **7**, pp. 258—265)

| Station | February | | | | | March | | | | | April | | | | |
|---|---|---|---|---|---|---|---|---|---|---|---|---|---|---|---|
| | Date | °C | Wind | Weather | $CO_2$ ml/10 l. | Date | °C | Wind | Weather | $CO_2$ ml/10 l. | Date | °C | Wind | Weather | $CO_2$ ml/10 l. |
| Kn | 10 | —3.0 | NE 12 | ✳ 10 | 2.94 | 20 | —4.0 | ENE 7 | 10 | 3.27 | 18 | —2.0 | S 5 | ✳ 9 | 3.15 |
| | 18 | —5.0 | ENE 20 | 8 | 3.21 | 21 | —5.0 | E 10 | 10 | 3.20 | 19 | —4.0 | SW 5 | 10 | 3.24 |
| | 19 | —11.0 | NNE 15 | 4 | 3.09 | 28 | —5.0 | E 7 | 7 | 3.17 | 20 | —2.0 | NE 15 | 9 | 3.19 |
| | 26 | —6.0 | S 5 | ✳° 9 | 2.98 | | | | | | | | | | |
| Ao | 10 | —12.5 | ENE 2 | ✳° 10 | 3.64 | 20 | —1.0 | W 11 | ▽*10 | 2.81 | 18 | —2.0 | N 1 | 1 | 2.96 |
| | 18 | —5.2 | Calm | 8 | 3.05 | 21 | —3.0 | Calm | 10 | 3.43 | 19 | —3.0 | SE 12 | 3 | 3.20 |
| | 19 | —6.0 | ESE 1 | 10 | 3.23 | 28 | —2.0 | W 10 | ▽*10 | 2.96 | 20 | — | — | — | — |
| | 26 | — | — | — | — | | | | | | | | | | |
| Öj | 10 | —10.6 | Calm | 10 | 3.20 | 20 | —1,8 | W 1 | = 1 | 2.86 | 18 | 0.8 | S 2 | 6 | 2.86 |
| | 18 | —7.4 | NW 1 | = 1 | 3.05 | 21 | 2.0 | W 1 | = 1 | 2.74 | 19 | 0.2 | SE 2 | 10 | 3.06 |
| | 19 | —10.2 | Calm | 10 | 3.54 | 28 | 0.5 | S 1 | 9 | 3.06 | 20 | 4.8 | Calm | 6 | 3.05 |
| | 26 | —12.8 | NW 1 | = | 3.42 | | | | | | | | | | |
| Br | 10 | —15.0 | NW 1 | 5 | 3.36 | 20 | —5.0 | Calm | 1 | 3.02 | 18 | 5.0 | W 2 | 1 | 2.92 |
| | 18 | —10,0 | NW 1 | 1 | 2.82 | 21 | —2.0 | Calm | 0 | 3.09 | 19 | 2.0 | SW 2 | 10 | 2.99 |
| | 19 | —6.0 | Calm | 0 | 2.84 | 28 | 0 | Calm | 0 | 3.22 | 20 | 1.0 | SE 2 | 9 | 2.87 |
| | 26 | —22.0 | Calm | 0 | 2.95 | | | | | | | | | | |
| Er | 10 | —8.5 | NW 1 | 8 | 3.10 | 20 | —4.8 | N 5 | 8 | 3.09 | 18 | 10.0 | SW 1 | 4 | 3.02 |
| | 18 | —3.8 | WNW 6 | 5 | 3.78 | 21 | —4.2 | NE 4 | 1 | 3.42 | 19 | 5.6 | S 5 | 6 | 3.10 |
| | 19 | —4.8 | W 4 | 4 | 3.15 | 28 | —3.5 | NE 1 | 0 | 2.97 | 20 | 2.1 | NW 6 | 10 | 2.91 |
| | 26 | — | — | — | — | | | | | | | | | | |
| Fl | 10 | 7.7 | NE 2 | 10 | 3.49 | 20 | —4.5 | N 1 | 8 | 3.04 | 18 | 2.8 | S 1 | 0 | 3.07 |
| | 18 | 4.3 | W 1 | 1 | 2.95 | 21 | —5.6 | N 1 | 0 | 2.99 | 19 | 3.8 | SW 1 | 10 | 3.00 |
| | 19 | 3.0 | SW 1 | 0 | 3.21 | 28 | —1.8 | SE 1 | 0 | 3.04 | 20 | 10.4 | W 1 | 0 | 2.96 |
| | 26 | 11.6 | N 2 | 8 | 3.36 | | | | | | | | | | |
| Pl | 10 | 5.0 | SW 4 | | 3.24 | 21 | —1.0 | E 2 | 1 | 2.95 | 19 | 6.0 | W 1 | ● 10 | 3.05 |
| | 19 | —3.0 | W 2 | | 2.82 | 22 | —1.0 | E 1 | 1 | 2.81 | 20 | 7.0 | W 1 | ●° 10 | 3.28 |
| | 20 | —3.0 | W 2 | 5 | 2.92 | 28 | —1.0 | E 8 | 0 | 3.00 | 21 | 8.0 | W 6 | 1 | 2.90 |
| | 26 | —5.0 | N 8 | 1 | 3.43 | | | | | | | | | | |
| So | 10 | —18.4 | Calm | ∞° 10 | 3.44 | 20 | 0.1 | W 2 | ∞ 0 | 3.32 | 18 | —3.1 | NE 1 | ∞° 10 | 3.38 |
| | 18 | —8.9 | N 0.5 | ∞ 10 | 3.46 | 21 | 0.1 | W 1.5 | ∞ 0 | 3.40 | 19 | —1.4 | E 2 | ∞° 10 | 3.19 |
| | 19 | —9.3 | N 1 | ✳° 10 | 3.03 | 28 | —2.8 | SW 2 | 5 | 3.09 | 20 | 0.2 | SSE 2 | ∞ 10 | 3.26 |
| | 26 | —6.0 | E 1 | ✳° 10 | 3.15 | | | | | | | | | | |
| Ka | 10 | —10.1 | WNW 0.5 | 0 | 3.33 | 20 | —3.7 | NNE 1 | 0 | 3.42 | 18 | 5.2 | Calm | 0 | 3.21 |
| | 18 | —5.3 | NNE 1 | 10 | 4.14 | 21 | — | — | — | — | 19 | 8.8 | S 1 | 0 | 3.01 |
| | 19 | —9.9 | W 0.5 | 8 | 3.47 | 28 | —1.2 | WSW 1.5 | 0 | 3.22 | 20 | — | — | — | — |
| | 26 | —21.7 | Calm | 10 | 3.53 | | | | | | | | | | |
| Ku | 10 | — | — | — | — | 20 | —6.8 | E 1 | 0 | 3.46 | 18 | 2.8 | N 1 | 5 | 3.17 |
| | 18 | —9.6 | N 0.5 | 5 | 3.21 | 21 | —5.3 | SW 0.5 | 5 | 3.52 | 19 | 6.2 | SE 1 | 0 | 3.34 |
| | 19 | —6.6 | NW 1 | 10 | 3.17 | 28 | —2.6 | WSW 1 | 0 | 3.30 | 20 | 5.6 | ESE 1 | 5 | 3.07 |
| | 26 | —17.6 | W 0.2 | 0 | 3.33 | | | | | | | | | | |
| Jy | 10 | —16.0 | Calm | 0 | 3.39 | 20 | —5.6 | NE 1.5 | 8 | 3.24 | 18 | 4.5 | WSW 1 | 7 | 3.22 |
| | 18 | —5.8 | NE 0.5 | ✳° 10 | 3.34 | 21 | —6.6 | SW 0.5 | 10 | 3.41 | 19 | 6.1 | WSW 1 | 7 | 3.10 |
| | 19 | —6.1 | NW 1 | 8 | 3.14 | 28 | —2.7 | WNW 2 | 9 | 3.30 | 20 | 6.4 | S 2 | 10 | 3.35 |
| | 26 | —16.2 | NE 0.2 | 10 | 3.06 | | | | | | | | | | |
| Pu | 10 | —16.9 | W 1 | 0 | 3.45 | 20 | —7.0 | NE 1 | 0 | 3.25 | 18 | 4.4 | W 2 | 1 | 3.26 |
| | 18 | —8.2 | N 2 | ✳° 10 | 3.09 | 21 | —6.8 | NE 1 | ✳° 7 | 3.14 | 19 | 5.2 | E 1 | 2 | 3.28 |
| | 19 | —6.4 | NW 2 | ✳° 10 | 3.10 | 28 | —3.4 | NE 1.5 | 1 | 3.20 | 20 | 5.0 | SE 2 | 0 | 3.25 |
| | 26 | —15.4 | NE 0.5 | 10 | 3.49 | | | | | | | | | | |

| Station | February | | | | | March | | | | | April | | | | |
|---|---|---|---|---|---|---|---|---|---|---|---|---|---|---|---|
| | Date | °C | Wind | Weather | $CO_2$ ml/10 l. | Date | °C | Wind | Weather | $CO_2$ ml/10 l. | Date | °C | Wind | Waether | $CO_2$ ml/10 l. |
| Tv | 10 | —11.0 | N 0.5 | 10 | 3.49 | 20 | —5.0 | E 2 | 0 | 3.24 | 18 | 7.0 | NW 2 | 0 | 3.34 |
| | 18 | —3.0 | NW 2 | 10 | 3.55 | 21 | —7.0 | NE 2 | 0 | 3.23 | 19 | 5.0 | SW 1 | 0 | 3.20 |
| | 19 | —3.0 | NW 1.5 | 10 | 3.43 | 28 | —3.0 | E 2 | 0 | 3.40 | 20 | 4.0 | SE 1 | 10 | 3.30 |
| | 26 | —11.0 | ENE 6 | ⚹ 10 | 3.50 | | | | | | | | | | |
| Ta | 10 | —18.0 | SSW 5 | | 3.02 | 20 | 2.0 | W 9 | 10 | 2.99 | 18 | —9.0 | SSW 2 | 0 | 2.92 |
| | 18 | —9.0 | Calm | =° | 2.95 | 21 | 1.2 | WNW 13 | ⚹ 10 | 3.04 | 19 | —13.0 | SSW 6 | 0 | 3.62 |
| | 19 | —12.0 | Calm | =° | 2.97 | 28 | —18.2 | Calm | 10 | 3.11 | 20 | —17.0 | SSW 2 | 0 | 3.09 |
| | 26 | —1.8 | NE 9 | = 10 | 2.89 | | | | | | | | | | |
| Vg | 10 | —10.2 | NE 4 | =° | 2.91 | 20 | —2.2 | E 1 | 2 | 2.85 | 18 | 2.8 | E 2 | 1 | 2.84 |
| | 18 | —2.3 | WSW 1 | ▽*10 | 3.05 | 21 | 1.2 | S 1 | =° 10 | 2.95 | 19 | 4.0 | NNW 5 | =° 10 | 3.08 |
| | 19 | —6.5 | ENE 2 | =° 3 | 3.10 | 28 | 0 | WSW 5 | ▽*10 | 3.03 | 20 | 5.8 | ESE 4 | 2 | 2.99 |
| | 26 | —11.4 | E 1 | =° 10 | 3.20 | | | | | | | | | | |
| Vå | 10 | —32.5 | SSW 2 | 1 | 3.07 | 20 | —9.0 | SSE 2 | 0 | 3.14 | 18 | 5.0 | SSW 2 | 5 | 3.18 |
| | 18 | —3.1 | WSW 9 | 10 | 2.99 | 21 | 9.0 | Calm | 0 | 2.99 | 19 | 6.3 | WNW 2 | 5 | 3.16 |
| | 19 | —10.3 | NE 5 | ⚹ 10 | 3.05 | 28 | —7.9 | ESE 2 | 0 | 2.92 | 20 | 5.2 | E 13 | 10 | 3.02 |
| | 26 | —24.0 | SSW 2 | 0 | 3.78 | | | | | | | | | | |
| Sd | 10 | —3.5 | E 8 | 10 | 2.87 | 20 | 0 | N 2 | 0 | 2.91 | 18 | 5.0 | S 4 | 10 | 2.79 |
| | 18 | —1.0 | NW 6 | 1 | 2.99 | 21 | | E 8 | 0 | 2.85 | 19 | 7.0 | S 2 | ▽●10 | 3.02 |
| | 19 | —1.0 | SW 12 | ⚹ | 3.36 | 28 | 3.0 | E 2 | 0 | 3.01 | 20 | 5.0 | SW 6 | ● 10 | 2.83 |
| | 26 | —5.0 | E 1 | 1 | 3.02 | | | | | | | | | | |
| Öd | 10 | —1.6 | SE 6 | ⚹²10 | 3.13 | 20 | —0.8 | NE 3 | 10 | 3.17 | 18 | 8.2 | SW 4 | 9 | 3.01 |
| | 18 | —1.0 | NW 3 | 9 | 2.94 | 21 | —3.2 | NE 3 | 10 | 3.15 | 19 | 7.4 | SSW 4 | 10 | 3.02 |
| | 19 | —0.1 | W 2 | 10 | 3.04 | 28 | 2.2 | E 5 | 7 | 3.20 | 20 | 7.6 | SW 5 | 10 | 2.96 |
| | 26 | —5.4 | NNE 4 | ≡ 7 | 3.24 | | | | | | | | | | |
| As | 10 | 1.0 | ESE 3 | | 3.30 | 20 | —0.6 | NE 4 | 4 | 3.04 | 18 | 6.2 | S 4 | 8 | 2.92 |
| | 18 | 2.2 | NNW 2 | | 2.92 | 21 | —2.0 | ENE 4 | 10 | 2.99 | 19 | 5.8 | W 4 | 6 | 3.08 |
| | 19 | 1.1 | W 1 | 8 | 2.72 | 28 | 3.7 | ENE 6 | 4 | 3.24 | 20 | 9.2 | W 5 | 8 | 3.18 |
| | 26 | —5.2 | NNE 2 | 3 | 3.27 | | | | | | | | | | |
| Vl | 10 | 8.3 | SW 17 | | 3.10 | 20 | — | — | — | — | 18 | 8.1 | SW 20 | — | 3.19 |
| | 18 | — | — | — | — | 21 | — | — | — | — | 19 | 9.8 | W 24 | — | 2.93 |
| | 19 | — | — | — | — | 28 | 6.7 | ESE 8 | ●° 10 | 3.07 | 20 | 10.1 | NNE 30 | — | 3.09 |
| | 26 | — | — | — | — | | | | | | | | | | |

## Coordinates of New Sampling Stations for Precipitation, Air and $CO_2$

| Station | Code | Altitude m | Latitude °N | Longitude | Green-wich | Precipita-tion | Air | $CO_2$ | Started sampling |
|---|---|---|---|---|---|---|---|---|---|
| Dublin Airport... | DA | | 53°26′ | 6°15′ | W | × | | | Feb. 1. 1958 |
| Belmullet ..... | Bt | | 54°14′ | 10°00′ | W | × | | | Mar. 1, 1958 |
| Birr..... | Bi | 71 | 53°05′ | 7°53′ | W | × | | | Apr. 1, 1958 |